Tratamiento térmico de lodos de la industria papelera. Utilización de subproductos para la adsorción de contaminantes emergentes del agua.

Ricardo Nuno de Coimbra Sampaio Gomes

Facultad de Ciencias Biológicas y Ambientales

Programa de doctorado: Ciencia y Tecnología del Medio Ambiente y Procesos

TESIS DOCTORAL UNIVERSIDAD DE LEÓN 2016

Thermal treatment of sludge from the paper industry. Utilization of byproducts for the adsorption of emerging contaminants from water.

Ricardo Nuno de Coimbra Sampaio Gomes

Faculty of Biological and Environmental Sciences

Doctoral Program: Environmental Science and Technology and Processes

PhD THESIS UNIVERSITY OF LEÓN 2016

Memoria presentada para optar al Grado de Doctor por la Universidad de León

Autor: Ricardo Nuno de Coimbra Sampaio Gomes

Directores: Dra. Marta Otero Cabero y Dr. Luis Fernando Calvo Prieto

Departamento de Química y Física Aplicadas

Facultad de Ciencias Biológicas y Ambientales

Universidad de León

Programa de doctorado: Ciencia y Tecnología del Medio Ambiente y Procesos

Aos meus pais e á minha irmã

Agradecimientos

En primer lugar, me gustaría manifestar un agradecimiento muy especial a mis directores de tesis, la Dra. Marta Otero y el Dr. Luis Fernando Calvo por su implicación, dedicación y apoyo incondicional.

À Universidade de Aveiro e, nomeadamente ao Dr. Valdemar e à sua equipa, agradeço, além da sua simpatia e profisionalidade, os meios e materiais disponibilizados.

Agradeço ao Instituto de Investigação da Floresta e do Papel (RAIZ), especialmente ao Eng. Luís Machado e ao Eng. José Luís Amaral, pelo fornecimento dos lodos objeto de estudo neste trabalho.

A la Estación Depuradora de Aguas Residuales (EDAR) de León y en especial a Patricia Quintans quiero expresarles mi gratitud por su amable contribución al proporcionar el efluente secundario utilizado en este trabajo.

Agradezco al Laboratorio Regional de Combustibles (LARECOM) y, en concreto, a José Alonso de Linaje y a María Pilar González, la atención prestada.

Doy las gracias a la Dra. Ana Isabel García tanto por su acogida como por apoyar mi integración y participación en el grupo de trabajo. Asimismo, a mis compañeros Carla y Sergio, además de agradecerles su colaboración, compañía y simpatía, les deseo lo mejor para su futuro.

También me gustaría dejar aquí una palabra de reconocimiento para Toyi, por esforzarse cada día en hacer un buen trabajo.

Finalmente, por tudo e mais alguma coisa, um GRANDE obrigado à minha família. Gosto muito de vocês!

Índice

Capítulo 1

1. Introducción

1.1. El papel y su relevancia como producto de consumo

El papel surgió para dar respuesta a la necesidad de un soporte de transmisión de información de fácil obtención, manejo y almacenamiento, ventajas que el papel presenta sobre otros soportes anteriormente utilizados como eran lajas de piedra y superficies de edificios. Desde su aparición, los usos del papel se fueron diversificando mucho más allá de los libros y material de escritura para pasar a incluir, entre otras, aplicaciones de empaquetado o de cuidado y aseo personal. Como resultado, actualmente, en media global, el mayor consumo de papel se destina al empaquetado (40%), seguido del papel de impresión (30%), papel de prensa (13%) y tisús (6%), porcentajes que pueden variar mucho de un país a otro. La expansión de los usos del papel se relaciona con la prosperidad de la zona o región, la substitución de otros materiales (servilletas o pañuelos de papel) y cambios estructurales hacia una economía basada en la información (Robins, 1996).

El cambio de un modelo de desarrollo industrial al basado en la información no ha llevado consigo una crisis del papel. Es muy significativo que, a pesar de las predicciones de disminución del consumo debido al auge de la era electrónica, el consumo global de papel ha venido aumentando desde mediados de los 80 (Techque, 2009). Más aún, se estima que el consumo global de papel continuará aumentando en más de un 1,6% anual hasta alcanzar los 500 millones de toneladas en 2025. Esta estimación se relaciona fundamentalmente con el aumento del consumo en Asia y, concretamente, en China (Bajpai, 2015a). En cualquier caso, el consumo de papel es muy desigual en las diferentes regiones del mundo, como se puede observar en la tabla 1.1. Los mayores consumidores de papel son Asia, Europa y América del Norte, que juntos consumen el 90% del papel mundial.

Tabla 1.1. Consumo mundial de papel en 2013 (adaptado de Bajpai (2015a)).

Región	**Consumo (%)**
Asia	46
Europa	24
América del Norte	20
América del Sur	7
Oceanía	2
África	1
Producción total (2013) = 403 millones de toneladas	

Se debe señalar que el consumo de papel posee un valor cultural inherente a la función que desempeña en el registro y difusión de la información. Por este motivo, la tasa de consumo de pasta y papel se suele utilizar como indicador del desarrollo socioeconómico de una nación (Techque, 2009). En la tabla 1.2. se muestra como el consumo de papel *per cápita* es muy diferente entre las distintas regiones y/o países del mundo.

Tabla 1.2. Consumo de papel per cápita en 2013 (Swedish Forest Industry Federation, 2014).

Región o país	**Consumo (kg/cápita)**
América del Norte	221
Unión Europea	156
Resto de Europa	52
Japón	215
China	75
Corea, Taiwán, Hong Kong, Singapur y Malasia	159
Resto de Asia	23
Oceanía	126
América del Sur	47
África	8

Estados Unidos y Canadá han sido, tradicionalmente, grandes consumidores de papel. Como se reflejaba en la tabla 1.1. América del Norte representa un 20% del consumo global, a pesar de contar con sólo el 5% de la población mundial. La media de consumo mundial fue, en

2013, de aproximadamente 57 kg de papel por persona, con valores entre los 300 kg/persona en Estados Unidos y los 7 kg/persona en el continente africano. En áreas densamente pobladas de Asia, el consumo aproximado *per cápita* es de unos 35 kg. Esto significa que, si el desarrollo sigue el mismo camino que en los países industrializados de Occidente, el potencial de crecimiento de la demanda en Asia es enorme (Bajpai, 2015a).

1.2. La industria papelera en números

Actualmente, la industria papelera se puede dividir en dos grandes sectores según su producción sea de pasta o papel. La pasta se elabora generalmente en grandes fábricas que normalmente se encuentran situadas en zonas próximas al lugar de recolección de la fibra. Muchas de estas fábricas también producen papel (por ejemplo: papel prensa, papel de escribir, papel para imprenta o papel de seda) o cartón. De hecho, tanto en Europa como a nivel mundial, se ha impuesto la tendencia de que las empresas productoras de pasta y de papel se organicen en forma de grandes compañías integradas de productos forestales. De esta manera pueden controlar todas las operaciones, desde la recolección forestal, las serrerías, la fabricación de pasta y de papel, hasta la transformación. Este tipo de estructura permite garantizar tanto la fuente de fibra como los compradores, y favorece una gestión más eficiente de los residuos, lo que supone un aumento de la cuota de mercado de las empresas (Techque, 2009).

La industria de la pasta y el papel es una de las mayores del mundo, cuyo peso está aumentando con gran rapidez en el continente asiático debido, sobre todo, a su gran expansión en China. Actualmente, el 22% de la producción global de pasta y el 45% de la de papel y cartón proceden de Asia. A nivel mundial, la producción de pasta en 2013 fue de 173 millones de toneladas y la de papel fue de 403 millones de toneladas. De esta producción mundial, la figura 1.1. representa el porcentaje correspondiente a cada región. Como se puede ver, Asia, Europa y América del Norte son los principales productores tanto de papel como de pasta. Por tanto, los principales productores son también los principales consumidores, tal y como se señaló en el apartado anterior.

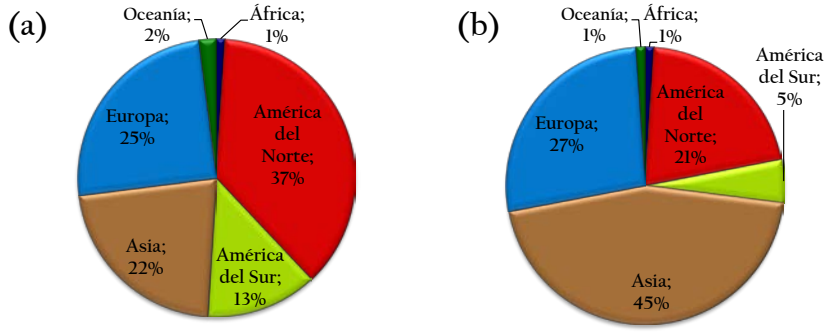

Producción total (2013) = 179 millones de toneladas. Producción total (2013) = 403 millones de toneladas.

Figura 1.1. Producción global de pasta (a) y papel (b) en 2013 (adaptado de Bajpai (2015a)).

En las diferentes regiones productoras, las grandes empresas del sector se han agrupado en asociaciones nacionales con el fin de representar a las empresas asociadas ante la Administración y grupos de interés, incentivar el desarrollo competitivo y sostenible y promocionar la imagen del sector, sus empresas y productos. Por ejemplo, en el Reino Unido está la CPI (*Confederation of Paper Industries*), en Portugal la CELPA (*Associação Portuguesa da Indústria do Papel*, que resultó de la fusión entre ACEL y FAPEL) y aquí en España la ASPAPEL (Asociación Española de Fabricantes de Pasta, Papel y Cartón). A nivel europeo, desde 1991, la asociación CEPI (*Confederation of European Paper Industries*) agrupa y representa a los productores de pasta y papel frente a las instituciones europeas, coordinando sus acciones y estrategias y apoyando sus objetivos. CEPI integra a los siguientes países europeos: Alemania, Austria, Bélgica, Eslovaquia, Eslovenia, España, Finlandia, Francia, Hungría, Italia, Noruega, Países Bajos, Polonia, Portugal, Reino Unido, República Checa, Rumanía, y Suecia. Y, de acuerdo con su último informe (CEPI - Confederation of European paper Industries, 2015), CEPI representa el 93% de la producción de la industria de la pasta y el papel en Europa, con una facturación de 75 millones de euros anuales y 180.000 puestos de trabajo directos y más 1,5 millones indirectos. En cuanto a la producción de pasta y de papel por parte de los países integrados en CEPI, la figura 1.2. muestra los datos correspondientes al año 2013.

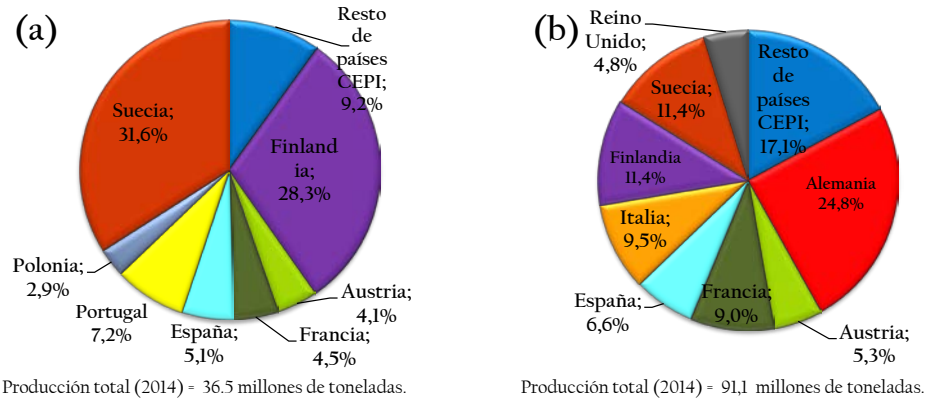

Figura 1.2. Producción total de pasta (a) y papel (b) por países pertenecientes a CEPI en el año 2013 (adaptado de CEPI-Confederation of European paper Industries (2015)).

En relación con el mercado de la pasta y del papel, la tabla 1.3. muestra los valores de importación y de exportación a otros países y/o regiones por parte de la CEPI. Según estos valores, la CEPI es importadora neta de pasta, principalmente de América del Sur. Por el contrario, hay una exportación neta de papel por parte de la CEPI, primordialmente a otros países europeos no pertenecientes a la CEPI.

Tabla 1.3. Importación y exportación de pasta y de papel (en miles de toneladas) por parte de la CEPI a otras regiones en el año 2014 (CEPI - Confederation of European paper Industries, 2015).

Región	Pasta		Papel	
	Importación	Exportación	Importación	Exportación
Otros países europeos	608 (7,8%)	791 (24,4%)	2417 (46,71%)	7188 (37,5%)
América del Norte	1578 (20,4%)	46 (1,4%)	1507 (29,1%)	1957 (10,2%)
América del Sur	5378 (69,4%)	65 (2,0%)	359 (6,9%)	1774 (9,3%)
Asia	97 (1,3%)	2200 (67,9%)	581 (11,2%)	5193 (27,1%)
Resto del mundo	83 (1,1%)	137 (4,2%)	313 (6,0%)	3053 (15,9%)
Total	*7745 (100%)*	*3239 (100%)*	*5177 (100%)*	*19164 (100%)*

1.3. La fabricación de papel

La fabricación de papel se cree que tuvo origen en China en torno al año 100 d.C. Como materia prima eran utilizados trapos, paja, hierba y cáñamo, que se golpeaban contra morteros de piedra con el fin de separar la fibra original. El uso del papel se extendió por Oriente y llegó a Europa con la conquista musulmana de la Península Ibérica. El sistema de producción por lotes basado en la utilización de fuentes agrícolas perduró hasta el siglo XIX, cuando, con la invención de la imprenta, fueron desarrollados los primeros métodos para obtener una fuente más abundante de fibra, la pasta de madera. Su obtención implicaba, además de abrasión mecánica, la aplicación de procesos químicos a base de sosa cáustica, sulfitos y sulfatos. Comenzó entonces la era moderna de la fabricación de pasta y de papel siendo que las primeras máquinas para la producción en continuo de papel fueron patentadas en la transición entre el siglo XIX y el XX (Techque, 2009).

La estructura básica de la pasta y el papel es un entramado de fibras de celulosa (polisacárido con 600 a 1.000 unidades de sacarosa) unidas mediante puentes de hidrógeno. Estas fibras tienen alta resistencia a la tracción, absorben los aditivos empleados para transformar la pasta en papel y cartón, y son flexibles, químicamente estables y blancas. Aunque la producción de papel reciclado es cada vez mayor, la principal fuente de fibra para la fabricación de pasta y de papel es la madera de coníferas y de especies arbóreas de hoja caduca. La figura 1.3. representa la secuencia de procesos para la fabricación de papel a partir de pasta termomecánica, de pasta química y de papel residual. A continuación se describen brevemente las etapas más relevantes (Techque, 2009).

Durante el proceso de elaboración de la pasta de papel, las fibras de celulosa se separan de los componentes no celulósicos (en el caso de la madera, principalmente, hemicelulosas, ligninas, extractos, minerales y otros compuestos inorgánicos). Al elaborarse la pasta, los enlaces dentro de la estructura de la madera se rompen mecánica o químicamente. En el último

caso, las pastas químicas se pueden producir en medio alcalino (por ejemplo, sulfato o kraft) o en medio ácido (por ejemplo, sulfito).

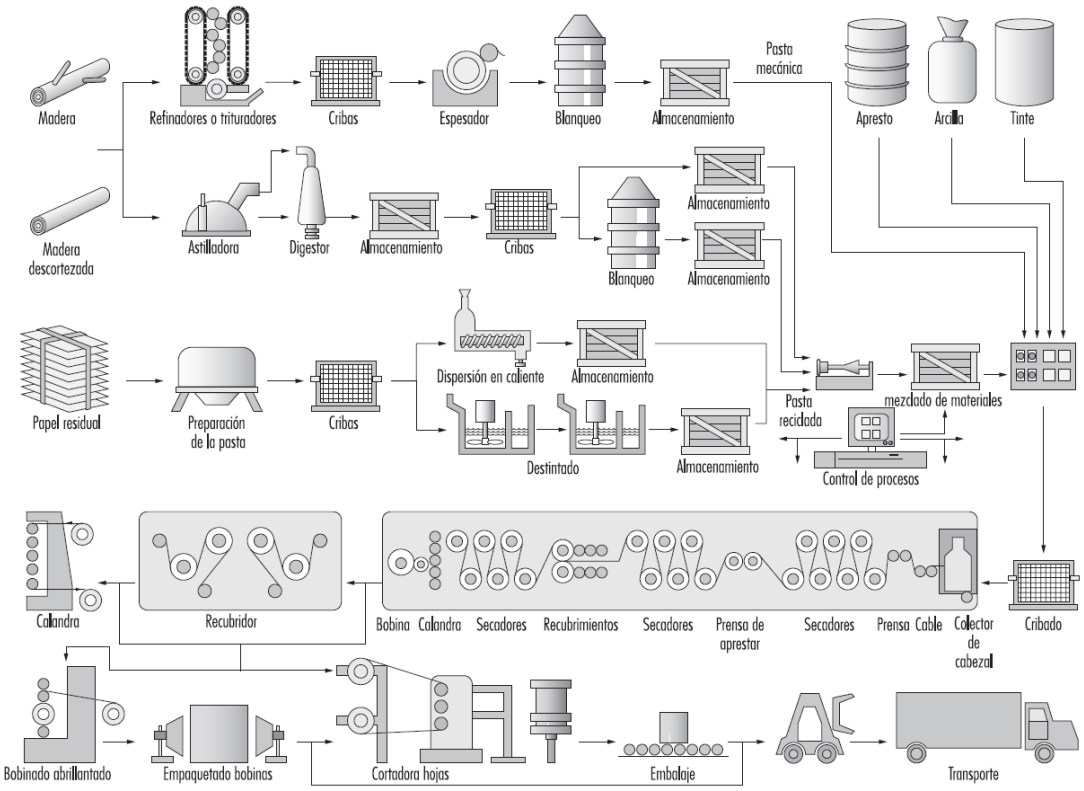

Figura 1.3. Esquema de la secuencia de procesos en la fabricación de pasta y de papel (adaptado de Weidenmüller (1984)).

Las pastas mecánicas se producen triturando la madera para conseguir que se separen las fibras. La lignina, que une celulosa y hemicelulosa, no se disuelve, sino que simplemente se ablanda, lo que permite que las fibras se asienten fuera de la estructura de la madera. La acción de las máquinas rompe estas fibras de celulosa, por lo que la pasta que se produce es más débil que la separada por métodos químicos. El rendimiento (proporción de la madera inicial en la pasta) suele ser superior al 85 %. La pasta química se produce disolviendo químicamente la lignina, con lo cual las fibras de madera se separan sin sufrir daños sustanciales. El procedimiento implica la cocción de las astillas junto con los reactivos en solución acuosa, lo que se realiza en un digestor que trabaja a temperatura y presión elevadas. Hoy en día, lo más frecuente es que estos digestores se recuperen y sean reconstituidos a partir del licor de cocción previamente empleado. En los procesos químicos se eliminan muchos de los componentes no fibrosos de la madera, por lo que los rendimientos son normalmente del 40 al 55 %.

Actualmente, la mayor parte de la pasta se obtiene por el procedimiento químico al sulfato (o kraft), que produce una pasta más fuerte y oscura, y requiere la recuperación química para ser competitivo. En el digestor, las astillas, junto con la mezcla de cocción (licor blanco),

compuesta por hidróxido sódico (NaOH) y sulfuro de sodio (Na_2S), se mantienen a temperaturas de unos 170 °C durante 3 ó 4 horas. La pasta que se obtiene (llamada "parda", por su color) se tamiza para separar los trozos de madera que hayan quedado sin digerir, se lava para separar la mezcla de cocción utilizada (ahora licor negro) y se envía o a la nave de blanqueado o a la de la máquina de producción de pasta. Los trozos de madera sin digerir se devuelven al digestor o a la caldera, donde se queman para producir energía. El licor negro recogido del digestor, cuya composición depende de la especie de madera y condiciones de cocción, se concentra por evaporación hasta tener un contenido en agua inferior al 40 %, y a seguir se pulveriza en la caldera de recuperación. La parte orgánica se consume como combustible, generando calor mientras que la parte inorgánica no quemada se recoge en el fondo de la caldera como una mezcla fundida. Este fundido se hace fluir fuera del horno y se disuelve en una solución cáustica débil, dando lugar a lo que se llama licor verde, el cual contiene primordialmente Na_2S disuelto y carbonato sódico (Na_2CO_3). Este licor se bombea a una planta de recaustificación, donde reacciona con cal apagada ($Ca(OH)_2$), formando NaOH y carbonato cálcico ($CaCO_3$). A seguir, se separa mediante filtración el $CaCO_3$ del licor blanco obtenido. Finalmente, el $CaCO_3$ se envía a un horno de cal, donde se calienta para regenerar cal viva (CaO) y el licor blanco se almacena para su uso posterior.

En el caso del procedimiento al sulfito, aunque fue el dominante en la industria papelera entre finales del siglo XIX y mediados del XX, su uso estaba limitado por los tipos de madera utilizables y por la contaminación relacionada con el licor residual. Por ello, hoy en día la pasta elaborada al sulfito representa un porcentaje muy pequeño del mercado de la pasta, porcentaje que es incluso inferior al de la pasta termomecánica.

Una vez producida la pasta, se realiza un proceso de blanqueo mediante el cual se refina y aclara la pasta en bruto siempre manteniendo la integridad de las fibras. El objetivo de este blanqueo, que consta de varias etapas, es disolver (pasta química) o modificar (pasta mecánica) la lignina parda que no se eliminó durante la elaboración de la pasta. Dependiendo del tipo de pasta, que cada fábrica produce por encargo, se ha de variar el orden de aplicación, la concentración y el tiempo de reacción de los agentes blanqueantes. Cada etapa del blanqueo se define por el agente químico blanqueante utilizado, el rango de pH, la temperatura y la duración. Por otro lado, tras cada una de las etapas, la pasta se debe lavar con agentes cáusticos para eliminar los agentes blanqueantes y disolver la lignina antes de pasar a la siguiente.

El uso de papel residual como materia prima para la obtención de pasta ha venido aumentado en las últimas décadas. El papel residual se puede transformar en pasta mediante un proceso relativamente suave, que utiliza agua y, a veces, NaOH. Los pequeños trozos de metal y de plástico se separan durante o después de la reconversión en pasta mediante métodos mecánicos. Por otro lado, las substancias de relleno (aditivos minerales usados para mejorar la

opacidad, resistencia y suavidad), colas y resinas se eliminan en la fase de lavado por corriente de aire a través de los lodos de la pasta. A seguir, la pulpa se destinta empleando una serie de lavados que pueden incluir o no el uso de reactivos químicos (por ejemplo, detergentes tensioactivos) para disolver las impurezas restantes. Finalmente, pueden también ser usados agentes blanqueantes que aclaran la pulpa, con la desventaja de que acortan las fibras. Después de estas operaciones, la producción de papel es muy similar a la que se sigue a partir de pasta de fibra virgen.

La pasta se puede destinar a la producción de diferentes productos de papel y cartón. Por ejemplo, la pasta mecánica, relativamente frágil, se transforma en productos de un único uso, como papel prensa y papel de seda. La pasta kraft se transforma en productos de papel de uso múltiple, como papel de escritorio de alta calidad, libros o bolsas para comestibles. Y la pasta a partir de papel residual, cuyas fibras suelen ser más cortas, menos flexibles y menos permeables, generalmente se utiliza para fabricar productos suaves y blandos, como papel higiénico, tisús o servilletas de papel. Sin embargo, algunas papeleras mezclan diferentes pastas para optimizar la calidad del papel (por ejemplo: una mezcla de madera dura, madera blanda, kraft, sulfito, pasta mecánica o reciclada). Dependiendo de la pasta utilizada, se seguirá una serie de pasos para obtener una hoja de papel.

Tras obtener la pasta palera, esta se mezcla con una serie de aditivos del "extremo húmedo" (talco, dióxido de Titanio, alumbre, resina, etc.) y se pasa a través de un conjunto final de cribas y lavaderos. En ese momento la pasta queda preparada para la máquina de papel. Mediante el esparcidor y el cabezal se distribuye una suspensión fina (1 a 3 %) de esa pasta en una rejilla móvil que forma con las fibras una lámina de fieltro. Esta lámina se desplaza a través de una serie de rodillos de prensado a la sección de secado, donde, mediante rodillos calientes se evapora gran parte del agua restante. En esta etapa se han desarrollado por completo los enlaces de hidrógeno entre las fibras. Finalmente, el papel se pasa por la calandra y se enrolla en bobinas. El calandrado permite alisar la superficie del papel y reducir su espesor, de manera que el papel seco alisado se puede enrollar en una bobina que a seguir es etiquetada y transportada al almacén. Hay que señalar que antes del calandrado se pueden añadir aditivos del "extremo seco", aunque estos pueden ser añadidos posteriormente, en el sector de transformación de la industria.

1.4. Generación y tratamiento de aguas residuales de la industria papelera

La industria de la pasta y del papel es un sector estratégico para la economía europea. A pesar de haber sufrido desde 2008 los efectos de la crisis, como la mayor parte de las industrias, continua siendo un actor importante en la recuperación, contribuyendo al crecimiento económico y a la creación de empleo. Como contrapartida, la industria papelera está

considerada una de las más contaminantes del mundo (Ince et al., 2011). Por otro lado, los procesos de producción de pasta y de papel implican, además de grandes necesidades energéticas, el consumo de un enorme volumen de agua (Pokhrel and Viraraghavan, 2004). De hecho, la localización de las industrias papeleras viene marcada por la disponibilidad de agua dulce que, en términos generales, proviene en un 75% de aguas superficiales (ríos, embalses, lagos, etc.) y en un 25% de las aguas subterráneas (Corrochano, 2006). En cualquier caso, las necesidades de agua de este tipo de industria pueden variar dependiendo del modo de producción y de los procesos empleados, si bien pueden llegar a ser en torno a los 60 m^3 por tonelada de papel producida (Thompson et al., 2001). Como consecuencia de tan elevado consumo, la industria papelera es generadora de grandes volúmenes de aguas residuales. En la figura 1.4. se representan las entradas, usos y salidas de agua en una industria papelera.

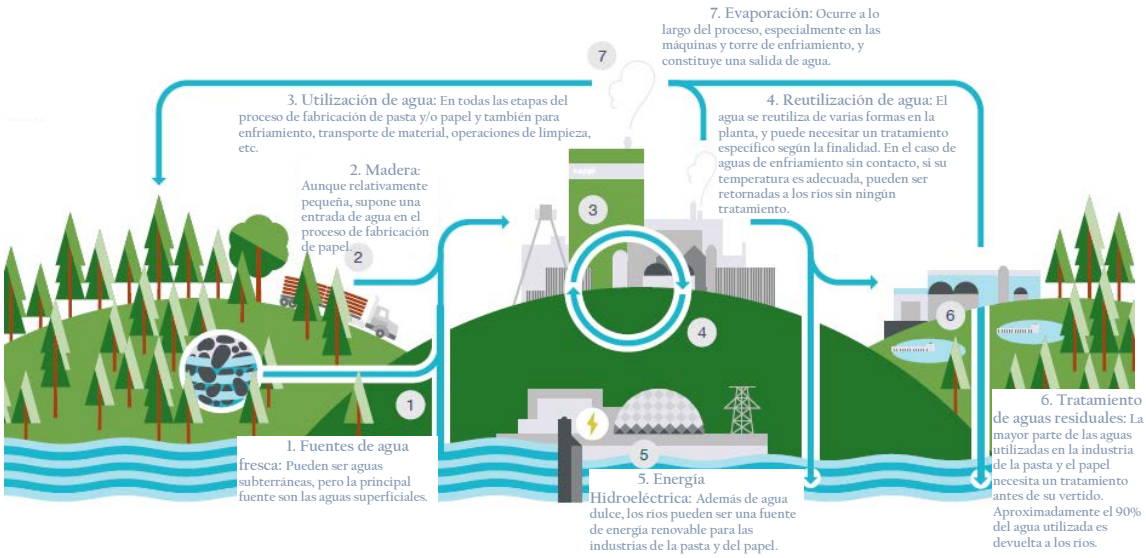

Figura 1.4. Esquema de las entradas, usos y salidas del agua en una industria papelera (adaptado de Sappi (2012)).

Existen grandes diferencias de calidad entre las aguas residuales que se generan a partir de la producción de pasta y aquellas resultantes de la fabricación de papel (Thompson et al., 2001). Esto se debe a que los procesos y agentes químicos utilizados son muy diferentes. La principal diferencia es que las aguas residuales de la producción de pasta contienen substancias derivadas de la madera, que se extraen de la misma durante las diferentes secuencias de producción y blanqueo de la pasta. Otra diferencia es el color del efluente final, que, en el caso de la producción de pasta, especialmente de pasta química, es muy acentuado debido a la lignina que lleva disuelta. Los efluentes de la fabricación de papel también pueden tener coloración, sobre todo en el caso de fábricas que usan tintes para producir papel de colores.

Para cada una de las etapas principales durante la fabricación de pasta y de papel, la tabla 1.4. muestra la contaminación típica del agua residual resultante.

La cantidad de contaminación producida individualmente por una fábrica de pasta y/o papel es un indicador clave para evaluar su desempeño. De cualquier manera, y a modo orientativo, en la tabla 1.5. se muestran algunos valores de generación y carga contaminante del agua residual resultante de diferentes procesos.

Tabla 1.4. Contaminación del agua residual resultante en cada una de las principales etapas del proceso de fabricación de pasta y de papel.

Etapa	Contaminación
Preparación de la madera	Se limpia la suciedad y restos de suelo de los troncos de madera. Se retira la corteza de la madera, que se lava con agua. El agua residual de esta etapa se caracteriza por su alto contenido en SS*, DBO*, arena, fibras etc.
Digestor	El agua residual de esta etapa se conoce como "licor negro" y contiene los agentes químicos utilizados en el digestor además de lignina y otros extractos de la madera. Por tanto, el agua residual de esta etapa se caracteriza por tener un alto contenido de resinas, ácidos grasos, color, DBO*, DQO*, AOX*, COVs*
Lavado de la pasta	El agua residual del lavado de la pasta posee elevados valores de pH, DBO, DQO, SS y un intenso color marrón oscuro
Blanqueado de la pasta	El agua residual de esta etapa contiene lignina y también hidratos de carbono en disolución. Además se caracteriza por poseer coloración, y elevados valores de DQO*, AOX*, COVs*, compuestos inorgánicos de cloro y compuestos organoclorados
Producción de papel	A partir de la producción de papel se genera agua residual con una DQO* elevada y que contiene material particulado, compuestos orgánicos y tintas.

*Abreviaturas: SS = Sólidos en Suspensión; DBO = Demanda Biológica de Oxígeno; DQO = Demanda Química de Oxígeno; AOX = (del inglés *adsorbable organic halogens*) Halógenos Orgánicos Adsorbibles; COVs = Compuestos Orgánicos Volátiles

Tabla 1.5. Valores típicos de volumen y carga contaminante de las aguas residuales generadas en la industria papelera (adaptado de Pokhrel and Viraraghavan (2004)).

Proceso	Efluente (m^3/t_{seca} de pasta o papel)	SS (kg/t_{seca} de pasta o papel)	DQO (kg/t_{seca} de pasta o papel)
Descortezado en húmedo	5-25	ND	5-20
Obtención mecánica de pasta	10-15	ND	15-32
Obtención termo-mecánica de pasta (sin blanquear)	10-30	10-40	40-60
Obtención termo-mecánica de pasta (blanqueada)	10-30	10-40	50-120
Obtención química-mecánica de pasta (sin blanquear)	10-15	20-50	70-120
Obtención químico-mecánica de pasta (blanqueada)	10-15	20-50	100-180
Pasta química al sulfito (sin blanquear)	80-100	20-50	ND
Pasta química al sulfito (blanqueada)	150-180	20-60	120-180
Pasta Kraft (sin blanquear)	40-60	10-20	40-60
Pasta Kraft (blanqueada)	60-90	10-40	100-140
Fabricación de papel	10-50	-	-

Para poder verter sus aguas residuales a los cauces naturales, las industrias de la pasta y el papel han de respetar la legislación ambiental que se aplique en cada país. Como orientación, la tabla 1.6. muestra los límites que se aplican a la producción de pasta Kraft blanqueada en varios países.

Tabla 1.6. Límites de vertido para las aguas residuales resultantes de la producción de pasta Kraft blanqueada (adaptado de Pokhrel and Viraraghavan (2004)).

País	SS (kg/t_{seca} de pasta)	DBO (kg/t_{seca} de pasta)	DQO (kg/t_{seca} de pasta)	AOX (kg/t_{seca} de pasta)
Canadá	9,5-14.5	5,5-30	-	1.4-1.5
Finlandia	5-15	6,8-34	90	1.4
Noruega	5	-	90	6
Suecia	0,3-5,8	7,5-17	39-107	1,5-2
Bélgica	7-14,4	2,3-5,4	22-63	1,5
Francia	6,5-10	3,3-30	48-95	-

En España, el 22 de Noviembre de 2005, ASPAPEL firmó un acuerdo voluntario con el Ministerio de Ambiente sobre el vertido de aguas residuales de la industria de pasta, papel y cartón (Corrochano, 2006). En la tabla 1.7 aparecen reflejados los valores de las cargas específicas máximas permitidas.

Como se puede ver, la casuística, en términos de exigencias y límites establecidos sobre la carga contaminante de los efluentes de la industria papelera es muy dispar, y depende del país, del tipo de industria y de los procesos que en ella se lleven a cabo. En cualquier caso, para minimizar la contaminación y el impacto ambiental de la industria papelera existen dos vías (Ince et al., 2011): (i) la aplicación de las mejores tecnologías disponibles (BAT, del inglés *best available technologies*) (Suhr et al., 2015) para disminuir el consumo de agua, el volumen de aguas residuales y su carga (Pokhrel and Viraraghavan, 2004); (ii) tratamientos fin de línea para reducir la contaminación antes del vertido o descarga. Esto es lo que ha permitido una significativa disminución de los impactos de la producción de pasta y papel por parte de las industrias papeleras de los países europeos CEPI, como se refleja en la figura 1.5. En ella se puede observar que, entre 1990 y 2013, la producción de pasta y papel por parte de los países CEPI ha venido aumentando, aunque a partir de 2007 son claros los efectos de la crisis económica. Por el contrario, el consumo de agua y la carga de DBO, DQO y AOX en los efluentes de las industrias han disminuido. Esta disminución fue muy acentuada entre 1990 y 1997 para el caso de los AOX. En relación con el consumo de agua y la carga de DBO y DQO en los efluentes, la reducción ha sido más progresiva y entre 1990 y 2005. Por tanto, aún hay mucho por hacer en este sentido, pues en los países desarrollados cada vez es mayor la preocupación social por la conservación del medio ambiente (Mahiout et al., 2016).

Tabla 1.7. Límites vigentes en España en cuanto a la emisión de vertidos líquidos de la industria papelera. Cargas específicas máximas permitidas expresadas en carga media mensual (adaptado de Corrochano (2006)).

Categoría de pasta y/o papel	Caudal de referencia (m^3/t_{seca} de pasta)	SS (kg/t_{seca} de pasta)	DQO (kg/t_{seca} de pasta)	AOX (kg/t_{seca} de pasta)
Pasta Kraft blanqueada (a partir de madera)	55	3	23	0,3
Pasta Kraft blanqueada (a partir de plantas anuales)	75	4	37	0,3
Pasta Kraft cruda	25	3	10	
Pasta destintada	15	0,9	4	
Papel de embalaje (a partir de papel residual)	10	1,6	4	
Papel Kraft liner o sacos	10	2	5	
Papel higiénico y sanitario	15	2	3,5	
Papel prensa	12	2	3,5	
Cartón	10	2	4,5	
Papel impresión o escritura	25	2	4,5	
Papel estucado	25	2	5	
Cartón estucado	10	2	5	
Papel decorativo y especiales	*	2	5	

NOTAS: (i) Las cifras de caudal son orientativas y no limitantes. (ii) Se tolerarán valores hasta un 50% más en carga diaria. (iii) En todo caso deben respetarse los objetivos medioambientales del cauce receptor. (iv) Las cargas específicas máximas permitidas en fábricas en las que se produzca pasta y papel, será el sumatorio de las correspondientes a cada uno de los procesos, independientemente de si la pasta se consume internamente en la fábrica para la fabricación de papel.
(*) La fabricación de papeles decorativos y especiales, por las singularidades de su propio proceso de producción, tienen requerimiento de caudal muy variable, no siendo posible establecer caudales orientativos con carácter general.

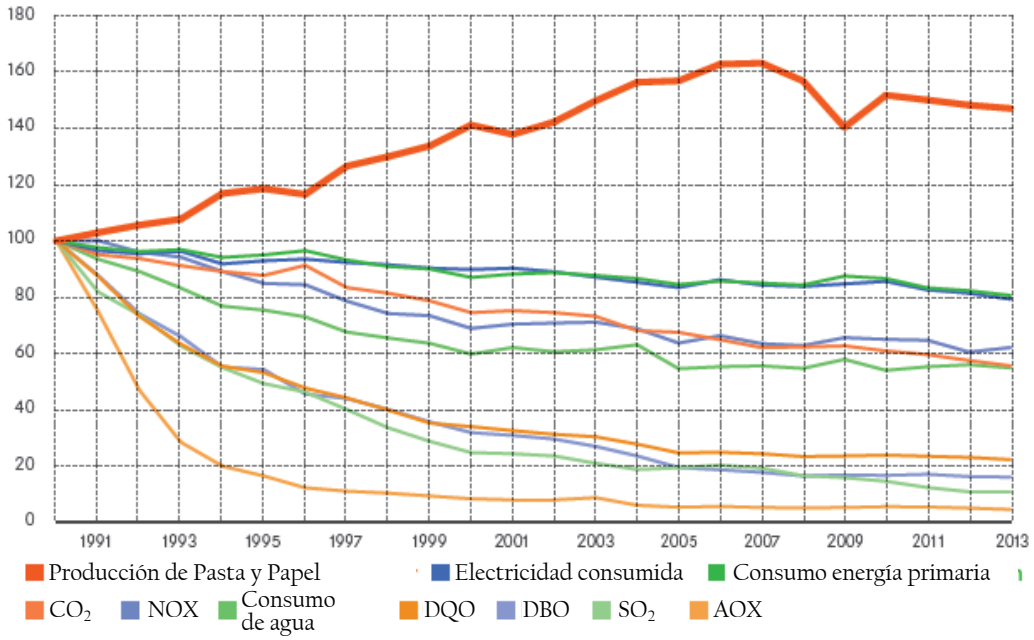

Figura 1.5. Evolución de los aspectos relacionados con el impacto del conjunto de las industrias de pasta y papel CEPI tomando como referencia (100%) el año 1990 (adaptado de CEPI - Confederation of European paper Industries (2015)).

Además de la aplicación de las BAT, el tratamiento de las aguas residuales en las industrias papeleras es esencial para que estas puedan cumplir con los límites de vertido exigidos (Pokhrel and Viraraghavan, 2004) y minimizar su impacto sobre los ecosistemas acuáticos.

Aparte de los tipos de contaminantes presentes en las aguas residuales de la industria papelera, que se mostraron en la tabla 1.4., en general, los efluentes de este tipo de industria se caracterizan por poseer: (i) grandes variaciones de carga y de concentración de los distintos contaminantes; (ii) una temperatura bastante alta y un pH lejos de ser neutro; (iii) baja relación entre el contenido de nutrientes y el de materia orgánica. Por ello, para el tratamiento de aguas residuales de este tipo de industria, se deben tener en consideración la necesidad de: (i) estabilizar la carga; (ii) controlar y ajustar el pH y la temperatura; (iii) añadir nutrientes. Por supuesto, la importancia de estos aspectos depende del tipo de tratamiento que se vaya a llevar a cabo. Siendo especialmente relevantes en el caso de que se vaya a aplicar algún tipo de tratamiento biológico, que es lo más común. En ese caso, la previa eliminación de los sólidos en suspensión es también un requisito indispensable.

El tratamiento de efluentes de la industria de la pasta y del papel incluye, típicamente, las siguientes etapas de tratamiento (Sappi, 2012):

- Tratamiento primario: Puede incluir un tratamiento de neutralización, cribado, sedimentación y flotación/hidrociclón para retirar los sólidos en suspensión. La mayoría de las plantas constan de un clarificador primario que puede retirar hasta un 95% de los sólidos decantables del efluente a tratar. En esta etapa también se consigue un enfriamiento de las aguas residuales.
- Tratamiento secundario o biológico: En esta etapa se reduce significativamente la carga orgánica y la toxicidad del efluente gracias a la biodegradación activa por parte de los microorganismos (bacterias, protozoos, etc.) que habitan en el reactor y usan el efluente como fuente de carbono (C). El tratamiento secundario más comúnmente utilizado para el tratamiento de aguas residuales en la industria de la pasta y del papel es mediante fangos activos o lagunas de estabilización aerobias. En estos sistemas, las condiciones de aerobiosis necesarias se mantienen mediante aireadores sumergidos o superficiales. Por otro lado, es clave la adición de nutrientes (N y P) para mantener una relación adecuada de C/N y C/P que permita sustentar una comunidad equilibrada y saludable de microorganismos. Mediante fangos activados y lagunas de estabilización aerobias, típicamente se consigue reducir la demanda biológica de oxígeno (DBO) más de un 80% y la demanda química de oxígeno (DQO) entre un 50 y un 90%.
- Tratamiento terciario: Su aplicación no es generalizada en las plantas de tratamiento de aguas residuales de la industria de la pasta y del papel (Thompson et al., 2001). Cuando

se lleva a cabo, consiste normalmente en una precipitación química para eliminar ciertos agentes químicos, reducir la toxicidad, los sólidos en suspensión y el color.

En la figura 1.6. se representa la secuencia típica en el tratamiento de aguas residuales de una industria papelera mediante fangos activos.

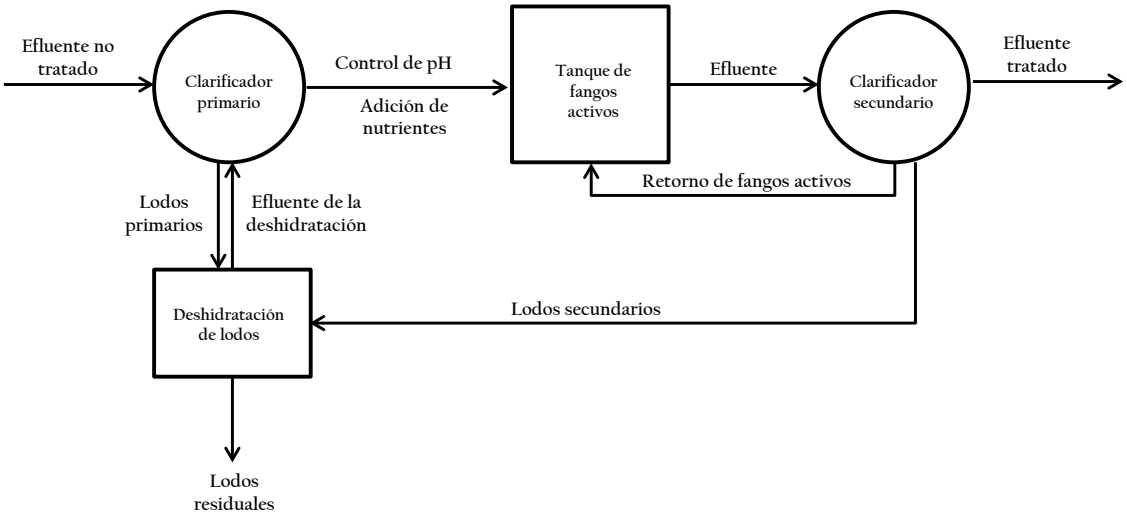

Figura 1.6. Esquema de una planta de tratamiento de aguas residuales de la industria papelera mediante fangos activos (adaptado de Sappi (2012)).

Además de las etapas que se muestran en el esquema anterior, es común que las plantas de tratamiento de aguas residuales de la industria de la pasta y del papel cuenten con tratamientos adicionales, como presas y cribas antes del clarificador primario, y después del mismo, adición de agentes antiespumantes y balsas de compensación (Mahiout et al., 2016), y, si es necesario, con tratamientos de regulación de la temperatura antes del vertido del efluente tratado (Sappi, 2012). En cualquier caso, como ya ha sido destacado, los tratamientos aplicados dependen en gran medida de la normativa local así como de los procesos de fabricación de pasta y/o papel en la planta.

1.5. Generación y gestión de lodos en la industria papelera

El elevado consumo de aguas por parte de industria papelera da lugar a la generación de grandes volúmenes de aguas residuales, que, después de su tratamiento generan grandes volúmenes de lodos, como residuo inevitable de dicho tratamiento (Pokhrel and Viraraghavan, 2004). De hecho, en general, los lodos procedentes del tratamiento de aguas residuales constituyen, en términos de volumen, la mayor corriente de residuos generados por las industrias de la pasta y del papel (Monte et al., 2009). En global, en una fábrica de pasta y papel, se generan aproximadamente 50 kg de lodos secos por cada tonelada de papel producida, siendo

que, aproximadamente el 70% son lodos primarios y el 30% lodos secundarios (Elliott and Mahmood, 2005).

Los lodos primarios se generan en el clarificador primario y están compuestos principalmente por fibras (principalmente celulosa), finos y substancias de relleno procedentes de una separación incompleta en las diferentes etapas de producción de la pasta y el papel. Estas pérdidas de material, pueden llegar a representar entre un 3-4% de la materia prima en la fabricación de pasta y 15-30% en la fabricación de papel (Trutschler, 1999). Por acción de la gravedad, decantan en el clarificador primario y en conjunto constituyen los lodos primarios, cuya tasa de generación depende de la eficiencia de los sistemas de recuperación de fibra durante la producción de pasta y papel. Por tanto, movidas sobre todo por motivos económicos, muchas industrias han optado por la aplicación de BAT para optimizar sus sistemas de recuperación y reducir costes, reduciendo así también la generación de lodos primarios y los gastos derivados de su gestión (Trutschler, 1999).

Los lodos secundarios proceden del clarificador secundario y se generan en menor volumen es inferior que los lodos primarios porque la mayor parte (aproximadamente el 80%) de los sólidos pesados, fibrosos y/o inorgánicos fueron retirados del agua en el clarificador primario (Monte et al., 2009). El agua que abandona el clarificador primario pasa al tanque de tratamiento biológico (secundario), donde los microorganismos utilizan la materia orgánica disuelta en el agua como fuente de carbono, dando como resultado, además de dióxido de carbono, una biomasa residual, cuyo exceso se decanta en el clarificador secundario como lodos secundarios, o, también llamados lodos biológicos (Bajpai, 2015b).

Básicamente, los lodos primarios contienen tanto materia orgánica como materia inorgánica, mientras que los lodos secundarios están constituidos fundamentalmente por materia orgánica. Por otro lado, los lodos secundarios son normalmente más difíciles de manejar que los primarios debido a su alto contenido de proteína de origen microbiano. Además, los lodos primarios, debido a su alto contenido en fibras, son más fácilmente deshidratables que los secundarios. En cualquier caso, en la mayoría de las industrias de pasta y papel, es habitual mezclar los lodos primarios con los secundarios para su posterior deshidratación, tratamiento y/o gestión. Sin embargo, dependiendo del destino final de los lodos, la gestión de lodos primarios y secundarios por separado podría ser ventajosa (Bajpai, 2015b).

La mezcla de lodos primarios y secundarios normalmente se refiere como lodos de papelera. Debido a su contenido en fibras son fácilmente deshidratables y, después de una deshidratación mecánica contienen un porcentaje de humedad entre el 40-80%, que es relativamente bajo si se compara con los lodos de la depuración de aguas residuales urbanas (Monte et al., 2009). Aun así, debido a los grandes volúmenes generados, la gestión de los lodos de papelera representa uno de los costes más elevados para la industria papelera (Stoica et al., 2009).

El depósito en vertederos de los lodos de papelera, a pesar de haber sido su destino final de durante mucho tiempo, hoy en día es una opción a descartar en los países desarrollados. Esto se debe bien a su prohibición expresa o bien a las altas tasas económicas asociadas, además de la falta de aceptación pública (Faubert et al., 2016). Desde el punto de vista ambiental, el depósito en vertederos de los lodos de papelera implica importantes problemas de lixiviación así como emisiones de gases de efecto invernadero (ha sido estimado que 1 ton de lodos de papelera en vertedero supone la emisión de unas 2,69 ton de CO_2 y 0,24 ton de CH_4 (Likon and Trebše, 2012)). Por otro lado, desde el punto de vista práctico, el depósito en vertederos es problemático para las industrias papeleras debido a los grandes volúmenes de lodos que este tipo de industria genera actualmente (Faubert et al., 2016). Por todo lo anterior, es necesario explorar otras opciones de gestión teniendo en consideración, en cada caso concreto, las características físico-químicas y microbiológicas de los lodos. En cualquier caso, por razones de sostenibilidad, siempre que sea posible, se debería dar prioridad a las opciones de recuperación, entre las que destacan las siguientes (Monte et al., 2009):

- Utilización en la fabricación de materiales de construcción: El contenido de material y energía de los lodos de papelera podría ser recuperado en la industria del cemento, de ladrillos y de otros materiales de construcción (Cusidó et al., 2015; Frías et al., 2015; Faubert et al., 2016). Para este tipo de aplicación, son especialmente adecuados los lodos primarios o lodos primarios mezclados con secundarios (Monte et al., 2009).
- Compostaje: Los composts producidos a partir de residuos orgánicos mezclados con residuos de papel y lodos de la industria papelera cumplen, en general, con los requisitos de grado de estabilidad y adecuación para favorecer el crecimiento de las plantas (Aycan and Turan, 2014). Sin embargo, debe prestarse atención a los límites de concentración de substancias peligrosas, especialmente de metales pesados (Monte et al., 2009).
- Aplicación al suelo: Los lodos de papelera tienen un alto contenido orgánico y pueden suponer una fuente de nutrientes para los cultivos. No obstante, su aplicación a suelos agrícolas puede acarrear graves peligros de salud pública y ambiental. Debido a ello, la presencia de sustancias peligrosas debe ser analizada con sumo rigor antes de plantear esta alternativa. Por otro lado, las restricciones de tipo legal en cada país deben ser respetadas. Aunque ha sido comprobado que los lodos de papelera pueden ser utilizados como enmienda orgánica y fertilizante (Abdullah et al., 2015), lo cierto es que, desde un punto de vista legal y social, su aplicación como cobertura en vertederos o en suelos degradados es más factible que su aplicación en suelos agrícolas (Monte et al., 2009).

- Digestión anaerobia: Se puede aplicar a residuos con un alto contenido orgánico, de manera que, en ausencia de oxígeno, este pueda ser convertido en biogás (metano y dióxido de carbono) y humus (que puede ser utilizado como enmienda para suelos). En el caso de residuos industriales, como los lodos de papelera, pueden servir como aditivo en la digestión anaerobia de residuos agrícolas y ganaderos, de manera que el biogás pueda ser utilizado en la propia industria papelera (Monte et al., 2009). La mono-digestión de lodos de papelera supone muy lentas tasas de hidrólisis, por lo que son necesarios tiempos de retención muy largos, grandes reactores, y, en último caso, grandes costes de inversión (Elliott and Mahmood, 2007). Para favorecer la digestión anaerobia de los lodos de papelera, se ha demostrado la efectividad de diferentes pretratamientos (Bayr et al., 2013), aunque los costes asociados deben ser evaluados para su implementación a escala real. En el caso de lodos de papelera mixtos (mezcla de primarios y secundarios) o lodos secundarios de difícil deshidratación, se podría considerar la digestión anaerobia después de un pre-tratamiento, mientras que en el caso de lodos primarios, que son fácilmente deshidratables, parece más factible la recuperación de energía mediante combustión (Meyer and Edwards, 2014).
- Procesamiento térmico: Existen diversas opciones de procesamiento térmico para los lodos de papelera, como son la combustión, la pirólisis y la gasificación, además de otros como la oxidación húmeda o la oxidación con agua supercrítica (Monte et al., 2009). En la práctica, entre estas alternativas, la combustión, que está regulada por la Directiva Europea 2000/76/EC (*Waste Incineration Directive*), es la más extendida. El modo más común de llevar a cabo la combustión de lodos de papelera es en lecho fluidizado, que se está convirtiendo en una solución consolidada para la gestión de este tipo de residuos, con alto contenido en cenizas y humedad, pues proporciona vapor y/o energía que pueden ser utilizados en la propia industria papelera, disminuyendo su dependencia de combustibles fósiles (Monte et al., 2009). Las propiedades de los lodos de papelera pueden dificultar su combustión (Ochoa de Alda, 2008), pero recientemente ha sido probado que la aplicación de pretratamientos puede mejorar significativamente la operación de lechos fluidizados para la combustión de este tipo de materiales (Areeprasert et al., 2016).

  La pirólisis, o, también llamada destilación destructiva, ha sido utilizada para el aprovechamiento de residuos con alto contenido en carbono y supone el calentamiento del residuo en ausencia de oxígeno, dando lugar a una mezcla de combustibles gaseosos y líquidos y a un residuo sólido inerte (carbonizado) (Monte et al., 2009). En el caso de los lodos de papelera, aunque aún no ha alcanzado la madurez suficiente, numerosos

estudios a nivel europeo apuntan a la pirólisis como una opción factible para la gestión y valorización de este tipo de materiales (Monte et al., 2009). Además, según las características de los lodos de papelera, se pueden aplicar distintas formas de pirólisis (al vacío, lenta, rápida) para rentabilizar el proceso (Ridout et al., 2016).

La gasificación es una combustión incompleta de materiales carbonosos que se realiza a alta temperatura y bajo atmósfera más o menos oxidante para producir una mezcla de gases combustibles (monóxido de carbono, hidrógeno, y metano) y un residuo inerte. A pesar de que no se trata de una tecnología reciente, su aplicación para la gestión de lodos de papelera está aún en una fase muy inicial de desarrollo (Monte et al., 2009).

En un estado aún más incipiente se encuentran la oxidación húmeda y la oxidación con agua supercrítica (Monte et al., 2009). En el caso de la oxidación húmeda, ha sido demostrado que también puede ser aplicada como pretratamiento para aumentar la eficiencia de la digestión anaerobia de los lodos de papelera (Baroutian et al., 2013). Por otro lado, la oxidación con agua supercrítica es una tecnología altamente innovadora mediante la cual se utiliza agua en estado supercrítico (temperatura y presión superiores a sus valores críticos, 374ºC y 221 bar, respectivamente) para disolver el oxígeno y los compuestos orgánicos no polares, permitiendo la oxidación del residuo orgánico hasta convertirlo en dióxido de carbono y agua (Monte et al., 2009). Puede ser una opción de futuro, pues ha sido comprobado que permite eliminar casi en su totalidad los compuestos orgánicos presentes en los lodos de papelera y obtener un producto líquido prácticamente transparente (Qian et al., 2014).

Es muy difícil estimar los costes de las diferentes formas de procesamiento térmico, pues dependerán de la composición del residuo, de su concentración, nivel de destrucción necesario, los volúmenes de lodos a tratar, etc. Debido a las diferencias significativas que puede haber en cuanto a estas variables, cualquier comparación de costes sólo será relevante en casos específicamente definidos o en términos relativos. En cualquier caso, las principales cuestiones con relación al procesamiento térmico se refieren a la energía consumida para alcanzar las temperaturas requeridas y a la necesidad de equipos de control de emisiones gaseosas y, por tanto, los altos costes de inversión asociados.

1.6. Referencias

Abdullah, R., Ishak, C.F., Kadir, W.R., Bakar, R.A., 2015. Characterization and feasibility assessment of recycled paper mill sludges for land application in relation to the environment. Int. J. Environ. Res. Public Health 12, 9314–9329.

Areeprasert, C., Scala, F., Coppola, A., Urciuolo, M., Chirone, R., Chanyavanich, P., Yoshikawa, K., 2016. Fluidized bed co-combustion of hydrothermally treated paper sludge with two coals of different rank. Fuel Process. Technol. 144, 230–238.

Aycan, N., Turan, N.G., 2014. Effects of Different Agro-Based Materials on Composting of Pulp/Paper-Mill Sludge. Arch. Environ. Prot. 40, 33–40.

Bajpai, P., 2015a. Pulp and Paper Industry: Chemicals. Elsevier Science.

Bajpai, P., 2015b. Generation of wastewater treatment sludge, in: Management of Pulp and Paper Mill Wastes. Springer, pp. 12–15.

Baroutian, S., Robinson, M., Smit, A.M., Wijeyekoon, S., Gapes, D., 2013. Transformation and removal of wood extractives from pulp mill sludge using wet oxidation and thermal hydrolysis. Bioresour. Technol. 146, 294–300.

Bayr, S., Kaparaju, P., Rintala, J., 2013. Screening pretreatment methods to enhance thermophilic anaerobic digestion of pulp and paper mill wastewater treatment secondary sludge. Chem. Eng. J. 223, 479–486.

CEPI - Confederation of European paper Industries, 2015. CEPI Key Statistics 2014. , European Pulp and Paper Industries (Published on the 6th of July, 2015). http://www.cepi.org/system/files/public/documents/publications/statistics/2015/Key%20Statistics%202014%20FINAL.pdf (último acceso: 25 de Junio de 2016)

Corrochano, A., 2006. La industria papelera "se moja." Ambienta, marzo 2006, 25–30. http://www.magrama.gob.es/ministerio/pags/Biblioteca/Revistas/pdf_AM%2FAM_2006_53_25_30.pdf (último acceso: 10 de Septiembre de 2016)

Cusidó, J.A., Cremades, L. V., Soriano, C., Devant, M., 2015. Incorporation of paper sludge in clay brick formulation: Ten years of industrial experience. Appl. Clay Sci. 108, 191–198.

Elliott, A., Mahmood, T., 2007. Pretreatment technologies for advancing anaerobic digestion of pulp and paper biotreatment residues. Water Res. 41, 4273–4286.

Elliott, A., Mahmood, T., 2005. Survey benchmarks generation, management of solid residues. Pulp Pap. 79, 49–55.

Faubert, P., Barnabé, S., Bouchard, S., Côté, R., Villeneuve, C., 2016. Pulp and paper mill sludge management practices: What are the challenges to assess the impacts on greenhouse gas emissions? Resour. Conserv. Recycl. 108, 107–133.

Frías, M., Rodríguez, O., Sánchez De Rojas, M.I., 2015. Paper sludge, an environmentally sound alternative source of MK-based cementitious materials. A review. Constr. Build. Mater. 74, 37–48.

Ince, B.K., Cetecioglu, Z., Ince, O., 2011. Pollution Prevention in the Pulp and Paper Industries, in: Broniewicz, E. (Ed.), Environmental Management in Practice. InTech, pp. 223–246.

Likon, M., Trebše, P., 2012. Recent Advances in Paper Mill Sludge Management. Ind. Waste 73–

90.

Mahiout, A., Damann, R., Pera, J., Luonsi, A., Kolari, M., Siivinen, J., Santos, J.F., Lapa, N., Pourcelly, G., Aslan, F., 2016. Industrial liquid effluents in the pulp and paper industry, in: Cox, Michael; Negré, Pascal; Yurramendi, L. (Ed.), A Guide Book on the Treatment of Effluents from the Mining/Metallurgy, Paper, Plating and Textile Industries. INASMET-Tecnalia, Donostia, Spain, pp. 33–73.

Meyer, T., Edwards, E.A., 2014. Anaerobic digestion of pulp and paper mill wastewater and sludge. Water Res. 65, 321–349.

Monte, M.C., Fuente, E., Blanco, A., Negro, C., 2009. Waste management from pulp and paper production in the European Union. Waste Manag. 29, 293–308.

Ochoa de Alda, J.A.G., 2008. Feasibility of recycling pulp and paper mill sludge in the paper and board industries. Resour. Conserv. Recycl. 52, 965–972.

Pokhrel, D., Viraraghavan, T., 2004. Treatment of pulp and paper mill wastewater - A review. Sci. Total Environ. 333, 37–58.

Qian, L.L., Wang, Z.Z., Zhang, J., 2014. No TitleExperimental Study on Supercritical Water Oxidation of Paper Mill Sludge. Adv. Mater. Res. 955-959, 711–715.

Ridout, A.J., Carrier, M., Collard, F.-X., Görgens, J., 2016. Energy conversion assessment of vacuum, slow and fast pyrolysis processes for low and high ash paper waste sludge. Energy Convers. Manag. 111, 103–114.

Robins, N., 1996. What on Earth is sustainable paper consumption?, in: International Institute for Environment and Development, IIED (Ed.), Towards a Sustainable Paper Cycle. World Business Council for Sustainable Development. IIED, London, Great Britain, pp. 1-56.

Sappi, 2012. Water Use and Treatment in the Pulp and Paper Industry. eQ Insights 5, 1–7.

Stoica, A., Sandberg, M., Holby, O., 2009. Energy use and recovery strategies within wastewater treatment and sludge handling at pulp and paper mills. Bioresour. Technol. 100, 3497–3505.

Suhr, M., Klein, G., Kourti, I., Rodrigo Gonzalo, M., Giner Santonja, G., Roudier, S., Delgado Sancho, L., 2015. Best Available Techniques (BAT). Reference Document for the Production of Pulp, Paper and Board. European Commission. Joint Research Center., Luxembourg.

Swedish Forest Industry Federation, S.I., 2014. Per capita paper comsumption. http://www.forestindustries.se/documentation/statistics_ppt_files/international/per-capita-paper-consumption (último acceso: 15 de Julio de 2016).

Techque, 2009. Industria del papel y de la pasta de papel, Perfil General, Enciclopedia de salud y seguridad en el trabajo. Sectores basados en recursos biológicos. Tomo 3, capítulo 72, pp.72.2-72.5.

http://www.insht.es/InshtWeb/Contenidos/Documentacion/TextosOnline/EnciclopediaOIT/tomo3/72.pdf (último acceso: 10 de Septiembre de 2016)

Thompson, G., Swain, J., Kay, M., Forster, C.F., 2001. The treatment of pulp and paper mill effluent: A review. Bioresour. Technol. 77, 275–286.

Trutschler, J.D., 1999. Fibre recovery—reducing operating costs and sludge. Pap. Technol. 40, 97–100.

Weidenmüller, R., 1984. Papermaking: the art and craft of handmade paper. Thorfinn International, San Diego, United States of America.

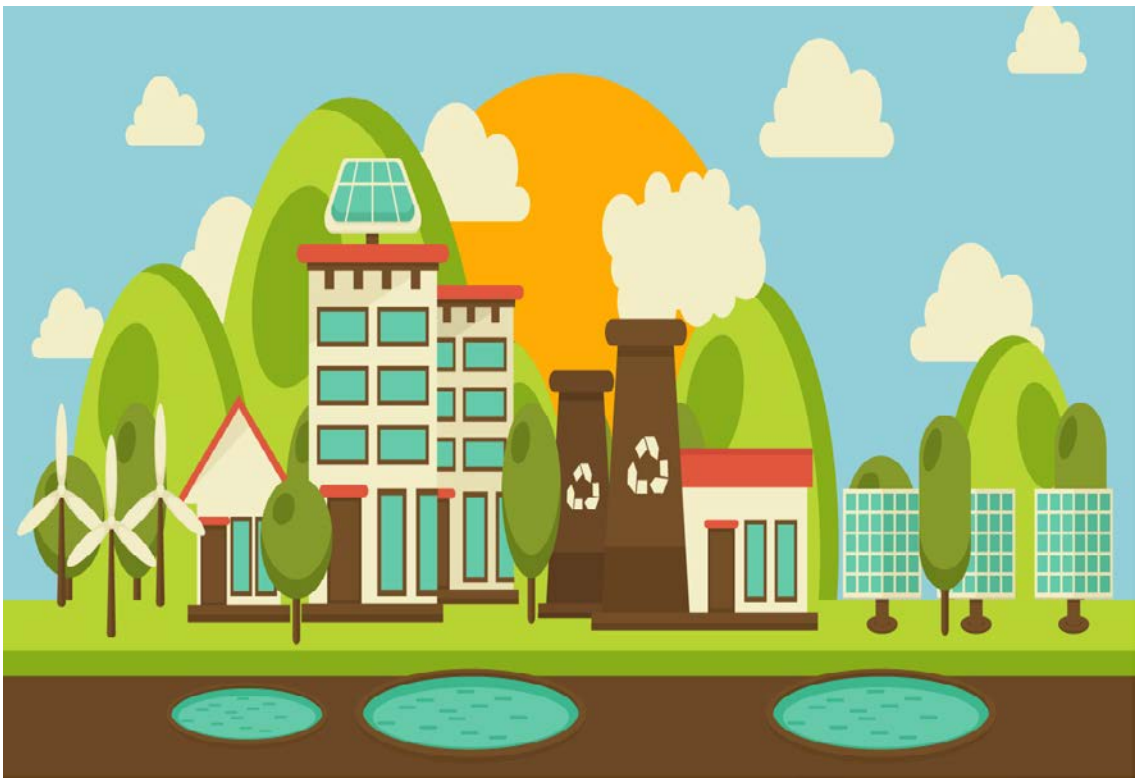

Capítulo 2

2. Antecedentes y objetivos

2.1. Procesamiento térmico de los lodos de papelera: Análisis termogravimétrico

El procesamiento térmico o conversión termoquímica de los lodos de la industria papelera, además de constituir una ruta de gestión para los lodos de la industria papelera, permite la recuperación de la energía contenida en este tipo de residuos (Ridout et al., 2016). Como ventaja añadida, una vez que la fracción orgánica de los lodos de papelera es renovable, no supone una contribución neta de emisiones de CO_2 (Gavrilescu, 2008). La recuperación energética a partir de lodos de la industria papelera incluye típicamente los siguientes pasos: (1) deshidratación y (2) secado para incrementar la capacidad calorífica efectiva, (3) conversión térmica (Faubert et al., 2016). Como ya fue señalado en el capítulo anterior, la pirólisis y,

especialmente, la combustión (o incineración) son actualmente las principales opciones de conversión térmica empleadas en la gestión de lodos de papelera (Monte et al., 2009).

2.1.1. Combustión de lodos de la industria papelera

En la industria de la pasta y el papel ha habido siempre una larga tradición en cuanto a la incineración de residuos (Bajpai, 2015). En los últimos tiempos, esta práctica se ha extendido como opción de gestión para los lodos, realizando su combustión en condiciones controladas para generar calor y luego producir electricidad que se utiliza en la propia planta o que se vende a la red nacional (Monte et al., 2009). Ejemplos de utilización de lodos de papelera como combustible los tenemos en las plantas de cogeneración operadas por Powergen en Aylesford Newsprint y en Kemsley site, Sittingbourne, Kent, ambas en Gran Bretaña (Kay, 2007). La incineración de residuos sólidos con alto contenido orgánico, como son los lodos de papelera, conlleva una gran reducción de volumen (Bajpai, 2015). Al llevar a cabo la combustión de los lodos, se genera vapor, que acciona turbinas que producen energía gracias a un generador eléctrico. Como alternativa, el vapor puede ser utilizado en la propia planta para diferentes procesos, disminuyendo así el gasto en combustibles fósiles para producir vapor (Monte et al., 2009). Los reactores de lecho fluidizado se han implantado como la tecnología más generalizada para la combustión de lodos de papelera pues permiten la combustión de residuos con alto contenido relativo en humedad y cenizas. En este proceso, se burbujea aire a través de un lecho de material inerte (normalmente arena o caliza), lo que mejora mucho el proceso de combustión de este tipo de materiales. Además, esta tecnología de combustión da lugar a menores emisiones de óxidos de azufre y nitrógeno que las calderas convencionales. Los lechos fluidizados operan generalmente a temperaturas entre 700 y 900ºC. Sin embargo, dependiendo de la zona o país, pueden existir normativas en cuanto a la temperatura de combustión. Por ejemplo, en Europa es obligatorio alcanzar una temperatura de 850ºC durante al menos 2 s, y si se trata de residuos peligrosos con más de 1% de contenido en substancias orgánicas halogenadas, se deben alcanzar los 1100ºC durante un mínimo de 2 s para así reducir la formación de compuestos tóxicos como las dioxinas (Monte et al., 2009).

Como subproducto de la combustión de los lodos de papelera están las cenizas, cuyo depósito en vertedero es más simple y barato que en el caso de los lodos. De hecho, como ya ha sido señalado, una de las ventajas de la combustión de lodos de papelera es que el volumen de vertedero necesario para las cenizas es alrededor del 25 % del que sería necesario para los lodos. Por otro lado, existen también opciones de recuperación para estos subproductos, como es el ejemplo de la aplicación de cenizas como enmienda para suelos (Faubert et al., 2016) o de su utilización en la producción de materiales de construcción (Monte et al., 2009). En cualquier caso, hay que tener en cuenta que en las cenizas se concentran los metales que estaban presentes en los lodos, generalmente en concentraciones relativamente bajas. De no ser así, y si

la concentración de metales alcanza valores peligrosos, es necesaria una gestión adecuada de las cenizas (Shin et al., 2005).

Además de las cenizas, la combustión de lodos de papelera genera emisiones que necesitan un tratamiento adecuado para evitar episodios de contaminación atmosférica. Comparados con los lodos de estaciones depuradoras de aguas residuales urbanas, los lodos de papelera tienen menores concentraciones de nitrógeno y fósforo. Por otro lado, comparados con la mayoría de combustibles fósiles, los lodos de papelera tienen contenidos de azufre, flúor, cloro, bromo e iodo relativamente bajos y por esa razón, normalmente no es necesario incorporar sistemas de purificación de alto coste si la combustión se realiza en infrastructuras ya existentes. Sin embargo, el contenido de compuestos orgánicos clorados en los lodos de la industria de la pasta y el papel puede causar problemas de emisiones durante la combustión, además de constituir un problema para su gestión mediante otras alternativas y su depósito en vertedero. Secar estos lodos hasta un 10 % de humedad de una manera eficiente desde el punto de vista energético, permitiría alcanzar temperaturas de combustión suficientemente elevadas como para destruir estos compuestos (Bajpai, 2015).

Entre las limitaciones asociadas a la incineración de lodos están las altas inversiones de capital, la necesidad de incorporar un combustible auxiliar (debido al alto contenido en humedad), las emisiones de dioxinas, NOx, metales, etc., además de los problemas de almacenamiento de los lodos y su relativamente baja eficiencia de combustión. Las propiedades de combustión de los lodos de papelera están generalmente relacionadas con su contenido en fibras. La energía disponible está normalmente inversamente relacionada con el contenido en cenizas, de manera que porcentajes de cenizas superiores al 50 % en base seca suelen correlacionarse con bajos poderes caloríficos. Pero además, para ser auto-sostenible, la combustión requiere deshidratar antes los lodos para incrementar el porcentaje de sólidos hasta un mínimo, que dependerá de la humedad y del contenido orgánico. Por ello, optimizar la combustión implica evaluaciones de coste-beneficio que indiquen el porcentaje ideal de humedad del lodo. Estas evaluaciones deben tener en cuenta que alcanzar porcentajes de sólidos por encima del 50 % puede requerir, además de filtros de prensa, un secado térmico, que puede realizarse utilizando gases de procesamiento en secadores de cinta transportadora (Bajpai, 2015). El secado mejora la eficiencia de la combustión, facilita el almacenamiento de lodos a largo plazo y reduce el crecimiento microbiano. Además, para facilitar la manipulación, almacenamiento y la combustión, los lodos pueden ser procesados en forma de briquetas o gránulos (David, 1995). Asimismo, la mezcla de lodos deshidratados con otros biocombustibles (astillas o serrín) puede mejorar las características para el transporte. En este sentido, la granulación (en inglés *pelletization*) ocupa un papel muy relevante en la práctica de utilizar

residuos sólidos como combustibles, contribuyendo así a resolver la crisis asociada al uso de vertederos (Bajpai, 2015).

Por último, aunque los reactores de lecho fijo son los más utilizados para la combustión de lodos, existen otras alternativas como son calderas de parrillas móviles, calderas de parrillas vibrantes, combustión en lecho burbujeante, calderas de circulación fluidizada, hornos rotativos, cámaras de combustión con pulso de pirólisis, etc., todas ellas dependientes de las características de los lodos, tales como humedad, tamaño de partícula, contenido en volátiles y cenizas, poder calorífico, presencia de contaminantes,..., y también, en gran medida, del volumen de lodos a quemar.

2.1.2. Pirólisis de lodos de la industria papelera

En el proceso de pirólisis de lodos de papelera, que implica el aporte de calor indirecto y en atmósfera inerte, es una alternativa a la incineración y al depósito en vertedero (Monte et al., 2009) y habitualmente requiere un flujo consistente de residuos para poder ser rentable (Fytili and Zabaniotou, 2008). En la práctica, el calentamiento de la fracción orgánica de los lodos en condiciones anaerobias y hasta temperaturas que generalmente se encuentran entre 400-800ºC da lugar a un carbonizado sólido (en inglés *char*), agua, compuestos orgánicos solubles en agua (ácidos piroleñosos, incluido el metanol y el ácido acético), compuestos orgánicos insolubles en agua (bioaceites, también conocidos bajo el término inglés *tar*), y gases no condensables (hidrógeno, metano, monóxido de carbono, dióxido de carbono). Durante la descomposición de la fracción orgánica no se permite la circulación de oxígeno, para evitar que ocurra combustión. Este tipo de tecnología se emplea para residuos con un alto contenido en carbono, como madera, petróleo y residuos plásticos. La temperatura de operación, velocidad de calentamiento y tiempo de residencia o de reacción han de ser optimizadas en función del material y del producto que se pretende obtener. Por ejemplo, si se utilizan temperaturas de pirólisis bajas y rampas de calentamiento lentas (Bajpai, 2015), se obtendrá principalmente carbonizado. Este carbonizado se caracteriza por poseer un elevado poder calorífico (30 MJ/kg) y puede ser utilizado como combustible para producir calor y/o electricidad. También, el carbonizado puede ser activado para ser convertido en carbón activado y utilizado como adsorbente. Para la producción de bioaceites, la pirólisis se realiza a velocidades de calentamiento rápidas hasta temperaturas de 500ºC o más que se mantienen durante tiempos de residencia cortos. En estas condiciones, se pueden alcanzar rendimientos de 70-75 % de bioaceite con un poder calorífico relativamente bajo (16–19 MJ/kg). Estos procesos de pirólisis rápida son comúnmente implementados en reactores de lecho fluidizado burbujeante, de lecho fluidizado circulante, en reactores de cono rotativo o en reactores al vacío (Mohan et al., 2006). Resumiendo, la pirólisis es un proceso que permite no sólo la recuperación de energía, a partir de los bioaceites, como también de material, a partir del carbonizado (Bajpai, 2015). Sin embargo, es importante señalar

que se necesitan lodos con un contenido en humedad igual o inferior al 20 %. Durante la pirólisis ocurre la degradación de la celulosa y hemicelulosa – polímeros de hidratos de carbono – presentes en los lodos y mediante la selección adecuada de temperatura, velocidad de calentamiento y tiempo de residencia, el proceso puede ser optimizado para producir carbonizado, bioaceites y/o gas. Cuando se alcanzan temperaturas superiores a los 300ºC, ocurre la despolimerización de la celulosa y hemicelulosa en cadenas cortas de polisacáridos. Esta despolimerización va acompañada de una lenta deshidratación y reacciones en cadena que dan lugar a polímeros insaturados intermedios que, eventualmente, condesan en forma de carbonizado sólido (Lomax et al., 1991). Cuando el calentamiento se realiza a alta velocidad y a temperaturas más altas, las reacciones de despolimerización liberan productos volátiles como aceites o *tar*. La ruptura de enlaces C-C ocurre a elevadas temperaturas, dando lugar a la formación de productos gaseosos. Por ello, si el objetivo es maximizar el rendimiento de la producción de bioaceites, se deben usar velocidades de calentamiento rápidas y tiempos de residencia cortos. Si se pretende maximizar la producción de carbonizado, será necesario emplear bajas temperaturas, lentas velocidades de calentamiento y tiempos de residencia prolongados. Los bioaceites, además de su alta concentración de agua (15-30 %), contienen una gran variedad de productos orgánicos oxigenados, carbohidratos poliméricos y fragmentos de lignina derivados del craqueo térmico de la celulosa, la hemicelulosa y la lignina presentes en los lodos de papelera (Mohan et al., 2006). Estos bioaceites, aunque tienen un poder calorífico (16–19 MJ/kg) inferior al del aceite pesado que se obtiene del petróleo (40 MJ/kg), pueden ser utilizados en lugar de combustibles fósiles en la producción de calor, energía y/o productos químicos. A corto plazo es posible su utilización en calderas (incluyendo centrales térmicas) y a un mayor plazo será factible su uso en turbinas y motores diésel. A partir de bioaceites y mediante procesos de gas de síntesis y/o el proceso Fischer-Tropsch es posible obtener combustibles para el transporte. Sin embargo, aunque técnicamente realizable, la transformación de bioaceites de la pirólisis de lodos en combustibles para el transporte está aún en fase de desarrollo (Bajpai, 2015). En otro sentido, existe un amplio abanico de productos químicos que pueden ser extraídos o derivados a partir de bioaceites de pirólisis.

Aunque menos convencional, la pirólisis de lodos de papelera puede ser ventajosa frente a la incineración en términos de gasto de combustible, recuperación de energía y control de emisiones. De hecho, la pirólisis permite la recuperación del 95-98 % de la energía contenida en los lodos secos a través de los varios productos que se obtienen (Bajpai, 2015). Sin embargo, la eficiencia del proceso de pirólisis es altamente dependiente del contenido en humedad de los lodos, y, teniendo en cuenta el secado y calentamiento necesarios para la pirólisis, el aporte de energía necesario es muy superior al de la incineración. Por ello, la co-pirólisis de lodos de

papelera con otros residuos o combustibles ha sido recomendada como estrategia para alcanzar el contenido de humedad requerido (Monte et al., 2009).

2.1.3. Análisis termogravimétrico de la combustión y la pirólisis de lodos de la industria papelera

El análisis termogravimétrico (TGA, del inglés *Thermogravimetric Analysis*) es una técnica analítica tradicionalmente utilizada para la caracterización de la descomposición térmica de carbones. La razón para ello es que permite el registro en continuo de la masa de una muestra cuando esta es sometida a un programa controlado de calentamiento o enfriamiento. La representación de la masa frente a la temperatura o frente al tiempo recibe el nombre de curva termogravimétrica. Por otro lado, la curva termogravimétrica derivada (DTG, del inglés *Derivative Thermogravimetry*) representa la primera derivada de la curva TG en función de la temperatura o el tiempo, y, por tanto, refleja la velocidad de variación de la masa frente a la temperatura o el tiempo, respectivamente.

Desde el siglo pasado, es sabido que el procesamiento térmico de biomasa y biorresiduos con recuperación de energía es una alternativa sostenible para la gestión de este tipo de materiales, que, además constituyen una fuente de energía renovable (Idris et al., 2010). Por ello, el uso del TGA se ha extendido para la caracterización de la descomposición térmica de biorresiduos (Sanchez et al., 2009) y/o biomasa (Saldarriaga et al., 2015), siendo muchas veces complementado mediante resultados de calorimetría diferencial de barrido (DSC, del inglés *Differential Scanning Calorimetry*).

Desde el punto de vista práctico, el TGA es ventajoso para la caracterización de materiales de comportamiento desconocido porque, utilizando una pequeña cantidad de muestra, permite una rápida determinación del contenido combustible, la temperatura de inicio y fin de degradación térmica, además de otros datos de interés como son, por ejemplo, la temperatura de máxima reactividad, el tiempo durante el que se está produciendo la reacción o la cantidad de residuo sólido que va a resultar al final del proceso. Por tanto, la información necesaria para predecir la eficacia del proceso, el tiempo de residencia, necesidad de exceso de aire, el diseño de caldera, etc., puede ser obtenida fácilmente mediante TGA. Sin embargo, para la comparación de resultados de TGA, hay que tener en cuenta que estos son altamente dependientes del rigor de la calibración, de las condiciones de operación (velocidad de calentamiento, atmósfera, caudal y presión de gas, etc.) y de las características de la muestra (masa, rango o grado de carbonificación, tamaño de partícula, etc.).

Comparativamente con la publicación científica de resultados TGA sobre lodos de estaciones depuradoras de aguas residuales urbanas, en el caso de los lodos de la industria papelera, el número de publicaciones es mucho menor (Magalhães et al., 2008) y son

relativamente recientes (Ferreira et al., 2016). Algunas de estas publicaciones están centradas exclusivamente en la combustión (Liu et al., 2010; Areeprasert et al., 2014) o en la pirólisis (Méndez et al., 2009b; Strezov and Evans, 2009) de lodos de la industria papelera. Si bien, la mayor parte de los trabajos contemplan el co-procesamiento térmico de los lodos de papelera, incluyendo la co-combustión con carbón (Vamvuka et al., 2009; Yanfen and Xiaoqian, 2010), la co-combustión con biomasa o biorresiduos (Hu et al., 2015; Cai et al., 2016) o la co-pirólisis con biomasa (Lin et al., 2014; Fang et al., 2015). Estas publicaciones coinciden en mostrar que los lodos de papelera tienen unas características muy peculiares y destacan las ventajas del co-procesamiento para la gestión y aprovechamiento energético de este tipo de residuos.

Como ya se refirió en el capítulo de introducción (sección 1.5. Generación y gestión de lodos en la industria papelera), los lodos primarios y secundarios de la industria papelera poseen propiedades muy dispares y se producen en diferentes proporciones, por lo que cabría esperar que no fueran igualmente aptos para las distintas opciones de tratamiento (Elliott and Mahmood, 2007). Esto contrasta con el hecho de que en la mayor parte de los estudios termogravimétricos sobre la combustión o pirólisis de lodos de papelera o sobre su co-procesamiento con carbón, biomasa o biorresiduos, se utilizan lodos primarios y secundarios mezclados (refiriendo esta mezcla como lodos de papelera o lodos mixtos). La única excepción encontrada es el trabajo de Méndez et al. (2009), en el que los autores caracterizaron ocho residuos diferentes de la industria papelera (entre los que se encontraban tanto los lodos primarios como los lodos secundarios) y realizaron el TGA de la pirólisis de estos residuos.

2.2. Producción de adsorbentes a partir de lodos de la industria papelera y aplicación para el tratamiento de aguas: eliminación de contaminantes emergentes

2.2.1. Producción de adsorbentes a partir de lodos de la industria papelera

La producción de adsorbentes a partir de lodos de papelera es una alternativa de gestión para estos residuos, aumenta el abanico de posibilidades en cuanto a materiales para ser utilizados en el tratamiento de aguas, y promueve la conservación de aquellos recursos naturales primarios normalmente utilizados para fabricar carbones activados (Bajpai, 2015).

Khalili et al. (2000) fueron los primeros en producir una serie de carbones activados micro- y mesoporosos a partir de lodos de la industria papelera mediante un proceso secuencial de activación química con cloruro de cinc, carbonización y activación física con una mezcla de monóxido y dióxido de carbono (75 % CO and 25 % CO_2). Estos autores (Khalili et al., 2000) destacaron que la utilización de los lodos de papelera como materia prima para la producción de adsorbentes era ventajosa con relación a los lodos de estaciones de depuradoras de aguas urbanas debido a que los primeros poseen una composición química más uniforme y con menos

impurezas. Los carbones activados producidos a partir de lodos de papelera (con áreas superficiales de hasta 1.000 m^2/g) fueron utilizados para la adsorción de fenol, alcanzando eficiencias de 65-75 % (Khalili et al., 2002). Posteriormente, otros autores realizaron una activación química de lodos de papelera con hidróxido de potasio para obtener un carbón activado con una elevada área superficial (1.002 m^2/g) y demostraron su capacidad para la adsorción de metales (Cd, Cr, Cu) del agua. La activación química de lodos de papelera mediante fluoruro de potasio seguida de una funcionalización con etilendiamina resultó en materiales adsorbentes con alta capacidad para la eliminación de colorantes orgánicos del agua (Auta and Hameed, 2014). Otros autores (Masomi et al., 2014) probaron la capacidad de adsorción de compuestos fenólicos (fenol, 2-clorofenol, y 4-nitrofenol) mediante carbones activados producidos mediante la activación con cloruro de cinc de lodos de papelera.

En los trabajos anteriores, como materia prima para la producción de carbones activados, fueron utilizados lodos de papelera mixtos, es decir, la mezcla de lodos primarios y secundarios. El proceso implicaba en todos los casos una activación química, lo que supone el consumo de reactivos químicos agresivos, con los gastos e implicaciones ambientales que esto conlleva. Alternativamente, algunos autores han demostrado la posibilidad de evitar la activación química y obtener, mediante la simple pirólisis de residuos de la industria papelera, adsorbentes capaces de eliminar cobre (Méndez et al., 2009a) y verde malaquita (Méndez et al., 2010) del agua. Posteriormente, (Calisto et al., 2014) trabajaron en la producción de adsorbentes mediante la pirólisis de, por un lado, lodos primarios y, por otro, de lodos secundarios de la misma papelera. Los materiales producidos fueron caracterizados mediante TGA; análisis inmediato, elemental y poder calorífico; carbono orgánico total (TOC, del inglés *Total Organic Carbon*); espectroscopía infra-rojo con transformada de Fourier (FTIR, del inglés *Fourier transform infra-red spectroscopy*); resonancia magnética nuclear (NMR, del inglés *Nuclear Magnetic Resonance)*; porosimetría de mercurio y de nitrógeno. Los autores (Calisto et al., 2014) probaron que las propiedades de los adsorbentes producidos dependían en gran medida de las condiciones operacionales de la pirólisis pero, sobre todo, de la materia prima (lodos primarios o lodos secundarios). Comparados con los secundarios, los lodos primarios de papelera proporcionaron materiales con mejores propiedades adsorbentes (Calisto et al., 2014).

2.2.2. Relevancia de la eliminación de contaminantes emergentes de las aguas y utilización de adsorbentes producidos a partir de lodos de la industria papelera con esta finalidad

El llamado grupo de los contaminantes emergentes (CEs) incluye un amplio y creciente espectro de compuestos (fármacos, fragancias, hormonas, antisépticos, surfactantes, etc.), que tienen como característica común la ausencia de regulación respecto a su vertido a pesar de que pueden constituir un riesgo para los ecosistemas y para la salud y seguridad humana (Farré et

al., 2008). Entre los CEs, los fármacos constituyen una clase especialmente preocupante, puesto que éstos fueron diseñados para provocar una respuesta fisiológica en los seres vivos y su presencia en el ambiente puede afectar a individuos y/o especies para los que no estaban destinados (Santos et al., 2010). Además, no se pueden descartar efectos negativos sobre la salud humana, pues, una vez que estos contaminantes son vertidos al medio acuático natural, pueden estar presentes en aguas utilizadas para el abastecimiento, cuyo tratamiento de potabilización no incluye la eliminación de CEs (Pal et al., 2014).

El modo de entrada de CEs en el ambiente depende de su patrón de utilización y modo de aplicación, pero, en el caso de los fármacos procedentes del consumo y excreción humana, las estaciones depuradoras de aguas residuales urbanas son importantes fuentes para el ambiente acuático (Farré et al., 2008). El motivo es que estas estaciones depuradoras fueron diseñadas para reducir la concentración de los parámetros legislados (demanda química de oxígeno, demanda biológica de oxígeno, sólidos en suspensión y nutrientes) pero no la de CEs como los fármacos. Sin embargo, teniendo en cuenta la atención que nivel público, político y científico está recibiendo la presencia de CEs en las aguas, en un futuro próximo son de esperar limitaciones legales en cuanto al vertido de este tipo de compuestos. En Europa este tipo de regulaciones son prácticamente inminentes en el contexto de la Directiva Marco del Agua (DMA, Directiva 2000/60/EC). La DMA, además de marcar objetivos en cuanto a calidad y protección del agua, define estrategias contra su contaminación. Entre estas estrategias está la limitación del vertido de las sustancias contenidas en la llamada lista de sustancias prioritarias, cuya primera versión fue lanzada en 2001 (Decisión 2455/2001/EC). Esta primera lista fue reemplazada por el Anexo II de la Directiva 2008/105/EC. Más tarde, y por primera vez, en la Comisión de 31 de Enero de 2012, se propuso la inclusión en la lista de sustancias prioritarias de tres fármacos: diclofenaco, 17-beta-estradiol (E2) y 17-alfa-etinilestradiol (EE2). Aunque esta inclusión no se llegó a concretizar, bajo la Directiva 2013/39/EU, la Comisión estableció la creación de una lista de observación de sustancias que deben ser monitorizadas en todos los países miembros de manera a justificar las futuras revisiones de la lista de sustancias prioritarias. Fue entonces establecido que los fármacos diclofenaco, E2 y EE2 formarían parte de la primera lista de observación. También mediante esta Directiva 2013/39/EU, la Comisión Europea estableció el compromiso de proponer, antes del 14 de Septiembre de 2017, "medidas a escala de la Unión y/o de los Estados miembros, según corresponda, para tratar las posibles consecuencias medioambientales de sustancias farmacéuticas [...] y para reducir sus descargas, emisiones y pérdidas en el medio acuático, teniendo en cuenta las necesidades de salud pública y la relación coste/eficacia de las medidas propuestas." Finalmente, la primera lista de observación ya publicada (Decisión 2015/495/EU) incluye, además de los tres fármacos

anteriores, tres antibióticos (azitromicina, claritromicina, eritromicina) y la hormona estrona (E1).

Teniendo en cuenta los riesgos de la presencia de fármacos en el ambiente y que es más que posible que en un futuro próximo existan normativas que limiten su vertido, en la última década ha sido realizada una intensa labor investigadora sobre tratamientos efectivos para la eliminación de este tipo de contaminantes de las aguas. Además, en el contexto actual de crisis es evidente la necesidad de desarrollar de estrategias sostenibles de bajo coste (Rivera-Utrilla et al., 2013). Entre las opciones más ventajosas para la eliminación de fármacos se encuentran los tratamientos de membrana y los de adsorción, puesto que no suponen la generación de compuestos de transformación, cuyos riesgos asociados pueden ser superiores a los de los compuestos originales (Bolong et al., 2009). En el caso de los tratamientos de membrana, los costes asociados son prohibitivos para su aplicación en el tratamiento de aguas residuales urbanas, mientras que la inclusión de los tratamientos de adsorción como tratamientos terciarios en estaciones depuradoras parece factible dada la efectividad y versatilidad de este tipo de tratamientos. Los carbones activados son los adsorbentes más comúnmente utilizados en el tratamiento de agua, si bien, su elevado precio constituye una desventaja para su aplicación a escala global. Es por ello que en los últimos años ha sido dedicado un gran esfuerzo al estudio de adsorbentes alternativos y de su uso para la eliminación de CEs en general y fármacos en particular. Entre estos adsorbentes alternativos y de bajo coste se encuentran los producidos mediante la pirólisis de lodos de papelera, cuya aplicación para la eliminación de fármacos en agua ultrapura ha sido probada. Específicamente, estos materiales han sido utilizados para la adsorción de fármacos humanos como el antidepresivo citalopram (Calisto et al., 2014), carbamazepina (antiepiléptico), oxazepan (ansiolítico), sulfametoxazol (antibiótico), piroxicam (antiinflamatorio no esteroideo), cetirizina (antihistamínico), venlafaxina (antidepresivo) y paroxetina (antidepresivo) (Calisto et al., 2015) y fármacos de uso veterinario como tricaina (Ferreira et al., 2015).

2.3.Objetivos

Planteada la necesidad de llevar a cabo una gestión sostenible de los lodos de la industria papelera así como el reto que actualmente supone la eliminación de contaminantes emergentes de las aguas residuales, esta tesis se plantea los siguientes objetivos:

2.3.1. Objetivo general

El objetivo general de esta tesis es determinar las características del procesamiento térmico de los lodos de la industria papelera y de su co-procesamiento con carbón. Además, se pretende también estudiar la utilización del carbonizado residual de la pirólisis de los lodos para la adsorción de fármacos en aguas residuales.

2.3.2. Objetivos específicos

i. Comparar las propiedades térmicas de los lodos primarios y de los lodos secundarios de una industria papelera con las de un carbón comercial para usos térmicos.

ii. Determinar mediante TGA las características de la combustión de los lodos primarios, los secundarios y el carbón así como evaluar las diferencias entre la combustión del carbón y su co-combustión con lodos primarios o secundarios.

iii. Determinar mediante TGA las características de la pirólisis de los lodos primarios, los lodos secundarios y el carbón así como evaluar las diferencias entre la pirólisis del carbón y su co-pirólisis con lodos primarios o secundarios.

iv. Calcular, a partir de un análisis cinético no-isotérmico de los resultados TGA, la energía de activación aparente correspondiente a la combustión y a la pirólisis de los lodos primarios, los lodos secundarios y el carbón.

v. Establecer si durante la co-combustión y/o durante la co-pirólisis de los lodos de papelera con carbón se produce interacción entre los materiales.

vi. Estudiar la velocidad y capacidad de adsorción de diclofenaco, ácido salicílico, ibuprofeno y acetaminofén por parte del carbonizado residual de la pirólisis de lodos primarios de papelera en agua ultrapura.

vii. Determinar si la velocidad y/o la capacidad de adsorción de estos fármacos se ven alteradas cuando la matriz acuosa es el efluente secundario de una estación depuradora de aguas residuales urbanas.

viii. Comparar la velocidad y capacidad de adsorción de diclofenaco por parte del carbonizado residual de la pirólisis de lodos primarios de papelera con la de adsorbentes comerciales (carbones activados y resinas poliméricas) en las dos matrices acuosas contempladas: agua ultrapura y el efluente secundario de una estación depuradora de aguas residuales urbanas.

2.4. Referencias

Areeprasert, C., Chanyavanich, P., Ma, D., Shen, Y., Prabowo, B., Yoshikawa, K., 2014. Combustion characteristics and kinetics study of hydrothermally treated paper sludge by thermogravimetric analysis. Biofuels 5, 673–685.

Auta, M., Hameed, B.H., 2014. Optimized and functionalized paper sludge activated with potassium fluoride for single and binary adsorption of reactive dyes. J. Ind. Eng. Chem. 20, 830–840.

Bajpai, P., 2015. Generation of wastewater treatment sludge, in: Management of Pulp and Paper Mill Wastes. Springer, Switzerland, pp. 12–15.

Bolong, N., Ismail, A.F., Salim, M.R., Matsuura, T., 2009. A review of the effects of emerging contaminants in wastewater and options for their removal. Desalination 239, 229–246.

Cai, Z., Ma, X., Fang, S., Yu, Z., Lin, Y., 2016. Thermogravimetric analysis of the co-combustion of eucalyptus residues and paper mill sludge. Appl. Therm. Eng. 106, 938–943.

Calisto, V., Ferreira, C.I.A., Oliveira, J.A.B.P., Otero, M., Esteves, V.I., 2015. Adsorptive removal of pharmaceuticals from water by commercial and waste-based carbons. J. Environ. Manage. 152, 83–90.

Calisto, V., Ferreira, C.I.A., Santos, S.M., Gil, M.V., Otero, M., Esteves, V.I., 2014. Production of adsorbents by pyrolysis of paper mill sludge and application on the removal of citalopram from water. Bioresour. Technol. 166, 335–344.

David, P.K., 1995. Converting paper, paper mill sludge and other industrial wastes into pellet fuel, in: T.W., J. (Ed.), Environmental Issues and Technology in the Pulp and Paper Industry-A Tappi Press Anthology of Published Papers 1991–1994. Tappi Press, Atlanta, Georgia, USA, pp. 365–367.

Elliott, A., Mahmood, T., 2007. Pretreatment technologies for advancing anaerobic digestion of pulp and paper biotreatment residues. Water Res. 41, 4273–4286.

Fang, S., Yu, Z., Lin, Y., Hu, S., Liao, Y., Ma, X., 2015. Thermogravimetric analysis of the co-combustion of paper mill sludge and municipal solid waste. Energy Convers. Manag. 99, 112–118.

Farré, M., Pérez, S., Kantiani, L., Barceló, D., 2008. Fate and toxicity of emerging pollutants, their metabolites and transformation products in the aquatic environment. Trends Anal. Chem. 27, 991–1007.

Faubert, P., Barnabé, S., Bouchard, S., Côté, R., Villeneuve, C., 2016. Pulp and paper mill sludge management practices: What are the challenges to assess the impacts on greenhouse gas emissions? Resour. Conserv. Recycl. 108, 107–133.

Ferreira, C.I.A., Calisto, V., Cuerda-Correa, E.M., Otero, M., Nadais, H., Esteves, V.I., 2016. Comparative valorisation of agricultural and industrial biowastes by combustion and pyrolysis. Bioresour. Technol. 218, 918–925.

Ferreira, C.I.A., Calisto, V., Santos, S.M., Cuerda-Correa, E.M., Otero, M., Nadais, H., Esteves, V.I., 2015. Application of pyrolysed agricultural biowastes as adsorbents for fish anaesthetic (MS-222) removal from water. J. Anal. Appl. Pyrolysis 112, 313–324.

Fytili, D., Zabaniotou, A., 2008. Utilization of sewage sludge in EU application of old and new methods-A review. Renew. Sustain. Energy Rev. 12, 116–140.

Gavrilescu, D., 2008. Energy from biomass in pulp and paper mills. Environ. Eng. Manag. J. 7, 537–546.

Hu, S., Ma, X., Lin, Y., Yu, Z., Fang, S., 2015. Thermogravimetric analysis of the co-combustion

of paper mill sludge and municipal solid waste. Energy Convers. Manag. 99, 112–118.

Idris, S.S., Rahman, N.A., Ismail, K., Alias, A.B., Rashid, Z.A., Aris, M.J., 2010. Investigation on thermochemical behaviour of low rank Malaysian coal, oil palm biomass and their blends during pyrolysis via thermogravimetric analysis (TGA). Bioresour. Technol. 101, 4584–4592.

Kay, M., 2007. The power of waste. Tappi J. 49, 21–22.

Khalili, N.R., Campbell, M., Sandi, G., Golaš, J., 2000. Production of micro- and mesoporous activated carbon from paper mill sludge. I. Effect of zinc chloride activation. Carbon N. Y. 38, 1905–1915.

Khalili, N.R., Vyas, J.D., Weangkaew, W., Westfall, S.J., Parulekar, S.J., Sherwood, R., 2002. Synthesis and characterization of activated carbon and bioactive adsorbent produced from paper mill sludge. Sep. Purif. Technol. 26, 295–304.

Lin, Y., Ma, X., Yu, Z., Cao, Y., 2014. Investigation on thermochemical behavior of co-pyrolysis between oil-palm solid wastes and paper sludge. Bioresour. Technol. 166, 444–450.

Liu, K., Ma, X.Q., Xiao, H.M., 2010. Experimental and kinetic modeling of oxygen-enriched air combustion of paper mill sludge. Waste Manag. 30, 1206–1211.

Lomax, D., Commandeur, J., Arisz, P., Boon, J., 1991. Characterization of oligomers and sugar ring-cleavage products in the pyrolysate of cellulose. J. Anal. Appl. Pyrolysis 19, 65–79.

Magalhães, W.L.E., Job, A.E., Ferreira, C.A., Da Silva, H.D., 2008. Pyrolysis and combustion of pulp mill lime sludge. J. Anal. Appl. Pyrolysis 82, 298–303.

Masomi, M., Ghoreyshi, A.A., Najafpour, G.D., Mohamed, A.R.D., 2014. Adsorption of Phenolic Compounds onto the Activated Carbon Synthesized from pulp and paper mill sludge: Equilibrium Isotherm, Kinetics, Thermodynamics and Mechanism Studies. Int. J. Eng. 27, 1485–1494.

Méndez, A., Barriga, S., Fidalgo, J.M., Gascó, G., 2009a. Adsorbent materials from paper industry waste materials and their use in Cu(II) removal from water. J. Hazard. Mater. 165, 736–743.

Méndez, A., Barriga, S., Saa, A., Gascó, G., 2010. Removal of malachite green by adsorbents from paper industry waste materials. J. Therm. Anal. Calorim. 99, 993–998.

Méndez, A., Fidalgo, J.M., Guerrero, F., Gascó, G., 2009b. Characterization and pyrolysis behaviour of different paper mill waste materials. J. Anal. Appl. Pyrolysis 86, 66–73.

Mohan, D., Pittman, C., Steele, P., 2006. Pyrolysis of wood/biomass for bio-oil: a critical review. Energy Fuel 20, 848–889.

Monte, M.C., Fuente, E., Blanco, A., Negro, C., 2009. Waste management from pulp and paper production in the European Union. Waste Manag. 29, 293–308.

Pal, A., He, Y., Jekel, M., Reinhard, M., Gin, K.Y.-H., 2014. Emerging contaminants of public

health significance as water quality indicator compounds in the urban water cycle. Review Article. Environ. Int. 71, 46–62.

Ridout, A.J., Carrier, M., Collard, F.-X., Görgens, J., 2016. Energy conversion assessment of vacuum, slow and fast pyrolysis processes for low and high ash paper waste sludge. Energy Convers. Manag. 111, 103–114.

Rivera-Utrilla, J., Sanchez-Polo, M., Angeles Ferro-Garcia, M., Prados-Joya, G., Ocampo-Perez, R., 2013. Pharmaceuticals as emerging contaminants and their removal from water. A review. Chemosphere 93, 1268–1287.

Saldarriaga, J.F., Aguado, R., Pablos, A., Amutio, M., Olazar, M., Bilbao, J., 2015. Fast characterization of biomass fuels by thermogravimetric analysis (TGA). Fuel 140, 744–751.

Sanchez, M.E., Otero, M., Gómez, X., Morán, A., 2009. Thermogravimetric kinetic analysis of the combustion of biowastes. Renew. Energy 34, 1622–1627.

Santos, L.H.M.L.M., Araujo, A.N., Fachinia, A., Pena, A., Delerue-Matos, C. Montenegro, M.C.B.S.M., 2010. Ecotoxicological aspects related to the presence of pharmaceuticals in the aquatic environment. J. Hazard. Mater. 175, 45–95.

Strezov, V., Evans, T.J., 2009. Thermal processing of paper sludge and characterisation of its pyrolysis products. Waste Manag. 29, 1644–1648.

Vamvuka, D., Salpigidou, N., Kastanaki, E., Sfakiotakis, S., Yanfen, L., Xiaoqian, M., 2009. Possibility of using paper sludge in co-firing applications. Fuel 88, 637–643.

Yanfen, L., Xiaoqian, M., 2010. Thermogravimetric analysis of the co-combustion of coal and paper mill sludge. Appl. Energy 87, 3526–3532.

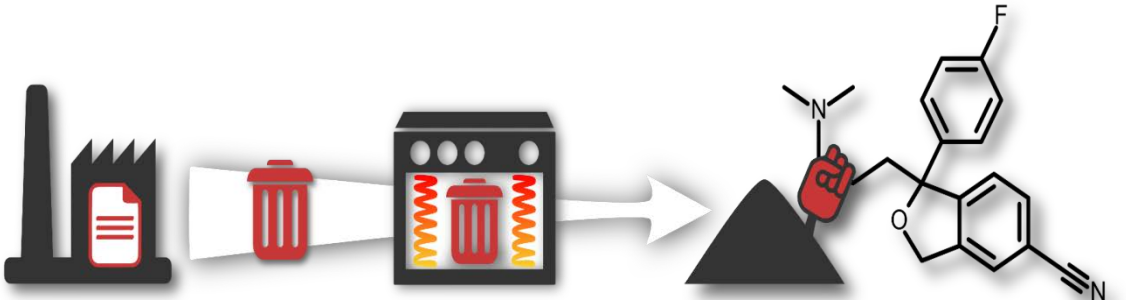

Capítulo 3

3. Resultados y discusión

3.1. Análisis termogravimétrico del procesamiento térmico de lodos de la industria papelera

3.1.1. Propiedades térmicas de los lodos de papelera y del carbón

Los resultados del análisis inmediato y elemental y el poder calorífico de los materiales carbonosos utilizados en este trabajo se muestran en la tabla 3.1. Como se puede ver, los materiales objeto de estudio poseen propiedades bien diferentes. Las humedades reflejan valores de los materiales en las condiciones de almacenamiento. Con relación al contenido en cenizas de los lodos primarios, es ligeramente superior al del carbón, siendo los lodos secundarios los que poseen un menor porcentaje. En el caso de los volátiles, el contenido de los lodos de papelera está dentro del rango de los valores encontrados en la literatura para biomasa (Saldarriaga et al., 2015), pero es muy superior (especialmente en los lodos primarios) al del carbón. Consecuentemente, los lodos de papelera tienen valores de carbono fijo inferiores al del carbón.

Con relación al análisis elemental, el carbón tiene un contenido superior en C, H, N y S que los lodos de papelera, excepto en el caso de los lodos secundarios, cuyo contenido en H y N es superior al del carbón. Por el contrario, el contenido de O de los lodos es muy superior al del carbón. Finalmente, el carbón tiene un poder calorífico superior que se encuentra en el rango típico de carbones sub-bituminosos y que es superior al de los lodos secundarios, y muy superior al de los lodos primarios.

Tabla 3.1. Análisis inmediato, análisis elemental y poder calorífico del carbón (C), los lodos primarios (L1) y los lodos secundarios (L2) de papelera utilizados en este trabajo.

Propiedades	**C**	**L1**	**L2**
Análisis inmediato (% en peso)			
Humedad	11,22	1,74	11,83
Volátiles/ b.s.	8,01	65,25	58,64
Cenizas/ b.s.	30,33	33,10	24,39
Carbono Fijo (CF)*/b.s	61,66	1,65	16,97
Análisis elemental (% en peso, b.s.)			
C	62,07	15,37	41,25
H	2,30	1,35	5,03
N	1,16	0,36	6,78
S	2,21	0,24	1,89
O*	1,93	49,58	20,66
Poder Calorífico (J g^{-1}, b.s.)			
PCS	24.382	2.489	16.429

b.s. = base seca
PCS = Poder calorífico superior
*calculado por diferencia

3.1.2. Análisis termogravimétrico de la combustión de lodos de papelera y de su co-combustión con carbón

Las curvas DTG (del inglés *Differential Termogravimetry*) y DSC (del inglés *Differential Scaning Calorimetry*) correspondientes a la combustión del carbón (C), los lodos primarios (L1) y los lodos secundarios (L2) de papelera se encuentran representadas en la figura 8.1. En esta figura también se representan las curvas de co-combustión del carbón con lodos (combustión de mezclas con 90% y 10% en peso de carbón y lodo).

En la figura 3.1., las curvas DTG y DSC del carbón muestran el perfil típico de pérdida de masa y de desprendimiento de calor para carbones y son muy similares y ocurren en una etapa principal. En ella ocurre la combustión del carbono fijo, con el correspondiente desprendimiento de calor. En el caso de los lodos primarios de papelera, la pérdida de peso ocurrió en dos fases separadas: la primera corresponde a la combustión de celulosa, que típicamente ocurre alrededor de los 600 K (Yanfen and Xiaoqian, 2010) y la segunda con la combustión de carbonato de calcio, que ocurre a altas temperaturas relativas (Idris et al., 2010).

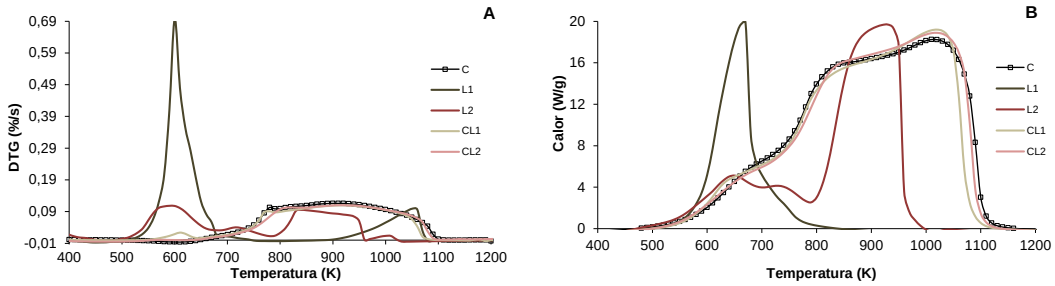

Figura 3.1. Curvas (A) DTG y (B) DSC correspondientes a la combustión de carbón (C), lodos primarios (L1), lodos secundarios (L2), mezcla de carbón con lodos primarios (CL1) y mezcla de carbón con lodos secundarios (CL2) a una velocidad de calentamiento de 0.5 K/s.

La curva DSC (figura 3.1. (B)) de los lodos primarios muestra que sólo la primera fase de pérdida tiene asociada un desprendimiento de calor, que se relaciona con la combustión de la materia orgánica y volátil. La segunda fase de pérdida de masa se debe a la descomposición de materia mineral, por lo que ocurre desprendimiento de calor en la curva DSC simultánea. Respecto a los lodos secundarios, la curva DTG muestra que a lo largo de la combustión tienen lugar cuatro etapas de pérdida de masa, que no se han podido contrastar con la literatura pues no hay resultados publicados sobre la combustión de lodos secundarios de la industria papelera. La primera etapa, que ocurre en el mismo rango que para los lodos primarios, debe relacionarse con la combustión de volátiles y celulosa; la segunda debe corresponder a la combustión de compuestos orgánicos biodegradables generados durante el tratamiento secundario; la tercera, que ocurre dentro del rango de la del carbón, debe relacionarse con la combustión del carbono fijo; y la cuarta, que está en el rango de la segunda etapa de los primarios, con la descomposición del contenido mineral. Así, la curva DSC de los lodos secundarios, muestra claramente que sólo hay desprendimiento de calor asociado a las tres primeras fases.

A pesar de las grandes diferencias entre las curvas DTG y DSC correspondientes a los tres materiales considerados, en el caso de la combustión de las mezclas de carbón con lodos (10% en peso), los perfiles de combustión son prácticamente iguales al del carbón tanto para las mezclas con lodos primarios como secundarios.

3.1.3. Análisis termogravimétrico de la pirólisis de lodos de papelera y de su co-pirólisis con carbón

La figura 3.2. representa las curvas DTG correspondientes a la pirólisis de lodos primarios de papelera, lodos sedundarios de papelera, carbón y sus respectivas mezclas. Las curvas DTG muestran que la pérdida de masa asociada a la pirólisis del carbón ocurre en una única etapa y es muy baja comparada con los lodos secundarios y, especialmente, con los primarios. Esto está de acuerdo con sus respectivos contenidos en volátiles, como se puede ver en la tabla 8.1. Además, durante la pirólisis del carbón, la pérdida de masa tiene lugar en una única etapa,

mientras que la pirólisis, tanto de los lodos primarios como de los secundarios, ocurre en dos etapas. Sin embargo, la pirólisis de los lodos primarios es muy diferente de la de los secundarios. En primer lugar, las dos etapas son mucho más intensas para la pirólisis de los primarios que para la de los secundarios, lo que está de acuerdo con el menor contenido en volátiles de los segundos (tabla 3.1.). Por otro lado, en el caso de los lodos secundarios, la primera etapa de pérdida de masa ocurre en un rango de temperaturas mayor que para los lodos primarios, mientras que en la segunda etapa es al contrario. Esto indica que las diferencias en cuanto al contenido volátil de los lodos primarios y secundarios no es sólo cuantitativa (tabla 3.1.) sino también cualitativa (figura 3.2.).

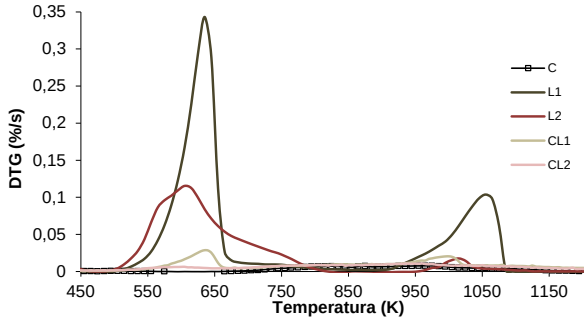

Figura 3.2. Curvas DTG correspondientes a la combustión de carbón (C), lodos primarios (L1), lodos secundarios (L2), mezcla de carbón con lodos primarios (CL1) y mezcla de carbón con lodos secundarios (CL2) a una velocidad de calentamiento de 0.5 K/s.

Durante la pirólisis de carbón con lodos primarios (10% en peso), la pérdida de masa es muy inferior a la de la pirólisis de lodos pudiéndose observar tres etapas de pérdida de masa. La primera y la tercera tienen lugar en el rango de temperatura de las dos etapas de los lodos primarios y la segunda (que es comparativamente menos relevante) en el rango de temperatura de la del carbón. Respecto a la mezcla de carbón con lodos secundarios (10% en peso), la curva DTG de la pirólisis es muy similar a la del carbón, pero se puede observar una pequeña pérdida de masa en el rango de temperaturas de la primera etapa de los lodos secundarios.

3.1.4. Energía de activación aparente asociada a la combustión y a la pirólisis de lodos de papelera y sus mezclas con carbón

Los valores de energía de activación aparente (E) asociada a los procesos de combustión y pirólisis de los lodos primarios, los lodos secundarios, el carbón y sus respectivas mezclas se encuentran representados en la tabla 3.2. La E determinada para la combustión de carbón es un orden de magnitud inferior a la de los lodos primarios y secundarios. Aunque significativa, esta diferencia se encuentra dentro del rango de las E correspondientes a carbones de diferente rango (Kök, 2005). Por otro lado, las E correspondientes a L1 y L2 están dentro de los valores determinados mediante el método de Flynn-Wall-Ozawa para lodos de papelera mixtos (Xie

and Ma, 2013) y también de los valores determinados para la combustión de biomasa (Xiao et al., 2009; Idris et al., 2012). Respecto a la combustión de las mezclas, los valores de E correspondientes a la combustión de CL1 y a CL2 son del mismo orden de magnitud que la del carbón y en ambos casos son ligeramente inferiores que los valores de E calculados a partir de la composición de la mezcla (92 and 96 KJ mol^{-1}, respectivamente), lo que apunta a algún tipo de interacción entre el carbón y ambos tipos de lodos de papelera.

Tabla 3.2. Valores medios de energía de activación aparente (E) estimados mediante el método de Flynn-Wall-Ozawa para la combustión y la pirólisis de lodos primarios (L1), lodos secundarios (L2), carbón (C) y sus respectivas mezclas (CL1 y CL2).

Tratamiento térmico	Material/Mezcla	$\bar{E}^{*}$ (kJ mol^{-1})
Combustión	C	85
	L1	155
	L2	199
	CL1	91
	CL2	88
Pirólisis	C	256
	L1	120
	L2	197
	CL1	165
	CL2	68

*Calculada como la media aritmética de los valores obtenidos para cada uno de los grados de conversión (α) considerados

En el caso de la pirólisis, la E determinada para el carbón es bastante superior a la de su combustión, y también superior a la de la pirólisis de L1 y L2. De cualquier manera, el valor de E correspondiente a C es similar a los valores encontrados en la literatura para carbones (Aboyade et al., 2013). En el caso de la pirólisis de lodos de papelera, no hay datos publicados sobre estimaciones de la energía de activación asociada, si bien los datos determinados en este trabajo son similares a los obtenidos por otros autores para la pirólisis de residuos lignocelulósicos (Aboyade et al., 2013; Wu et al., 2014). Respecto a los valores determinados para la pirólisis de CL1 y CL2, estos son inferiores de lo que correspondería de acuerdo a la composición de las mezclas (247 y 250 KJ mol^{-1}, respectivamente). Las diferencias, que son especialmente evidentes para CL2, indican que durante la pirólisis deben ocurrir interacciones entre los materiales de las mezclas. Algunos autores han señalado la ocurrencia de interacciones entre el carbón y la celulosa durante el procesamiento térmico (Wu et al., 2014; Guo et al., 2015). Una vez que la celulosa es un constituyente importante de los lodos de papelera, esta puede tener un papel relevante en las interacciones detectadas.

3.1.5. Interacción entre el carbón, los lodos primarios y los lodos secundarios de papelera durante el procesamiento térmico de sus respectivas mezclas

En este trabajo se han estudiado mediante análisis termogravimétrico la combustión y la pirólisis de carbón, lodos primarios y los lodos secundarios de papelera. Comparando combustión y pirólisis, la figura 3.3. refleja que las diferencias entre las curvas DTG correspondientes son más o menos evidentes dependiendo del material. En el caso del carbón, la pirólisis apenas supone pérdida de peso comparada con la combustión de este combustible fósil. Esto no es así para los lodos de papelera, cuya pirólisis supone una importante pérdida de peso relativamente a su combustión. Además, mientras que la pérdida de peso durante la pirólisis del carbón tiene lugar en una única etapa, la de los lodos de papelera ocurre en dos etapas diferenciadas. De cualquier manera, existen diferencias notables entre las curvas DTG de la pirólisis de los lodos primarios y de los secundarios. En primer lugar, en las dos etapas de la pirólisis, la pérdida de peso de los primarios es superior a la de los secundarios, lo que está de acuerdo con el mayor contenido en volátiles de los primarios (tabla 3.1.). Por otro lado, la primera etapa de la pirólisis tiene lugar en un rango de temperaturas más amplio en el caso de los lodos secundarios. Además, en el caso de los primarios, la curva DTG de la pirólisis se asemeja mucho a la de la combustión, lo que se asocia al bajo contenido de carbono fijo de los lodos primarios (tabla 3.1.).

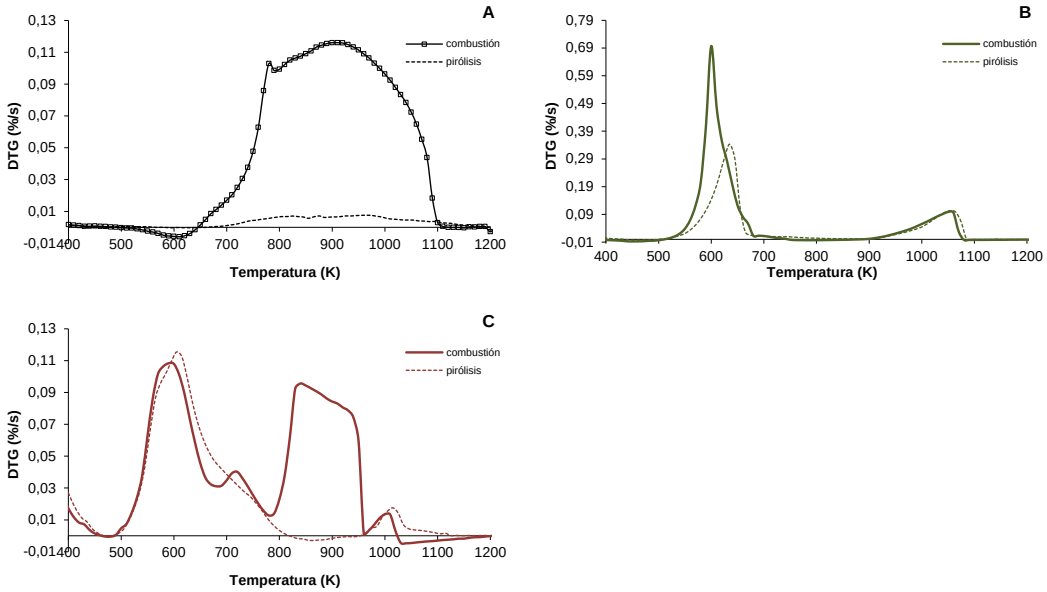

Figura 3.3. Curvas DTG obtenidas a una velocidad de calentamiento de 0.5 K/s para la combustión y para la pirólisis de: (A) carbón; (B) lodos primarios; y (C) lodos secundarios. Nota: La escala de las figuras (A), (B) y (C) es diferente y ha sido ajustada para permitir la visualización de las curvas.

La figura 3.4. representa las curvas DTG de la co-combustión y co-pirólisis de carbón con lodos primarios y secundarios así como las curvas calculadas a partir de la composición de las mezclas carbón:lodos (90:10). Las curvas DTG de la co-combustion de lodos primarios con carbón (figura 3.4. (A)) son muy similares a las de la combustión de carbón (figura 3.3. (A)), si

bien, existe una pérdida de peso asociada a la combustión del contenido en celulosa de los lodos primarios. Sin embargo, esa pérdida de peso es más relevante en la curva DTG calculada (figura 3.3. (C)). Lo mismo ocurre para la co-combustión de los lodos secundarios con carbón, siendo que la pérdida de peso debida a la combustión de celulosa aparece en la curva calculada (figura 3.4. (D)), pero no en la obtenida experimentalmente (figura 3.4. (B)).

A diferencia de la co-combustión, las curvas DTG de co-pirólisis (figura 3.4. (A) y (B)) son muy diferentes y reflejan una pérdida de peso mayor que la DTG correspondiente a la pirólisis del carbón (figura 3.3. (A)). En cualquier caso, e igual que ocurría para la co-combustión, la pérdida de peso determinada experimentalmente (figura 3.4. (A) y (B)) para las co-pirólisis es menor que las calculadas (figura 3.4. (C) y (D)). De esto se deducen efectos sinérgicos negativos durante la pirólisis y la combustión de mezclas de lodos de papelera, tanto primarios como secundarios, con carbón.

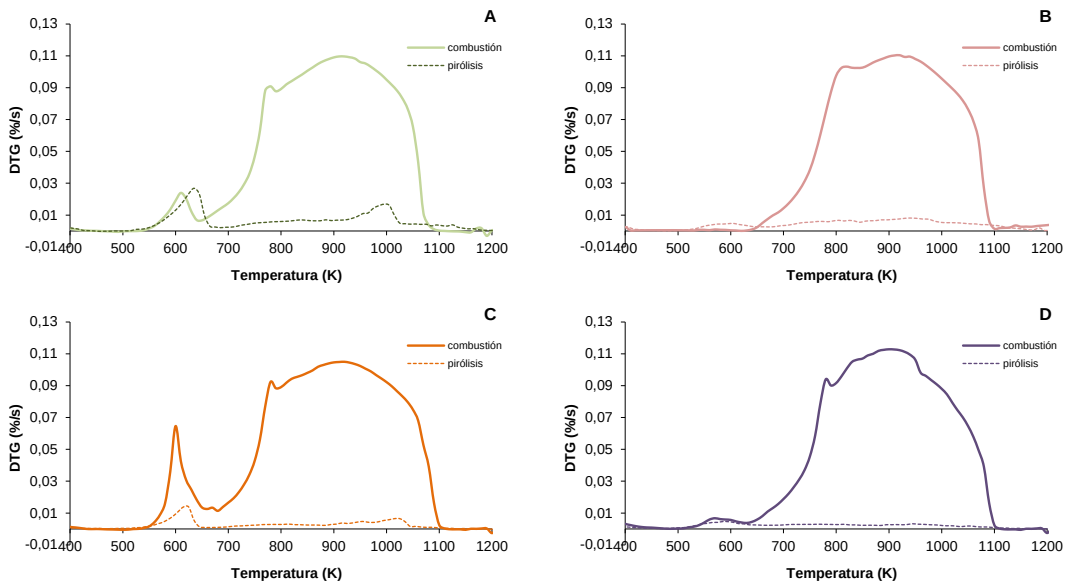

Figura 3.4. Curvas DTG obtenidas a una velocidad de calentamiento de 0.5 K/s para la co-combustión y co-pirólisis (A) de los lodos primarios con carbón; y (B) de los lodos secundarios con carbón. Curvas DTG calculadas a partir de la composición de la mezcla para la co-combustión y co-pirólisis (C) de los lodos primarios con carbón; y (D) de los lodos secundarios con carbón.

Los parámetros característicos de las curvas DTG obtenidas experimentalmente y de las calculadas se muestran en la tabla 3.3. Tanto para la combustión como para la pirólisis, la T_v, T_m y la T_f correspondientes al carbón son más elevadas que las de los lodos primarios o de los lodos secundarios. Por otro lado, destaca el valor de DTG_{max} correspondiente a los lodos primarios cuando se comparan con los secundarios y, especialmente con el carbón. En el caso de las mezclas, los parámetros característicos de las curvas calculadas coinciden en gran medida con los de las curvas experimentales. Sin embargo, la T_v correspondiente a $CL2_{CALCULADA}$ es inferior

que la correspondiente a CL2, como se puede ver al comparar la Figura 3.4. (B) con la Figura 3.4. (D). Esto confirma la ausencia del primer pico de la combustión de los lodos secundarios en la co-combustión de estos lodos con carbón. En el caso de la co-combustión de lodos primarios con carbón, la Tv de $CL1_{CALCULADA}$ también es inferior a la de CL1, lo que confirma que la pérdida de peso asociada a la combustión de la celulosa es inferior de lo que sería en ausencia de interacción entre lodos y carbón.

En el caso de las co-pirólisis, la DTG_{max} de CL1 es inferior a la de $CL1_{CALCULADA}$ y lo mismo ocurre para la T_v de CL2 cuando se compara con la de $CL2_{CALCULADA}$. Por ello, tanto en la co-combustión como en la co-pirólisis la pérdida de peso asociada a la combustión y/o desvolatilización del contenido celulósico de los lodos de papelera es inferior a la calculada en función de la composición de la mezcla lodo:carbón. Esto apunta a que durante el calentamiento deben ocurrir interacciones entre celulosa y carbón, de manera que parte de los volátiles de la celulosa pueden haber quedado retenidos en las partículas de carbón. Hay que destacar que el contenido en volátiles de los lodos de papelera es muy superior al del carbón (tabla 3.1.) y está asociado principalmente a la composición celulósica de estos lodos, especialmente en el caso de los primarios.

Tabla 3.3. Parámetros característicos de las curvas DTG correspondientes a la combustión (atmósfera oxidante) y pirólisis (atmósfera inerte) del carbón (C), lodos primarios de papelera (L1), lodos secundarios de papelera (L2) y sus respectivas mezclas con carbón (CL1 y CL2). En el caso de las mezclas, se representan también los parámetros correspondientes a las curvas DTG calculadas en función de la composición de la mezcla de carbón con lodos primarios y secundarios ($CL1_{CALCULADA}$ y $CL2_{CALCULADA}$).

Material	Atmósfera	T_v (K)	T_m (K)	T_f (K)	DTG_{max} (%/s)	t_q (s)
C	Inerte (Pirólisis)	620	964	1250	0.0097	1260
	Oxidante (Combustión)	649	915	1114	0.1162	930
L1	Inerte (Pirólisis)	500	636	1090	0.3446	1180
	Oxidante (Combustión)	490	598	1077	0.6969	1174
L2	Inerte (Pirólisis)	475	608	1150	0.1156	1350
	Oxidante (Combustión)	485	596	1030	0.1090	1090
CL1	Inerte (Pirólisis)	500	637	1250	0.0269	1500
	Oxidante (Combustión)	529	923	1105	0.1097	1152
CL2	Inerte (Pirólisis)	475	945	1250	0.0114	1550
	Oxidante (Combustión)	627	933	1100	0.1112	942
$CL1_{CALCULADA}$	Inerte (Pirólisis)	500	635	1250	0.0341	1500
	Oxidante (Combustión)	530	910	1105	0.1048	1150
$CL2_{CALCULADA}$	Inerte (Pirólisis)	475	605	1250	0.0114	1550
	Oxidante (Combustión)	505	900	1105	0.1128	1200

T_v = Temperatura de inicio de la desvolatilización. T_m = Temperatura del pico de máxima velocidad de pérdida de peso. T_f = Temperatura del final de la combustión o de la pirólisis. DTG_{max} = Máxima velocidad de pérdida de peso. t_q = Tiempo de duración de la combustión o de la pirólisis.

3.2. Utilización del carbonizado procedente de la pirólisis de lodos de papelera para la adsorción de contaminantes emergentes del agua

3.2.1. Adsorción de fármacos mediante el carbonizado de los lodos primarios de papelera

Como se ha visto en la sección anterior, los lodos primarios y secundarios poseen propiedades diferentes. Estas diferencias se reflejan en su comportamiento térmico, tanto en atmósfera oxidante como inerte. En lo que se refiere al co-procesamiento con carbón, los resultados anteriores muestran que las modificaciones que sufren la combustión o la pirólisis del carbón al añadir un porcentaje de lodos de papelera (10%) son menos relevantes en el caso de los secundarios que de los primarios. Esto se debe fundamentalmente a la intensa desvolatilización que tiene lugar a bajas temperaturas relativas durante el calentamiento de los lodos primarios, debido a su elevado contenido en celulosa.

En el caso de los lodos de depuración de aguas residuales urbanas, existen numerosos artículos científicos acerca de la utilización del carbonizado resultante de su pirólisis como adsorbente (Calvo et al., 2001; Rozada et al., 2005; Rozada et al., 2007; Otero et al., 2009; Tan et al., 2014; Tan et al., 2015). Sin embargo, no es así para los lodos de papelera, que, quizás debido a su peculiar composición, han recibido menos atención en este sentido. El primer estudio con residuos de la industria papelera (Méndez et al., 2009) se centró en la aplicación como adsorbente del carbonizado de la pirólisis de lodos de destintado y lodos secundarios. Este carbonizado fue utilizado como adsorbente de Cu (II) (Méndez et al., 2009) y, después, de verde malaquita (Méndez et al., 2010) en agua. Sin embargo, el estudio de la adsorción de fármacos mediante adsorbentes producidos a partir de lodos de la industria papelera es muy reciente (Calisto et al., 2014). Estos autores (Calisto et al., 2014) llevaron a cabo la caracterización física y química de los carbonizados obtenidos a partir de lodos primarios y de aquellos obtenidos partir de lodos secundarios, para después estudiar su aplicación para la adsorción de citalopram (un fármaco antidepresivo). Así pudieron concluir que el carbonizado obtenido a partir de los lodos primarios contaba con unas propiedades más adecuadas para su utilización como adsorbente que el obtenido a partir de lodos secundarios (Calisto et al., 2014). Con este antecedente, en el presente trabajo se estudió la adsorción de fármacos del grupo de los analgésicos, específicamente diclofenaco, ibuprofeno, ácido salicílico y acetaminofén (paracetamol) mediante el carbonizado de los lodos primarios. El grupo de fármacos considerado fue seleccionado debido a su elevado consumo, de lo que se deriva su presencia habitual en aguas residuales urbanas y su relevancia como contaminantes emergentes.

El carbonizado utilizado como adsorbente se obtuvo mediante la pirólisis de lodos primarios (PS, abreviatura del inglés *primary sludge*) bajo atmósfera inerte (N_2) a una

temperatura de 800ºC, y un tiempo de residencia de 150 minutos a esa temperatura, denominándose al material final PS800-150. Estas condiciones de producción fueron señaladas como las más favorables en un estudio previo que contempló varias temperaturas de pirólisis y tiempos de residencia, caracterizando los productos finales (Calisto et al., 2014). En la tabla 3.4. se representan las principales propiedades de los lodos primarios (PS) y del carbonizado (PS800-150) utilizados en el presente trabajo.

Uno de los objetivos de este trabajo fue comparar la influencia de la matriz acuosa en la adsorción de los fármacos antes referidos. Para ello, las experiencias de adsorción se realizaron de forma idéntica utilizando dos tipos de matrices: (i) agua ultrapura; y (ii) el efluente secundario de la estación depuradora de aguas residuales urbanas (EDAR) de León, cuyas principales propiedades se representan en la tabla 3.5.

Tabla 3.4. Propiedades de los lodos primarios de papelera (PS) y el carbonizado obtenido a partir de los mismos (PS800-1500) (adaptada de Calisto et al. (2014)).

Propiedades	**PS**	**PS800-150**
Análisis inmediato (% en peso)		
Humedad	1,57	3,16
Cenizas/ b.s.	55,31	61,25
Volátiles/ b.s.	36,09	20,77
Carbono Fijo (CF)*/ b.s.	8,60	17,98
VM/FC	4,2	1,2
Análisis elemental (% en peso, b.s.)		
C	14,83	27,05
H	1,26	0,82
N	0,40	0,33
S	0,29	0,82
O*	27,91	9,73
Propiedades físicas		
Densidad aparente (g cm^{-3})	NM	0,52
S_{BET} (m^2 g^{-1})	NM	209,12
V_p (cm^3 g^{-1})	NM	0,13
W_0 (cm^3 g^{-1})	NM	0,078
L (nm)	NM	1,30
D (nm)	NM	0,84

b.s. = base seca
NM = no medido
S_{BET} = área superficial calculada con base en la teoría de Brunauer-Emmet-Teller
V_p =volumen total de poros
W_0 = volumen total de microporos
L = diámetro medio de los microporos
D = diámetro medio de poro
*calculado por diferencia

Para cada fármaco y matriz acuosa considerados, se realizaron experiencias cinéticas de adsorción seguidas de experiencias de equilibrio, todas ellas en discontinuo y bajo agitación a temperatura controlada (25± 2 ºC). Tras ello, se determinaron los ajustes de los resultados experimentales a modelos empíricos o teóricos comúnmente utilizados en la literatura. En el caso de los resultados cinéticos, se utilizaron dos modelos: (i) el de pseudo-primer orden o Lagergren (Lagergren, 1808); y (ii) el modelo de pseudo-segundo orden (Ho and McKay, 1999). En cuanto a los resultados de equilibrio, se determinaron los ajustes a los modelos de isoterma de: (i) Freundlich (Freundlich, 1906); (ii) Langmuir (Langmuir, 1918); y (iii) Sips (Sips, 1948), también conocida como isoterma de Langmuir-Freundlich.

Tabla 3.5. Principales propiedades del efluente de EDAR utilizado en este trabajo. Nota: se representan los valores medios junto (±) la desviación estándar correspondiente.

Parámetro	
pH	7.6±0.1
Conductividad (µS cm^{-1})	612±3
SST (mg L^{-1})	22±1
DBO_5 (mg L^{-1})	21±2
DQO (mg L^{-1})	47±3
NTK (mg L^{-1})	17±2
$N\text{-}NH_4$ (mg L^{-1})	13.1±0.4
$N\text{-}NO_3$ (mg L^{-1})	1.7±0.2
$N\text{-}NO_2$ (mg L^{-1})	0.5±0.1
$P\text{-}PO_4$ total (mg L^{-1})	1.8±0.1

SST = sólidos en suspensión totales
DBO_5 = demanda biológica de oxígeno a los 5 días
DQO = demanda química de oxígeno

Los parámetros obtenidos a partir del ajuste de los resultados experimentales a los modelos referidos están representados en la tabla 3.6 en el caso de los resultados cinéticos y en la tabla 3.7. para los resultados de equilibrio.

Los resultados cinéticos y los parámetros de ajuste a las ecuaciones de pseudo-primer y pseudo-segundo orden (tabla 3.6.) muestran que, bajo idénticas condiciones experimentales, el acetaminofén es el fármaco que se adsorbe más lentamente en PS800-150. Por otro lado, fue el ácido salicílico el fármaco para el que se obtuvo el menor q_e. Además, los ajustes al modelo de pseudo-segundo orden son mejores que los del pseudo-primer orden, tal y como se puede concluir por los valores de R^2 y S_{xy} en la tabla 3.6. La constante cinética k_2 disminuye en el sentido ácido salicílico > diclofenaco > ibuprofeno > acetaminofén, tanto en agua ultrapura como

en el efluente de EDAR. Bajo las condiciones experimentales seguidas, el tiempo de equilibrio para la adsorción de estos fármacos en PS800-150 fue en todos los casos inferior a 200 min, tanto en agua ultrapura como en el efluente de EDAR. Por otro lado, los valores de k_2 determinados en el efluente de EDAR fueron iguales (acetaminofén) o ligeramente superiores (diclofenaco, ácido salicílico, ibuprofeno) que los obtenidos en agua ultrapura.

Con relación a las isotermas de equilibrio y los parámetros de ajuste en la tabla 3.7., el modelo de Sips fue el que ofreció mejores ajustes para diclofenaco, ibuprofeno y acetaminofén tanto en agua ultrapura como en el efluente de EDAR. Sin embargo, para el ácido salicílico fue la isoterma de Freundlich, la que mejor describió el equilibrio de adsorción sobre PS800-150. En cuanto a la capacidad de adsorción de PS800-150, esta fue diferente según el fármaco y disminuyó en el sentido diclofenaco > ibuprofeno ≈ acetaminofén > ácido salicílico, tal y como confirman los valores de Q_m (tabla 3.7.). Estas diferencias deben estar relacionadas con las propiedades de los propios fármacos, entre las cuales se ha podido constatar que la solubilidad en agua (S_w) y el coeficiente octanol-agua (K_{ow}) son especialmente determinantes (Calisto et al., 2015). Considerando las desviaciones estándar asociadas, en el caso del diclofenaco, ibuprofeno y acetaminofén, la capacidad máxima de adsorción (Q_m de Sips en la tabla 3.7.) fue similar en agua ultrapura y en el efluente de EDAR. Sin embargo, la K_{LF}, que normalmente se relaciona con la afinidad del adsorbente hacia el adsorbato, mostró diferente tendencia según el fármaco. Valores similares de K_{LF} fueron determinados para el equilibrio de adsorción de diclofenaco en agua ultrapura y en el efluente de EDAR mientras que en el caso del ibuprofeno y del acetaminofén, los valores en agua ultrapura fueron superiores. Para estos últimos, la menor afinidad entre adsorbente y adsorbato en el efluente de EDAR puede asociarse a la complejidad de esta matriz. Respecto al equilibrio de adsorción del ácido salicílico, los valores de K_F reflejaron una mayor afinidad adsorbente-adsorbato en agua ultrapura que en el efluente de EDAR, de la misma manera que los valores de n mostraron una adsorción más favorable en agua ultrapura. De ello se desprende que el equilibrio de adsorción del ácido salicílico en PS800-150 ha debido verse afectada por efectos de matriz en el efluente de EDAR. En cualquier caso, como para los otros fármacos, la capacidad máxima de adsorción del ácido salicílico fue equivalente en agua ultrapura y en el efluente de EDAR. Esto es especialmente relevante para la aplicación del carbonizado de lodos primarios de papelera como adsorbente para el tratamiento terciario de efluentes.

Tabla 3.6. Parámetros cinéticos de las ecuaciones de pseudo-primer y pseudo-segundo orden obtenidos a partir del ajuste de los resultados experimentales de la adsorción de cada fármaco sobre el carbonizado de lodos primarios de papelera (PS800-1500) en las dos matrices acuosas consideradas (efluente secundario de EDAR (ES-EDAR) y agua ultrapura (AUP). Nota: Se muestran los valores medios junto con la desviación estándar de tres réplicas experimentales.

		Fármacos							
		Diclofenaco		Ácido salicílico		Ibuprofeno		Acetaminofén	
		ES-EDAR	AUP	ES-EDAR	AUP	ES-EDAR	AUP	STP-SE	AUP
pseudo-primer orden	k_1 (min^{-1})	0,235 ± 0,130	0,153 ± 0,017	0,207 ± 0,038	0,129 ± 0,025	0,198 ± 0,033	0,138 ± 0,022	0,052 ± 0,005	0,061 ± 0,004
	q_e ($mg\ g^{-1}$)	19,94 ±0,02	22,77 ±0,31	7,94 ± 0,15	8,01 ± 0,22	12,19 ± 0,19	12,68 ± 0,27	12,64 ± 0,31	12,53 ± 0,21
	R^2	0,9971	0,9883	0,9861	0,9712	0,9832	0,9720	0,9774	0,9883
	S_{xy}	0,36	0,82	0,36	0,52	0,53	0,71	0,66	0,47
pseudo-segundo orden	k_2 ($g\,mg^{-1}\,min^{-1}$)	0,042 ± 0,003	0,015 ± 0,000	0,063 ± 0,015	0,027 ± 0,005	0,038 ± 0,006	0,021 ± 0,003	0,006 ± 0,001	0,007 ± 0,001
	q_e ($mg\ g^{-1}$)	20,30 ± 0,06	23,64 ± 0,05	8,13 ± 0,11	8,36 ± 0,15	12,60 ± 0,13	13,26 ± 0,16	13,50 ± 0,23	13,31 ± 0,17
	R^2	0,9996	0,9998	0,9944	0,9912	0,9956	0,9940	0,9914	0,9948
	S_{xy}	0,13	0,11	0,23	0,29	0,27	0,33	0,41	0,31

Tabla 3.7. Parámetros de equilibrio de los modelos de isoterma de Freundlich, Langmuir y Sips obtenidos a partir del ajuste de los resultados experimentales de la adsorción de cada fármaco sobre el carbonizado de lodos primarios de papelera (PS800-1500) en las dos matrices acuosas consideradas (efluente secundario de EDAR (ES-EDAR) y agua ultrapura (AUP). Nota: Se muestran los valores medios junto con la desviación estándar de tres réplicas experimentales.

		Fármacos							
		Diclofenaco		Ácido salicílico		Ibuprofeno		Acetaminofén	
		ES-EDAR	AUP	ES-EDAR	AUP	ES-EDAR	AUP	ES-EDAR	AUP
Freundlich	$K_F[mg\,g^{-1}\,(mg\,L^{-1})^{-1/n}]$	3,07 ± 0,31	3,70 ± 0,36	0,50 ± 0,04	0,90 ± 0,05	2,55 ± 0,29	4,91 ± 0,29	2,86 ± 0,38	3,95 ± 0,31
	n	2,32 ± 0,14	2,41 ± 1,40	1,62 ± 0,04	1,97 ± 0,05	2,76 ± 0,22	4,36 ± 0,31	2,73 ± 0,27	3,66 ± 0,28
	R^2	0,9744	0,9805	0,9949	0,9954	0,9617	0,9534	0,9438	0,9720
	S_{yx}	1,10	1,18	0,19	0,17	0,731	0,77	1,07	0,73
Langmuir	$Q_m\,(mg\,g^{-1})$	23,38 ± 1,28	26,69 ± 1,53	15,12 ± 1,06	12,08 ±1,99	12,93 ± 0,45	12,66 ± 0,30	15,53 ± 0,71	12,33 ± 0,65
	$K_L(L\,mg^{-1})$	0,058 ± 0,009	0,060 ± 0,012	0,013 ± 0,002	0,025 ± 0,005	0,098 ± 0,014	0,359 ± 0,046	0,077 ± 0,012	0,265 ± 0,077
	R^2	0,9714	0,9643	0,9875	0,9622	0,9739	0,9580	0,9721	0,9303
	S_{yx}	1,16	1,61	0,29	0,48	0,60	0,73	0,76	1,15
Sips	$Q_m\,(mg\,g^{-1})$	34,84 ± 8,44	53,16 ± 22,62			16,05 ± 2,30	15,36 ± 1,05	16,79 ± 2,25	19,74 ± 4,55
	$K_{LF}[mg\,g^{-1}\,(mg\,L^{-1})^{-1/n}]$	0,069 ± 0,012	0,062 ± 0,022			0,118 ± 0,017	0,372 ± 0,035	0,092 ± 0,021	0,230 ± 0,063
	n	1,49 ± 0,21	1,77 ± 0,29			1,38 ± 0,22	1,69 ± 0,20	1,15 ± 0,21	2,15 ± 0,379
	R^2	0,9852	0,9845			0,9824	0,9851	0,9734	0,9846
	S_{yx}	0,88	1,10			0,52	0,45	0,77	0,57

3.2.2. Adsorción de diclofenaco mediante adsorbentes comerciales

Como ya ha sido referido, los contaminantes emergentes (CEs) incluyen un amplio abanico de compuestos entre los cuales están los fármacos. Una vez que estas substancias fueron concebidas para provocar una respuesta fisiológica, la preocupación acerca de su presencia en el ambiente es creciente debido a su posible toxicidad y efectos negativos. Prueba de ello es que, en Enero de 2012, fue propuesta, por primera vez, la incorporación de 3 fármacos (diclofenaco, 17-betaestradiol (E2) y 17-alfa-etinilestradiol (EE2)) a la lista de sustancias prioritarias de la Directiva Marco del Agua (DMA, 2000/60/EC). Más tarde, bajo la Directiva 2013/39/EU, la Comisión estableció que estos tres fármacos estarían incluidos en la primera lista de observación de substancias que deben ser monitorizadas en los países miembros. Finalmente, la Decisión 2015/495/EU estableció la primera lista de observación, lista en la que se encuentran siete fármacos, siendo uno de ellos el diclofenaco.

El diclofenaco es un antiinflamatorio que posee actividades analgésicas y antipiréticas y está indicado por vía oral e intramuscular para el tratamiento de enfermedades reumáticas agudas, artritis reumatoidea, espondilitis anquilosante, artrosis, lumbalgia, gota en fase aguda, inflamación postraumática y postoperatoria, cólico renal y biliar, migraña aguda, y como profilaxis para dolor postoperatorio y dismenorrea. Se trata de un fármaco con elevado consumo que ha sido frecuentemente detectado en aguas residuales y también en aguas superficiales pues, debido a su baja biodegradabilidad, su eliminación en EDARs convencionales es incompleta (Vieno and Sillanpaa, 2014). Los tratamientos de adsorción han sido señalados como tratamientos terciarios adecuados para la eliminación de este tipo de contaminantes con la ventaja de que no suponen la generación de productos de transformación (Bolong et al., 2009). En este sentido, y dada la relevancia como contaminante del diclofenaco, este fármaco fue seleccionado en este trabajo para estudiar su adsorción, tanto en agua ultrapura como en el efluente de una EDAR, utilizando adsorbentes comerciales. Específicamente, fueron utilizados dos carbones activados (GPP20 y Pulsorb WP70, de Chemviron Carbon) y una resina polimérica no-iónica (Sepabeads SP207, de Resindion). En la tabla 3.8. se pueden ver las principales propiedades físicas de estos materiales.

Tabla 3.8. Principales propiedades físicas de los adsorbentes comerciales utilizados para el estudio de la adsorción de diclofenaco.

Adsorbente	**GPP20**	**Pulsorb WP270**	**Sepabeads SP207**
Matriz	Coal based steam activated carbon	Coal based steam activated carbon	Styrene and DVD copolymer
Color	Black carbon	Black carbon	Yellowish opaque beads
S_{BET} (m^2g^{-1})	725	1050	630
D (nm)	0.04	0.03	0.4

S_{BET} = área superficial calculada con base en la teoría de Brunauer-Emmet-Teller
D = diámetro medio de poro

Al comparar los valores de las tablas 3.4. y 3.8., es evidente que estos tres adsorbentes comerciales poseen mayores S_{BET} y menores D que el carbonizado obtenido a partir de lodos primarios de papelera (PS800-150) utilizado en la sección anterior para la adsorción de fármacos. Para poder compararlos en cuanto a su utilización, los adsorbentes comerciales de la tabla 3.8. se usaron bajo las mismas condiciones experimentales que PS800-150 para la adsorción de diclofenaco. Además de agua ultrapura, también se usó el efluente de EDAR cuya caracterización se mostró en la tabla 3.5. como matriz acuosa para el estudio de la eliminación de diclofenaco mediante los adsorbentes comerciales referidos en la tabla 3.8.

Igualmente, para el ajuste de los resultados cinéticos experimentales se utilizaron los modelos de pseudo-primer orden o Lagergren (Lagergren, 1808) y de pseudo-segundo orden (Ho and McKay, 1999). Respecto a los resultados de equilibrio, se determinaron los ajustes a los modelos de isoterma de Freundlich (Freundlich, 1906), de Langmuir (Langmuir, 1918) y de Sips (Sips, 1948).

Los parámetros obtenidos a partir del ajuste de los resultados experimentales a los modelos considerados están representados en la tabla 3.9. en el caso de los resultados cinéticos y en la tabla 3.10. para los resultados de equilibrio.

Los resultados experimentales y los valores de R^2 y S_{xy} en la tabla 3.9. muestran que el modelo de pseudo-segundo orden ofrece mejores ajustes que el de pseudo-primer orden para los adsorbentes comerciales utilizados y tanto en agua ultrapura como en el efluente de EDAR. Por otro lado, para cada adsorbente, no existen diferencias significativas entre las k_2 obtenidas en agua ultrapura y en el efluente de EDAR, por lo que se puede afirmar que, en estos casos, la velocidad de adsorción del diclofenaco no se ha visto afectada por la matriz acuosa. Además, se puede observar que la velocidad de adsorción en ambos carbones activados (GPP20 y WP270) es equivalente, mientras que la cinética es más lenta en la resina polimérica (SP207).

Con relación a las isotermas de equilibrio, los resultados experimentales se ajustan bastante bien a los tres modelos considerados. Sin embargo, es el modelo de isoterma de Sips, o modelo de Langmuir-Freundlich, el que mejor describe el equilibrio de adsorción de diclofenaco sobre los adsorbentes utilizados y en ambas matrices acuosas. Según este modelo, la capacidad máxima de adsorción (Q_m) de la resina polimérica es un orden de magnitud inferior a la de los carbones activados. Teniendo en cuenta las desviaciones estándar, para cada adsorbente, la capacidad máxima es equivalente en agua ultrapura y en el efluente de EDAR. En cualquier caso, hay que señalar que, para el carbón activado GPP20, la Q_m de Sips en el efluente de EDAR tiene una desviación estándar muy elevada. Esto se debe a que la isoterma no tiene un "plateau" bien definido sino que también se ajusta a la isoterma de Freundlich.

Tabla 3.9. Parámetros cinéticos de las ecuaciones de pseudo-primer y pseudo-segundo orden obtenidos a partir del ajuste de los resultados experimentales de la adsorción de diclofenaco sobre cada adsorbente comercial en las dos matrices acuosas consideradas (efluente secundario de EDAR (ES-EDAR) y agua ultrapura (AUP). Nota: Se muestran los valores medios junto con la desviación estándar de tres réplicas experimentales.

		Adsorbentes					
		GPP20		WP270		SP207	
		ES-EDAR	AUP	ES-EDAR	AUP	ES-EDAR	AUP
pseudo-primer orden	k_1 (min^{-1})	0,108 ± 0,015	0,104 ± 0,011	0,119 ± 0,007	0,115 ± 0,008	0,0023 ± 0,0003	0,0017 ± 0,0002
	q_e ($mg\ g^{-1}$)	184,40 ± 2,96	180,90 ± 2,13	291,90 ± 1,89	293,50 ± 2,27	28,45 ± 0,84	30,64 ± 0,83
	R^2	0,9820	0,9903	0,9972	0,996	0,9692	0,9734
	S_{xy}	8,33	5,99	5,14	6,16	1,98	1,92
pseudo-segundo orden	k_2 ($g mg^{-1} min^{-1}$)	0,00118 ± 0,00020	0,00119 ± 0,00010	0,00117 ± 0,00008	0,00106 ± 0,00003	0,00010 ± 0,00002	0,00007 ± 0,00001
	q_e ($mg\ g^{-1}$)	188,40 ± 2,09	188,70 ± 1,01	296,90 ± 1,09	299,1 ± 0,45	31,83 ± 0,92	33,94 ± 0,83
	R^2	0,993	0,9983	0,9993	0,9999	0,9835	0,9869
	S_{xy}	5,22	2,50	2,58	1,06	1,45	1,35

Tabla 3.10. Parámetros de equilibrio de los modelos de isoterma de Freundlich, Langmuir y Sips obtenidos a partir del ajuste de los resultados experimentales de la adsorción de diclofenaco sobre cada adsorbente comercial en las dos matrices acuosas consideradas (efluente secundario de EDAR (ES-EDAR) y agua ultrapura (AUP). Nota: Se muestran los valores medios junto con la desviación estándar de tres réplicas experimentales.

		Adsorbentes					
		GPP20		WP270		SP207	
		ES-EDAR	AUP	ES-EDAR	AUP	ES-EDAR	AUP
Freundlich	$K_F[mg\,g^{-1}\,(mg\,L^{-1})^{-1/n}]$	94,30 ± 5,39	74,53 ± 2,73	167,20 ± 12,05	96,07 ± 19,17	10,28 ± 0,63	5,12 ± 0,70
	n	6,252 ± 0,598	4,689 ± 0,214	6,186 ± 0,8822	3,343 ± 0,678	3,454 ± 0,225	2,212 ± 0,182
	R^2	0,954	0,9932	0,9074	0,8116	0,9689	0,9728
	S_{yx}	13,72	5,14	31,3	48,62	1,85	2,042
Langmuir	$Q_m\,(mg\,g^{-1})$	169,00 ± 8,10	182,10 ± 11,06	268,10 ± 12,78	333,00 ± 15,82	30,23 ± 1,19	36,90 ± 0,86
	$K_L(L\,mg^{-1})$	5,334 ± 1,440	0,327 ± 0138	7,157 ± 1,890	0,246 ± 0,038	0,551 ± 0,078	0,084 ± 0,006
	R^2	0,9252	0,9019	0,9371	0,9712	0,9695	0,9959
	S_{yx}	17,49	19,57	25,79	19,02	1,836	0,89
Sips	$Q_m\,(mg\,g^{-1})$	202,60 ± 12,59	445,50 ± 254,70	315,00 ± 18,64	300,80 ± 5,17	37,94 ± 2,31	38,63 ± 2,59
	$K_{LF}[mg\,g^{-1}\,(mg\,L^{-1})^{-1/n}]$	1,198 ± 0,259	0,158 ± 0,086	1,698 ± 0,422	0,182 ± 0,015	0,385 ± 0,038	0,087 ± 0,008
	n	2,208 ± 0,302	3,670 ± 0,495	1,912 ± 0,261	0,646 ± 0,038	1,628 ± 0,126	1,070 ± 0,092
	R^2	0,9896	0,9952	0,9868	0,9969	0,9953	0,9962
	S_{yx}	6,98	4,62	12,78	6,72	0,76	0,81

Respecto a las K_{LF} determinadas para el ajuste a isoterma de Sips, las correspondientes a la resina polimérica son un orden de magnitud inferior a las de los carbones activados, tanto en agua ultrapura como en el efluente de EDAR. Sin embargo, cabe destacar que, para cada adsorbente, las K_{LF} fueron un orden de magnitud superior en el efluente de EDAR que en agua ultrapura. Esto se corresponde con unas pendientes más acentuadas en las isotermas de adsorción en el efluente de EDAR y se relaciona con una mayor afinidad adsorbente-adsorbato en esta matriz. Este incremento de afinidad en aguas residuales comparando con agua ultrapura coincide con los resultados de otros autores utilizando carbón activado para la adsorción de ácido ftálico (Méndez-Díaz et al., 2012). Estos investigadores (Méndez-Díaz et al., 2012) atribuyeron la mayor afinidad al incremento de la hidrofobicidad de la superficie del carbón debido a la adhesión de micro-organismos presentes en el agua residual. También la presencia de sales en las aguas residuales puede afectar a la afinidad entre el adsorbente y el adsorbato (Pastrana-Martínez et al., 2010), aumentar la tensión superficial y disminuir la energía libre de los solutos orgánicos (Sahu et al., 2010). De hecho, algunos autores han verificado que la presencia de sales inorgánicas aumenta la eliminación de compuestos orgánicos en fase acuosa mediante carbón activado (Chang et al., 2013).

Comparando con los resultados de la sección anterior, cabe destacar que la capacidad de adsorción de diclofenaco por parte de PS800-150 (Q_m, en la tabla 3.7.), aunque un orden de magnitud inferior a la de los carbones activados comerciales utilizados en esta sección, es similar a la de la resina polimérica comercial (tabla 3.10.). En cualquier caso, para ninguno de los adsorbentes utilizados en este trabajo ha sido observada una disminución de la capacidad de adsorción en el efluente de EDAR respecto al agua ultrapura. Otros autores (Sotelo et al., 2012) sí verificaron una disminución de la capacidad de adsorción de varios fármacos en el efluente de una EDAR, lo que asociaron a la presencia de materia orgánica natural. A pesar de que la aplicación práctica sea el tratamiento de aguas residuales, la mayor parte de resultados publicados sobre adsorción de fármacos en fase acuosa refieren la utilización de agua ultrapura o destilada, lo que limita las posibles comparaciones de resultados.

3.3. Referencias

Aboyade, A.O., Görgens, J.F., Carrier, M., Meyer, E.L., Knoetze, J.H., 2013. Thermogravimetric study of the pyrolysis characteristics and kinetics of coal blends with corn and sugarcane residues. Fuel Process. Technol. 106, 310–320.

Bolong, N., Ismail, A.F., Salim, M.R., Matsuura, T., 2009. A review of the effects of emerging contaminants in wastewater and options for their removal. Desalination 239, 229–246.

Calisto, V., Ferreira, C.I.A., Oliveira, J.A.B.P., Otero, M., Esteves, V.I., 2015. Adsorptive removal of pharmaceuticals from water by commercial and waste-based carbons. J. Environ. Manage. 152, 83–90.

Calisto, V., Ferreira, C.I.A., Santos, S.M., Gil, M.V., Otero, M., Esteves, V.I., 2014. Production of adsorbents by pyrolysis of paper mill sludge and application on the removal of citalopram from water. Bioresour. Technol. 166, 335–344.

Calvo, L., Otero, M., Morán, A., García, A., 2001. Upgrading sewage sludges for adsorbent preparation by different treatments. Bioresour. Technol. 80, 143–148.

Chang, G., Bao, Z., Zhang, Z., Xing, H., Su, B., Yang, Y., Ren, Q., 2013. Salt-enhanced removal of 2-ethyl-1-hexanol from aqueous solutions by adsorption on activated carbon. J. Colloid Interface Sci. 412, 7–12.

Freundlich, H., 1906. Über die Adsorption in Lösungen. Zeitschrift für Phys. Chemie 57, 385–470.

Guo, Z., Bai, Z., Bai, J., Wang, Z., Li, W., 2015. Synergistic effects during co-pyrolysis and liquefaction of biomass and lignite under syngas. J. Therm. Anal. Calorim. 119.

Ho, I.S., McKay, G., 1999. Pseudo-second order model for sorption processes. Process Biochem. 34, 451–465.

Idris, S.S., Rahman, N.A., Ismail, K., 2012. Combustion characteristics of Malaysian oil palm biomass, sub-bituminous coal and their respective blends via thermogravimetric analysis (TGA). Bioresour. Technol. 123, 581–591.

Idris, S.S., Rahman, N.A., Ismail, K., Alias, A.B., Rashid, Z.A., Aris, M.J., 2010. Investigation on thermochemical behaviour of low rank Malaysian coal, oil palm biomass and their blends during pyrolysis via thermogravimetric analysis (TGA). Bioresour. Technol. 101, 4584–4592.

Kök, M. V, 2005. Temperature-controlled combustion and kinetics of different rank coal samples. J. Therm. Anal. Calorim. 79, 175–180.

Lagergren, S., 1808. Zur theorie der sogenannten adsorption gelöster stoffe. K. Sven. Vetenskapsakademiens, Handl. 24, 1–39.

Langmuir, I., 1918. the Adsorption of Gases on Plane Surfaces of Glass, Mica and Platinum. J. Am. Chem. Soc. 40, 1361–1403.

Méndez, A., Barriga, S., Fidalgo, J.M., Gascó, G., 2009. Adsorbent materials from paper industry

waste materials and their use in Cu(II) removal from water. J. Hazard. Mater. 165, 736–743.

Méndez, A., Barriga, S., Saa, A., Gascó, G., 2010. Removal of malachite green by adsorbents from paper industry waste materials. J. Therm. Anal. Calorim. 99, 993–998.

Méndez-Díaz, J.D., Abdel daiem, M.M., Rivera-Utrilla, J., Sánchez-Polo, M., Bautista-Toledo, I., 2012. Adsorption/bioadsorption of phthalic acid, an organic micropollutant present in landfill leachates, on activated carbons. J. Colloid Interface Sci. 369, 358–365.

Otero, M., Rozada, F., Morán, A., Calvo, L.F., García, A.I., 2009. Removal of heavy metals from aqueous solution by sewage sludge based sorbents: competitive effects. Desalination 239, 46–57.

Pastrana-Martínez, L.M., López-Ramón, M. V., Fontecha-Cámara, M.A., Moreno-Castilla, C., 2010. Batch and column adsorption of herbicide fluroxypyr on different types of activated carbons from water with varied degrees of hardness and alkalinity. Water Res. 44, 879–885.

Rozada, F., Otero, M., Parra, J.B., Morán, A., García, A.I., 2005. Producing adsorbents from sewage sludge and discarded tyres: Characterization and utilization for the removal of pollutants from water. Chem. Eng. J. 114, 161–169.

Rozada, F., Otero, M., García, A. I., Morán, A., 2007. Application in fixed-bed systems of adsorbents obtained from sewage sludge and discarded tyres. Dye. Pigment. 72, 47–56.

Sahu, K., McNeill, V.F., Eisenthal, K.B., 2010. Effect of salt on the adsorption affinity of an aromatic carbonyl molecule to the air-aqueous interface: Insight for aqueous environmental interfaces. J. Phys. Chem. C 114, 18258–18262.

Saldarriaga, J.F., Aguado, R., Pablos, A., Amutio, M., Olazar, M., Bilbao, J., 2015. Fast characterization of biomass fuels by thermogravimetric analysis (TGA). Fuel 140, 744–751.

Sips, R., 1948. Combined form of Langmuir and Freundlich equations. J. Chem. Phys. 16, 490–495.

Sotelo, J.L., Rodriguez, A.R., Mateos, M.M., Hernandez, S.D., Torrellas, S.A., Rodriguez, J.G., 2012. Adsorption of pharmaceutical compounds and an endocrine disruptor from aqueous solutions by carbon materials. J Env. Sci Heal. B 47, 640–652.

Tan, C., Yaxin, Z., Hongtao, W., Wenjing, L., Zeyu, Z., Yuancheng, Z., Lulu, R., 2014. Bioresource Technology Influence of pyrolysis temperature on characteristics and heavy

metal adsorptive performance of biochar derived from municipal sewage sludge. Bioresour. Technol. 164, 47–54.

Tan, C., Zeyu, Z., Rong, H., Ruihong, M., Hongtao, W., Wenjing, L., 2015. Chemosphere Adsorption of cadmium by biochar derived from municipal sewage sludge : Impact factors and adsorption mechanism. Chemosphere 134, 286–293.

Vieno, N., Sillanpaa, M., 2014. Fate of diclofenac in municipal wastewater treatment plant - A review. Environ. Int. 69, 28–39.

Wu, Z., Wang, S., Zhao, J., Chen, L., Meng, H., 2014. Synergistic effect on thermal behavior during co-pyrolysis of lignocellulosic biomass model components blend with bituminous coal. Bioresour. Technol. 169, 220–228.

Xiao, H. min, Ma, X. qian, Lai, Z. yi, 2009. Isoconversional kinetic analysis of co-combustion of sewage sludge with straw and coal. Appl. Energy 86, 1741–1745.

Xie, Z., Ma, X., 2013. The thermal behaviour of the co-combustion between paper sludge and rice straw. Bioresour. Technol. 146, 611–618.

Yanfen, L., Xiaoqian, M., 2010. Thermogravimetric analysis of the co-combustion of coal and paper mill sludge. Appl. Energy 87, 3526–3532.

Capítulo 4

4.Conclusiones

A partir del trabajo realizado, cuyos resultados se encuentran expuestos con detalle en las publicaciones incluidas como Anexos, las principales conclusiones que se pueden extraer son las siguientes:

i. En cuanto a sus propiedades térmicas, los lodos de papelera y muy especialmente los primarios, mostraron evidentes diferencias con relación al carbón comercial, destacando por su relativamente elevado contenido en volátiles, reducido porcentaje de carbono fijo y bajo poder calorífico.

ii. Las curvas DTG y DSC de la combustión del carbón evidenciaron un perfil típico de carbones bituminosos. En el caso de los lodos primarios, la pérdida de masa durante la combustión ocurrió en dos etapas: la primera y exotérmica, asociada al contenido volátil de la celulosa; y la segunda, sin desprendimiento de calor asociado, a la descomposición del carbonato cálcico (sin desprendimiento de calor). En el caso de los lodos secundarios, las curvas DTG y DSC revelaron tres etapas exotérmicas

(desvolatilización de la celulosa; combustión de la materia orgánica biodegradable; combustión del carbono fijo), seguidas de la descomposición del carbonato cálcico (sin desprendimiento de calor). A pesar de las grandes diferencias entre el carbón y los lodos de papelera, la combustión a temperatura programada de las mezclas (10 % en peso de lodos) permitió comprobar que la pérdida de masa (curvas DTG) y el desprendimiento de calor (curvas DSC) fueron muy similares a los de la combustión del carbón, especialmente en el caso de la mezcla con lodos secundarios.

iii. Al contrario que en el caso del carbón, las curvas DTG correspondientes a la pirólisis de los lodos, además de mostrar una pérdida de masa apreciable, reflejaron bastantes semejanzas con las de su combustión. Por otro lado, las curvas DTG de la pirólisis de las mezclas de carbón con lodos (10 % en peso) revelaron un incremento de la reactividad del carbón durante la pirólisis que fue especialmente significativo para la mezcla con lodos primarios.

iv. La energía de activación aparente media (E) determinada mediante el método de análisis cinético no-isotérmico de Flynn–Wall–Ozawa para la combustión del carbón, los lodos primarios y los secundarios fue de 85 kJ/mol, 155 y 199 kJ/mol, respectivamente. A pesar de las diferencias, la E determinada para la combustión de las mezclas de carbón con lodos primarios y de carbón con lodos secundarios fueron muy próximas a las del carbón (91 y 88 kJ/mol, respectivamente). Al contrario, la E determinada para la pirólisis del carbón (256 kJ/mol) fue superior a las de los lodos primarios (120 kJ/mol) y secundarios (197 kJ/mol). En cuanto que la E determinada para las pirólisis de las mezclas de carbón con lodos primarios y secundarios, las E (165 y 68 kJ/mol, respectivamente) fueron próximas, e incluso inferiores, a las de los lodos.

v. Tanto para la combustión como para la pirólisis de las mezclas, las E determinadas fueron inferiores a las calculadas a partir de la composición de dichas mezclas (10 % en peso de lodos), indicando la existencia de interacciones entre los constituyentes del carbón y de los lodos probablemente asociadas al contenido celulósico de los últimos. Del mismo modo, las curvas DTG calculadas para combustión y pirólisis de las mezclas de carbón con lodos, tanto primarios como secundarios, mostraron pérdidas de masa superiores a las experimentales, permitiendo inferir efectos sinérgicos negativos.

vi. Bajo las condiciones experimentales empleadas y en agua ultrapura, el carbonizado obtenido a partir de lodos primarios de papelera fue capaz de adsorber los fármacos considerados (diclofenaco, ácido salicílico, ibuprofeno y acetaminofén) en tiempos de equilibrio inferiores a 200 min y siguiendo una cinética de pseudo-segundo orden. La velocidad de adsorción decreció para los fármacos considerados en el sentido: ácido salicílico > diclofenaco > ibuprofeno > acetaminofén. En cuanto al equilibrio, la isoterma

de Sips fue la que mejor describió los resultados experimentales, excepto para el ácido salicílico, que se ajustó mejor a la isoterma de Freundlich. En agua ultrapura la capacidad de adsorción de los fármacos considerados varió entre 38,84 y 15,12 mg/g, disminuyendo en el sentido diclofenaco > ibuprofeno ≈ acetaminofén > ácido salicílico.

vii. Bajo idénticas condiciones experimentales, utilizando como fase acuosa el efluente secundario de una estación depuradora de aguas residuales urbanas (EDAR), la velocidad y capacidad de adsorción de los fármacos considerados no disminuyeron comparativamente a las determinadas en agua ultrapura.

viii. Fueron utilizados tres adsorbentes comerciales: dos carbones activados (WP270 y GPP20) y una resina polimérica (SP207) para estudiar la adsorción de diclofenaco en fase acuosa. Para los tres materiales, la cinética siguió el modelo de pseudo-segundo orden y el equilibrio la isoterma de Sips. Las constantes cinética k_2 determinadas para los carbones activados y la resina polimérica fueron alrededor de 0,001 y 0,0001 g/mg min, respectivamente, valores que no se vieron afectados por efectos de matriz cuando se usó el efluente secundario de EDAR. La capacidad de adsorción de los carbones activados fue un orden de magnitud superior a la de la resina polimérica (38 mg/g). Esta capacidad es similar a la determinada para el carbonizado de lodos primarios de papelera, que mostraron una cinética más rápida (k_2 ≈ 0,006 mg/g min). Por otro lado, aunque no se observaron variaciones significativas de la velocidad o capacidad de adsorción relacionadas con la matriz acuosa considerada (agua ultrapura o efluente secundario de EDAR), si se verificó un incremento de la afinidad adsorbente-adsorbato (dada por la constante K_{LF} de la isoterma de Sips) en el efluente de EDAR.

Capítulo 5

5. Anexos: Publicaciones que integran la tesis doctoral

Anexo I

Coimbra, R.N., Paniagua, S., Escapa, C., Calvo, L.F., Otero, M., 2015. Combustion of primary and secondary pulp mill sludge and their respective blends with coal: A thermogravimetric assessment. Renewable Energy 83, 1050-1058.
http://dx.doi.org/10.1016/j.renene.2015.05.046

Renewable Energy 83 (2015) 1050–1058

Contents lists available at ScienceDirect

Renewable Energy

journal homepage: www.elsevier.com/locate/renene

Combustion of primary and secondary pulp mill sludge and their respective blends with coal: A thermogravimetric assessment

Ricardo N. Coimbra [a], Sergio Paniagua [a], Carla Escapa [a], Luis F. Calvo [a], Marta Otero [a, b, *]

[a] Department of Applied Chemistry and Physics, IMARENABIO (Institute of Environment, Natural Resources and Biodiversity), Campus de Vegazana, University of León, 24071 León, Spain

[b] Department of Chemistry and CESAM (Centre for Environmental and Marine Studies), University of Aveiro, Campus de Santiago, 3810-193 Aveiro, Portugal

ARTICLE INFO

Article history:
Received 16 December 2014
Received in revised form
24 April 2015
Accepted 24 May 2015
Available online 9 June 2015

Keywords:
TGA/DSC analysis
Paper industry
Isoconversion model
Co-combustion
Vyazovkin

ABSTRACT

Properties of primary and secondary pulp mill sludge are unalike and are also very different from those of coal. Thermogravimetric analysis was used to assess the separate combustion of coal, primary and secondary pulp mill sludge. Then, the co-combustion of coal with primary and with secondary pulp mill sludge was studied under identical experimental conditions. Both Differential Thermogravimetry burning profiles (DTG) and Differential Scanning Calorimetric analysis (DSC) showed remarkable differences between the combustion of coal, primary and secondary paper mill sludge. However, compared with the combustion of coal, the effects of adding a 10 wt.% of either primary or secondary paper mill sludge were not relevant in terms of weight loss or heat release. This was further proved by non-isothermal kinetic analysis, which was used to evaluate the apparent activation energy corresponding to the single combustions and to the co-combustion of blends.

© 2015 Elsevier Ltd. All rights reserved.

1. Introduction

The pulp and paper industry is a strategic economic sector in Europe, which production is concentrated in a few countries [1]. Along with most of industrial sectors, it has suffered significantly from the economic crisis in 2008 and 2009 and it has been largely affected by the economic slowdown that began in mid-2011. Yet, European pulp and paper industry remains an important contributor to EU economic growth and job creation, with its performance still stronger than other energy-intensive sectors in Europe [2]. As a counterpart, pulp and paper production processes are very demanding in terms of energy and water consumption and the pulp and paper industry is considered one of the most polluting in the world [3].

In pulp and paper mills, the high water usage results in the generation of large wastewater volumes, which must be treated to accomplish with environment regulations on effluents discharge [4] and therefore sludge is produced as an unavoidable waste from pulp and paper mill wastewater treatment. Globally, in a pulp and paper mill, around 50 kg of dry sludge result from the production of a tonne of paper, approximately 70% being primary sludge and 30% secondary sludge [5]. Primary sludge is generated in the clarification of process water treatments while secondary sludge is generated in the clarifier of the biological units of the wastewater treatment. Secondary sludge volumes are generally lower than those corresponding to the primary sludge, since most of the heavy, fibrous or inorganic solids are removed in the primary clarifier [6]. In any case, due to the large volumes of sludge generated, the management of these wastes in an economically and environmentally acceptable manner has been a critical issue for the mills [7–9].

Due to legislation and increasing taxes, landfilling has being disregarded as a final destination for wastes. The problems associated with the landfilling of paper mill sludge are the large volumes involved and the possibility of hazardous substances leaking into the environment. In consequence, it is obvious the necessity of considering other management options. Under the appropriate control, thermal valorisation has been pointed out as a main management option for such wastes, although research is still needed for optimization of the processes [6]. In fact, thermal valorisation has already been used for large-scale disposal of sludge from paper industry [10] and different technologies have been studied at a laboratory scale [11]. Among thermal conversion

* Corresponding author. Department of Applied Chemistry and Physics, IMARENABIO (Institute of Environment, Natural Resources and Biodiversity), University of León, Campus de Vegazana, León 24071, Spain.
E-mail addresses: marta.otero@unileon.es, marta.otero@ua.pt (M. Otero).

http://dx.doi.org/10.1016/j.renene.2015.05.046
0960-1481/© 2015 Elsevier Ltd. All rights reserved.

options, co-combustion of paper mill sludge together with coal in existing infrastructures may be an interesting option, since these facilities are already equipped with appropriate devices for emission control [12,13].

Thermogravimetric analysis (TGA) has been largely used to characterize the thermal decomposition of coal and, more recently, to characterize biomass fuels [14,15] and their co-combustion with coal [16,17]. The advantage of TGA is that provides a rapid assessment of the fuel value, the temperatures at which combustion starts and ends and other characteristics such as maximum reactivity temperature or total combustion time. For any fuel or blend, the necessary information to estimate combustion efficiency, residence time, excess air, boiler design, etc., may be obtained by TGA in an easy way. Furthermore, TGA has proved to provide a way of rapidly assessing the kinetics of thermally induced reaction such as the combustion of carbonaceous materials [18].

Comparatively with sewage sludge, TGA results on the combustion of sludge from the treatment of industrial effluents are scarce in the literature. In the specific case of the pulp and paper industry, a few recent works [19–22] dealing with paper mill sludge (mixed primary and secondary sludge) have shown that combustion and co-combustion with coal may be feasible waste to energy management options for such wastes. In this context, Yanfen et al. [21] studied the combustion of different paper sludge ratios (10, 20 and 50%) with coal and found that blends with a low weight percentage of paper sludge ($\leq$10 wt.%) resulted in combustion profiles similar to that of coal. This is coincident with findings on the co-combustion of sewage sludge with coal [16,17], which recommended the utilization of relative low percentages ($\leq$10 wt.%) of such wastes in view of their co-combustion with coal in existing infrastructures.

Primary and secondary sludge from the pulp and paper industry have different properties, are produced in different proportion and are not equally amenable for the different treatment options [23]. However, to our best knowledge, the separate combustion of primary and secondary pulp mill sludge or their co-combustion with other fuels has never been studied. Thus, in this manuscript, TGA and differential scanning calorimetry (DSC) were used to determine the combustion behaviour of primary pulp mill sludge, secondary pulp mill sludge and their blends with coal. The main aim was to evaluate the effect that adding a low percentage (10 wt.%) of primary or secondary pulp mill sludge has on the combustion of coal and its kinetics.

2. Materials and methods

2.1. Materials

For this study, a bituminous coal (C) coming from the north coalfield of León (Spain) and commonly exploited in thermal power stations has been used. Primary and secondary pulp mill sludge were provided by a mill that uses eucalyptus wood (*Eucalyptus globulus*) for the production of pulp by the kraft ECD (elemental chlorine free) process. At this mill, primary and secondary sludge are generated at an average rate of 20 and 10 kg per ton of air dried pulp produced, respectively. Primary sludge (L1) results from fibres rejected after the cooking/digestion at the pulping step, losses of fibres and other solids within liquid streams involved in the process (for example, washing and bleaching). The composition of the L1 is very similar to that of the pulp and basically consists of fibres. Secondary sludge (L2) results from the biological treatment to which wastewater is submitted after the primary clarification. Essentially, secondary sludge is dehydrated biomass that results from the action of microorganisms used to reduce, under aerobic conditions, the wastewater organic matter content.

Before thermal analysis, C, L1 and L2 were air-dried at room temperature (298 ± 3 K) until constant weight (which took about 10 days), disaggregated manually and grinded in a ball mill. Then a Humboldt sieve shaker was used (30 min) in order to have a 0.105 mm < particle diameter < 0.210 mm, which is within the size range commonly used in circulating fluidized boilers (CFBs), minimize differences in heat of combustion values and is large enough to ensure homogeneous ignition [15, and references therein]. Then, C, L1 and L2 were characterized as it is next described. Moisture content was determined gravimetrically by the oven drying method. Higher heating value (HHV) at a constant volume was measured by means of an isoperibol oxygen bomb calorimeter LECO AC-600 according to the procedure UNE EN/4918. Proximate determinations were made according to modified procedures from ASTM D 3172 to D 3175 (Standard Practice for Proximate Analysis of Coal and Coke), E 870 (Standard Methods for Analysis of Wood Fuels), D 1102 (ash in wood) and E 872 (volatile matter). For the elemental determination, a LECO equipment model CHN-600 was used to determine the carbon, hydrogen and nitrogen content. Sulphur was determined by means of a LECO equipment, model SC-132.

2.2. Thermogravimetric analysis

Non-isothermal combustion runs were carried out in a Setaram equipment, model SETSYS Evolution, which was calibrated (baseline, weight, temperature and heat flow) prior utilization. Throughout these runs, TG and DSC (Differential Scanning Calorimetry) signals were simultaneously registered. For this purpose, samples of C, L1 and L2 and their blends were submitted to dynamic runs carried out up to 1200 K at the following heating rates ($\beta = dT/dt$): 0.1, 0.2, 0.4 and 0.5 K/s. For each sample and heating rate, three repetitive TG-DSC curves were obtained in order to guarantee reproducibility of the results. All dynamic runs were carried out on a pan containing 25 ± 1 mg of the corresponding sample or blend, which was verified to be an appropriate sample size to ensure representativeness and to avoid heat or mass transfer limitations. Oxidizing atmosphere inside the furnace during temperature-programmed combustion was obtained by means of a continuous air flow of 100 cm^3/min at 1 atm (101 kPa).

2.3. Kinetic theory

The rate of heterogeneous solid-state reactions can be generally described by:

$$\frac{d\alpha}{dt} = k(T)f(\alpha) \tag{1}$$

where t is time, $k(T)$ is the temperature-dependent constant and $f(\alpha)$ is a function called the reaction model, which describes the dependence of the reaction rate on the extent of reaction or fractional conversion, α.

The mathematical description of decomposition from a solid-state is commonly defined in terms of a kinetic triplet, as activation energy, E, Arrhenius parameter, A, and an algebraic expression of the kinetic model in function of the fractional conversion $f(\alpha)$, which can be related to experimental data as follows:

$$\frac{d\alpha}{dt} = Ae^{-E/RT}f(\alpha) \tag{2}$$

Next, the above rate expression (2) can be converted into non-isothermal rate expressions describing reaction rates as a function of temperature at a constant heating rate, β:

$$\frac{d\alpha}{dT} = \frac{A}{\beta} A e^{-E/RT} f(\alpha) \tag{3}$$

Integrating up to conversion, α, Eq. (3) gives:

$$\int_0^{\alpha} \frac{d\alpha}{f(\alpha)} = g(\alpha) = \frac{A}{\beta} \int_{T_0}^{T} e^{-E/RT} dT \tag{4}$$

where $g(\alpha)$ is the integral kinetic function or integral reaction model when its form is mathematically defined.

Kinetic analysis is usually carried out to acquire an appropriate description of the process in terms of the apparent activation energy (E). Different methods may be used to analyse solid-state kinetic data [24], which may be classified according to the selected experimental conditions and the performed mathematical analysis. Experimentally, either isothermal or non-isothermal methods are employed. Although the concepts of solid-state kinetics were established on the basis of isothermal experiments, the sample takes some time to reach the experimental temperature in this kind of experiments [24]. Non-isothermal experiments avoid this drawback. Matematically, there are two possible approaches, the model-fitting and isoconversional (free model). Model-fitting methods were the first and most popular, especially for isothermal experiments, but they have lost popularity with respect to isoconversional methods, which can compute kinetic parameters without modelling assumptions [25,26]. Model-free isoconversional methods allow estimating the activation energy as a function of α without pre-fixing the reaction model. The essential assumption is that the reaction rate for a constant extent of conversion, α, depends only on the temperature [27–29].

In non-isothermal kinetics, several isoconversional methods may be used. To use these methods, a series of experiments has to be conducted at different heating rates [30,26]. During the last decade, these methods have been frequently used to study the thermal decomposition kinetics of very different types of biofuels [16,17,31–35].

In this work, the activation energy from non-isothermal thermogravimetric (TG) data corresponding to the combustion of C, L1, L2 and their blends (CL1 and CL2, respectively) was carried out by the application of the Vyazovkin kinetic model [30,24], which is next described.

In Eq. (4), since E/2RT » 1, the temperature integral can be approximated by:

$$\int_{T_0}^{T} e^{-E/RT} dT \approx \frac{R}{E} T^2 e^{-E/RT} \tag{5}$$

Substituting the temperature integral and taking the logarithm, we have that:

$$\ln \frac{\beta}{T^2} = \ln \left[\frac{RA}{Eg(\alpha)} \right] - \frac{E}{R} \frac{1}{T} \tag{6}$$

To apply this method, it is necessary to obtain at least three different heating rates (β), the respective conversion curves being evaluated from the measured TG curves. For each conversion value (α), $ln(\beta/T^2)$ plotted versus $1/T$, gives a straight line with slope $-E/R$, and thus the activation energy is obtained as a function of the conversion.

3. Results and discussion

3.1. Characterization of materials

The results of the elementary and proximate analysis for the coal, the primary and secondary pulp mill sludge here used are depicted in Table 1. As it may be seen, these carbonaceous materials have very different properties.

The proximate analysis showed that moisture values are comprised between 1.7 and 11.8%, which are typical equilibrium values for the storeroom conditions of temperature and moisture. With respect to the ash yield, that of C (30.33%) is slightly lower than that of L1 (33.10%) but higher than that of L2 (24.39%). Relative high ash contents are undesirable in many combustion facilities and care should be taken in the design stage to overcome derived difficulties. However, in this work, the ashes content of L2 is lower than that of C and the ash percentage of L1 is only slightly higher than that of C. Regarding the amount of volatiles, L1 (65.25%) and L2 (58.64%) yield much higher amount of volatiles than C (8.01%). Volatile contents here determined for L1 and L2 are in the range of typical values determined for biomass fuels [14]. The higher volatile matter content of biomass, as compared with coal is known to improve the combustion of the latter, resulting in a better burn out and lower unburned carbon in the ashes. However, for the co-combustion of C with L1 or L2, the combustor should be previously adapted due to the relative high volatiles content of these wastes, especially in the case of L1. Finally, it is to highlight that, as a consequence of their higher volatile content, both L1 and L2 have much lower fixed-carbon (1.65 and 16.97%, respectively) than C (61.66%), which is expected to largely affect their separate combustion profiles.

With respect to the elementary analysis, C has much higher carbon content (62.07%) than L2 (41.25%) and, especially, than L1 (15.37%). Therefore, from an environmental point of view, a desirable reduction of CO_2-emissions may be expected in the combustion or co-combustion of L1 and/or L2 with respect to that of C. On the contrary, C has much lower oxygen content (1.93%) than L1 and L2 (49.58 and 20.66%, respectively). Both C and L2 have a similar sulphur content (2.21 and 1.89%, respectively), which is higher than that of L1 (0.24%). In any case, the combustion of L2 and, especially, L1, would imply lower SO_x emissions than that of C. The trends of the hydrogen and the nitrogen are similar, L2 having the highest contents of both elements (5.03 and 6.78%, respectively), followed by C (2.30 and 1.16%, respectively) and then L1 (1.35 and 0.36%, respectively). Therefore, in order to minimise NO_x emissions, the co-combustion of L1 with C would be more favourable than that of C. Regarding L2 co-combustion with C, however it could be expected an increase of NO_x emissions, Tsai et al. [12] showed that, when co-firing paper mill sludge and coal in a CFB boiler, NO_x emissions did not increase due to the higher N content of sludge. In order to justify this finding, these authors [12] highlighted that it is known that NO emissions are not strongly dependent on the fuel nitrogen content.

Finally, as regards the calorific value, C, which has a HHV typical of a bituminous coal, showed the highest value. The HHV of L2 is relatively high, and similar to lignite coal characteristic values. Meanwhile, L1 has a relative low HHV, which is even lower than values typical of peat. Therefore, the co-combustion of C with L2 and, especially, with L1, would mean a decrease in the energy input as compared with the combustion of C. Apart from the energy related consequences, the smaller the energy input, the less air is needed. However, the decrease in air flow rate also depends on the oxygen content of L1 and L2. Therefore, in the co-combustion of C with pulp mill sludge, the relative high oxygen content of L2 and, especially, of L1 would decrease the oxygen required for combustion.

Table 1
Proximate analysis, elementary analysis, and calorific values for the coal (C), the primary (L1) and the secondary (L2) pulp sludge used in combustion studies.

Sample	Moisture content	Volatiles (d.b.)	Ashes (d.b.)	FC (d.b.)	C (d.b.)	H (d.b.)	N (d.b.)	S (d.b.)	O[a] (d.b.)	HHV (d.b.)
	%	%	%	%	%	%	%	%	%	J g^{-1}
C	11.2	8.01	30.33	61.66	62.07	2.30	1.16	2.21	1.93	24381.61
L1	1.7	65.25	33.10	1.65	15.37	1.35	0.36	0.24	49.58	2488.86
L2	11.8	58.64	24.39	16.97	41.25	5.03	6.78	1.89	20.66	16428.99

FC = fixed carbon.
HHV = high heat value.
d.b. = dry basis.
[a] Calculated by difference.

3.2. Thermogravimetric analysis

The DTG (Differential Thermogravimetric) and DSC (Differential Scanning Calorimetry) results obtained from the temperature programmed combustions of the samples are shown in Figs. 1 and 2, respectively, for the different heating rates used (β = 0.1, 0.2, 0.4 and 0.5 K/s). The results corresponding to the coal (C), to the primary pulp mill sludge (L1), to the secondary pulp mill sludge (L2) and to their respective blends (CL1 and CL2) are represented together.

On raising the temperature, combustion of the sample takes place with an associated weight loss and a heat release, which may be observed both in DTG (Fig. 1) and DSC (Fig. 2) curves. Once the fuel content of the sample is exhausted, the mass, corresponding to the ashes remains stable and heat is not further released.

Fig. 1 shows the combustion profiles (DTG curves) corresponding to coal C, which may be considered typical of a bituminous coal. In the DTG curves corresponding to C, the thermal decomposition and loss of volatiles as well as char gasification occur in two steps at the lower heating rates (β = 0.1, 0.2 K/s) and practically together at higher heating rates (β = 0.4, 0.5 K/s), which points to the large contribution of fixed carbon content in C (see Table 1) to the mass loss during combustion. Moreover, a slight weight gain due to oxygen chemisorption may be observed during the combustion of coal [36]. This chemisorption was not observable in the DTG curves corresponding to L1 and L2, neither in those corresponding to CL1 and CL2. Also, the DTG combustion curves corresponding to L1 and L2 were different between them and also very different from C. In the case of L1, the weight loss associated to the process took place in two main and well separated stages. This is coincident with results found by Yanfen et al. [21] who related these two stages to the burning of combustible components and the decomposition of mineral filling, respectively. The first stage must include the combustion of cellulose, which typically occurs at around 600 K [21] while the second stage must be related to the combustion of calcium carbonate, which is characterized by burning at relative high temperatures [37]. Still, the DTG curves corresponding to the blend (CL1) mostly resembled those of coal, although a small weight loss peak in the temperature range of the first stage of L1 combustion remained in DTG curves of CL1. This peak, which was more evident at relative large β, may be related to the cellulose content of L1 and its existence should be considered when planning co-combustion. Moreover, the combustion of CL1 ended at slightly lower temperatures than that of C, which was also more evident for relative large β. This delay trend suggests that some interaction may occur between C and L1 that retards the combustion of blends. Therefore, when planning the co-combustion of L1 with coal, these differences must be taken into account for the appropriate design of the process.

Regarding L2, four combustion steps may be observed throughout combustion, which are especially plain for the largest β used in this work (0.5 K/s). These steps may not been contrasted

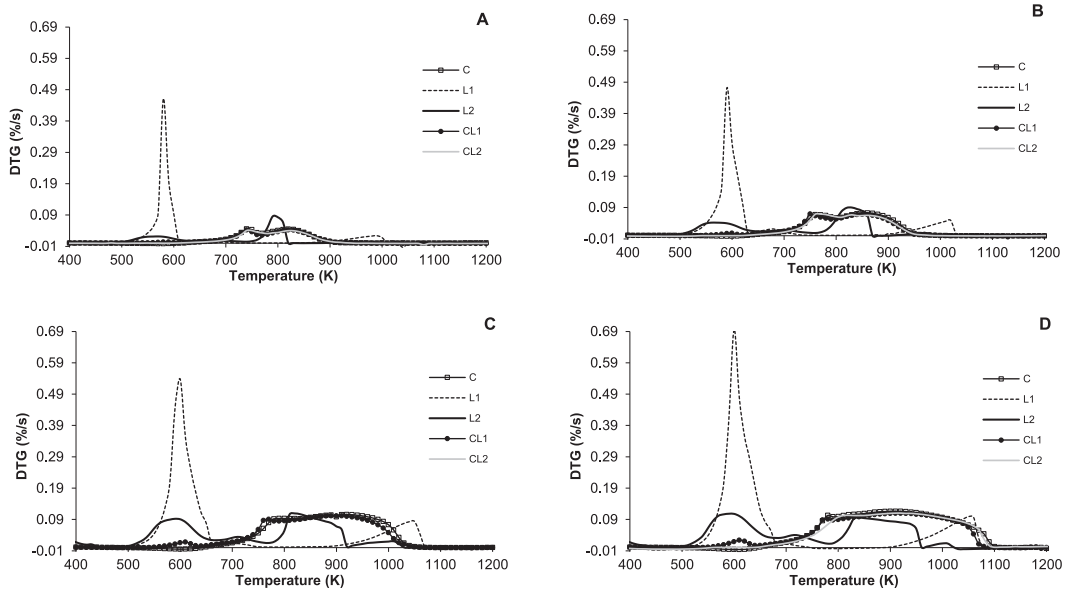

Fig. 1. Combustion and co-combustion DTG curves for coal (C), primary pulp mill sludge (L1), secondary pulp mill sludge (L2) and their blends (CL1 and CL2, respectively) at the heating rates (β) of: A: 0.1 K/s; B: 0.2 K/s; C: 0.4 K/s; and D: 0.5 K/s.

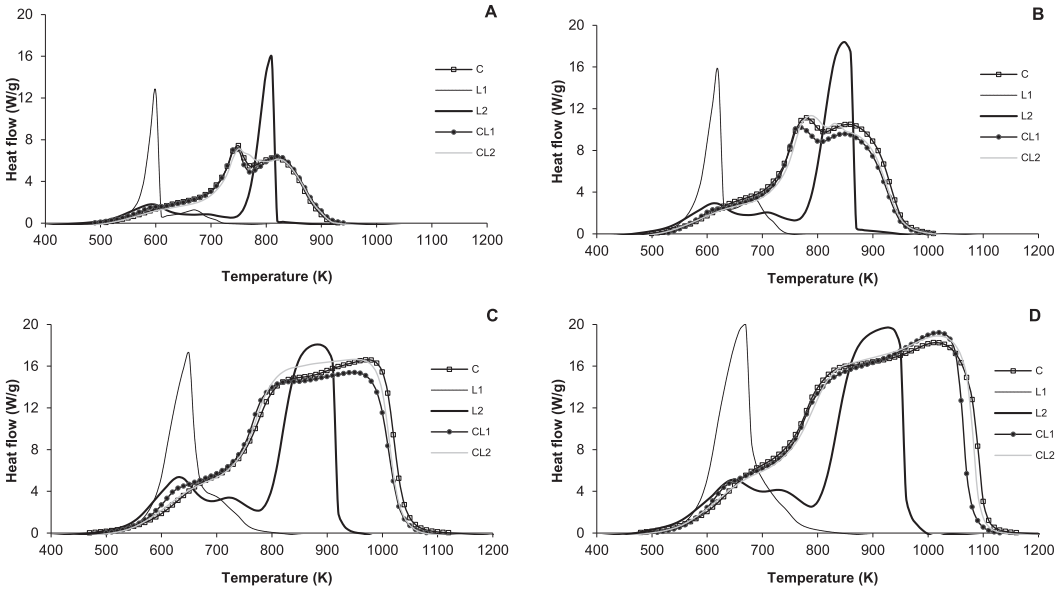

Fig. 2. Combustion and co-combustion DSC curves for coal (C), primary pulp mill sludge (L1), secondary pulp mill sludge (L2) and their blends (CL1 and CL2, respectively) at the heating rates (β) of: A: 0.1 K/s; B: 0.2 K/s; C: 0.4 K/s; and D: 0.5 K/s.

with the literature, since, to our best knowledge, there are not published DTG curves on the combustion of secondary paper or pulp mill sludge, but only on the combustion of mixed primary and secondary sludge. The first step, may be related to volatiles yield and combustion of cellulose [21,37]. The associated mass loss occurred in the same temperature range that the first step of the L1 combustion, although it was not as sharp as in the case of L1. Then, a second step, which relevance increases with increasing β, must correspond to the combustion of biodegradable organics, probably produced during the biological treatment of PS. The combustion of fixed carbon occurred next, in the same temperature range as for C. Finally, there is a small peak related to the decomposition of mineral content [21]. This last step is more evident with increasing β and occurred in the same temperature range as the second stage of the combustion of L1.

The DTG curves corresponding to C, L1 and L2 displayed clear modifications with increasing heating rate (β): (i) an increase of the temperature at which thermal decomposition starts; (ii) a broadening in the combustion range of temperature; (iii) an increase of the rate of weight loss (%/s) at each peak; (iv) an overlapping of the two separate steps in the combustion of C. In the case of the blends, even for increasing heating rates (β), the combustion profiles have kept analogous to those of coal.

The DSC (Differential Scanning Calorimetry) curves shown in Fig. 2 evidenced that the chemisorption stage, which was seen at around 600 K in the DTG curves (Fig. 1) of coal, is exothermic. Also, and contrary to weight loss (Fig. 1), exothermicity in DSC curves (Fig. 2) starts at around 500 K either in the combustion of C, L1, L2 or their respective blends. In the case of L1, heat release must be related to the release and combustion of volatile matter and organics. There was not heat release associated to the second stage of weight loss that occurred in the DTG curve corresponding to L1, given that it was due to the decomposition of mineral content. The same applies to L2, for which, heat was released at three different steps, corresponding to the combustion of volatiles, organic material and fixed carbon. Even when DTG curves corresponding to L1, L2 and C were very different, heat release during the combustion of CL1 and CL2 followed the same trend than that of C.

The characteristic parameters of the combustion profiles are shown in Table 2. As may be seen in Fig. 1, combustion profiles corresponding to C, L1 and L2 were quite unalike. The curves corresponding to each material showed characteristic stages with different relative weight and occurring at different temperatures. On the contrary, combustion profiles corresponding to blends were nearly coincident to those of C. Parameters in Table 2 further support these differences and/or similitudes. In this sense, the T_v and T_f in Table 2 correspond to the temperatures at which volatiles start to be released and at which weight stabilizes, respectively. Meanwhile, for each DTG curve, the T_m corresponds to the temperature at which occurs the maximum weight loss rate, that is, the DTG_{max}.

Table 2
Characteristic parameters obtained from burning profiles of coal (C), primary mill sludge (L1), secondary mill sludge (L2) and their respective blends with coal (CL1 and CL2).

Sample	T_v (K)	T_m (K)	T_f (K)	DTG_{max} (%/s)	t_q (s)
C (0.1 K/s)	614	744	944	0.0465	3300
C (0.2 K/s)	623	777	1016	0.0731	1965
C (0.4 K/s)	642	906	1100	0.1058	1145
C (0.5 K/s)	649	915	1114	0.1162	930
L1 (0.1 K/s)	479	579	1009	0.4606	5300
L1 (0.2 K/s)	481	591	1034	0.4707	2765
L1 (0.4 K/s)	487	595	1067	0.5379	1455
L1 (0.5 K/s)	490	598	1077	0.6969	1174
L2 (0.1 K/s)	465	792	975	0.0866	5100
L2 (0.2 K/s)	475	824	995	0.0907	2600
L2 (0.4 K/s)	480	814	1030	0.1117	1375
L2 (0.5 K/s)	485	596	1030	0.1090	1090
CL1 (0.1 K/s)	516	740	970	0.0424	4540
CL1 (0.2 K/s)	523	752	1015	0.0700	2460
CL1 (0.4 K/s)	525	899	1083	0.1017	1395
CL1 (0.5 K/s)	529	923	1105	0.1097	1152
CL2 (0.1 K/s)	584	744	963	0.0423	3790
CL2 (0.2 K/s)	608	765	1010	0.0704	2010
CL2 (0.4 K/s)	613	901	1076	0.1033	1158
CL2 (0.5 K/s)	627	933	1098	0.1112	942

T_v = onset temperature for volatile release and weight loss.
T_m = temperature of maximum weight loss rate.
T_f = final combustion temperature detected as weight stabilization.
DTG_{max} = maximum weight loss rate.
t_q = burning time; time interval from the moment the dried sample starts to lose weight until the moment combustion ends and weight stabilizes.

The T_v are similar in the combustion of L1 and L2 but lower than in the combustion of CL1, CL2 and C. Regarding the temperature at which the maximum weight loss rate occurs (Tm), L1 showed lower values than CL1, CL2 and C. In the case of L2, T_m is higher than that of C, CL1 and CL2 for the DTG curves obtained at relative low β (0.1 and 0.2 K/s). However, at relative high β (0.4 and 0.5 K/s), overlapping of oxidative pyrolysis and char combustion stages in the DTG curves of C, CL1 and CL2 occurred. Then, at these β (0.4 and 0.5 K/s), L2 showed lower T_m than C, L1 and L2. Furthermore, at the highest β, it may be observed in Fig. 1 that the main peak in the combustion of L2 is the corresponding to the volatiles, which are more reactive than fixed carbon. Regarding the T_f, the highest values were those corresponding to L1, but with increasing β, T_f corresponding to C, CL1 and CL2 increased until becoming slightly higher than that of L1. The maximum weight loss rate values (DTG_{max}) corresponding to L1 were outstanding, so reflecting the pronounced weight loss associated to the combustion of cellulosic matter. With respect to L2, the combustion of fixed carbon showed a DTG_{max} slightly higher than that of C at β = 0.1, 0.2 and 0.4 K/s. This was not true at β = 0.5 K/s, due to overlapping of stages in the DTG curve of C. In any case, at each β, DTG_{max} corresponding to C, CL1 and CL2 are alike. Finally, with respect to the burning times (t_q), they were much longer for the combustion of L1 and L2 than for that of C, which t_q were close to those of CL1 and CL2. For all materials and their blends, t_q decreased with increasing β, but those corresponding to C, CL1 and CL2 remained comparable. Parameters in Table 2 make plain that the combustion of L1 and L2 could not been carried out in the facilities were coal is currently burned but would require adapted infrastructures. On the contrary, the parameters given in Table 2 for the combustion of C, CL1 and CL2 support the possibility of using existing infrastructures for the co-combustion of coal with either primary or secondary pulp mill sludge. Therefore, direct co-combustion of C with either L1 or L2 may be a feasible waste to energy management option for pulp mill sludge. In direct co-combustion, biomass and coal are burned in the same boiler, although separate mills and burners should be used due to the large differences between the fuels properties.

The enthalpies and characteristic temperatures corresponding to the DSC curves are shown in Table 3. In the case of the onset temperatures for heat release (T_i), these are very similar and close to 500 °C for all the materials and blends. In the case of the final combustion temperature (T_e), this was higher for C than for L1 and L2, since there is not heat release associated to the decomposition of the mineral content of L1 and L2. With respect to the temperature of maximum energy release (T_{max}), L1 showed the lowest values, which is associated to the combustion of its high volatiles content. On the other hand, in agreement with the corresponding T_m (Table 2) from DTG curves (Fig. 1), L2 displayed higher T_{max} than C for β = 0.1 and 0.2 K/s but lower values than C for β = 0.4 and 0.5 K/s. These differences are related to overlapping of heat peaks corresponding to the oxidative pyrolysis and char combustion of C with increasing β. Differently release associated to the combustion of L2 is related to its fixed carbon content. Regarding the higher maximum heat flow (HF_{max}), at β = 0.1 K/s, L2 displayed a higher maximum heat flow (HF_{max}) than L1, and L1 higher than C. However, differences were decreasing with increasing β, so at β = 0.5 K/s, HF_{max} corresponding to C, L1 and L2 were quite similar. With respect to the enthalpy from DSC curves (ΔH), L1 displayed quite lower values than L2 and, especially, than C. No results have been found in the literature regarding heat release during the combustion of sludge from the paper industry. Otero et al. [38] reported heat release associated to the combustion of sewage sludge (SS) and there are main differences between the corresponding DSC curves and the here determined for L1 and L2. In the case of T_i the determined for SS are similar to those of L1 and L2. Also, the T_e determined for SS are comparable to that of L2, although higher than that of L1. Most noticeable, the T_{max} in the combustion of SS is in between the here determined from the DSC curves corresponding to L1 and that of L2. However the big differences in parameters determined in the present work between C, L1 and L2, in the case of CL1 and CL2, the T_e, T_{max}, HF_{max} and ΔH values were very similar to those of C, as it corresponds to DSC curves in Fig. 2. In fact, from a heat release point of view, the co-combustion of C with L1 and L2 (10 wt.%) in this work is more similar to that of C than in the case of the co-combustion of SS (10 wt.%) with C [38]. From a practical point of view of the co-combustion, apart from weight loss, heat release is of upmost importance. Results in this work evidence that, also from an energetic point of view, the direct co-combustion of C with L1 or L2 (10 wt.%) may be a feasible management option for the latter.

Table 3
Characteristic parameters obtained from DSC profiles for the combustion of coal (C), primary mill sludge (L1), secondary mill sludge (L2) and their respective blends with coal (CL1 and CL2).

Sample	T_i (K)	T_{max} (K)	T_e (K)	HF_{max} (W/g)	ΔH (J/g)
C (0.1 K/s)	500	748	934	7.48	12,753
C (0.2 K/s)	496	779	1016	11.11	12,571
C (0.4 K/s)	467	973	1125	16.60	12,291
C (0.5 K/s)	465	1014	1169	18.25	12,829
L1 (0.1 K/s)	492	602	730	13.00	3197
L1 (0.2 K/s)	478	622	750	15.99	3772
L1 (0.4 K/s)	487	654	811	17.38	3172
L1 (0.5 K/s)	491	667	840	19.95	3367
L2 (0.1 K/s)	465	808	860	15.95	7408
L2 (0.2 K/s)	465	850	995	18.36	7587
L2 (0.4 K/s)	475	882	957	18.08	6572
L2 (0.5 K/s)	471	927	997	19.70	6762
CL1 (0.1 K/s)	485	745	945	7.35	12,874
CL1 (0.2 K/s)	523	766	1005	10.23	11,242
CL1 (0.4 K/s)	496	948	1083	15.39	11,797
CL1 (0.5 K/s)	502	1019	1132	19.20	12,154
CL2 (0.1 K/s)	513	750	928	7.12	12,272
CL2 (0.2 K/s)	508	788	1010	11.39	11,745
CL2 (0.4 K/s)	510	951	1076	16.65	12,302
CL2 (0.5 K/s)	498	1018	1137	18.89	12,622

T_i = onset temperature for energy release and peak integration.
T_{max} = temperature of maximum energy release during combustion.
T_e = temperature at the end of energy release during combustion.
HF_{max} = maximum heat flow.
ΔH = enthalpy from the DSC combustion profile.

On the whole, parameters in Tables 2 and 3 confirm the above said with respect to Figs. 1 and 2 and make plain differences between the combustion of coal, primary and secondary pulp mill sludge while evidence similarities between the combustion of C, CL1 and CL2.

3.3. Kinetic analysis

The TG curves obtained from the temperature programmed combustions of the pure samples and blends at the heating rates (β) of 0.1, 0.2, 0.4 and 0.5 K/s are depicted in Fig. S-1 as Supplementary Material. The weight loss during combustion is shown for C, L1, L2 and their respective blends, CL1 and CL2. As it was previously said, for all the heating rates, burning of coal starts at higher temperatures than that of L1 or L2. Meanwhile, depending on β, burning of coal ended before or at similar temperature than burning of L1 and/or L2. Regarding the ash yield, or residual weight after burning, it was 31, 32 and 23% for C, L1 and L2, respectively. Six different percentages of conversion are pointed out in each curve: 10, 20, 30, 40, 50 and 60%.

Fig. 3 shows the plots of $ln\,(\beta/T^2)$ *vs.* $1/T$ to the several conversion degrees (α) corresponding to the combustion of *C*, *SS* and their blends. According with the Vyazovkin method [30], straight lines with the angular coefficient $-E/R$ were obtained.

Table 4 shows the values of *E* estimated by the Vyazovkin method at each α together with R^2 of the corresponding fitting. The average *E* determined for the coal C was 65 kJ/mol, while the obtained *E* for L1 and L2 were 151 and 198 kJ/mol, respectively. Comparing the coal with L1 and L2, the differences obtained for *E* are the same magnitude than those obtained for different rank coals [39]. Compared with *E* values determined for paper mill sludge those here estimated for L1 and L2 were slightly lower than those determined by Xie et al. [22] and slightly higher than those obtained by Liu et al. [20]. Apparent activation energies determined in other studies from non-isothermal TG data on the combustion of biomass, are mostly the same order than those here estimated for L1 and L2 [31,33,34,40].

However the *E* determined for the combustion of L1 and L2 is an order of magnitude higher than that estimated for C, the same order *E* were estimated for the blends (10 wt.%) as for the C combustion. Nevertheless, it must be highlighted that, although *E* obtained for L1 was lower than that obtained for L2, in the blends with coal *E* estimated for CL1 was higher than for CL2. This must be related to the very different combustion profile of L1 compared with that of C, given that L1 did not show a fixed carbon combustion step. Also, the E estimated for the combustion of CL1 is slightly higher than what would proportionally correspond for the relative L1 and coal contents (73.6 kJ mol^{-1}). While the E value estimated for CL2 is equivalent to the one calculated on a proportional basis (78.3 kJ mol^{-1}).

Globally, results obtained in this work showed that, under the appropriate conditions, co-combustion of primary and, especially secondary pulp mill sludge with coal may play an important role for the disposal of such wastes accounting for not big extra costs. Once more, thermogravimetric analysis was used in this work as a first and fast assessment tool for the consideration of co-combustion in existing infrastructures. This sort of assessment is essential for the evaluation of this management option for wastes such as these under study, since sludge from the treatment of industrial effluents may be quite different.

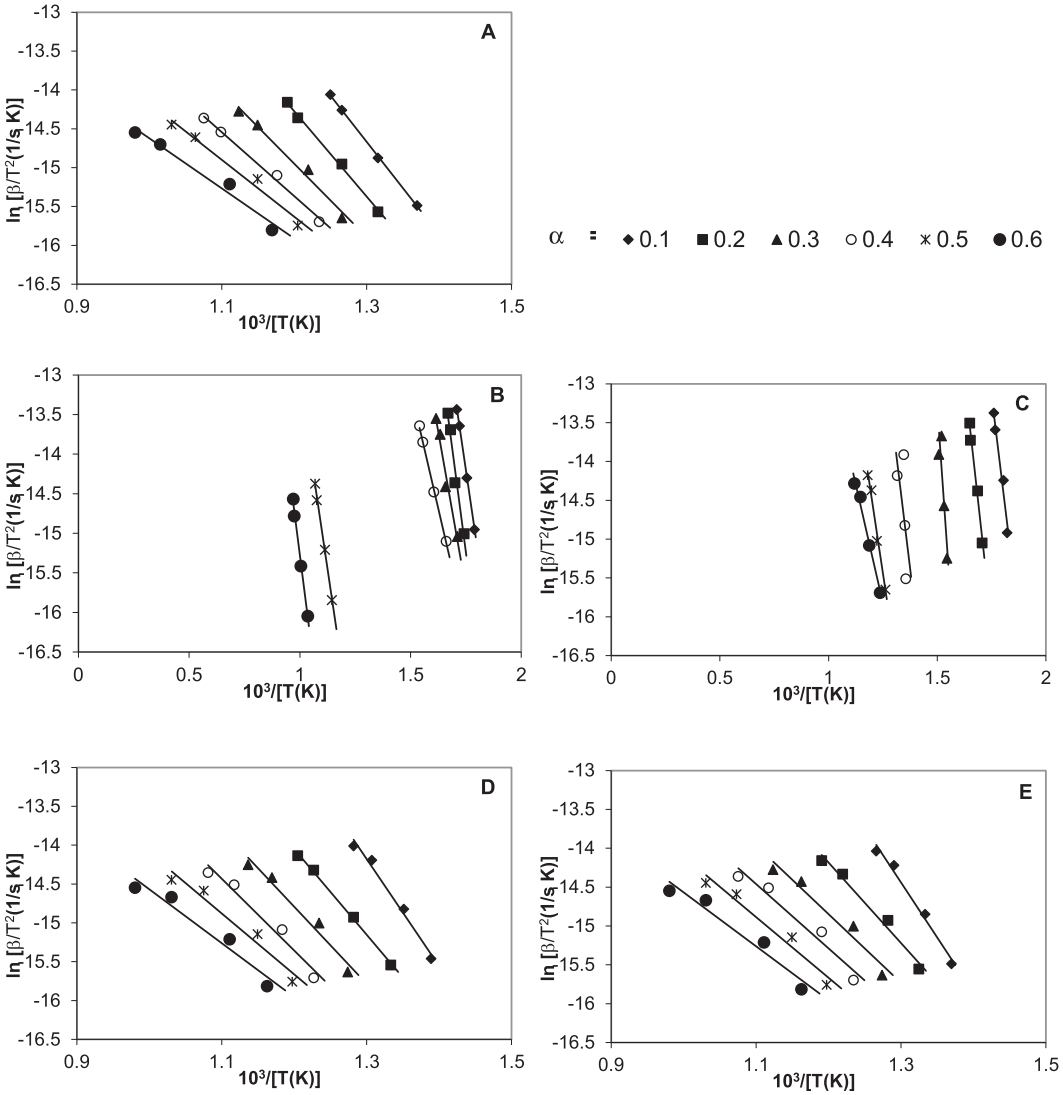

Fig. 3. Curves of fitting to kinetic model proposed by Vyazovkin to various conversion degrees (α) corresponding to the combustion of coal (C), primary pulp mill sludge (L1), secondary pulp mill sludge (L2) and their blends (CL1 and CL2, respectively) at different heating rates.

Table 4
Apparent activation energy (E) estimated for the combustion of C, L1, L2 and their blends at the considered conversion degrees (α).

Sample	α	Activation energy (kJ/mol)	
		Vyazovkin model	R^2
C	0.1	99.1	0.9950
	0.2	91.3	0.9971
	0.3	78.6	0.9831
	0.4	6.8	0.9926
	0.5	60.8	0.9778
	0.6	53.6	0.9726
		65.0[a]	
L1	0.1	159.7	0.9999
	0.2	177.0	0.9715
	0.3	132.1	0.9684
	0.4	100.6	0.9984
	0.5	156.4	0.9969
	0.6	181.4	0.9924
		151.2[a]	
L2	0.1	192.6	0.9665
	0.2	210.8	0.9824
	0.3	334.8	0.8223
	0.4	192.4	0.9374
	0.5	155.4	0.9858
	0.6	102.2	0.9869
		198.0[a]	
CL1	0.1	114.6	0.9842
	0.2	91.7	0.9976
	0.3	82.4	0.9637
	0.4	77.0	0.9651
	0.5	65.1	0.9541
	0.6	57.6	0.9448
		81.4[a]	
CL2	0.1	117.9	0.9842
	0.2	86.0	0.9782
	0.3	73.5	0.9487
	0.4	68.8	0.9519
	0.5	64.8	0.9579
	0.6	57.6	0.9448
	0.1	117.9	0.9842
		78.1[a]	

[a] Calculated as arithmetic average of the several E values obtained for the different conversion degrees shown in Fig. 3.

4. Conclusions

The elementary and proximate analysis, calorific values, DTG and DSC curves showed remarkably differences between coal, primary and secondary sludge. However these differences, both the DTG and the DSC curves corresponding to the temperature programmed combustion of their blends (sludge wt. 10%) were nearly coincident with those corresponding to coal combustion. Moreover, the apparent activation energy estimated for the co-combustion of coal with primary or secondary pulp mill sludge approached that of coal. On the whole, these results point to co-combustion of coal with primary and, especially, with secondary pulp mill sludge as a feasible management option for such wastes, which, furthermore, may provide a reduction on CO_2 and NO_x derived emissions.

Acknowledgements

We would like to thank assistance given by María Pilar González Alonso and José Alonso de Linaje, from LARECOM (Spain). Authors also thank the kind collaboration of Luís Machado and José Luís Amaral from RAIZ – Instituto de Investigação da Floresta e do Papel (Portugal). FCT funding to the Associated Laboratory CESAM is acknowledged. C. Escapa acknowledges the Spanish Ministry of Education, Culture and Sports for her PhD fellowship (FPU12/03073). S. Paniagua thanks University of León for his grant, funded by the research program ULE-2014. M. Otero acknowledges support by the Spanish Ministry of Economy and Competitiveness, State Secretariat for Research, Development and Innovation (RYC-2010-05634).

Appendix A. Supplementary data

Supplementary data related to this article can be found at http://dx.doi.org/10.1016/j.renene.2015.05.046.

References

[1] CEPI, Key Statistics 2013, Confederation of European Paper Industries (CEPI), 2014 (accessed 15.11.14), http://www.cepi.org/topics/statistics/keystatistics2013.
[2] CEPI, CEPI'S Online Sustainability Report, Confederation of European Paper Industries (CEPI), 2013 (accessed 15.11.14), http://www.cepi-sustainability.eu/.
[3] B.K. Ince, Z. Cetecioglu, O. Ince, Pollution prevention in the pulp and paper industries, environmental management in practice, in: Dr Elzbieta Broniewicz (Ed.), InTech, 2011, ISBN 978-953-307-358-3, http://dx.doi.org/10.5772/23709. Available from: http://www.intechopen.com/books/environmental-management-in-practice/pollution-prevention-in-the-pulp-and-paper-industries.
[4] D. Pokhrel, T. Viraraghavan, Treatment of pulp and paper mill wastewater- a review, Sci. Total Environ. 333 (2004) 37–58.
[5] A. Elliott, T. Mahmood, Survey benchmarks generation, management of solid residues, Pulp Pap. 79 (2005) 49–55.
[6] M.C. Monte, E. Fuente, A. Blanco, C. Negro, Waste management from pulp and paper production in the European Union, Waste Manag. 29 (2009) 293–308.
[7] Y. Wei, R.T. VanHouten, A.R. Borger, D.H. Eikelboom, Y. Fan, Minimization of excess sludge production for biological wastewater treatment, Water Res. 37 (2003) 4453–4467.
[8] T. Mahmood, A. Elliott, A review of secondary sludge reduction technologies for the pulp and paper industry, Water Res. 40 (2006) 2093–2112.
[9] A. Stoica, M. Sandberg, O. Holby, Energy use and recovery strategies within wastewater treatment and sludge handling at pulp and paper mills, Bioresour. Technol. 100 (2009) 3497–3505.
[10] A.C. Caputo, P.M. Pelagagge, Waste-to-energy plant for paper industry sludges disposal: technical-economic study, J. Hazard. Mater. B 81 (2001) 265–283.
[11] D. Shin, S. Jang, J. Hwang, Combustion characteristics of paper mill sludge in a lab-scale combustor with internally cycloned circulating fluidized bed, Waste Manag. 25 (2005) 680–685.
[12] M.Y. Tsai, K.T. Wu, C.C. Huang, H.T. Lee, Co-firing of paper mill sludge and coal in an industrial circulating fluidized bed boiler, Waste Manag. 22 (2002) 439–442.
[13] W.L.E. Magalhães, A.E. Job, C.A. Ferreira, H.D. da Silva, Pyrolysis and combustion of pulp mill lime sludge, J. Anal. Appl. Pyrol. 82 (2008) 298–303.
[14] J.F. Saldarriaga, R. Aguado, A. Pablos, M. Amutio, M. Olazar, J. Bilbao, Fast characterization of biomass fuels by thermogravimetric analysis (TGA), Fuel 140 (2015) 744–751.
[15] M.E. Sanchez, M. Otero, X. Gómez, A. Morán, Thermogravimetric kinetic analysis of the combustion of biowastes, Renew. Energy 34 (2009) 1622–1627.
[16] M. Otero, L.F. Calvo, M.V. Gil, A.I. García, A. Morán, Co-combustion of different sewage sludge and coal: a non-isothermal thermogravimetric kinetic analysis, Bioresour. Technol. 99 (14) (2008) 6311–6319.
[17] M. Otero, M.E. Sánchez, X. Gómez, Co-firing of coal and manure biomass: a TG/MS approach, Bioresour. Technol. 102 (2011) 8304–8309.
[18] R. López-Fonseca, I. Landa, M.A. Gutiérrez-Ortiz, J.R. González-Velasco, Non-isothermal analysis of the kinetics of the combustion of carbonaceous materials, J. Therm. Anal. Calorim. 80 (2005) 65–69.
[19] D. Vamvuka, N. Salpigidou, E. Kastanaki, S. Sfakiotakis, Possibility of using paper sludge in co-firing applications, Fuel 88 (2009) 637–643.
[20] K. Liu, X.Q. Ma, H.M. Xiao, Experimental and kinetic modeling of oxygen-enriched air combustion of paper mill sludge, Waste Manag. 30 (2010) 1206–1211.
[21] L. Yanfen, M. Xiaoqian, Thermogravimetric analysis of the co-combustion of coal and paper mill sludge, Appl. Energy 87 (2010) 3526–3532.
[22] Z. Xie, X. Ma, The thermal behaviour of the co-combustion between paper sludge and rice straw, Bioresour. Technol. 146 (2013) 611–618.
[23] A. Elliott, T. Mahmood, Pretreatment technologies for advancing anaerobic digestion of pulp and paper biotreatment residues, Water Res. 41 (2007) 4273–4286.
[24] S. Vyazovkin, C.A. Wight, Isothermal and non-isothermal kinetics of thermally stimulated reactions of solids, Int. Rev. Phys. Chem. 17 (1998) 407–433.
[25] S. Vyazovkin, C.A. Wight, Model-free and model-fitting approaches to kinetic analysis of isothermal and nonisothermal data, Thermochim. Acta 340–341 (1999) 53–68.
[26] A. Khawam, D.R. Flanagan, Role of isoconversional methods in varying activation energies of solid-state kinetics: I. isothermal kinetic studies, Thermochim. Acta 429 (2005) 93–102.

[27] H. Friedman, Kinetics of thermal degradation of char-forming plastics from thermo-gravimetry. Application to a phenolic plastic, J. Polym. Sci. Part C6 (1965) 183–195.
[28] T. Ozawa, A new method of analyzing thermogravimetric data, B. Chem. Soc. Jpn. 38 (1965) 1881–1886.
[29] J.H. Flynn, L.A. Wall, A quick, direct method for the determination of activation energy from thermogravimetric data, Polym. Lett. 4 (1966) 323–328.
[30] S. Vyazovkin, Evaluation of activation energy of thermally stimulated solid-state reactions under arbitrary variation of temperature, J. Comput. Chem. 18 (1997) 393–402.
[31] B. Ramajo-Escalera, A. Espina, J.R. García, J.H. Sosa-Arnao, S.A. Nebra, Model-free kinetics applied to sugarcane bagasse combustion, Thermochim. Acta 448 (2006) 111–116.
[32] M. Benbouzid, S. Hafsi, Thermal and kinetic analyses of pure and oxidized bitumens, Fuel 87 (2008) 1585–1590.
[33] H.-m. Xiao, X.-q. Ma, Z.-y. Lai, Isoconversional kinetic analysis of co-combustion of sewage sludge with straw and coal, Appl. Energy 86 (2009) 1741–1745.
[34] S.S. Idris, N.A. Rahman, K. Ismail, Combustion characteristics of Malaysian oil palm biomass, sub-bituminous coal and their respective blends via thermogravimetric analysis (TGA), Bioresour. Technol. 123 (2012) 581–591.
[35] P. Tiwari, M. Deo, Compositional and kinetic analysis of oil shale pyrolysis using TGA-MS, Fuel 94 (2012) 333–341.
[36] P.-f. Fu, N. Wang, B. Yu, B. Zhang, Y. Liu, H.-ch Zhou, Investigation on the transient enthalpy of coal combustion, in: H. Qui, B. Zhao (Eds.), Cleaner Combustion and Sustainable World, Springer, 2013, p. 423.
[37] S.S. Idris, N. Abd Rahman, K. Ismail, A.B. Alias, Z. Abd Rashid, M.J. Aris, Investigation on thermochemical behaviour of low rank Malaysian coal, oil palm biomass and their blends during pyrolysis via thermogravimetric analysis (TGA), Bioresour. Technol. 101 (2010) 4584–4592.
[38] M. Otero, X. Gomez, A.I. García, A. Morán, Effects of sewage sludge blending on the coal combustion: a thermogravimetric assessment, Chemosphere 69 (2007) 1740–1750.
[39] M.V. Kök, Temperature-controlled combustion and kinetics of different rank coal samples, J. Therm. Anal. Calorim. 79 (2005) 175–180.
[40] S. Munir, S.S. Daood, W. Nimmo, A.M. Cunliffe, B.M. Gibbs, Thermal analysis and devolatilization kinetics of cotton stalk, sugar cane bagasse and shea meal under nitrogen and air atmospheres, Bioresour. Technol. 100 (2009) 1413–1418.

Anexo II

Coimbra, R.N., Paniagua, S., Escapa, C., Calvo, L.F., Otero, M., 2015. Thermogravimetric analysis of the co-pyrolysis of a bituminous coal and pulp mill sludge. Journal of Thermal Analysis and Calorimetry 122, 1385-1394.
http://dx.doi.org/10.1007/s10973-015-4834-3

J Therm Anal Calorim (2015) 122:1385–1394
DOI 10.1007/s10973-015-4834-3

Thermogravimetric analysis of the co-pyrolysis of a bituminous coal and pulp mill sludge

R. N. Coimbra[1] · S. Paniagua[1] · C. Escapa[1] · L. F. Calvo[1] · M. Otero[1,2]

Received: 16 February 2015 / Accepted: 2 June 2015 / Published online: 26 June 2015
© Akadémiai Kiadó, Budapest, Hungary 2015

Abstract Thermal valorization of organic wastes by co-processing with coal may be a management option for such wastes. In this work, the separate pyrolysis of coal and primary and secondary pulp mill sludge was assessed by thermogravimetric (TG) analysis. Then, under the same experimental conditions, the pyrolysis TG curves of the coal blends with a 10 mass% of either primary or secondary pulp mill sludge were obtained. The corresponding differential thermogravimetry curves made evident that the devolatilization of coal starts at higher temperature and reaches higher char yields than that of primary or secondary paper mill sludge. Under blending, lower devolatilization temperatures and char yields, close to the weighted calculated ones, are observed. Non-isothermal kinetic analysis showed that the Arrhenius activation energy (E) corresponding to the pyrolysis of coal was lower than that corresponding to either L1 or L2. Moreover, lower E than the weighted calculated ones was determined for the co-pyrolysis of the blends.

Keywords Carbonization · Thermal conversion · Kinetics · Paper industry · Wastes

✉ M. Otero
marta.otero@unileon.es; marta.otero@ua.pt

[1] Department of Applied Chemistry and Physics, IMARENABIO (Institute of Environment, Natural Resources and Biodiversity), University of León, Campus de Vegazana, 24071 León, Spain

[2] Department of Chemistry and CESAM (Centre for Environmental and Marine Studies), University of Aveiro, Campus de Santiago, 3810-193 Aveiro, Portugal

Introduction

In the European Union (EU), the pulp and paper industry is a key economic sector, contributing to the EU growth and job creation [1, 2]. However, from an environmental point of view, it is well known that the pulp and paper industry is very demanding in terms of energy and water consumption, and it is one of the most polluting in the world [3]. Given the large water usage, huge volumes of wastewater are generated, which must be treated before discharge in order to accomplish environment regulations [4]. Thorough the primary and secondary wastewater treatment steps, sludge is produced as an unavoidable waste. Globally, in a pulp and paper mill, around 50 kg of dry sludge results from the production of a tonne of paper, approximately 70 % being primary sludge and 30 % secondary sludge [5, 6]. Thus, the management of these wastes in an economically and environmentally sustainable way is a critical issue for the pulp and paper industry [7–9].

In the EU, landfilling has been prohibited as a final destination for this sort of wastes. Other alternatives such as agriculture application or composting are not viable due to the composition of sludge from the pulp and paper industry [10]. Thermal valorization by combustion, gasification, and/or pyrolysis, which has been widely studied as a management option for organic waste materials, has been pointed as a possible management option for wastes from the pulp and paper industry [10]. In any case, research is still needed for the optimization of the associated processes [6].

Among thermal conversion options, pyrolysis of organic waste materials produces three fractions: liquid, solid and gaseous fractions [11]. The gaseous and liquid fractions are potential fuels, whereas the solid fraction produced may be used as an adsorbent for pollutants removal from contaminated water [12, 13].

Thermogravimetric (TG) analysis has been largely used to characterize the thermal decomposition during the pyrolysis [14] and co-pyrolysis [15] of different carbonaceous wastes. TG analysis provides a rapid assessment of the temperatures at which pyrolysis starts and ends and other characteristics such as maximum reactivity temperature or total pyrolysis time. Furthermore, TG analysis may provide a way of rapidly assessing the pyrolysis kinetics, reaction rates and activation energy [15].

In this work, properties of primary and secondary sludge from the pulp and paper industry were evaluated and compared with those of a bituminous coal. Then TG analysis was used to determine the thermal behaviour and apparent activation energy related to the pyrolysis of primary pulp mill sludge, secondary pulp mill sludge and their respective blends with coal. The main aims were: (1) to assess differences between the separate pyrolysis of these materials and (2) in view of co-processing in existing infrastructures, to evaluate how the addition of a low percentage (10 mass%) of primary or secondary pulp mill sludge affects the pyrolysis of coal.

Materials and methods

Materials

For this study, a bituminous coal (C) coming from the north coalfield of León (Spain) and commonly exploited in thermal power stations has been used. Primary sludge and secondary pulp mill sludge were provided by a mill that uses eucalyptus wood (*Eucalyptus globulus*) for the production of pulp by the kraft elemental chlorine-free (ECD) process. At this mill, primary sludge and secondary sludge are generated at an average rate of 20 and 10 kg per ton of air-dried pulp produced, respectively. Primary sludge (L1) results from fibres rejected after the cooking/digestion at the pulping step, losses of fibres and other solids within liquid streams involved in the process (for example, washing and bleaching). The composition of the L1 is very similar to that of the pulp and basically consists of cellulosic fibres. Secondary sludge (L2) results from the biological treatment to which wastewater is submitted after the primary clarification. During the biological treatment, microorganisms are used to reduce the organic content of this wastewater. Essentially, secondary sludge is the resulting dehydrated biomass, including recalcitrant organic matter, e.g., lignocellulose residues.

Before TG analysis, C, L1 and L2 air-dried samples were sieved so to have a 0.105 mm < particle diameter < 0.210 mm and characterized as it is next described. Moisture content was determined gravimetrically by the oven-drying method. Higher heating value (HHV) at a constant volume was measured by means of an adiabatic oxygen bomb calorimeter. Proximate determinations were made according to modified procedures from ASTM D 3172 to D 3175 (Standard Practice for Proximate Analysis of Coal and Coke), E 870 (Standard Methods for Analysis of Wood Fuels), D 1102 (ash in wood) and E 872 (volatile matter). For the elemental determination, a LECO equipment model CHN-600 was used to determine the carbon, hydrogen and nitrogen content. Sulphur was determined by means of a LECO equipment, model SC-132.

Thermogravimetric analysis

Non-isothermal TG runs were carried out under inert atmosphere in a Setaram equipment, model SETSYS Evolution, which was calibrated (baseline, mass and temperature) prior to utilization. Samples of C, L1 and L2 and their respective blends CL1 (containing 10 mass% of L1) and CL2 (containing 10 mass% L2) were submitted to dynamic runs at four different heating rates ($\beta = \mathrm{d}T/\mathrm{d}t$) in order to determine the apparent activation energy by the isoconversional kinetic model of Vyazovkin [16]. With this purpose, samples and blends were heated at 0.5, 0.4, 0.2 and 0.1 K s^{-1} up to 1200 K. Relative low heating rates here used are in the range of those commonly used for isoconversional kinetic analysis of biomass pyrolysis [17]. For each sample and heating rate, three repetitive TG curves were obtained in order to guarantee reproducibility of the results. All dynamic runs were carried out on a pan containing 25 ± 1 mg of the corresponding sample or blend. Inert atmosphere inside the furnace during temperature-programmed pyrolysis was obtained by means of a continuous flow of N_2 (100 cm^3 min^{-1}) at a pressure of 1 atm (101 kPa).

Kinetic theory

The rate of heterogeneous solid-state reactions can be generally described by:

$$\frac{\mathrm{d}\alpha}{\mathrm{d}t} = k(T)f(\alpha) \quad (1)$$

where t is time, $k(T)$ is the temperature-dependent constant and $f(\alpha)$ is a function called the reaction model, which describes the dependence of the reaction rate on the extent of reaction or fractional conversion, α.

The mathematical description of decomposition from a solid state is commonly defined in terms of a kinetic triplet, as activation energy, E, Arrhenius parameter, A, and an algebraic expression of the kinetic model in function of the fractional conversion $f(\alpha)$, which can be related to experimental data as follows:

$$\frac{d\alpha}{dt} = Ae^{-E/RT} f(\alpha) \quad (2)$$

Next, the above rate expression (2) can be converted into non-isothermal rate expressions describing reaction rates as a function of temperature at a constant heating rate, β:

$$\frac{d\alpha}{dT} = \frac{A}{\beta} Ae^{-E/RT} f(\alpha) \quad (3)$$

Integrating up to conversion, α, Eq. (3) gives:

$$\int_0^{\alpha} \frac{d\alpha}{f(\alpha)} = g(\alpha) = \frac{A}{\beta} \int_{T_0}^{T} e^{-E/RT} dT \quad (4)$$

where $g(\alpha)$ is the integral kinetic function or integral reaction model when its form is mathematically defined.

Kinetic analysis is usually carried out to acquire an appropriate description of the process in terms of the Arrhenius activation energy (E). Different methods may be used to analyse solid-state kinetic data [18], which may be classified according to the selected experimental conditions and the performed mathematical analysis. Experimentally, either isothermal or non-isothermal methods are employed. Although the concepts of solid-state kinetics were established on the basis of isothermal experiments, the sample takes some time to reach the experimental temperature in this kind of experiments [18]. Non-isothermal experiments avoid this drawback. Mathematically, there are two possible approaches, the model-fitting and isoconversional (model-free). Model-fitting methods were the first and most popular, especially for isothermal experiments, but they have lost popularity with respect to isoconversional methods, which can compute kinetic parameters without modelling assumptions [19, 20]. Model-free isoconversional methods allow estimating the activation energy as a function of α without pre-fixing the reaction model. The essential assumption is that the reaction rate for a constant extent of conversion, α, depends only on the temperature [18].

In non-isothermal kinetics, several model-free isoconversional methods may be used. To use these methods, a series of experiments has to be conducted at different heating rates [16]. During the last decade, these methods have been frequently used to study the pyrolysis decomposition kinetics and apparent activation energy for very different materials [21–27]. Among these methods, the one developed by Vyazovkin [16] allows for the calculation of the activation energy from dynamic data and may be applied to both simple and complex reactions.

In Eq. 4, since $E/2RT >> 1$, the temperature integral can be approximated by:

$$\int_{T_0}^{T} e^{-E/RT} dT \approx \frac{R}{E} T^2 e^{-E/RT} \quad (5)$$

Substituting the temperature integral and taking the logarithm, we have that:

$$\ln \frac{\beta}{T^2} = \ln \left[\frac{RA}{Eg(\alpha)} \right] - \frac{E}{R} \frac{1}{T} \quad (6)$$

To apply this method, it is necessary to obtain at least at three different heating rates (β), the respective conversion curves given by the measured TG data. For each conversion value (α), $\ln [\beta T^{-2}]$ plotted versus T^{-1}, gives a straight line with slope $-E/R$, and thus the activation energy is obtained as a function of the conversion (α).

Results and discussion

Characterization of materials

The results of the elementary and proximate analysis for the coal and the primary and secondary pulp mill sludge here used are depicted in Table 1. The proximate analysis showed that the ash yield of C (30.33 %) is lower than that of L1 (33.10 %) but higher than that of L2 (24.82 %). Regarding the amount of volatiles, L1 (65.25 %) and L2 (58.64 %) yield much higher amount of volatiles than the coal (8.01 %). Then, both L1 and L2 have much lower fixed carbon (1.65 and 16.97 %, respectively) than C (61.66 %). The here-obtained results for L1 and L2 are in

Table 1 Proximate analysis, elementary analysis, and calorific values for the coal (C), the primary (L1) and the secondary (L2) pulp sludge used in combustion studies

Properties	C	L1	L2
Proximate analysis/mass%			
Moisture	11.22	1.74	11.83
Volatiles/d.b.	8.01	65.25	58.64
Ashes	30.33	33.10	24.39
FC	61.66	1.65	16.97
Elemental analysis/mass%, d.b.			
C	62.07	15.37	41.25
H	2.30	1.35	5.03
N	1.16	0.36	6.78
S	2.21	0.24	1.89
O[a]	1.93	49.58	20.66
Elemental analysis/J g^{-1}, d.b.			
HHV	24,382	2489	16,429

FC fixed carbon, *HHV* high heat value, *d.b.* dry basis

[a] Calculated by difference

the range of those by [10] for different wastes from the paper industry, except for L2, which has a slightly higher fixed carbon content.

With respect to the elementary analysis, C has a higher carbon content (62.07 %) than L2 (41.25 %) and, especially, than L1 (15.37 %). On the contrary, C has much lower oxygen content (1.93 %) than L1 and L2 (49.58 and 20.66 %, respectively). Both C and L2 have a similar sulphur content (2.21 and 1.89 %, respectively), which is higher than that of L1 (0.24 %). The trend of the hydrogen and the nitrogen is similar, L2 having the highest contents of both elements (5.03 and 6.78 %, respectively), followed by C (2.3 and 1.16 %, respectively) and then L1 (1.35 and 0.36 %, respectively). It is to highlight the high nitrogen content of L2, compared with results published by [10] on wastes from the paper industry.

Finally, as regards the calorific value, as expected, C, which has a HHV typical of a bituminous coal, showed the highest value. The HHV of L2 is relatively high, and similar to lignite coal characteristic values. Meanwhile, L1 has a low HHV, which is even lower than typical values for peat.

Thermogravimetric analysis

The differential thermogravimetric (DTG) results obtained from the temperature-programmed pyrolysis of the samples and blends here considered are shown in Fig. 1 for the different heating rates used. As may be seen, on raising the temperature at each heating rate, pyrolysis of the sample or blend takes place with an associated mass loss. Once the volatile content of the sample is exhausted, the mass progressively remains stable.

DTG curves in Fig. 1 make evident that the mass loss associated with the pyrolysis of coal is very low compared with the case of L2 and, especially, L1. This is in agreement with their respective volatiles content, as displayed in Table 1. Furthermore, during the pyrolysis of C, mass loss occurs in an only step, while it occurs in two steps for L1 and L2. For increasing heating rates ($\beta = 0.1$, 0.2, 0.4 and 0.5 K s^{-1}), the pyrolysis mass loss started at increasing temperatures for all samples and blends. In any case, it must be highlighted that, at all the tested β, the pyrolysis mass loss started at higher temperatures for coal than for L1, L2 and their respective blends with coal. Regarding L1 and L2, although pyrolysis mass loss occurred in two steps for both of them, their DTG pyrolysis curves show relevant differences. First, a more intense mass of loss takes place at both steps of the pyrolysis of L1 than of L2, which is in agreement with the lower volatiles content of the latter (Table 1). Furthermore, the first pyrolysis step occurs in a broader range of temperatures for L2 than for L1, while the contrary occurs for the second pyrolysis step. Thus, differences between L1 and L2 in the volatile content are not only quantitative, as indicated by results in Table 1, but also qualitative, as indicated by DTG curves.

The pyrolysis DTG curves of the blends (CL1 and CL2) in Fig. 1 differ from those corresponding to the coal. In the case of CL1, three steps of mass loss may be observed. The first and the third one occur in the range of temperatures of the two steps observed for L1, while the second one, which is comparatively less relevant, is coincident with the only mass loss step observed for C. With respect to CL2, a first mass loss step occurs in the same range of temperatures than the first one corresponding to L2. Then, that first mass loss peak overlaps with the mass loss associated with C, the C and the CL2 curves being nearly coincident from 800 K.

In order to check interaction between coal and L1 or L2 during co-pyrolysis, the theoretical DTG curve was calculated, for each blend and heating rate (β), as a weighted average of the blend composition:

$$\mathrm{DTG_{CALCULATED}} = 0.9 * \mathrm{DTG_{coal}} + 0.1 * \mathrm{DTG_{sludge}} \quad (7)$$

where $\mathrm{DTG_{coal}}$ is the mass loss rate of coal and $\mathrm{DTG_{sludge}}$ is the mass loss rate of either L1 or L2 at each heating rate (β).

Experimental and calculated DTG curves corresponding to the pyrolysis of the blends are shown in Fig. 2. As may be seen, experimental curves (CL1 and CL2, in Fig. 2a, b, respectively) differ from the calculated ones ($\mathrm{CL1_{CALCULATED}}$ and $\mathrm{CL2_{CALCULATED}}$, in Fig. 2a, b, respectively) for all the heating rates here used. Differences are especially in the case of CL1, which points to strong interactions among coal and primary pulp mill sludge. Also, depending on the heating rate and on the type of sludge, either primary or secondary, different synergistic effects occur on the pyrolysis of coal.

The characteristic parameters of the pyrolysis DTG profiles are shown in Table 2. At each heating rate (β), the temperatures at which volatiles start to be released (T_v) are similar for L1 and L2 but lower than for C, whose reactivity to pyrolysis is lower. On the contrary, it is to highlight coincidences of T_v for L1 with CL1 and for L2 with CL2. Regarding the temperature at which occurs the maximum mass loss rate (T_m), those corresponding to L2 are only slightly lower than for L1. In any case, T_m corresponding to C is higher than those corresponding to L1 and L2, confirming the lower reactivity of coal towards pyrolysis. Again, as it was for T_v, CL1 and CL2 show T_m values that resemble those of L1 and L2, respectively. With respect to the temperature at which mass stabilizes (T_f), values corresponding to C are higher than those corresponding to L1 and L2. Moreover, T_f corresponding to CL1 and CL2 are equivalent to those of C. The maximum mass loss rate ($\mathrm{DTG_{max}}$) corresponding to both L1 and L2 are quite higher than those corresponding to C. In any case, it is to highlight the outstanding $\mathrm{DTG_{max}}$ associated with L1,

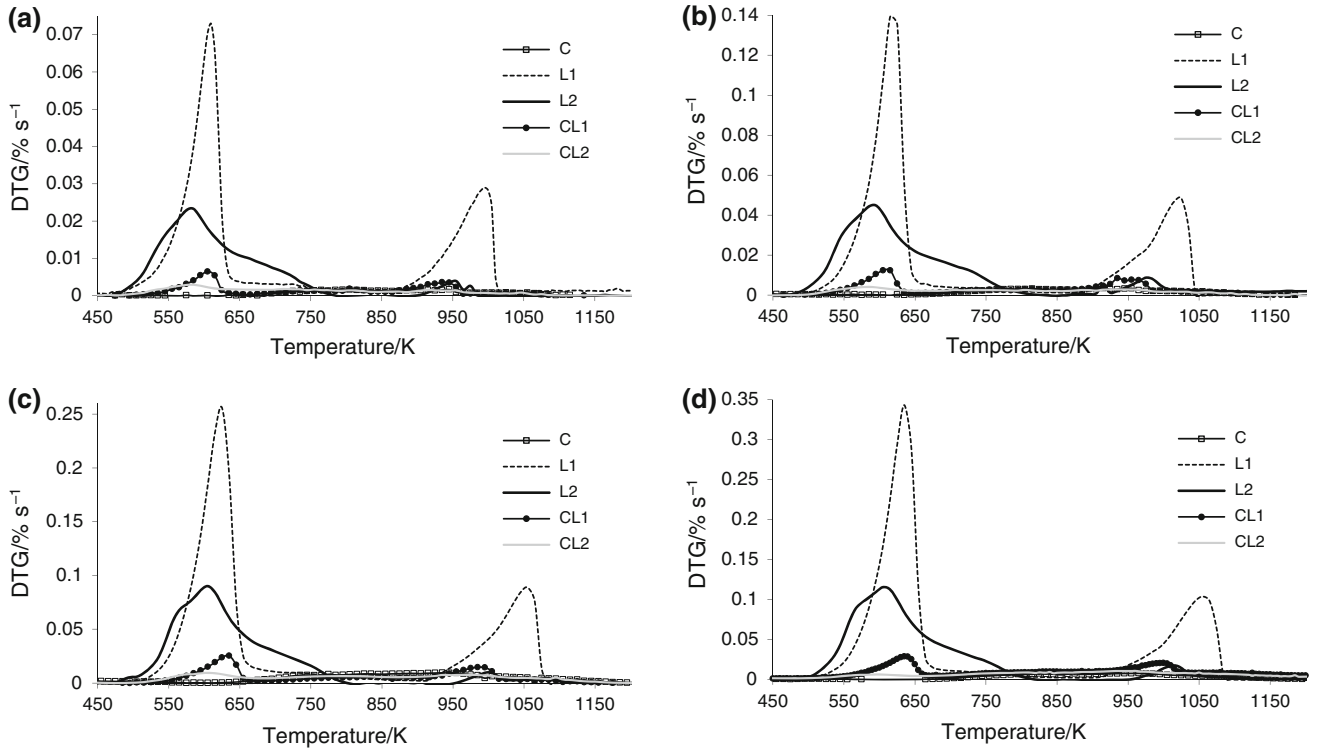

Fig. 1 Pyrolysis DTG curves for coal (C), primary pulp mill sludge (L1), secondary pulp mill sludge (L2) and their blends (CL1 and CL2, respectively) at the heating rates (β) of: **a** 0.1 K s^{-1}; **b** 0.2 K s^{-1}; **c** 0.4 K s^{-1}; and **d** 0.5 K s^{-1}. *Note* the scale of the *Y* axis has been adjusted for a better visualization of results

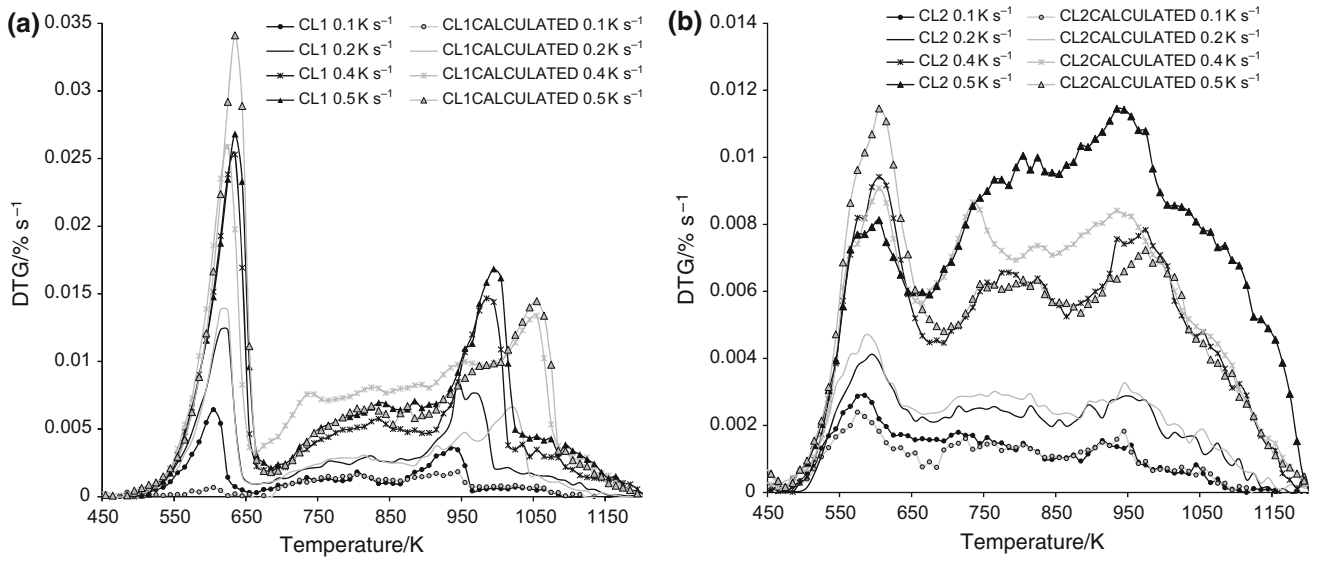

Fig. 2 Experimental pyrolysis DTG curves of CL1 and CL2 (in *black*) together with the corresponding weighted average curves ($CL1_{CALCULATED}$ and $CL2_{CALCULATED}$, in *grey*) at the heating rates (β) of: **a** 0.1 K s^{-1}; **b** 0.2 K s^{-1}; **c** 0.4 K s^{-1}; and **d** 0.5 K s^{-1}. *Note* the scale of the *Y* axis has been adjusted for a better visualization of results

reflecting the pronounced mass loss associated with the volatiles yield. The DTG_{max} corresponding to the blends is higher than those observed for the coal and lower than those of either L1 or L2. Also, for all samples and blends, increasing DTG_{max} occur with increasing heating rate (β). With respect to the devolatilization times (t_q), they are

Table 2 Characteristic parameters obtained from the DTG pyrolysis curves in Fig. 1 for coal (C), primary mill sludge (L1), secondary mill sludge (L2) and their respective blends with coal (CL1 and CL2)

Sample	β/K s^{-1}	T_v/K	T_m/K	T_f/K	DTG$_{max}$/% s^{-1}	t_q/s
C	0.1	608	809	1120	0.0016	5231
	0.2	610	934	1174	0.0034	2736
	0.4	615	938	1210	0.0077	1500
	0.5	620	964	1,250	0.0097	1260
L1	0.1	475	609	1015	0.0731	5428
	0.2	490	620	1050	0.1459	2810
	0.4	495	623	1085	0.2558	1475
	0.5	500	636	1090	0.3446	1180
L2	0.1	452	581	985	0.0238	5348
	0.2	463	591	1024	0.0451	2812
	0.4	470	604	1135	0.0902	1662
	0.5	475	608	1150	0.1156	1350
CL1	0.1	475	607	1120	0.0064	6469
	0.2	490	619	1174	0.0130	3420
	0.4	495	633	1210	0.0255	1787
	0.5	500	637	1250	0.0269	1500
CL2	0.1	452	581	1120	0.0029	6693
	0.2	465	593	1175	0.0044	3550
	0.4	470	606	1210	0.0095	1850
	0.5	475	945	1250	0.0114	1550
CL1$_{CALCULATED}$	0.1	475	945	1120	0.0018	6469
	0.2	490	615	1174	0.0138	3420
	0.4	495	625	1210	0.0259	1787
	0.5	500	635	1250	0.0341	1500
CL2$_{CALCULATED}$	0.1	452	575	1120	0.0024	6693
	0.2	465	585	1175	0.0047	3550
	0.4	470	605	1210	0.0091	1850
	0.5	475	605	1250	0.0114	1550

Parameters from the calculated weighted average DTG curves for the blends (CL1$_{CALCULATED}$ and CL2$_{CALCULATED}$) in Fig. 2 have been also included

T_v onset temperature for volatile release and mass loss, T_m temperature of maximum mass loss rate, T_f final combustion temperature detected as mass stabilization. DTG$_{max}$ maximum mass loss rate, t_q devolatilization time; time interval from the moment the dried sample starts to lose mass until the moment that the pyrolysis ends and mass trends to stabilize

similar for the pyrolysis of C, L1 and L2. Comparatively, longer devolatilization times are required to complete the pyrolysis of CL1 and CL2, since their respective pyrolysis start at the T_v of L1 or L2 but end at the T_f of coal. Finally, for all materials and blends, t_q decreases with increasing β.

Characteristic parameters obtained from the calculated weighted average curves (CL1$_{CALCULATED}$ and CL2$_{CALCULATED}$) in Fig. 2 have been depicted in Table 2 for comparison purposes. Although the T_v and T_f, and, consequently, the t_q, from the calculated curves are equivalent to those from the experimental ones, different T_m and, especially, different DTG$_{max}$ values may be observed.

Parameters in Table 2 confirm the above said with respect to Fig. 1 and make plain differences between the pyrolysis of coal, primary and secondary pulp mill sludge and their respective blends with coal. Also, parameters in Table 2 obtained from the calculated weighted average curves, corroborate interactions between coal and either L1 or L2 during pyrolysis.

Kinetic analysis

The TG curves obtained from the temperature-programmed pyrolysis of the pure samples and blends at the heating rates (β) of 0.1, 0.2, 0.4 and 0.5 K s^{-1} are depicted in Fig. 3 together with six different percentages of conversion. These TG curves represent the mass loss at increasing temperature during the pyrolysis of C, L1 and L2 and their respective blends, CL1 and CL2. As it was previously said, for all the heating rates, the devolatilization of coal both

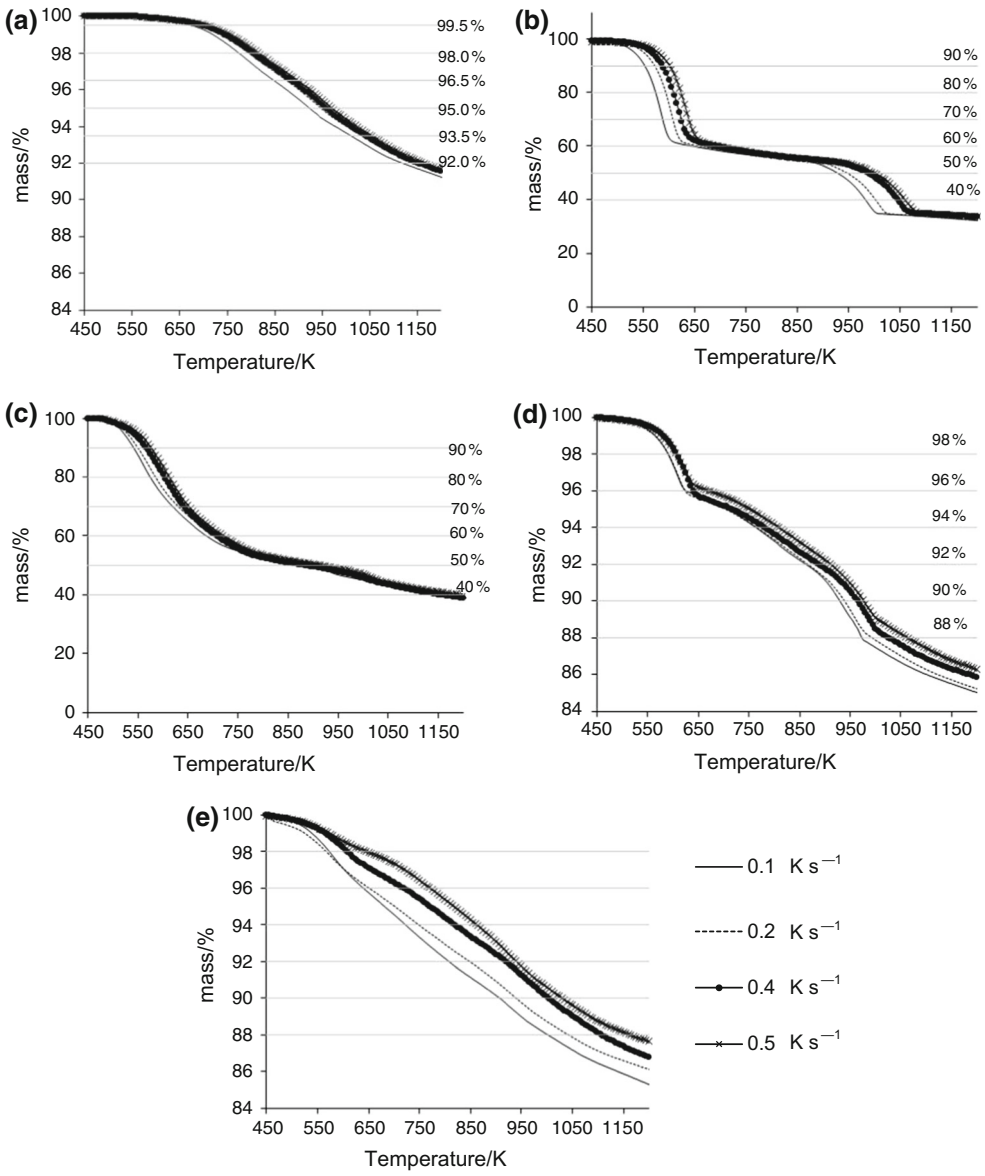

Fig. 3 TG curves corresponding to the pyrolysis at different heating rates of: **a** coal (C); **b** primary pulp mill sludge (L1); **c** secondary pulp mill sludge (L2); **d** coal and primary pulp mill sludge (CL1); and **e** coal and secondary pulp mill sludge (CL2). Conversion percentages (α) have been represented by *straight lines* crossing experimental data. *Note* the scale of the *Y* axis has been adjusted for a better visualization of results

starts and ends at higher temperatures than that of L1 or L2. Regarding the average char yields, or residual mass after pyrolysis, they were 91.5, 32.5 and 38.5 % for C, L1 and L2, respectively. The char yield here determined for coal is higher than values found in the literature, which are around 70–80 % [26, 27]. Also, the char yields here determined for the pyrolysis of primary and secondary pulp mill sludge are in the range of values published for the pyrolysis of wastes from the paper industry [10]. Meanwhile, it is to highlight that the char yields of the pyrolysis of CL1 and CL2 are 85.3 and 86.1 %, which remain quite close to the values that would proportionally correspond to the blends mass composition. Contrary, differences from the calculated weighted values of the char yield from the co-pyrolysis of coal and lignocellulosic biomass have been obtained by other authors [26, 27].

Figure 4 shows the plots of $\ln[\beta T^{-2}]$ versus T^{-1} to the several conversion degrees (α) corresponding to the pyrolysis of C, L1 and L2 and their blends. According with the Vyazovkin method [16], straight lines with the angular coefficient $-E/R$ were obtained. Then, the values of E calculated by the Vyazovkin method are shown in Table 3.

The average E determined for C by the Vyazovkin method (254 kJ mol^{-1}) is higher than that of L2 (194 kJ mol^{-1}) and, especially, than that of L1 (114 kJ mol^{-1}). The here-obtained E values for the pyrolysis of coal are equivalent to those found in the literature for such a fuel [27]. With respect to the

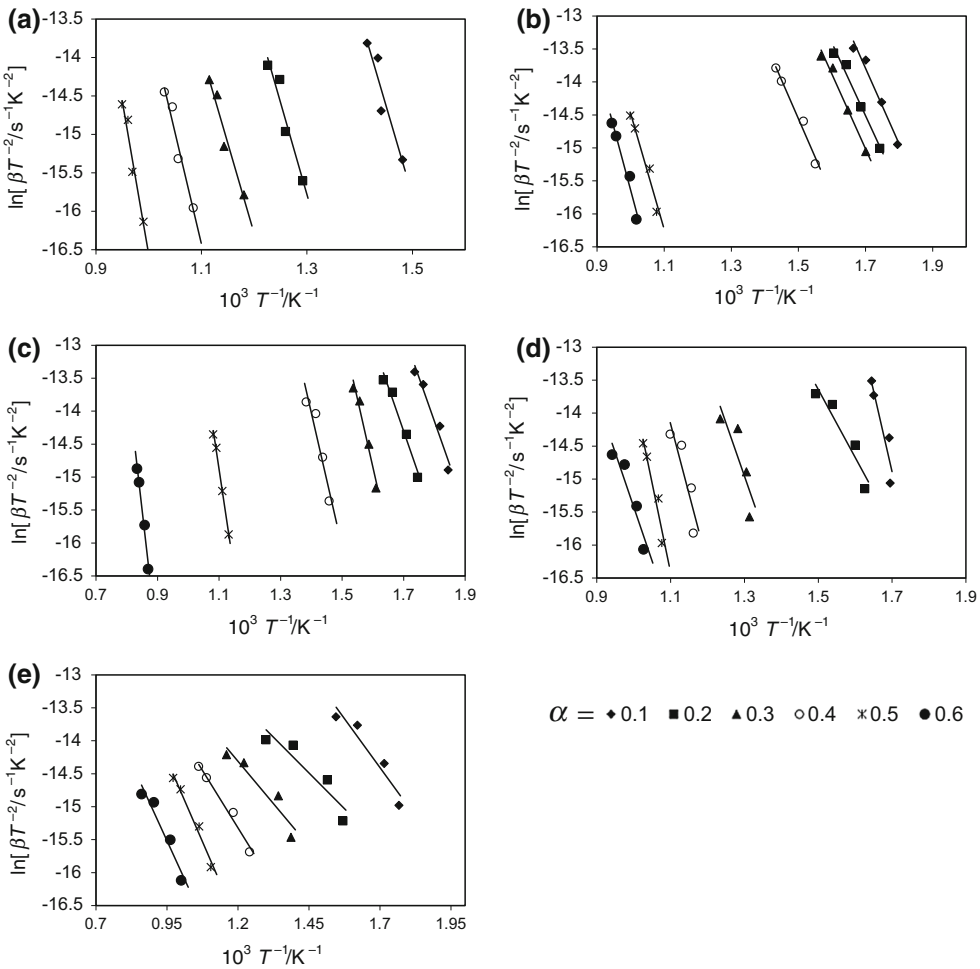

Fig. 4 Fittings of TG results to kinetic model proposed by Vyazovkin at the considered conversion percentages (α) corresponding to the pyrolysis at different heating rates of: **a** coal (C); **b** primary pulp mill sludge (L1); **c** secondary pulp mill sludge (L2); **d** coal and primary pulp mill sludge (CL1); and **e** coal and secondary pulp mill sludge (CL2)

Table 3 Values of pyrolysis activation energy (E) obtained by the application of the Vyazovkin model

Thermal treatment	Sample/blend	E^a/kJ mol^{-1} Vyazovkin model
Pyrolysis	C	254
	L1	114
	L2	194
	CL1	160
	CL2	58

[a] Activation energy E was calculated as arithmetic average of the several E values obtained for different conversion degrees shown in Fig. 3

pyrolysis of pulp mill sludge, no data are available in the literature. However, the here-obtained results are close to E values published for the pyrolysis of lignocellulosic wastes [17, 27].

Regarding the E estimated for the blends, the obtained values for CL1 (160 kJ mol^{-1}) and CL2 (58 kJ mol^{-1}) are lower than for the calculated weighted E that would correspond as proportional to the blends composition (10 mass% of either primary or secondary pulp mill sludge). This is especially true in the case of the co-pyrolysis of CL2 and points to the occurrence of synergistic interactions between coal and primary or secondary pulp mill sludge during their co-pyrolysis. E values lower than the weighted calculated ones have been found by other authors [26] for the co-pyrolysis of lignocellulosic biomass and bituminous coal. This reduction may be related to coal interactions with cellulose, which have been shown by different authors [26, 28]. Given the source of primary and secondary pulp mill sludge, lignocellulose must be an important constituent, which may lead to the reduction of the E associated to the pyrolysis of coal.

Globally, results obtained in this work showed that blending coal with pulp mill sludge is a way to increase coal pyrolysis reactivity and to decrease the associated activation energy. In any case, it must be highlighted that primary and secondary pulp mill sludge display different properties and behaviour during pyrolysis. Compared to secondary pulp mill sludge, primary sludge has a relative higher volatiles

yield, which evidently shapes the DTG curve corresponding to its blend with coal (CL1). However, when comparing the *E* corresponding to the pyrolysis of blends with that of coal, blending effects of the secondary pulp mill sludge are more notable than those of primary sludge. Thermogravimetric analysis may be a useful tool for the assessment of co-pyrolysis of coal in existing infrastructures.

Conclusions

In this work, the DTG pyrolysis curves showed remarkably differences between coal, primary and secondary sludge, which are related to the different properties of these materials. Compared to coal, pyrolysis of pulp mill sludge starts at lower temperatures and involves larger devolatilization and smaller char yields. These differences are more evident for primary than for secondary pulp mill sludge. Blending of pulp mill sludge (10 mass%) causes an increase in the pyrolysis reactivity of coal and a decrease in the corresponding apparent activation energy, as calculated by the Vyazovkin model. This reduction is more evident for the pyrolysis of coal blended with secondary than with primary pulp mill sludge. Moreover, although the char yields of the pyrolysis of blends are close to the weighted calculated ones, the co-pyrolysis activation energies are lower than the weighted calculated ones, which points to non-additive performance.

Acknowledgements We would like to thank assistance given by María P. González Alonso and José A. de Linaje Aguirre, from LARECOM (Spain). Authors also thank the kind collaboration of Luís Machado and José Luís Amaral from RAIZ—Instituto de Investigação da Floresta e do Papel. FCT funding to the Associated Laboratory CESAM is acknowledged. C. Escapa acknowledges the Spanish Ministry of Education, Culture and Sports for her PhD fellowship (FPU12/03073). S. Paniagua acknowledges the grant for doctorate studies given by University of León in the framework of its own research programme ULE-2014. Also, M. Otero acknowledges support from the Spanish Ministry of Economy and Competitiveness, State Secretariat for Research, Development and Innovation Spanish Ministry of Science and Innovation (RYC-2010-05634).

References

1. CEPI. Confederation of European Paper Industries (CEPI). Key statistics 2013. http://www.cepi.org/topics/statistics/keystatistics2013. Last accessed 15 January 2015.
2. CEPI. Confederation of European Paper Industries (CEPI). CEPI'S online sustainability report. http://www.cepi-sustainability.eu/. Last accessed 15 January 2015.
3. Ince BK, Cetecioglu Z, Ince O. Pollution prevention in the pulp and paper industries. In: Broniewicz E, editor. Environmental management in practice. InTech; 2011. ISBN: 978-953-307-358-3. doi:10.5772/23709. http://www.intechopen.com/books/environmental-management-in-practice/pollution-prevention-in-the-pulp-and-paper-industries.
4. Pokhrel D, Viraraghavan T. Treatment of pulp and paper mill wastewater—a review. Sci Total Environ. 2004;333:37–58.
5. Elliott A, Mahmood T. Survey benchmarks generation, management of solid residues. Pulp Pap. 2005;79:49–55.
6. Monte MC, Fuente E, Blanco A, Negro C. Waste management from pulp and paper production in the European Union. Waste Manage. 2009;29:293–308.
7. Wei Y, VanHouten RT, Borger AR, Eikelboom DH, Fan Y. Minimization of excess sludge production for biological wastewater treatment. Water Res. 2003;37:4453–67.
8. Mahmood T, Elliott A. A review of secondary sludge reduction technologies for the pulp and paper industry. Water Res. 2006;40:2093–112.
9. Stoica A, Sandberg M, Holby O. Energy use and recovery strategies within wastewater treatment and sludge handling at pulp and paper mills. Bioresource Technol. 2009;100:3497–505.
10. Méndez A, Fidalgo JM, Guerrero F, Gasco G. Characterization and pyrolysis behaviour of different paper mill waste materials. J Anal Appl Pyrolysis. 2009;86:66–73.
11. Inguanzo M, Domínguez A, Menéndez JA, Blanco CG, Pis JJ. On the pyrolysis of sewage sludge: the influence of pyrolysis conditions on solid, liquid and gas fractions. J Anal Appl Pyrolysis. 2002;63:209–22.
12. Calisto V, Ferreira CIA, Santos SM, Gil MV, Otero M, Esteves VI. Production of adsorbents by pyrolysis of paper mill sludge and application on the removal of citalopram from water. Bioresour Technol. 2014;166:335–44.
13. Ferreira CIA, Calisto V, Santos SM, Cuerda-Correa EM, Otero M, Nadais H, Esteves VI. Application of pyrolysed agricultural biowastes as adsorbents for fish anaesthetic (MS-222) removal from water. J Anal Appl Pyrolysis. 2015;112:313–24.
14. Zhu F, Feng Q, Xu Y, Liu R, Li K. Kinetics of pyrolysis of ramie fabric wastes from thermogravimetric data. J Therm Anal Calorim. 2015;119:651–7.
15. Zhu X, Chen Z, Xiao B, Hu Z, Hu M, Liu C, Zhang Q. Co-pyrolysis behaviors and kinetics of sewage sludge and pine sawdust blends under non-isothermal conditions. J Thermal Anal Calorim. 2015;119:2269–79.
16. Vyazovkin S. Evaluation of activation energy of thermally stimulated solid-state reactions under arbitrary variation of temperature. J Comput Chem. 1997;18:393–402.
17. Baroni ÉDG, Tannous K, Rueda-Ordóñez YJ, Tinoco-Navarro LK. The applicability of isoconversional models in estimating the kinetic parameters of biomass pyrolysis. J Thermal Anal Calorim. (in press). doi:10.1007/s10973-015-4707-9.
18. Vyazovkin S, Wight CA. Isothermal and non-isothermal kinetics of thermally stimulated reactions of solids. Int Rev Phys Chem. 1998;17:407–33.
19. Vyazovkin S, Wight CA. Model-free and model-fitting approaches to kinetic analysis of isothermal and nonisothermal data. Thermochim Acta. 1999;340–341:53–68.
20. Khawam A, Flanagan DR. Role of isoconversional methods in varying activation energies of solid-state kinetics: I. Isothermal kinetic studies. Thermochim Acta. 2005;429:93–102.
21. Bhavanam A, Sastry RC. Kinetic study of solid waste pyrolysis using distributed activation energy model. Bioresource Technol. 2015;178:126–31.
22. Mishra G, Bhaskar T. Non isothermal model free kinetics for pyrolysis of rice straw. Bioresource Technol. 2014;169:614–21.
23. Jeong HM, Seo MW, Jeong SM, Na BK, Yoon SJ, Lee JG, Lee WJ. Pyrolysis kinetics of coking coal mixed with biomass under non-isothermal and isothermal conditions. Bioresource Technol. 2014;155:442–5.

24. Devrim YG. Pyrolysis kinetics of blends of yeni Çeltek lignite and sugar beet pulp. Energy Sources Part A Recovery Util Environ Effects. 2008;30:238–46.
25. Tiwari P, Deo M. Compositional and kinetic analysis of oil shale pyrolysis using TGA-MS. Fuel. 2012;94:333–41.
26. Wu Z, Wang S, Zhao J, Chen L, Meng H. Synergistic effect on thermal behavior during co-pyrolysis of lignocellulosic biomass model components blend with bituminous coal. Bioresource Technol. 2014;169:220–8.
27. Aboyade AO, Görgens JF, Carrier M, Meyer EL, Knoetze JH. Thermogravimetric study of the pyrolysis characteristics and kinetics of coal blends with corn and sugarcane residues. Fuel Processing Technol. 2013;106:310–20.
28. Guo Z, Bai Z, Bai J, Wang Z, Li W. Synergistic effects during co-pyrolysis and liquefaction of biomass and lignite under syngas. J Therm Anal Calorim. 2015;119:2133–40.

Anexo III

Coimbra, R.N., Paniagua, S., Escapa, C., Calvo, L.F., Otero, M., 2016. Thermal valorization of pulp mill sludge by co-processing with coal. Waste and Biomass Valorization 7, 995-1006.
http://dx.doi.org/10.1007/s12649-016-9524-2

Thermal Valorization of Pulp Mill Sludge by Co-processing with Coal

R. N. Coimbra, S. Paniagua, C. Escapa, L. F. Calvo & M. Otero

Waste and Biomass Valorization

ISSN 1877-2641
Volume 7
Number 4

Waste Biomass Valor (2016) 7:995-1006
DOI 10.1007/s12649-016-9524-2

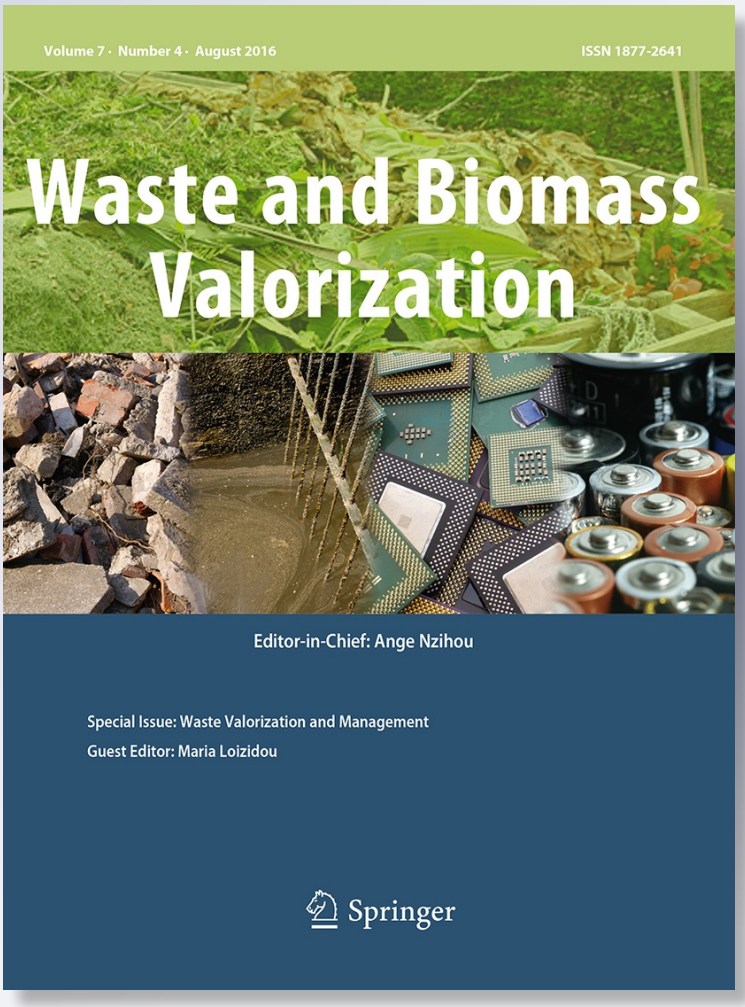

Springer

Your article is protected by copyright and all rights are held exclusively by Springer Science +Business Media Dordrecht. This e-offprint is for personal use only and shall not be self-archived in electronic repositories. If you wish to self-archive your article, please use the accepted manuscript version for posting on your own website. You may further deposit the accepted manuscript version in any repository, provided it is only made publicly available 12 months after official publication or later and provided acknowledgement is given to the original source of publication and a link is inserted to the published article on Springer's website. The link must be accompanied by the following text: "The final publication is available at link.springer.com".

Author's personal copy

Waste Biomass Valor (2016) 7:995–1006
DOI 10.1007/s12649-016-9524-2

ORIGINAL PAPER

Thermal Valorization of Pulp Mill Sludge by Co-processing with Coal

R. N. Coimbra[1] · S. Paniagua[1] · C. Escapa[1] · L. F. Calvo[1] · M. Otero[1,2]

Received: 28 September 2015 / Accepted: 7 March 2016 / Published online: 10 March 2016
© Springer Science+Business Media Dordrecht 2016

Abstract At the pulp and paper industries, large volumes of primary and secondary sludge are generated from wastewater treatment. Aiming to assess the co-processing of each type of sludge with coal, thermogravimetric (TG) analysis has been used in this work. First, combustion and pyrolysis TG curves of coal (C), primary (L1) and secondary (L2) pulp mill sludge were obtained under oxidizing and inert atmosphere, respectively. Then, under identical experimental conditions, TG analysis was carried out on the primary sludge–coal (CL1) and the secondary sludge–coal (CL2) blends. The corresponding differential thermogravimetric (DTG) curves showed evident differences between C, L1 and L2, which were mainly related to the relative large fixed carbon and low volatiles content of C. However these differences, the combustion of CL1 and CL2 mostly resembled that of C. Meanwhile, the pyrolysis of CL1 and CL2 showed lower devolatilization temperatures and char yields than that of C. Non-isothermal kinetic analysis of TG data showed slightly lower apparent activation energy (E) for the combustion of C than for the combustion of either CL1 or CL2. Contrarily, much lower E values were determined for the pyrolysis of CL1 and CL2 than for the pyrolysis of C. Yet, lower E values than the weighted calculated ones were determined for the combustion and, especially, for the pyrolysis of the blends.

Keywords Thermal conversion · Kinetics · Flynn–Wall–Ozawa · Paper industry · Wastes

Introduction

In Europe, the pulp and paper manufacturing and converting industries employ about 647.500 workers in 21.000 companies, generating an annual turnover of around 180 billion Euro [1]. As a counterpart, the pulp and paper industry is energy—and raw materials—intensive and considered one of the most polluting in the world [2]. Given the large water usage, huge volumes of wastewater are generated during various stages of pulping and papermaking activities [3]. In fact, this sort of industry is the third largest producer of wastewater after primary metals and chemicals industries [4].

In the pulp and paper industry, the main wastewater producing stages are wood preparation, pulp washing, pulp bleaching and paper making processes as well as the digester house [3]. At each stage, the wastewaters volume generated is closely related to the quantity of generated pulp in that particular process [5]. Depending on the type of applied processes, these wastewaters are characterized for having a high BOD content and various concentrations of other contaminants [3] so they can cause slime growth, thermal impacts, scum formation, colour problems, and loss of aesthetic beauty in receiving waters [6]. Also, they may be a source of toxic substances in the aquatic environment, leading to the zooplankton and fish death, as well as profoundly affecting ecosystems [6]. Therefore, the pulp and paper industry must treat effluents before discharging

✉ M. Otero
marta.otero@unileon.es; marta.otero@ua.pt

[1] Department of Applied Chemistry and Physics, IMARENABIO (Institute of Environment, Natural Resources and Biodiversity), University of León, Campus de Vegazana, 24071 León, Spain

[2] Department of Chemistry and CESAM (Centre for Environmental and Marine Studies), University of Aveiro, Campus de Santiago, 3810-193 Aveiro, Portugal

Author's personal copy

them into the environment in order to comply with environmental regulations [6]. Then, sludge is generated throughout primary and secondary wastewater treatment as a main end-product and must be treated before disposal [3]. In fact, handling, treatment and disposal of sludge produced from wastewater treatment represent an important percentage of total costs of pulp and paper industries [3, 7].

Given prohibitions on landfilling and since other alternatives such as agricultural applications or composting are not viable due to the composition of sludge from the pulp and paper industry, other management options must be undertaken. Nowadays, several waste recovery options may be considered for this sort of wastes, which include thermal processes such as combustion and/or, pyrolysis [7]. Ashes and char, which are the solid products from combustion and pyrolysis of sludge, respectively, represent an important reduction of volume for the pulp and paper industries [7]. Furthermore, these thermal processes allow for the valorization of such wastes through energy recovery by power and steam generation during combustion or by the production of gaseous or liquid fuels during pyrolysis [7, 8]. On the other hand, and from an economic and practical point of view, the possibility of a joint processing of sludge from the pulp and paper industry with coal in existing plants may be an interesting option, since it allows for the use of existing infrastructures already equipped with appropriate devices for emission control, reducing at the same time fossil fuels consumption [9]. In this sense, the utilization of relative low percentages ($\leq$10 wt%) of sludge has been recommended for their co-processing with coal in current infrastructures [10–12].

Thermogravimetric (TG) analysis has been widely employed for the study of the thermal processing and co-processing of different wastes, including those from the pulp and paper industry [10–17]. The main reason is that TG allows not only for a rapid assessment of the characteristic temperatures, maximum reactivity, or decomposition time, but also for assessing the process kinetics, reaction rates and activation energy [16]. In the case of the paper industry wastewater treatment, primary and secondary sludge are generated in unequal volumes and hold very different properties [8]. Thus, it could be expected that they are not equally suitable for their co-processing with coal, either by combustion or pyrolysis. However, a comparison of both sludge and valorization options is missed in the literature. Therefore, this work aimed to assess and compare the thermal behaviour during combustion and during pyrolysis of primary pulp mill sludge, secondary pulp mill sludge, a bituminous coal and their respective blends (10 wt% of either primary or secondary pulp mill sludge). For this purpose, thermogravimetric analysis was carried out and the Flynn–Wall–Ozawa non-isothermal kinetic model was applied in order to determine the apparent activation energy associated to the single combustion and pyrolysis as well to the co-combustion and co-pyrolysis of primary and secondary pulp mill sludge with coal.

Materials and Methods

Materials

A bituminous coal (C) from the north coalfield of León (Spain), which is actually exploited in thermal power stations, was used in this study. Both primary and secondary pulp mill sludge were provided by a mill that uses eucalyptus wood (*Eucalyptus globulus*) for the production of pulp by the kraft ECD (elemental chlorine free) process. At this mill, primary and secondary sludge are generated at an average rate of 20 and 10 kg per tonne of air dried pulp produced, respectively. Primary sludge (L1) results from fibres rejected after the cooking/digestion at the pulping step, losses of fibres and other solids within liquid streams involved in the process (for example, washing and bleaching). The composition of the L1 is very similar to that of the pulp and basically consists of cellulosic fibres. Secondary sludge (L2) results from the clarification stage following the biological treatment to which wastewater is submitted after the primary clarification. During the biological treatment microorganisms are used to reduce the organic content of wastewater. Essentially, secondary sludge is the resulting dehydrated biomass, including recalcitrant organic matter, e.g. lignocellulose residues.

C, L1 and L2 air dried samples were sieved so to have a 0.105 mm $<$ particle diameter $<$ 0.210 mm. From these materials, primary sludge–coal (CL1) and secondary sludge–coal (CL2) blends with a sludge weight content of 10 % were prepared and homogenized by vigorous mixing. A fuel blend of 90 % C and 10 wt% pulp mill sludge (either L1 or L2) ratio was selected on the basis of results by Yanfen and Xiaoqian [12], who used TGA to study the thermal decomposition profiles of paper mill sludge blended with a typical semi-anthracite coal. These authors concluded that, according with both TG profiles and activation energy, the combustion of blends with low percentages of sludge, such as 10 wt%, was similar to that of coal. The same conclusion had already been established in the case of sewage sludge [10, 11].

Air dried and sieved C, L1 and L2 were characterized for their heating value, proximate and elemental analysis. Higher heating value (HHV) at a constant volume was measured by means of an adiabatic oxygen bomb calorimeter. Proximate determinations were made according to modified procedures from ASTM D 3172 to D 3175 (Standard Practice for Proximate Analysis of Coal and

Author's personal copy

Coke), E 870 (Standard Methods for Analysis of Wood Fuels), D 1102 (ash in wood) and E 872 (volatile matter). For the elemental determination, a LECO equipment model CHN-600 was used to determine the carbon, hydrogen and nitrogen content. Sulphur was determined by means of a LECO model SC-132. Next, the corresponding weighted data were calculated for the blends.

Thermogravimetric Analysis

Non-isothermal thermogravimetric analysis was carried out in a Setaram equipment, model SETSYS Evolution, which was calibrated (baseline, mass and temperature) prior to utilization. Then, C, L1, L2 and their respective blends, CL1 and CL2, were submitted to dynamic runs up to 1200 K under a heating rate ($\beta = dT/dt$) of 0.5 K/s. These dynamic runs were all carried out on a pan containing 25 ± 1 mg of the corresponding sample or blend. Temperature-programmed combustion and pyrolysis runs were performed under oxidizing and under inert atmosphere, respectively. Oxidizing atmosphere inside the furnace was obtained by means of a continuous airflow (100 cm^3/min) at a pressure of 1 atm (101 kPa). Inert atmosphere was provided by a continuous flow of N_2 (100 cm^3/min) at a pressure of 1 atm (101 kPa). Three replicates were analysed for each sample or blend, both under oxidizing or inert atmosphere. Mean TG values and the corresponding deviations were calculated for each three replicates, deviations ≤ 1 % having been obtained in all cases. In this way, reproducibility is guaranteed and mean values were used for comparison between samples and/or blends.

In order to check interaction between C, L1 or L2 during co-combustion or co-pyrolysis, the theoretical DTG curves ($DTG_{CALCULATED}$) were calculated for each blend (CL1 and CL2) as a weighted average of the blend composition:

$$DTG_{CALCULATED} = 0.9 \times DTG_{coal} + 0.1 \times DTG_{sludge} \quad (1)$$

where DTG_{coal} is the weight loss rate of C and DTG_{sludge} is the weight loss rate of either L1 or L2.

Non-isothermal Kinetic Analysis

The rate of heterogeneous solid-state reactions can be generally described by:

$$\frac{d\alpha}{dt} = k(T)f(\alpha) \quad (2)$$

where t is time, k(T) is the temperature-dependent constant and f(α) is a function called the reaction model, which describes the dependence of the reaction rate on the extent of reaction or fractional conversion, α.

The mathematical description of decomposition from a solid-state is commonly defined in terms of a kinetic triplet, as apparent activation energy, E, Arrhenius parameter, A, and an algebraic expression of the kinetic model in function of the fractional conversion f(α), which can be related to experimental data as follows:

$$\frac{d\alpha}{dt} = Ae^{-E/RT}f(\alpha) \quad (3)$$

Next, the above rate expression (3) can be converted into non-isothermal rate expressions describing reaction rates as a function of temperature at a constant heating rate, β:

$$\frac{d\alpha}{dT} = \frac{A}{\beta}Ae^{-E/RT}f(\alpha) \quad (4)$$

Integrating up to conversion, α, Eq. (4) gives:

$$\int_0^{\alpha} \frac{d\alpha}{f(\alpha)} = g(\alpha) = \frac{A}{\beta}\int_{T_0}^{T} e^{-E/RT}dT \quad (5)$$

where g(α) is the integral kinetic function or integral reaction model when its form is mathematically defined.

Kinetic analysis is usually carried out to acquire an appropriate description of the process in terms of the apparent activation energy (E). Different methods may be used to analyse solid-state kinetic data [18], which may be classified according to the selected experimental conditions and the performed mathematical analysis. Experimentally, either isothermal or non-isothermal methods may be employed, while, mathematically, there are two possible approaches, the model-fitting and the iso-conversional (model-free). In this work, the model-free iso-conversional model by Flynn–Wall–Ozawa [19, 20] using Doyle's approximation [21] of the temperature integral was applied to non-isothermal TG data as described elsewhere [10]. Therefore, in order to determine the activation energy of the combustion and pyrolysis of C, L1, L2 and their blends, TG runs were carried out as described in the previous section (for $\beta = 0.5$ K/s) at three more β: 0.1, 0.2 and 0.4 K/s.

Results and Discussion

Materials

The HHV, proximate and elemental results from the analysis of C, L1 and L2, are depicted in Table 1, which also shows the weighted calculated data corresponding to the blends ($CL1_{CALCULATED}$ and $CL2_{CALCULATED}$). As shown in Table 1, properties of C largely differ from those of L1 and L2, which, as discussed elsewhere [17] are also quite different among them. On the contrary, $CL1_{CALCULATED}$ and $CL2_{CALCULATED}$ data are quite close, with a higher volatiles and lower fixed carbon content than C.

Author's personal copy

Table 1 Proximate analysis, elementary analysis, and calorific values determined for the coal (C), the primary pulp mill sludge (L1) and the secondary pulp mill sludge (L2) together with weighted calculated data for blends ($CL1_{CALCULATED}$ and $CL2_{CALCULATED}$)

Properties	C	L1	L2	$CL1_{CALCULATED}$	$CL2_{CALCULATED}$
Proximate analysis (wt%)					
Moisture	11.22	1.74	11.83	10.27	11.28
Volatiles (d.b.)	8.01	65.25	58.64	13.73	13.07
Ashes	30.33	33.10	24.39	30.61	29.74
FC	61.66	1.65	16.97	55.66	57.19
Elemental analysis (wt%, d.b.)					
C	62.07	15.37	41.25	57.40	59.99
H	2.30	1.35	5.03	2.21	2.57
N	1.16	0.36	6.78	1.08	1.72
S	2.21	0.24	1.89	2.01	2.18
O[a]	1.93	49.58	20.66	6.69	3.80
Elemental analysis (J/g, d.b.)					
HHV	24,382	2489	16,429	22,193	23,587

FC Fixed carbon, *HHV* high heat value, *d.b.* dry basis

[a] Calculated by difference

Thermogravimetric Analysis

The differential thermogravimetric (DTG) results obtained from the temperature programmed combustion and pyrolysis of C, L1 and L2 at $\beta = 0.5$ K/s are shown in Fig. 1, while those corresponding to their respective blends, CL1 and CL2, are shown in Fig. 2. Also, weighted calculated DTG curves corresponding to the combustion and pyrolysis of the blends are shown in Fig. 2 together with experimental curves.

On raising the temperature, combustion or the pyrolysis of the sample takes place with an associated weight loss. Then, when the fuel and/or volatiles content of the sample is exhausted, the mass corresponding to the ashes or char remains stable in the combustion or pyrolysis DTG curves, respectively.

In Fig. 1, the combustion DTG curves corresponding to C may be considered typical of a bituminous coal, the loss of volatiles and char gasification occurring in a single step, as for the large contribution of fixed carbon content in C (see Table 1) to the mass loss during combustion. Moreover, a slight weight gain due to oxygen chemisorption may be observed during the combustion of coal, which is not present in the DTG curves corresponding to L1 and L2. With respect to L1 and L2, their DTG combustion curves were different between them and also very different from C. In the case of L1, the weight loss during combustion occurred in two clear stages, which is in agreement with results found by Yanfen et al. [12]. These authors [12] stated that the first and the second steps correspond to the decomposition of combustible components and of mineral filling, respectively. The first stage must include the combustion of cellulose, which typically occurs at around 600 K [12] while the second stage must be related to the combustion of calcium carbonate, which is characterized by burning at relative high temperatures. Regarding L2, four combustion steps may be observed throughout combustion. The first step, which is in the same temperature range than for L1, may be related to volatiles yield and combustion of cellulose [12, 17]. Then, there is a shoulder that may be related to the combustion of biodegradable organics, probably generated during the wastewater biological treatment. The combustion of fixed carbon occurred next, in the same temperature range as for C. The last step, in the same temperature range as the second stage of the combustion of L1, must correspond to the decomposition of mineral content [12].

With respect to the pyrolysis DTG curves in Fig. 1, it is evident that the mass loss associated to the pyrolysis of coal is very low compared to its combustion, as corresponds to the low volatiles content of coal (see Table 1). This is not the case of either L1 or L2, which pyrolysis DTG curves are more similar to their respective combustion profiles. Furthermore, weight loss during the pyrolysis of C occurs in a single step, while two steps are evident in the pyrolysis DTG curves of either L1 or L2. In any case, the pyrolysis DTG curves of L1 and L2 show plain peculiarities. As may be seen in Fig. 1 (see the scale of Y axis), more intense weight loss occurs during both steps of the pyrolysis of L1, as compared with L2, which is in agreement with the higher volatiles content of the first (see Table 1). On the other hand, the first pyrolysis step occurs in a broader range of temperatures for L2 than for L1. In fact, the pyrolysis DTG curve corresponding to L1 mostly resembles its combustion profile, which is in agreement with the low fixed carbon of L1 (see Table 1). However,

Author's personal copy

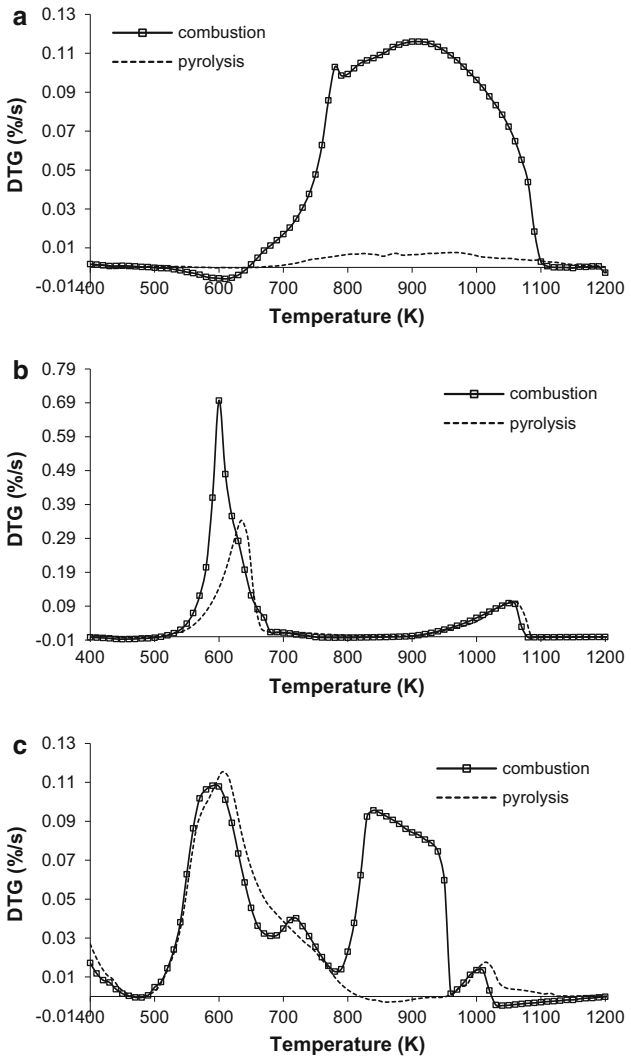

Fig. 1 Combustion and pyrolysis DTG curves for C (**a**), L1 (**b**) and L2 (**c**). Note that the *scale* of figures has been adjusted for a better visualisation of DTG curves

for L2, the step corresponding to the combustion of fixed carbon is missed in its DTG pyrolysis curve while the shoulder corresponding to the second combustion step is still present in the pyrolysis curve. It may be said that differences between the here used coal and pulp mill sludge are relevant, but, there are also apparent differences between L1 and L2, either from a quantitative or qualitative point of view, as indicated by properties in Table 1 and DTG curves in Fig. 1.

Experimental co-combustion curves in Fig. 2a, b mostly resemble the DTG combustion curve of C (Fig. 1). However, it is to highlight the absence of the chemisorption weight gain, and moreover, in the case of CL1, remains the first step of the L1 combustion curve, which was associated to the combustion of the cellulosic content. Nevertheless, according to the weighted calculated DTG curves in Fig. 2c, d, a more intense peak would correspond to the first stage of the combustion of CL1 and also CL2. Differently from combustion, experimental co-pyrolysis curves in Fig. 2a, b are quite different from the pyrolysis of coal with a larger weight loss associated to the pyrolysis of CL1 and CL2. In any case, as for combustion, lower weight loss occurred for the experimental pyrolysis of CL1 and CL2 (Fig. 2a, b) than for their respective weighted calculated pyrolysis (Fig. 2c, d). Therefore, negative synergistic effects could be inferred for both the combustion and the pyrolysis of coal with either L1 or L2.

The characteristic parameters of the combustion and pyrolysis DTG experimental and calculated curves in Figs. 1 and 2 are shown in Table 2. These parameters confirm the aforementioned observation with respect to the corresponding curves. In this sense, under oxidizing atmosphere, the combustion of C starts (T_v), peaks (T_m) and ends (T_f) at higher temperatures than the combustion of L1 or L2. Also, a quite higher DTG_{max} was observed for L1, as compared with L2 and also with C. Then, the characteristic temperatures and DTG_{max} corresponding to the combustion of CL1 and CL2 are comparable with those of C, except for the lower T_v of CL2 and, especially, CL1. This lower T_v may be favourable from a practical point of view in the sense that helps the initiation of C combustion. With respect to the characteristic parameters determined for the weighted calculated combustion curves ($CL1_{CALCULATED}$ and $CL2_{CALCULATED}$), these are mostly coincident with the experimental ones (CL1 and CL2). However, it must be highlighted that the T_v corresponding to $CL2_{CALCULATED}$ is lower than for CL2. This is plain by comparing the combustion of $CL2_{CALCULATED}$ (Fig. 2d) with that CL2 (Fig. 2b), which evidences the absence of the first devolatilization step of L2 in the combustion of CL2. Equally, the first devolatilization peak in the combustion of CL1 (Fig. 2a) is less relevant than in the case of $CL1_{CALCULATED}$ (Fig. 2c). Therefore, and also considering the larger volatiles content of $CL1_{CALCULATED}$ and $CL2_{CALCULATED}$ comparatively with C (Table 1), it may be said that negative synergism has occurred in the combustion of CL1 and CL2.

As for combustion, the T_v, T_m and T_f determined for the pyrolysis of C are higher than those of L1 or L2. Also a quite higher DTG_{max} was observed for L1, as compared with L2 and, especially with C. Contrarily to their combustion, the characteristic parameters determined for the pyrolysis of CL1 and CL2 are unlike than those of C. Differences with C are evident for the lower T_v of CL1 and CL2 and, especially, for the higher DTG_{max} of CL1. However, as indicated by the parameters corresponding to the pyrolysis of $CL1_{CALCULATED}$ and $CL2_{CALCULATED}$, these differences are less relevant than would correspond. In this sense, DTG_{max} of CL1 is lower than that of

Author's personal copy

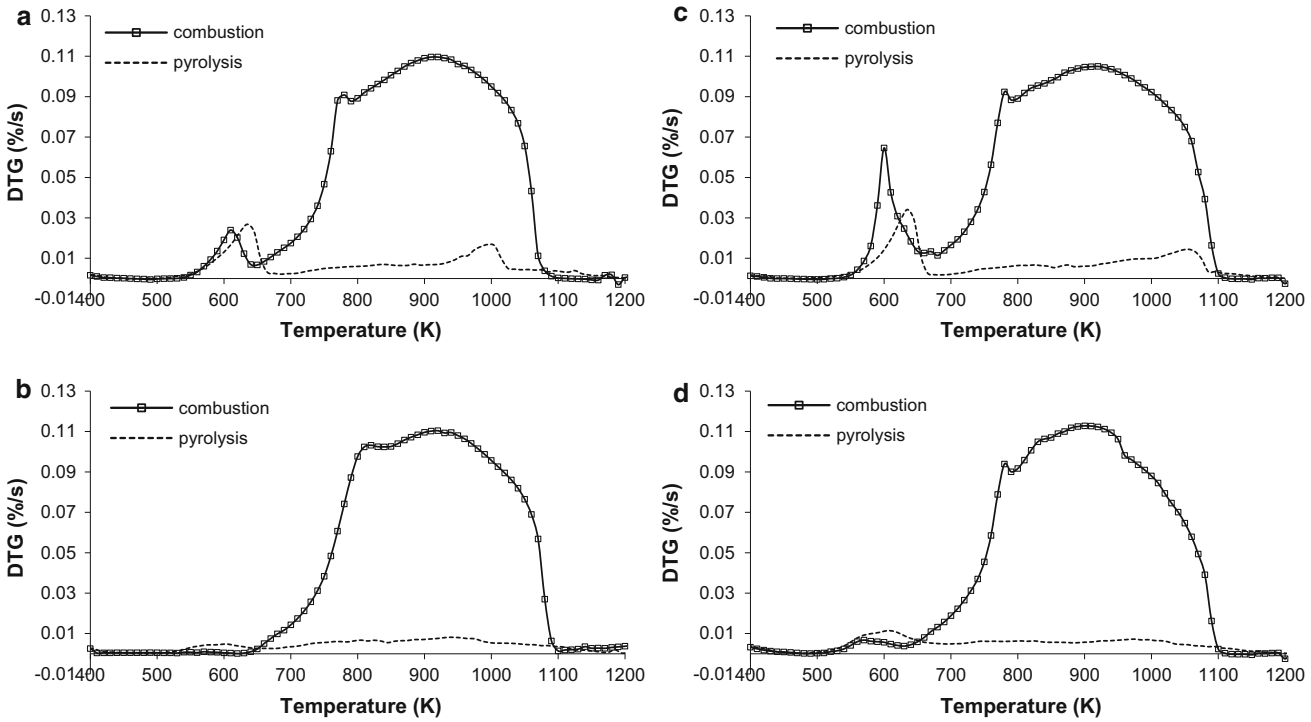

Fig. 2 Experimental co-combustion and co-pyrolysis DTG curves for CL1 (**a**) and CL2 (**b**) and weighted average calculated co-combustion and co-pyrolysis DTG curves for CL1 (**c**) and CL2 (**d**)

Table 2 Characteristic parameters obtained from the experimental DTG combustion and pyrolysis curves of coal (C), primary mill sludge (L1), secondary mill sludge (L2) and their respective blends with coal (CL1 and CL2)

Sample	Atmosphere	T_v (K)	T_m (K)	T_f (K)	DTG_{max} (%/s)	t_q (s)
C	Inert (pyrolysis)	620	964	1250	0.0097	1260
	Oxidizing (combustion)	649	915	1114	0.1162	930
L1	Inert (pyrolysis)	500	636	1090	0.3446	1180
	Oxidizing (combustion)	490	598	1077	0.6969	1174
L2	Inert (pyrolysis)	475	608	1150	0.1156	1350
	Oxidizing (combustion)	485	596	1030	0.1090	1090
CL1	Inert (pyrolysis)	500	637	1250	0.0269	1500
	Oxidizing (combustion)	529	923	1105	0.1097	1152
CL2	Inert (pyrolysis)	475	945	1250	0.0114	1550
	Oxidizing (combustion)	627	933	1100	0.1112	942
$CL1_{CALCULATED}$	Inert (pyrolysis)	500	635	1250	0.0341	1500
	Oxidizing (combustion)	530	910	1105	0.1048	1150
$CL2_{CALCULATED}$	Inert (pyrolysis)	475	605	1250	0.0114	1550
	Oxidizing (combustion)	505	900	1105	0.1128	1200

T_v = Onset temperature for volatile release. Determined as the temperature at which the rate of weight loss reached the value of 0.005 %/s, T_m = temperature of maximum rate of weight loss or peak temperature, T_f = final combustion or pyrolysis temperature. Determined as the temperature at which the rate of weight loss reached a value of 0.005 %/s then stabilizing. DTG_{max} = maximum weight loss rate, t_q = combustion or pyrolysis time. Determined as the time between T_v and T_f

$CL1_{CALCULATED}$ and the T_v of CL2 is lower than the corresponding to $CL2_{CALCULATED}$. On the basis of these differences and the weighted average properties of $CL1_{CALCULATED}$ and $CL2_{CALCULATED}$ in Table 1, namely the volatiles content, it could be stated that a slight negative synergism occurred in the pyrolysis of blends. This is patent by a less intense devolatilization than would correspond in the first stage of pyrolysis and combustion of

Author's personal copy

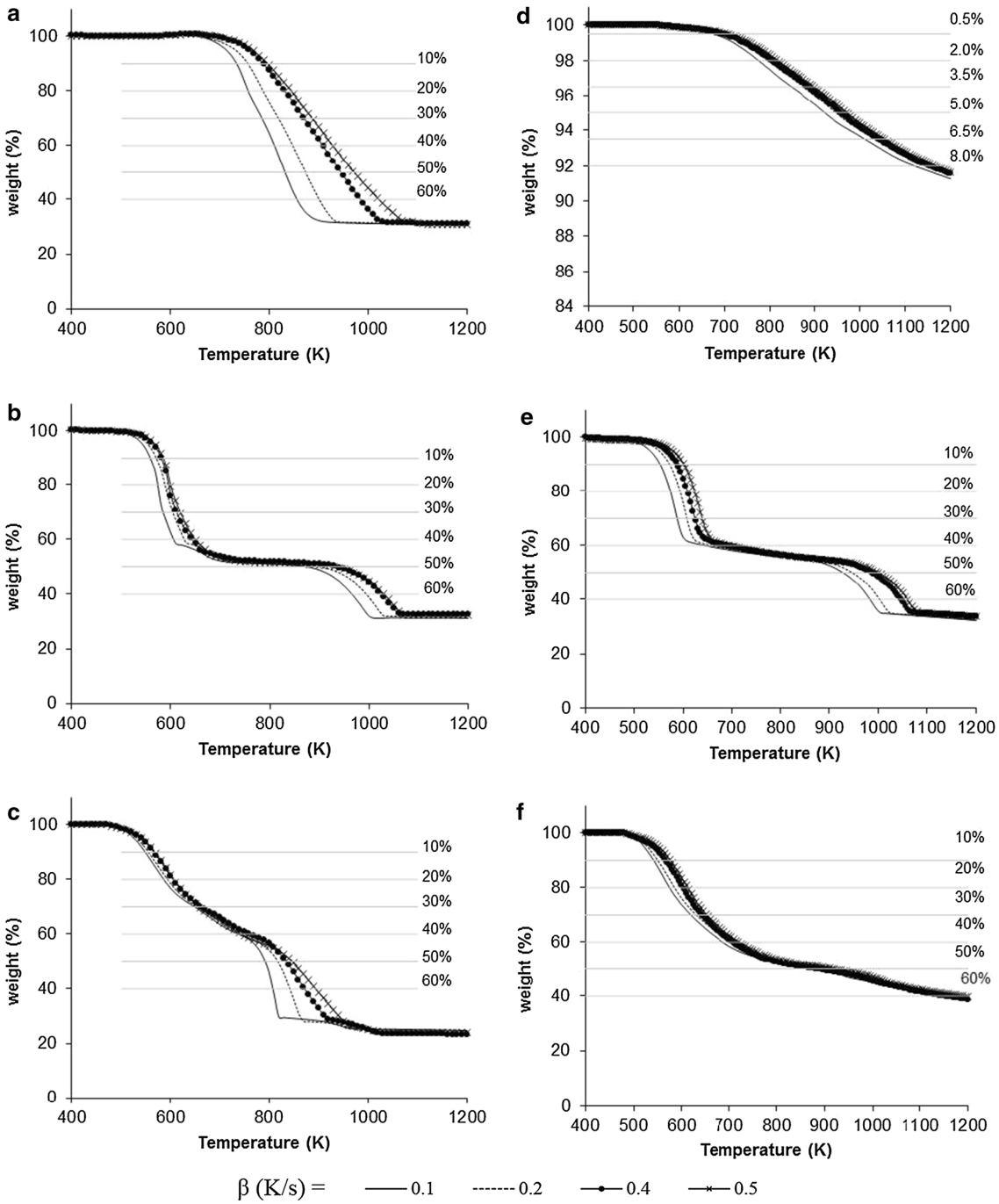

Fig. 3 TG curves corresponding to the combustion of C (**a**), L1 (**b**) and L2 (**c**) and to the pyrolysis of C (**d**), L1 (**e**) and L2 (**f**) at different heating rates (β). The conversion percentages considered for kinetic analysis have been represented by straight lines crossing experimental data. Note that the *scale* of the Y axis has been adjusted for a better visualization of results

blends (Fig. 2). According with results by Méndez et al. [15], this stage must be related to the cellulosic content of L1 and L2. Therefore, interactions during heating must have occurred between cellulose and C and part of the cellulose volatiles may have gathered on C particles, so hindering their release. It must be taken into account that the volatile content of L1 and L2 is above seven times higher than that of C, and highly related to the cellulosic content of sludge, particularly in the case of L1. This supports the fact that, although the volatiles content of $CL1_{CALCULATED}$ and $CL2_{CALCULATED}$ (Table 1) is quite similar, the first combustion and pyrolysis stage is more intense for CL1 than for CL2, both in the experimental and, especially, in the weighted calculated curves (Fig. 2).

Author's personal copy

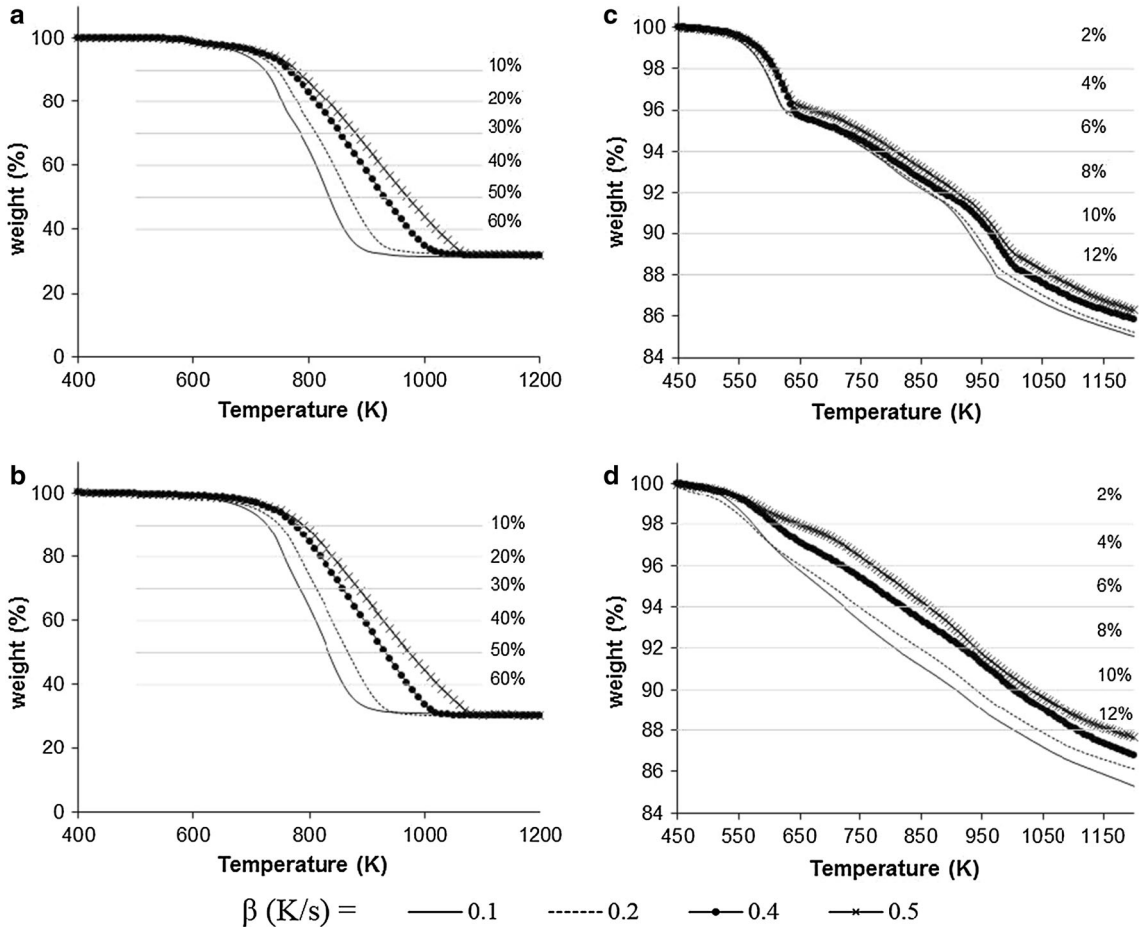

Fig. 4 TG curves corresponding to the combustion of CL1 (**a**) and CL2 (**b**) and to the pyrolysis of CL1 (**c**) and CL2 (**d**) at different heating rates (β). The conversion percentages considered for kinetic analysis have been represented by straight lines crossing experimental data. Note that the *scale* of the Y axis has been adjusted for a better visualization of results

Non-isothermal Kinetic Analysis

The TG curves obtained from the temperature programmed combustion and pyrolysis of the single samples at the heating rates (β) of 0.1, 0.2, 0.4 and 0.5 K/s are depicted in Fig. 3 together with the percentages of conversion considered for the kinetic analysis. In the same way, Fig. 4 represents the TG combustion and pyrolysis curves corresponding to blends CL1 and CL2.

Curves in Fig. 3 confirm large differences between weight loss during combustion and pyrolysis of C and similarities between these processes in the case of L1. Meanwhile, for L2, main differences between combustion and pyrolysis TG curves are related to the weight loss associated to the combustion of fixed carbon, which is absent in pyrolysis TG curves. In Fig. 4, TG combustion curves corresponding to blends CL1 and CL2 mostly resemble those of C in Fig. 3a. However, synergetic effects of blending are evidenced by the TG pyrolysis of CL1 and CL2, as compared with the pyrolysis curves of C (Fig. 3d)

The plots of $ln\beta$ versus $1/T$ corresponding to the several conversion degrees (α) considered for the combustion and pyrolysis are shown in Fig. 5 for C, L1 and L2 and in Fig. 6 for the blends CL1 and CL2. As may be seen, there is linearity for the several conversion percentages so, according with the Flynn–Wall–Ozawa kinetic method [19–21], the activation energy E may be calculated from the corresponding slope.

Table 3 shows the E values determined for the combustion and pyrolysis of C, L1 and L2 and their respective blends CL1 and CL2. The average E determined for the combustion of coal C was 85 kJ/mol, while for L1 and L2 it was 155 and 199.4 kJ/mol, respectively. Differences between E values determined for the combustion of C, L1 and L2 are the same magnitude than those obtained for different rank coals [22]. Xie and Ma [23], using the Flynn–Wall–Ozawa method determined E values between 133 and 253 kJ/mol for the combustion of paper sludge, which means a larger range than that of E values here determined for the combustion of L1 but

Author's personal copy

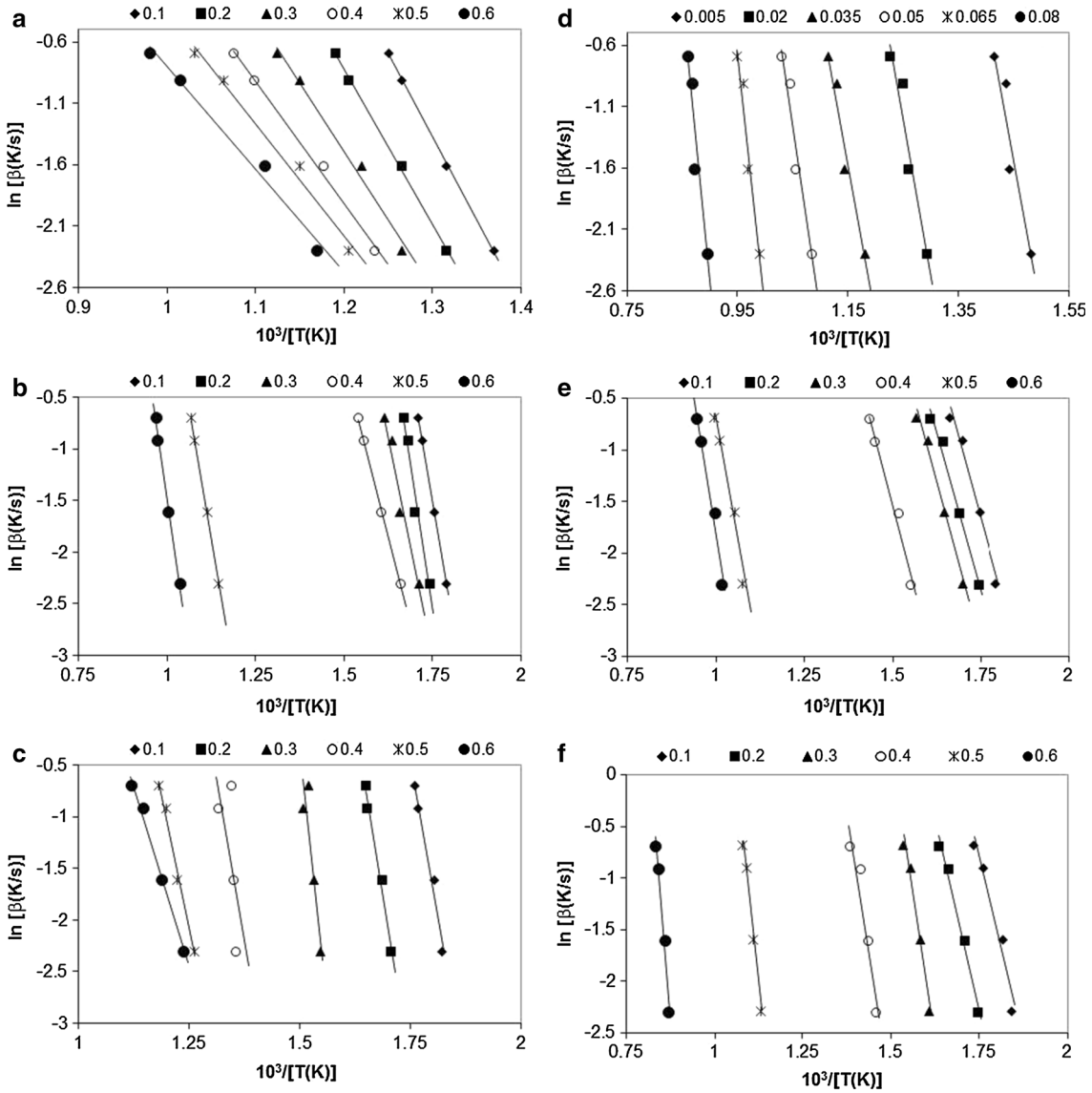

Fig. 5 Fittings corresponding to the kinetic model proposed by Ozawa–Flynn–Wall to various conversion degrees (α) corresponding to the combustion of C (**a**), L1 (**b**) and L2 (**c**) and to the pyrolysis of C (**d**), L1 (**e**) and L2 (**f**). Note that the *scales* of axis have been adjusted for a better visualization of results

shorter than for L2. Also, in the literature, apparent activation energies determined by non-isothermal thermogravimetric analysis for the combustion of biomass [24, 25] are mostly the same order than those here estimated for L1 and L2. Regarding the combustion of blends (10 wt%), average E values corresponding to CL1 and CL2 are 90.8 and 87.7 kJ/mol, respectively, which are both the same order as for the C combustion (85.0 kJ/mol). Then, although the average E determined for the combustion of L1 was lower than for L2, in the blends with coal, the average E of the combustion of CL1 was slightly higher than that of CL2. This is probable related to the large differences between the combustion profiles of C and L1, which did not show the fixed carbon combustion step but an intense peak associated to the decomposition of its cellulose content. In any case, for both the combustion of CL1 and, especially, of CL2, the determined average E values were slightly lower than the weighted average calculated ones (92 and 96.4 kJ/mol, respectively), pointing to interactions between coal and both types of sludge.

The average E determined for the pyrolysis of C (255.6 kJ/mol) was quite higher than the one determined for its combustion (85 kJ/mol), and also higher than values determined for the pyrolysis of L1 (119.7 kJ/mol) and L2 (196.6 kJ/mol). Anyway, the determined E values for the

Author's personal copy

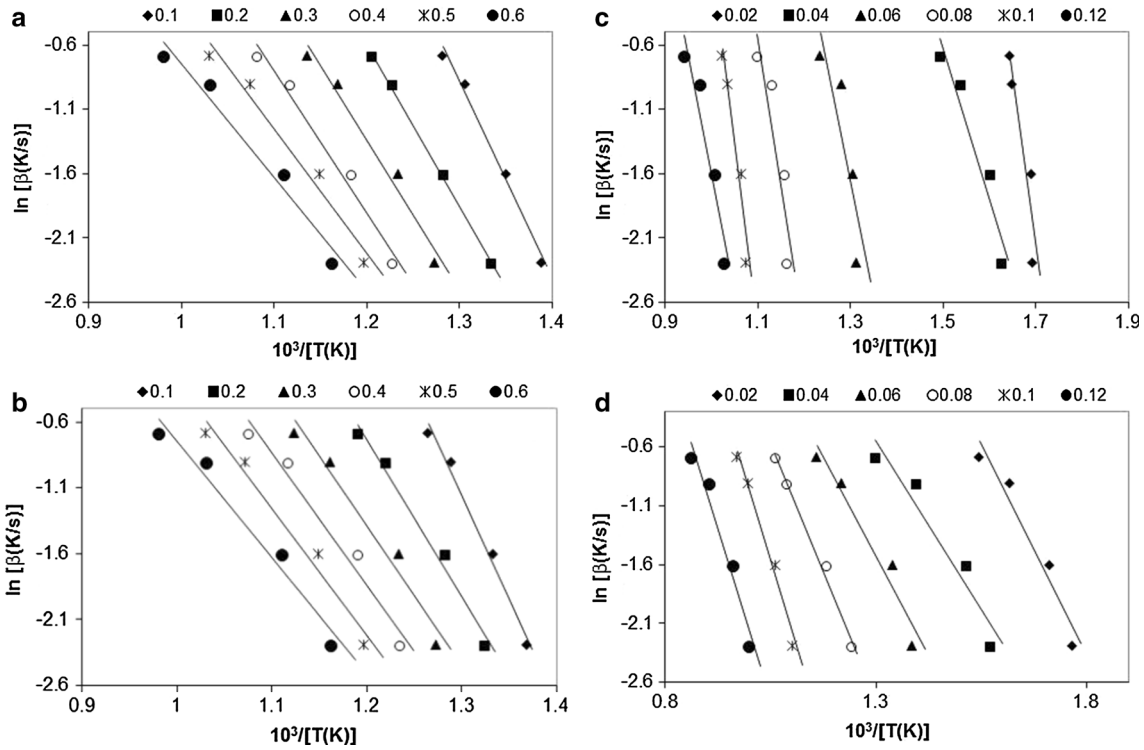

Fig. 6 Fittings corresponding to the kinetic model proposed by Ozawa–Flynn–Wall to various conversion degrees (α) corresponding to the combustion of CL1 (**a**) and CL2 (**b**) and to the pyrolysis of CL1 (**c**) and CL2 (**d**). Note that the *scales* of axis have been adjusted for a better visualization of results

Table 3 Apparent activation energy (E) estimated by the Flynn–Wall–Ozawa method for the combustion and pyrolysis of C, L1, L2 and their blends, at the considered conversion degrees (α)

Sample	α	Combustion		Pyrolysis	
		E (kJ/mol)	R^2	E (kJ/mol)	R^2
C	0.1	106.3	0.9995	195.1	0.9995
	0.2	99.5	0.9978	201.4	0.9978
	0.3	88.0	0.9882	199.9	0.9882
	0.4	78.7	0.9953	243.7	0.9953
	0.5	72.0	0.9864	329.8	0.9864
	0.6	65.8	0.9844	363.7	0.9844
		85.0[a]		255.6[a]	
L1	0.1	160.9	0.9999	99.6	0.9999
	0.2	177.6	0.9742	96.6	0.9742
	0.3	135.1	0.9724	99.1	0.9724
	0.4	105.5	0.9986	103.1	0.9986
	0.5	163.0	0.9974	154.2	0.9974
	0.6	188.2	0.9935	165.7	0.9935
		155.0[a]		119.7[a]	
L2	0.1	192.0	0.9694	113.5	0.9694
	0.2	209.9	0.9840	115.9	0.9840
	0.3	328.7	0.9315	173.7	0.9315
	0.4	194.8	0.9661	172.0	0.9661
	0.5	160.7	0.9880	259.6	0.9880
	0.6	110.6	0.9901	344.7	0.9901
		199.4[a]		196.6[a]	

Author's personal copy

Table 3 continued

Sample	α	Combustion		Pyrolysis	
		E (kJ/mol)	R^2	E (kJ/mol)	R^2
CL1	0.1	120.9	0.9874	201.9	0.9874
	0.2	99.7	0.9983	91.7	0.9983
	0.3	91.4	0.9737	140.0	0.9737
	0.4	86.9	0.9758	181.0	0.9758
	0.5	76.1	0.9704	229.8	0.9704
	0.6	69.6	0.9667	146.5	0.9667
		90.8[a]		165.2[a]	
CL2	0.1	124.1	0.9873	56.6	0.9873
	0.2	94.4	0.9840	45.4	0.9840
	0.3	83.1	0.9640	53.1	0.9640
	0.4	79.1	0.9677	68.9	0.9677
	0.5	75.8	0.9729	93.9	0.9729
	0.6	69.6	0.9667	91.4	0.9667
		87.7[a]		68.2[a]	

[a] Calculated as arithmetic average of the E values determined for the different α

pyrolysis of C are similar to those found in the literature for coals [26]. No data were found in the literature on the pyrolysis of pulp mill sludge, but it may be said that E values corresponding to the pyrolysis of L1 and L2 resemble those determined by other authors for the pyrolysis of lignocellulosic wastes [26, 27]. Concerning the E determined for the pyrolysis of blends, the obtained values for CL1 (165.2 kJ/mol) and for CL2 (68.2 kJ/mol) are lower than the calculated weighted E (246.6 and 249.7 kJ/mol, respectively). Differences, which are especially evident for CL2, hint that synergism may be occurring between C and L1 or L2 during their co-pyrolysis. This could be related to coal interactions with cellulose, as highlighted by other authors [27, 28], since lignocellulose is an important constituent of L1 and L2.

Thermogravimetric results obtained in this work indicated that the addition of a relative low percentage (≤10 wt%) of either L1 or L2 favoured the initiation of C combustion while the E associated to the process remained practically the same. With respect to pyrolysis, adding primary or secondary pulp mill sludge, favoured coal devolatilization with a significant decrease of E. In any case, when blending C with L1, attention must be given to volatiles emission related to the cellulose decomposition. Thus, under the appropriate conditions, thermal co-processing of coal with primary and, especially, with secondary pulp mill sludge may be a management route for these wastes, which, furthermore, accounts for their valorization. Moreover, it was confirmed that TG analysis is very useful as a first and fast assessment tool for the consideration of thermal co-processing of wastes in existing infrastructures.

Conclusions

Large differences between C, L1 and L2 were plain by their respective DTG combustion and pyrolysis curves. These differences are mainly related to the higher fixed carbon and lower volatile content of C, as compared with L2 and, especially with L1. However these differences, the combustion of blends CL1 and CL2, mostly resembled that of coal, except for the absence of the oxygen chemisorption weight gain, the lower onset temperature for volatiles release (T_v) and, in the case of CL1, also for the presence of the cellulose decomposition stage. On the contrary, the DTG pyrolysis curves of blends showed evident differences with respect to C, especially for a more intense devolatilization stage related to the decomposition of cellulose during the pyrolysis of CL1 and CL2. A slightly negative synergism occurred during the combustion and pyrolysis of blends, as indicated by differences between the experimental and the weighted average DTG curves. Sludge–coal interactions were further confirmed by the lower than calculated apparent activation energies (E) determined for the combustion and pyrolysis of blends. Globally, results obtained in this work showed the potential of thermal valorization of pulp mill sludge by co-processing with coal, which means an increase of coal reactivity with equal (for co-combustion) or lower (for co-pyrolysis) associated activation energy. In any case, from a practical point of view, for co-processing in existing plants, it must be taken into account the large volatiles content of L2 and, especially, of L1.

Acknowledgments We would like to thank assistance given by María P. González Alonso and José A. de Linaje Aguirre, from

Author's personal copy

LARECOM (Spain). Authors also thank the kind collaboration of Luís Machado and José Luís Amaral from RAIZ—Instituto de Investigação da Floresta e do Papel. FCT funding to the Associated Laboratory CESAM is acknowledged. C. Escapa acknowledges the Spanish Ministry of Education, Culture and Sports for her PhD fellowship (FPU12/03073). S. Paniagua acknowledges the grant for doctorate studies given by University of León in the framework of its own research program ULE-2014. Also, M. Otero acknowledges support from the Spanish Ministry of Economy and Competitiveness, State Secretariat for Research, Development and Innovation Spanish Ministry of Science and Innovation (RYC-2010-05634) and from MaSTherPro CESAM's project.

References

1. European Comission: A blueprint for the EU forest-based industries (woodworking, furniture, pulp & paper manufacturing and converting, printing). http://eur-lex.europa.eu/legal-content/EN/TXT/PDF/?uri=CELEX:52013SC0343&from=EN (2013). Last accessed 26 May 2015
2. Ince, B.K., Cetecioglu, Z., Ince, O.: Pollution Prevention in the Pulp and Paper Industries, Environmental Management in Practice.In: Elzbieta Broniewicz (ed.), ISBN: 978-953-307-358-3, InTech. doi: 10.5772/23709. http://www.intechopen.com/books/environmental-management-in-practice/pollution-prevention-in-the-pulp-and-paper-industries (2011). Last accessed 26 May 2015
3. Ashrafi, O., Yerushalmi, L., Haghighat, F.: Wastewater treatment in the pulp-and-paper industry: a review of treatment processes and the associated greenhouse gas emission. J. Environ. Manag. (2015). doi:10.1016/j.jenvman.2015.05.010
4. Savant, D.V., Abdul-Rahman, R., Ranade, D.R.: Anaerobic degradation of adsorbable organic halides (AOX) from pulp and paper industry wastewater. Bioresour. Technol. **97**, 1092–1104 (2006)
5. The World Bank Group: Pollution Prevention and Abatement Handbook, 1998: Toward Cleaner. The International Bank for Reconstruction and Development, Washington, DC (1999)
6. Pokhrel, D., Viraraghavan, T.: Treatment of pulp and paper mill wastewater—a review. Sci. Total Environ. **333**, 37–58 (2004)
7. Monte, M.C., Fuente, E., Blanco, A., Negro, C.: Waste management from pulp and paper production in the European Union. Waste Manag **29**, 293–308 (2009)
8. Elliott, A., Mahmood, T.: Survey benchmarks generation, management of solid residues. Pulp Pap. **79**, 49–55 (2005)
9. Vamvuka, D., Salpigidou, N., Kastanaki, E., Sfakiotakis, S.: Possibility of using paper sludge in co-firing applications. Fuel **88**, 637–643 (2009)
10. Otero, M., Calvo, L.F., Gil, M.V., García, A.I., Morán, A.: Co-combustion of different sewage sludge and coal: a non-isothermal thermogravimetric kinetic analysis. Bioresour. Technol. **99**, 6311–6319 (2008)
11. Otero, M., Sanchez, M.E., García, A.I., Morán, A.: Simultaneous thermogravimetric mass spectrometric study on the co-combustion of coal and sewage sludge. J. Therm. Anal. Calorim. **86**, 489–495 (2006)
12. Yanfen, L., Xiaoqian, M.: Thermogravimetric analysis of the co-combustion of coal and paper mill sludge. Appl. Energy **87**, 3526–3532 (2010)
13. Liu, K., Ma, X.Q., Xiao, H.M.: Experimental and kinetic modeling of oxygen-enriched air combustion of paper mill sludge. Waste Manag **30**, 1206–1211 (2010)
14. Fang, S., Yu, Z., Lin, Y., Hu, S., Liao, Y., Ma, X.: Thermogravimetric analysis of the co-pyrolysis of paper sludge and municipal solid waste. Energy Convers. Manag. **101**, 626–631 (2015)
15. Méndez, A., Fidalgo, J.M., Guerrero, F., Gasco, G.: Characterization and pyrolysis behaviour of different paper mill waste materials. J. Anal. Appl. Pyrolysis **86**, 66–73 (2009)
16. Zhu, X., Chen, Z., Xiao, B., Hu, Z., Hu, M., Liu, C., Zhang, Q.: Co-pyrolysis behaviors and kinetics of sewage sludge and pine sawdust blends under non-isothermal conditions. J. Therm. Anal. Calorim. **119**, 2269–2279 (2015)
17. Coimbra, R.N., Paniagua, S., Escapa, C., Calvo, L.F., Otero, M.: Combustion of primary and secondary pulp mill sludge and their respective blends with coal: a thermogravimetric assessment. Renew. Energy **83**, 1050–1058 (2015)
18. Vyazovkin, S., Wight, C.A.: Isothermal and non-isothermal kinetics of thermally stimulated reactions of solids. Int. Rev. Phys. Chem. **17**, 407–433 (1998)
19. Ozawa, T.: A new method of analyzing thermogravimetric data. Bull. Chem. Soc. Jpn **38**, 1881–1886 (1965)
20. Flynn, J.H., Wall, L.A.: A quick, direct method for the determination of activation energy from thermogravimetric data. Polym. Lett. **4**, 323–328 (1966)
21. Doyle, C.D.: Estimating isothermal life from thermogravimetric data. J. Appl. Polym. Sci. **6**, 639–642 (1962)
22. Kök, M.V.: Temperature-controlled combustion and kinetics of different rank coal samples. J. Therm. Anal. Calorim. **79**, 175–180 (2005)
23. Xie, Z., Ma, X.: The thermal behaviour of the co-combustion between paper sludge and rice straw. Bioresour. Technol. **146**, 611–618 (2013)
24. Xiao, H.-M., Ma, X.-Q., Lai, Z.-Y.: Isoconversional kinetic analysis of co-combustion of sewage sludge with straw and coal. Appl. Energy **86**, 1741–1745 (2009)
25. Idris, S.S., Rahman, N.A., Ismail, K.: Combustion characteristics of Malaysian oil palm biomass, sub-bituminous coal and their respective blends via thermogravimetric analysis (TGA). Bioresour. Technol. **123**, 581–591 (2012)
26. Aboyade, A.O., Görgens, J.F., Carrier, M., Meyer, E.L., Knoetze, J.H.: Thermogravimetric study of the pyrolysis characteristics and kinetics of coal blends with corn and sugarcane residues. Fuel Process. Technol. **106**, 310–320 (2013)
27. Wu, Z., Wang, S., Zhao, J., Chen, L., Meng, H.: Synergistic effect on thermal behavior during co-pyrolysis of lignocellulosic biomass model components blend with bituminous coal. Bioresour. Technol. **169**, 220–228 (2014)
28. Guo, Z., Bai, Z., Bai, J., Wang, Z., Li, W.: Synergistic effects during co-pyrolysis and liquefaction of biomass and lignite under syngas. J. Therm. Anal. Calorim. **119**, 2133–2140 (2015)

Anexo IV

Coimbra, R.N., Calisto, V., Ferreira, C.I.A., Esteves, V.I., Otero, M., *in press*. Removal of pharmaceuticals from municipal wastewater by adsorption onto pyrolyzed pulp mill sludge. Arabian Journal of Chemistry. http://dx.doi.org/10.1016/j.arabjc.2015.12.001

Arabian Journal of Chemistry (2015) xxx, xxx–xxx

King Saud University

Arabian Journal of Chemistry

www.ksu.edu.sa
www.sciencedirect.com

ORIGINAL ARTICLE

Removal of pharmaceuticals from municipal wastewater by adsorption onto pyrolyzed pulp mill sludge

R.N. Coimbra [a], V. Calisto [b], C.I.A. Ferreira [b], V.I. Esteves [b], M. Otero [a,*]

[a] Department of Applied Chemistry and Physics, Institute of Environment, Natural Resources and Biodiversity (IMARENABIO), University of León, León 24071, Spain
[b] Department of Chemistry and CESAM (Centre for Environmental and Marine Studies), University of Aveiro, Campus de Santiago, 3810-193 Aveiro, Portugal

Received 22 August 2015; accepted 1 December 2015

KEYWORDS

Paper sludge;
Pyrolysis;
Wastewater treatment;
Emerging contaminants;
Pain reliever;
Sorption

Abstract A charcoal was produced from primary pulp mill sludge and then used for the adsorptive removal of diclofenac, salicylic acid, ibuprofen and acetaminophen. A main aim was to assess the utilization of this material for the tertiary treatment of sewage. For this purpose, the adsorption of the selected pharmaceuticals from the secondary effluent of a sewage treatment plant (STP) was compared with their adsorption from ultrapure water. Differences in the adsorption kinetics and equilibrium were evident between the four pharmaceuticals considered. However, differences between the adsorption from the two aqueous matrixes considered were negligible. It was hypothesized that synergetic microorganism removal compensated the competitive effects in wastewater.
© 2015 The Authors. Production and hosting by Elsevier B.V. on behalf of King Saud University. This is an open access article under the CC BY-NC-ND license (http://creativecommons.org/licenses/by-nc-nd/4.0/).

1. Introduction

The pulp and paper industry is a strategic economic sector in Europe that largely contributes to the European Union (EU) financial growth and job creation (CEPI, 2013). However, a main counterpart is that pulp and paper production processes are very demanding in terms of energy and water and this industry is considered one of the most polluting in the world (Ince et al., 2011). As a consequence of the high water consumption, large wastewater volumes are generated by the pulp and paper industry. This wastewater must be treated before discharge in order to accomplish with environmental regulations (Pokhrel and Viraraghavan, 2004). Therefore sludge from wastewater treatment is an unavoidable waste for the pulp and paper industry. Elliott and Mahmood (2005) estimated that around 50 kg of dry sludge result from the production of a tonne of paper, of which approximately 70% is primary sludge and 30% is secondary sludge. Thermal valorization may be considered a viable management choice for such wastes given that landfilling has been prohibited at the EU and that alternatives such as agriculture application or composting are not viable due to the composition of sludge from the pulp and paper industry (Méndez et al., 2009).

Among thermal valorization options for the pulp and paper wastes it is pyrolysis, also called destructive distillation (Monte et al., 2009). It involves the heating of the organic waste in the absence of oxygen

* Corresponding author.
E-mail address: marta.otero@unileon.es (M. Otero).
Peer review under responsibility of King Saud University.

ELSEVIER Production and hosting by Elsevier

http://dx.doi.org/10.1016/j.arabjc.2015.12.001
1878-5352 © 2015 The Authors. Production and hosting by Elsevier B.V. on behalf of King Saud University.
This is an open access article under the CC BY-NC-ND license (http://creativecommons.org/licenses/by-nc-nd/4.0/).

Please cite this article in press as: Coimbra, R.N. et al., Removal of pharmaceuticals from municipal wastewater by adsorption onto pyrolyzed pulp mill sludge. Arabian Journal of Chemistry (2015), http://dx.doi.org/10.1016/j.arabjc.2015.12.001

yielding a mixture of gaseous and liquid fuels, with a solid inert residue (char). Yang et al. (2013) reported that gas, liquid (bio-oil) and char and gas yields were 11, 10 (27.9 daf, wt%) and 79 wt%, respectively, and that the bio-oil, with a higher heating value (HHV) of 36.5 MJ kg^{-1} and low oxygen content, supplied heat enough to power a diesel engine. Then, Ridout et al. (2015) proved that the bio-oil yield could be increased by fast pyrolysis. However, in practice, pyrolysis is not a preferred management option for paper industry wastes (Monte et al., 2009). Adding some value to the solid residue (char) from pyrolysis would undoubtedly boost this waste-to-energy management choice. The practical utilization of char as adsorbent for wastewater treatment is a way to do it. In this sense, chars from different paper waste materials have been used to adsorb trace metals (Méndez et al., 2009) and pharmaceuticals (Calisto et al., 2014) from water.

Traditionally, pharmaceuticals were not considered as environmental pollutants, but at present they constitute a group of great concern among emerging contaminants (ECs). Pharmaceuticals were designed to cause a physiological response and their presence in the environment may affect non-target individuals and species, which has raised alarms for possible impacts on human health (Santos et al., 2010). The way that ECs enter the environment depends on their pattern of usage and mode of application but, in the case of pharmaceuticals coming from human use and/or excretion, municipal sewage treatment plants (STPs) are important sources in the aquatic environment (Farré et al., 2008). Actually, STPs were conceived to reduce the concentration of legislated parameters, such as chemical oxygen demand (COD), biological oxygen demand (BOD), total suspended solids (TST) and nutrients but not emerging contaminants (ECs), such as pharmaceuticals. However, it is expected that in the nearer future more strict legislation will come out on the discharge of pharmaceuticals. In fact, pharmaceuticals have been included in the first observation list of the Water Framework Directive (WFD). Removal of these pollutants at STPs could be attained by the inclusion of a tertiary treatment before discharge. Among the several treatment options, adsorptive processes have been pointed to have large potential for the removal of ECs from water as they do not imply the generation of transformation products (Bolong et al., 2009; Priac et al., 2014). Furthermore, adsorptive treatments are advantageous from a practical point of view, due to their convenience incorporation into current water treatment processes (Domínguez et al., 2011).

In this context, research on the adsorptive removal of ECs and, namely, pharmaceuticals from water has largely increased in the last years. However, most of the published works report the adsorption of this sort of pollutants onto different adsorbents from distilled or ultrapure water but not from real wastewater. However, a main issue for the applicability of any adsorbent in tertiary treatment is the study of its utilization for pharmaceuticals adsorption from real wastewater. Therefore, this work aimed to assess the utilization of pyrolyzed paper mill sludge for the removal of pharmaceuticals from wastewater by comparing their adsorption from the secondary effluent of a STP with their adsorption from ultrapure water. For this purpose, the selected pharmaceuticals were pain relievers, namely diclofenac, ibuprofen, salicylic acid and acetaminophen. These pharmaceuticals belong to the anti-inflammatory and/or analgesic groups and among the most commonly used of all medications in the world and, consequently, also among the most frequently found drugs in STP effluents and natural waters.

2. Materials and methods

2.1. Adsorbent materials

Primary sludge (PS) was collected from a mill that employs the kraft elemental chlorine free (ECF) pulp production process, which operates exclusively with eucalyptus wood (Eucalyptus globulus). PS, which is produced at an average rate of 20 kg per ton of air-dried pulp, results from fibers rejected after the cooking/digestion pulping step and losses of fibers and other solids which occur when liquid effluents are involved (for example, washing and bleaching). After collection, PS was dried at room temperature and then subjected to oven drying at 60 °C, blade milled and pyrolyzed in a Nüve muffle (MF 106, Turkey). The pyrolysis was carried out at 800 °C under N_2 saturated atmosphere (N_2 flow of 0.5 dm^3 min^{-1}) during 150 min. The pyrolysis of PS to obtain PS800-150 was meticulously described by Calisto et al. (2014), and a summary of the main properties of this char is displayed in Table 1. A detailed characterization of PS800-150, namely total organic carbon, FTIR, ^{13}C and ^{1}H solid state NMR and SEM analysis may be found elsewhere (Calisto et al., 2014).

2.2. Chemicals and analytic methods

Diclofenac sodium (⩾99%), salicylic acid (⩾99%) and acetaminophen (⩾99%) were purchased from Sigma–Aldrich (Steinheim, Germany) while ibuprofen sodium (⩾98%) was purchased from Fluka. Main properties of these compounds are depicted in Table 2.

The target pharmaceuticals were analyzed by a Jasco HPLC apparatus equipped with a PU-980 pump, a detector UV–Vis Barspec, a phenomenex C18 column (5 μm, 110 Å, 250 × 4.6 mm), a Rheodyne injector and a 50 μL loop. The wavelengths of detection were 276.5, 220, 236 and 246 for diclofenac, ibuprofen, salicylic acid and acetaminophen,

Table 1 Main properties of primary sludge from the paper industry before (PS) and after pyrolysis (PS800-150) (adapted from Calisto et al. (2014)).

	PS	PS800-150
Proximate analysis (wt%)		
Moisture content	1.57	3.16
Ash	55.31	61.25
Volatile Matter (VM)	36.09	20.77
Fixed Carbon (FC)	8.60	17.98
VM/FC	4.2	1.2
Ultimate analysis (wt%)		
C	14.83	27.05
H	1.26	0.82
N	0.40	0.33
S	0.29	0.82
O	27.91	9.73
Physical properties		
Apparent density (g cm^{-3})	NM	0.52
S_{BET} (m^2 g^{-1})	NM	209.12
V_p (cm^3 g^{-1})	NM	0.13
W_0 (cm^3 g^{-1})	NM	0.078
L (nm)	NM	1.30
D (nm)	NM	0.84

Note: Proximate analysis and ultimate analysis are presented on a dry basis (with the exception of the moisture content). Fixed carbon (proximate analysis) and oxygen (ultimate analysis) were calculated by difference. The following abbreviations have been used: Not measured (nm), surface area (S_{BET}), total pore volume (V_p), total micropore volume (W_0), average micropore width (L) and average pore diameter (D).

Please cite this article in press as: Coimbra, R.N. et al., Removal of pharmaceuticals from municipal wastewater by adsorption onto pyrolyzed pulp mill sludge. Arabian Journal of Chemistry (2015), http://dx.doi.org/10.1016/j.arabjc.2015.12.001

respectively. The mobile phase consisted of a mixture of aceto nitrile:water:orthophosphoric acid (70:30:0.1, v/v/v) for the analysis of diclofenac and salicylic acid, a mixture of metha nol:water:orthophosphoric acid (75:25:0.3) for the analysis of ibuprofen and a mixture of acetonitrile:water (30:70, v/v) for the analysis of acetaminophen. HPLC quality acetonitrile (CH_3CN) from LabScan, orthophosphoric acid (H_3PO_4) from Panreac and ultrapure water obtained by a Millipore System were used for the preparation of the mobile phase. Before use, each mixture was passed through a Millipore 0.45 μm pore size filter and degasified in an ultrasound bath during 30 min. For the chromatographic determination of concentration, four replicated injections were carried out under a mobile phase flow rate of 1 mL min^{-1}.

2.3. Wastewater from a municipal STP

Aiming the practical utilization of pyrolyzed primary pulp mill sludge in tertiary wastewater treatment, adsorption of pharmaceuticals from real wastewater was tested. Thus, for this work, the secondary effluent was collected from the STP of León (Spain). This secondary effluent is directly discharged at the Bernesga river, a tributary of the Esla river that is 77 km long and goes through the town of León. This STP consists of primary and secondary stage treatments. The primary stage comprises the following treatments: screening, sand removal, fat removal and primary clarification. Then, the secondary stage involves a plug-flow activated sludge with nitrification/denitrification followed by secondary clarification. The plant was designed to treat the wastewater of 330,000 equivalent inhabitants and has an inflow of 123,000 m^3 day^{-1} with a hydraulic retention time (HRT) of about 6 h.

Wastewater quality parameters, namely pH, conductivity, total suspended solids (TSS), biological oxygen demand at five days (BOD_5), chemical oxygen demand (DQO), NTK, N-NH_4, N-NO_3, N-NO_2, total P-PO_4, were determined by using Standard Methods (APHA-AWWA-WPCF, 2001). Obtained results are given in Table 3.

2.4. Adsorption experiments

Adsorption experiments were performed using a batch experimental approach. For each pharmaceutical, adsorption kinetic experiments were first carried out in order to determine the time necessary to attain equilibria (t_{eq}). Then equilibrium experiments were done to determine the corresponding adsorption isotherm. All experiments were carried out by shaking (250 rpm) a known mass of PS800-150 together with 100 mL of wastewater in 250 mL Erlenmeyer flasks. Initial concentration of each target pharmaceutical in wastewater was 100 ± 1 mg L^{-1}. All experiments were done in triplicate and at a constant temperature of 25 ± 2 °C by means of a thermostatically regulated incubator. Triplicate control experiments, with no adsorbent, were run in parallel with adsorption experiments in order to verify whether the concentration of the target pharmaceutical was stable throughout the duration of the experiments.

In the kinetic experiments, Erlenmeyer flasks were progressively withdrawn from the shaker after pre-set time intervals. Then, from each flask, three aliquots were taken, filtered and chromatographically analyzed to determine the concentration of the target pharmaceutical. The amount of each pharmaceutical adsorbed onto PS800-150 at each time, q_t (mg g^{-1}), was calculated by a mass balance relationship as follows:

$$q_t = (C_0 - C_t)\frac{V}{W} \quad (1)$$

where C_0 (mg L^{-1}) is the initial liquid-phase concentration of pharmaceutical, C_t (mg L^{-1}) is the liquid-phase concentration of pharmaceutical at a time t (min), V is the volume of the solution (L) and W is the mass (g) of PS800-150.

For equilibrium experiments, Erlenmeyer flasks were shaken during 1000 min in order to guarantee the equilibrium,

Table 2 Physico-chemical properties of the pharmaceuticals used in this study. *Source:* ChemSpider

Pharmaceutical (formula)	Structure	M_w (g mol^{-1})	S_w[a] (mg L^{-1})	pKa	*log* K_{ow}	PSA (A^2)	HBAC
Diclofenac Sodium ($C_{14}H_{10}Cl_2NNaO_2$)	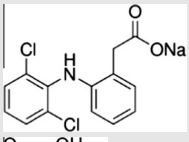	318.13	50,000	4	0.57	52.2	3
Salicylic acid ($C_7H_6O_3$)	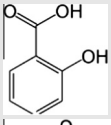	138.12	2240	2.97	2.26	57.5	3
Ibuprofen Sodium ($C_3H_{17}NaO_2$)	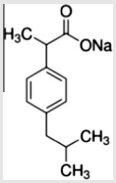	228.26	100,000	4.91	3.8	40.1	2
Acetaminophen ($C_8H_9NO_2$)	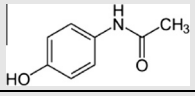	151.17	14,000	9.48	0.46	49.3	2

PSA = Polar Surface Area.
HBAC = Hydrogen Bound Acceptor Count.
[a] S_w = water solubility (25 °C).

Table 3 Main properties of the STP secondary effluent used in this work.

Parameter	
pH	7.6 ± 0.1
Conductivity (μS cm^{-1})	612 ± 3
TSS (mg L^{-1})	22 ± 1
BOD_5 (mg L^{-1})	21 ± 2
COD (mg L^{-1})	47 ± 3
NTK (mg L^{-1})	17 ± 2
N-NH_4 (mg L^{-1})	13.1 ± 0.4
N-NO_3 (mg L^{-1})	1.7 ± 0.2
N-NO_2 (mg L^{-1})	0.5 ± 0.1
Total P-PO_4 (mg L^{-1})	1.8 ± 0.1

Note: Each ± stands for standard deviation of three analytical replications.

as inferred from kinetic results. Then, from each flask, three aliquots were taken, filtered and chromatographically analyzed to determine the equilibrium concentration (C_e, mg L^{-1}) of the target pharmaceutical. The amount of each pharmaceutical adsorbed onto PS800-150 at the equilibrium, q_e (mg g^{-1}) was calculated by the following mass balance relationship:

$$q_e = (C_0 - C_e)\frac{V}{W} \quad (2)$$

For comparison purposes in terms of capacity, equilibrium experiments were also carried out following the same procedure but using ultrapure water as aqueous matrix.

2.5. Modeling of adsorption results

The experimental kinetic results were fitted with the pseudo first-order (Lagergren, 1898) and the pseudo second-order (Ho and McKay, 1999) equations. Both the pseudo-first order (Eq. (3)) and the pseudo-second order (Eq. (4)) are empirical rate equations based on the overall sorption rate:

$$q_t = q_e(1 - e^{-k_1 t}) \quad (3)$$

$$q_t = \frac{q_e^2 k_2 t}{1 + q_e k_2 t} \quad (4)$$

where k_1 (min^{-1}) and k_2 (mg g^{-1} min) are the pseudo-first and the pseudo-second order rate constants, respectively.

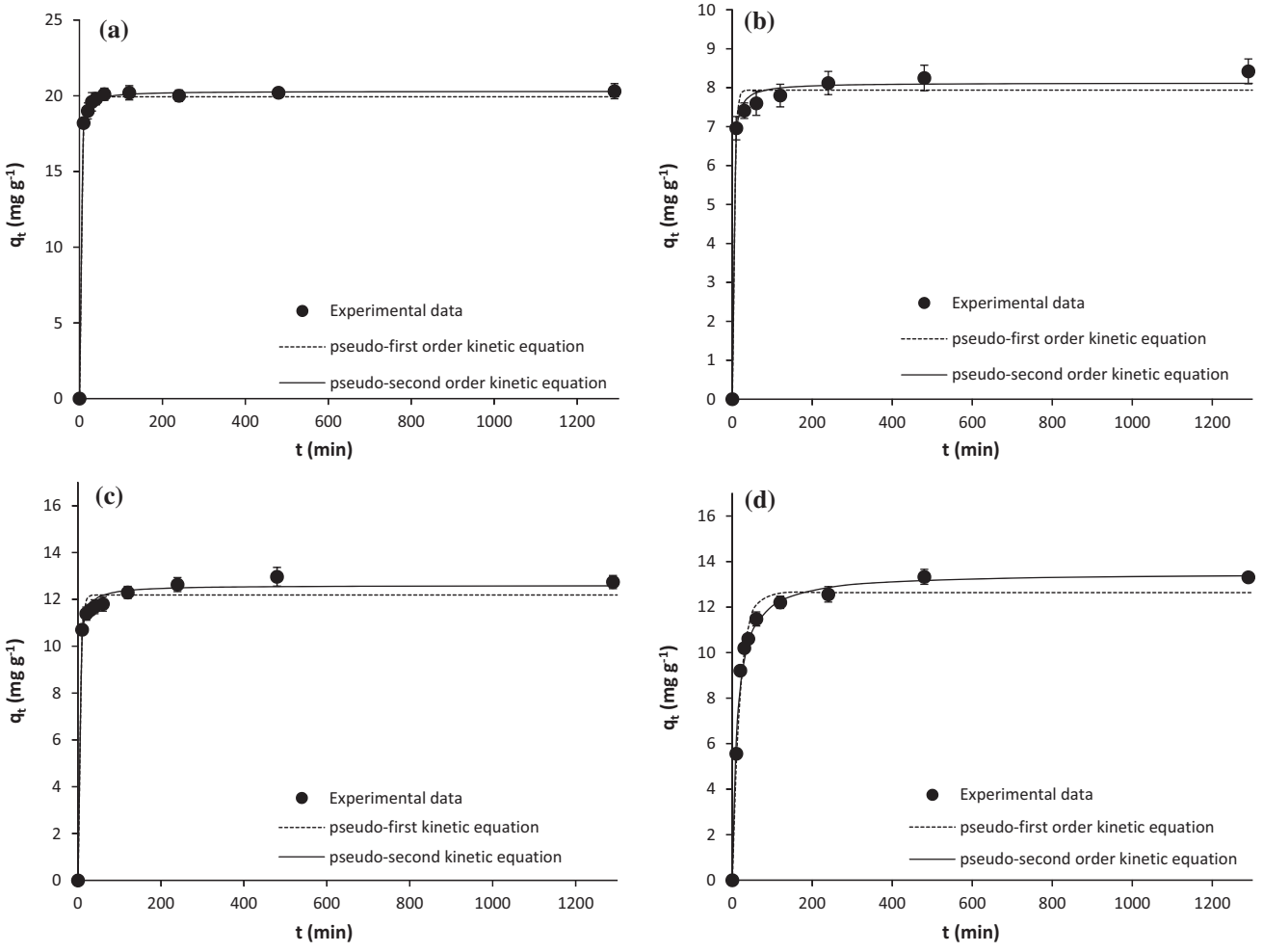

Figure 1 Kinetic results on the removal of (a) diclofenac, (b) salicylic acid, (c) ibuprofen, and (d) acetaminophen from a secondary effluent of a STP by adsorption onto PS800-150. Experimental results throughout time are shown together with the corresponding fittings to the pseudo-first and to the pseudo-second order kinetic equations. *Note:* error bars stand for standard deviation of three experimental replications.

In order to describe the adsorption equilibrium results, different non-linear models were tried. First of all, fittings to the main two parameter isotherms, namely the Freundlich isotherm (Freundlich, 1906) and the Langmuir isotherm (Langmuir, 1918), which are described by Eqs. (5) and (6), were determined. Then, the Sips isotherm (Sips, 1948), which is a combined form of Langmuir and Freundlich and a three parameter model, as described by Eq. (7), was also tried.

$$q_e = K_F C_e^{1/n} \tag{5}$$

$$q_e = \frac{Q_m K_L C_e}{1 + K_L C_e} \tag{6}$$

$$q_e = \frac{Q_m K_{LF} C_e^{1/n}}{1 + K_{LF} C_e^{1/n}} \tag{7}$$

where K_F is the Freundlich adsorption constant (mg g^{-1} (mg L^{-1})$^{-1/n}$); n is the degree of non-linearity; Q_m is the maximum adsorption capacity (mg g^{-1}); K_L (L mg^{-1}) and K_{LF} (mg g^{-1} (mg L^{-1})$^{-1/n}$) are the Langmuir and Langmuir–Freundlich affinity coefficients, respectively.

3. Results and discussion

The parameters analyzed on the secondary effluent used in this work (Table 3) showed typical values of a municipal STP effluent and accomplished with European regulations on the discharge of this sort of effluents (35 mg L^{-1} TSS, 25 mg L^{-1} BOD_5 and 125 mg L^{-1} COD as established by the EU Council Directive 91/271/EEC).

The kinetic experimental data on the adsorption of diclofenac, ibuprofen, salicylic acid and acetaminophen from the secondary effluent of a STP and from ultrapure water are shown in Figs. 1 and 2, respectively, together with fittings to the pseudo-first order and the pseudo-second order kinetic equations. Parameters determined from these fittings are depicted in Table 4.

As it may be seen in Fig. 1, under identical experimental conditions, when the equilibrium is reached, the adsorbed mass of each pharmaceutical on PS800-150 from the secondary effluent was different. Clearly, the drug showing the lowest adsorbed mass is salicylic acid. Furthermore, it is evident that the adsorption of acetaminophen is slower than that of the rest of drugs. Mostly, experimental results are better fitted

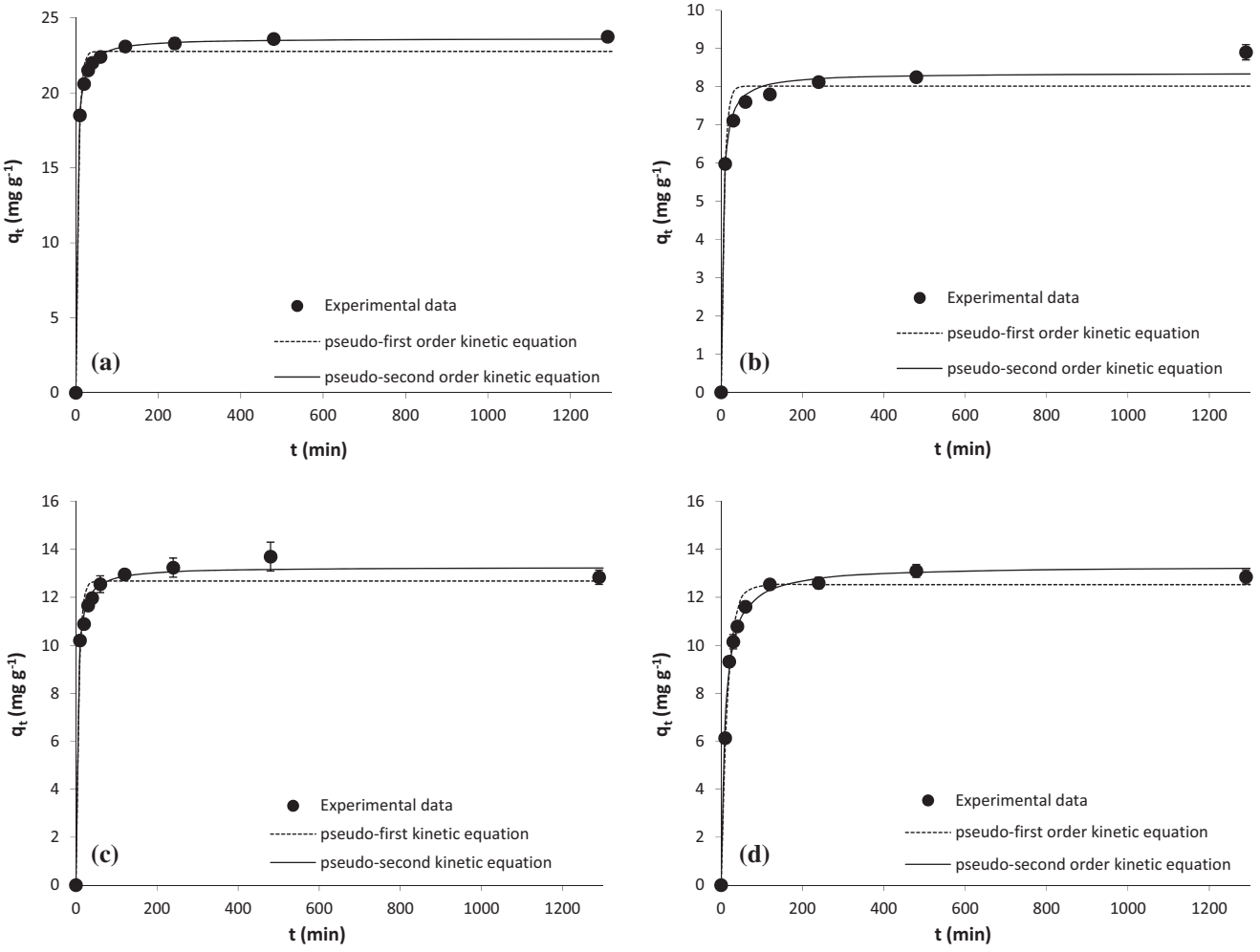

Figure 2 Kinetic results on the removal of (a) diclofenac, (b) salicylic acid, (c) ibuprofen, and (d) acetaminophen from ultrapure water by adsorption onto PS800-150. Experimental results throughout time are shown together with the corresponding fittings to the pseudo-first and to the pseudo-second order kinetic equations. *Note:* error bars stand for standard deviation of three experimental replications.

by the pseudo-second order equation than by the first order one, which is confirmed by the R^2 and S_{yx} values in Table 4. The kinetic constant k_2 decreases from salicylic acid > diclofenac > ibuprofen > acetaminophen. Furthermore, the k_2 corresponding to the adsorption of acetaminophen is an order of magnitude lower than the k_2 determined for the adsorption of the other pharmaceuticals here considered. On the other hand, the fitted q_e for the adsorption of salicylic acid is an order of magnitude lower than for the rest of drugs.

Kinetic results on the adsorption of the considered pharmaceuticals from ultrapure water are given in Fig. 2. As for the adsorption from the secondary effluent, fittings to the pseudo-second order equation are better than those to the pseudo-first order one; salicylic acid was the one showing the lowest adsorbed equilibrium concentration (q_e), which was an order of magnitude lower than for the rest of pharmaceuticals; and the adsorption of acetaminophen was the slowest one with a k_2 an order of magnitude lower than for the rest of drugs. From ultrapure water, the kinetic constant k_2 also decreases from salicylic acid > diclofenac > ibuprofen > acetaminophen. When comparing the adsorption kinetics of each pharmaceutical from wastewater (Fig. 1) with its adsorption from ultrapure water (Fig. 2), differences are not especially relevant as confirmed by the pseudo-second order kinetic parameters in Table 4. Equilibrium was attained quite quickly from either the STP secondary effluent or ultrapure water, for all the pharmaceuticals equilibrium being attained within 200 min. In any case, under the experimental conditions here used, the kinetic constant k_2 was slightly higher (diclofenac, salicylic acid, ibuprofen) or equal (acetaminophen) for the adsorption from the secondary STP effluent than from ultrapure water. On the other hand, the adsorbed concentration in the equilibrium (q_e) was slightly higher (diclofenac, ibuprofen) or equivalent (salicylic acid, acetaminophen) from ultrapure than from the secondary STP effluent.

The equilibrium experimental data on the adsorption of diclofenac, ibuprofen, salicylic acid and acetaminophen from the secondary STP effluent and from ultrapure water are shown in Figs. 3 and 4, respectively, together with fittings to the isotherm models considered. Parameters determined from these fittings are depicted in Table 5.

The equilibrium isotherms obtained for the adsorption of the pharmaceuticals from the STP effluent (Fig. 3) show some differences regarding the adsorption capacity and shape of isotherm. The adsorption capacity decreases from diclofenac > ibuprofen ≈ acetaminophen > salicylic acid. These capacity differences must be related to the drugs properties, among which S_w and *log* K_{ow} seem to have been especially determinant (Calisto et al., 2015). With respect to the isotherm, fittings to the Sips model are the most accurate for diclofenac, ibuprofen and acetaminophen. However, for salicylic acid, ambiguous fittings to the Sips isotherm were obtained, while both the Langmuir and, especially, the Freundlich isotherm models fitted experimental results. These observations are confirmed by parameters in Table 5, which make evident differences between the capacity and the isotherm model fittings.

As shown in Fig. 4, the adsorption equilibrium of pharmaceuticals from ultrapure water mostly resembles their adsorption from the STP secondary effluent. The equilibrium capacity also decreases from diclofenac > ibuprofen ≈ acetaminophen > salicylic acid and the Sips isotherm model

Table 4 Kinetic parameters obtained from the fittings of experimental results on the adsorption of each pharmaceutical to the pseudo-first and to the pseudo-second order equations.

	Pharmaceuticals							
	Diclofenac		Salicylic acid		Ibuprofen		Acetaminophen	
	STP-SE	UP-W	STP-SE	UP-W	STP-SE	UP-W	STP-SE	UP-W
Pseudo-first order								
k_1 (min^{-1})	0.235 ± 0.130	0.153 ± 0.017	0.207 ± 0.038	0.129 ± 0.025	0.198 ± 0.033	0.138 ± 0.022	0.052 ± 0.005	0.061 ± 0.004
q_e (mg g^{-1})	19.94 ± 0.02	22.77 ± 0.31	7.94 ± 0.15	8.01 ± 0.22	12.19 ± 0.19	12.68 ± 0.27	12.64 ± 0.31	12.53 ± 0.21
R^2	0.9971	0.9883	0.9861	0.9712	0.9832	0.9720	0.9774	0.9883
S_{xy}	0.36	0.82	0.36	0.52	0.53	0.71	0.66	0.47
Pseudo-second order								
k_2 (g mg^{-1} min^{-1})	0.042 ± 0.003	0.015 ± 0.000	0.063 ± 0.015	0.027 ± 0.005	0.038 ± 0.006	0.021 ± 0.003	0.006 ± 0.001	0.007 ± 0.001
q_e (mg g^{-1})	20.30 ± 0.06	23.64 ± 0.05	8.13 ± 0.11	8.36 ± 0.15	12.60 ± 0.13	13.26 ± 0.16	13.50 ± 0.23	13.31 ± 0.17
R^2	0.9996	0.9998	0.9944	0.9912	0.9956	0.9940	0.9914	0.9948
S_{xy}	0.13	0.11	0.23	0.29	0.27	0.33	0.41	0.31

Note: Each ± stands for standard deviation of three experimental replications.

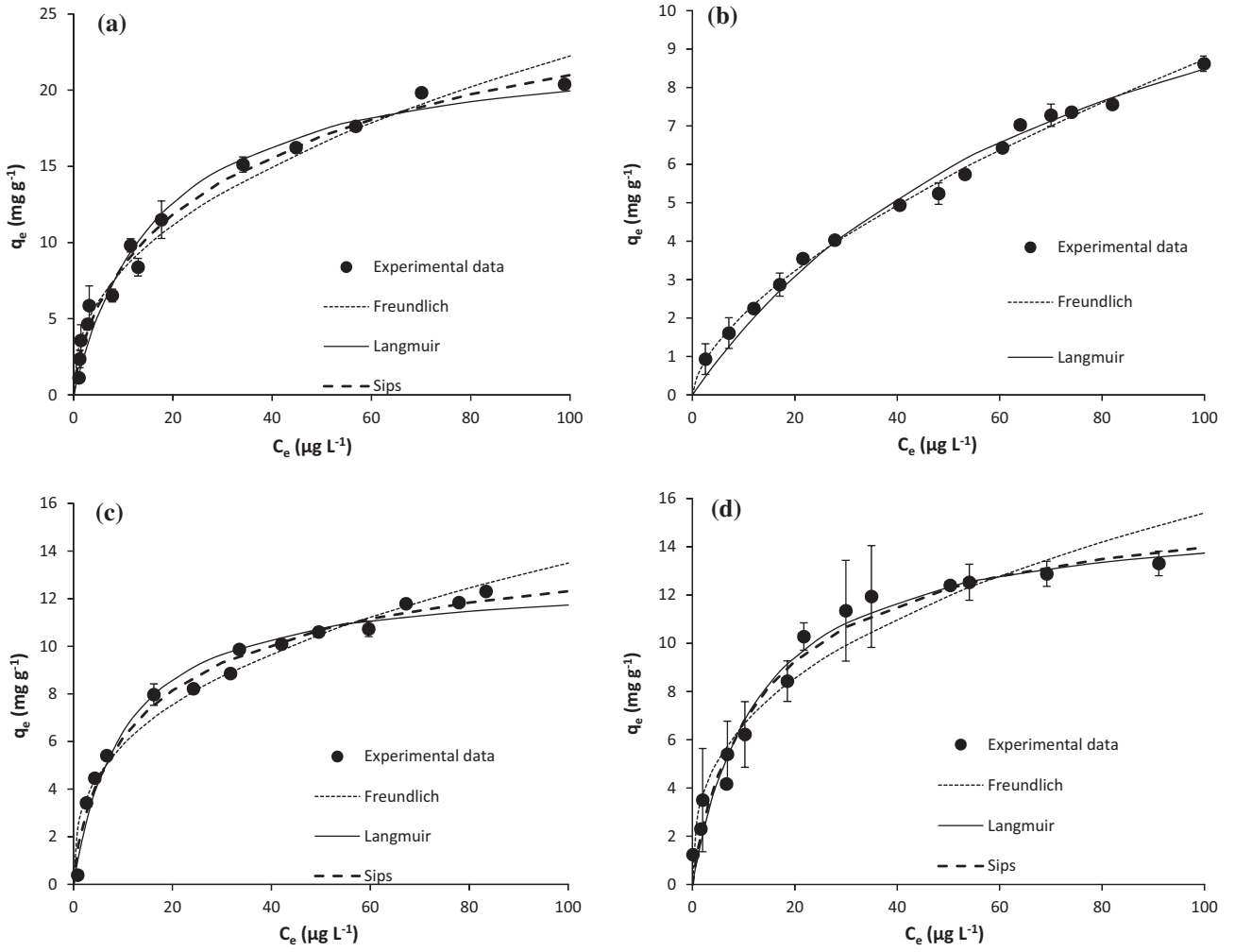

Figure 3 Equilibrium results on the removal of (a) diclofenac, (b) salicylic acid, (c) ibuprofen, and (d) acetaminophen from a secondary effluent of a STP by adsorption onto PS800-150. Experimental results are shown together with fittings to the Freundlich, to the Langmuir and to the Sips isotherm models. *Note:* error bars stand for standard deviation of three experimental replications.

is the one that better fits experimental results, except for salicylic acid. In this last case, the best fittings were obtained by the Freundlich isotherm model. Parameters in Table 5 support these remarks, as it may be seen by the Q_m and the R^2 and S_{yx} obtained for each pharmaceutical.

When comparing the equilibrium isotherms obtained for the adsorption of the considered pharmaceuticals from the STP secondary effluent and ultrapure water, differences are not outstanding. Focusing on the Sips isotherm model parameters (Table 5) for comparing the adsorption of diclofenac, ibuprofen and acetaminophen, several remarks may be made. First, considering the associated deviations, the Q_m values determined for the adsorption from the STP effluent and from ultrapure water are equivalent. In the case of the K_{LF}, which is usually related to the affinity of the adsorbent toward the adsorbate, each pharmaceutical showed a different pattern. Equal K_{LF} were determined for diclofenac while higher values were determined in ultrapure water than in the STP secondary effluent for ibuprofen and acetaminophen. Therefore, it may be inferred that the adsorption affinity for these last pharmaceuticals may be affected by the complex matrix of the STP effluent.

Finally, the shape of the adsorption isotherms revealed a favorable process, with $n > 1$, which points to the fact that the adsorbents are efficient not only removing high but also low concentrations of these pharmaceuticals. In any case, higher n values were determined for the adsorption of these pharmaceuticals from ultrapure water than from the STP effluent. With respect to salicylic acid, the Freundlich isotherm parameters in Table 5 will be used for the comparison of its adsorption from the two different aqueous matrixes. In terms of adsorption affinity, a higher salicylic acid adsorption coefficient K_F was obtained for the adsorption from ultrapure water. In the case of n, it was larger than 1 either from ultrapure water or from the STP secondary effluent, but a larger value was determined for the adsorption from ultrapure water. Therefore, some matrix effects must have affected the salicylic acid adsorption from the STP effluent. In any case, as it was for the rest of the pharmaceuticals, the adsorption capacity remained the same from both ultrapure water and the STP secondary effluent, which is a key issue for the application of the charcoal here produced for an adsorptive tertiary treatment of wastewater.

Please cite this article in press as: Coimbra, R.N. et al., Removal of pharmaceuticals from municipal wastewater by adsorption onto pyrolyzed pulp mill sludge. Arabian Journal of Chemistry (2015), http://dx.doi.org/10.1016/j.arabjc.2015.12.001

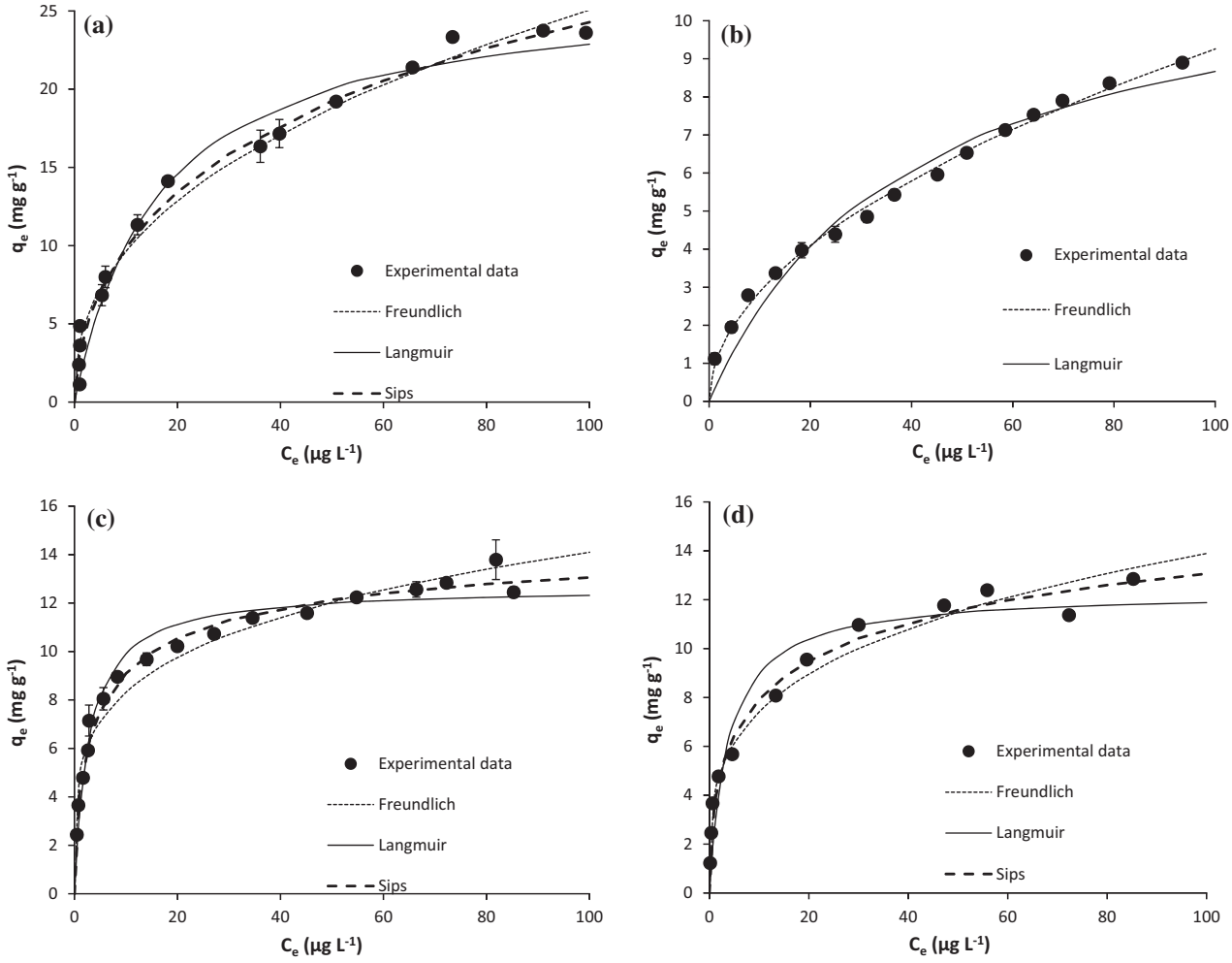

Figure 4 Equilibrium results on the removal of (a) diclofenac, (b) salicylic acid, (c) ibuprofen, and (d) acetaminophen from ultrapure water by adsorption onto PS800-150. Experimental results are shown together with fittings to the Freundlich, to the Langmuir and to the Sips isotherm models. *Note:* error bars stand for standard deviation of three experimental replications.

Our results differ from those by Sotelo et al. (2012), who determined the adsorption isotherms of diclofenac and isoproturon using three carbonaceous materials (activated carbon, multiwalled carbon nanotubes and carbon nanofibers), found that the single adsorption capacity of these drugs was higher in ultrapure water than in real wastewater. Similarly, Kovalova et al. (2013) determined the adsorption isotherm and batch kinetic data using two powdered activated carbons to assess the removal of the pharmaceuticals 5-fluorouracil (5-Fu) and cytarabine (CytR) from ultrapure water and from a wastewater treatment plant effluent. These authors (Sotelo et al., 2012; Kovalova et al., 2013) found that the presence of organic matter in wastewater lowered the pharmaceuticals adsorption uptake. Using natural organic matter (NOM), Saravia and Frimmel (2008) showed that its presence slightly reduced the adsorption of pharmaceuticals, namely carbamazepine, clofibric, diclofenac, and iohexol on activated carbon. On the contrary, Méndez-Díaz et al. (2012) found that an increased adsorption capacity of phthalic acid (PA) from wastewater than from ultrapure water occurred onto two different activated carbons, which was attributed to the action of microorganisms in wastewater. In fact, Combarros et al. (2014) proved that the formation of bacterial biofilm on the surface of a commercial activated carbon increased the adsorptive removal of salicylic acid from water. In fact, it is possible that the synergetic microorganism action may have compensated the competitive effect of organic matter so that the removal capacity remains the same when using the produced charcoal for the removal of diclofenac, salicylic acid, ibuprofen and acetaminophen. It must be highlighted that, it was verified in this work that the pharmaceuticals concentration in controls (ultrapure or STP secondary effluent, in the absence of charcoal) remained constant throughout the duration of all the experiments.

Unfortunately, no other than the here referred works have been found in the literature on the comparative kinetics or isotherms in ultrapure and wastewater for the adsorption of pharmaceuticals. Therefore, it is not possible to further contrast our findings with results by other authors and with other adsorbent materials. From our point of view, this sort of study is essential for the application of any adsorbent in the tertiary treatment of wastewater.

Please cite this article in press as: Coimbra, R.N. et al., Removal of pharmaceuticals from municipal wastewater by adsorption onto pyrolyzed pulp mill sludge. Arabian Journal of Chemistry (2015), http://dx.doi.org/10.1016/j.arabjc.2015.12.001

Table 5 Isotherm parameters obtained from the fittings of experimental results on the adsorption of each pharmaceutical from the secondary effluent of a STP (STP-SE) or from ultrapure water (UP-W).

	Pharmaceuticals							
	Diclofenac		Salicylic acid		Ibuprofen		Acetaminophen	
	STP-SE	UP-W	STP-SE	UP-W	STP-SE	UP-W	STP-SE	UP-W
Freundlich								
K_F (mg g^{-1} (mg L^{-1})$^{-1/n}$)	3.07 ± 0.31	3.70 ± 0.36	0.50 ± 0.04	0.90 ± 0.05	2.55 ± 0.29	4.91 ± 0.29	2.86 ± 0.38	3.95 ± 0.31
n	2.32 ± 0.14	2.41 ± 1.40	1.62 ± 0.04	1.97 ± 0.05	2.76 ± 0.22	4.36 ± 0.31	2.73 ± 0.27	3.66 ± 0.28
R^2	0.9744	0.9805	0.9949	0.9954	0.9617	0.9534	0.9438	0.9720
$S_{y.x}$	1.10	1.18	0.19	0.17	0.731	0.77	1.07	0.73
Langmuir								
Q_m (mg g^{-1})	23.38 ± 1.28	26.69 ± 1.53	15.12 ± 1.06	12.08 ± 1.99	12.93 ± 0.45	12.66 ± 0.30	15.53 ± 0.71	12.33 ± 0.65
K_L (L mg^{-1})	0.058 ± 0.009	0.060 ± 0.012	0.013 ± 0.002	0.025 ± 0.005	0.098 ± 0.014	0.359 ± 0.046	0.077 ± 0.012	0.265 ± 0.077
R^2	0.9714	0.9643	0.9875	0.9622	0.9739	0.9580	0.9721	0.9303
$S_{y.x}$	1.16	1.61	0.29	0.48	0.60	0.73	0.76	1.15
Sips								
Q_m (mg g^{-1})	34.84 ± 8.44	53.16 ± 22.62			16.05 ± 2.30	15.36 ± 1.05	16.79 ± 2.25	19.74 ± 4.55
K_{LF} (mg g^{-1} (mg L^{-1})$^{-1/n}$)	0.069 ± 0.012	0.062 ± 0.022			0.118 ± 0.017	0.372 ± 0.035	0.092 ± 0.021	0.230 ± 0.063
n	1.49 ± 0.21	1.77 ± 0.29			1.38 ± 0.22	1.69 ± 0.20	1.15 ± 0.21	2.15 ± 0.379
R^2	0.9852	0.9845			0.9824	0.9851	0.9734	0.9846
$S_{y.x}$	0.88	1.10			0.52	0.45	0.77	0.57

Note: Each ± stands for standard deviation of three experimental replications.

Please cite this article in press as: Coimbra, R.N. et al., Removal of pharmaceuticals from municipal wastewater by adsorption onto pyrolyzed pulp mill sludge. Arabian Journal of Chemistry (2015), http://dx.doi.org/10.1016/j.arabjc.2015.12.001

4. Conclusions

A charcoal, obtained by the pyrolysis of primary pulp mill sludge, was proved to be able to adsorb diclofenac, salicylic acid, ibuprofen and acetaminophen either from ultrapure or from an STP secondary effluent. Adsorption equilibrium of these pharmaceuticals was attained within 200 min in all cases, the kinetics being described by the pseudo-second order equation. Both from ultrapure water and from the STP secondary effluent, the kinetic constant k_2 decreased from salicylic acid > diclofenac > ibuprofen > acetaminophen. Equilibrium results were appropriately described by the Sips isotherm model, except for salicylic acid, adsorption equilibrium of which was better described by the Freundlich isotherm. Both from ultrapure water and from the STP secondary effluent, the adsorption capacity decreased from diclofenac > ibuprofen ≈ acetaminophen > salicylic acid. For each of these pharmaceuticals, neither the removal velocity nor the capacity decreased when using the produced charcoal in a real wastewater matrix with respect to its utilization in ultrapure water. Competitive effects of substances present in wastewater may have been compensated by the synergetic removal of pharmaceuticals by microorganisms.

Acknowledgments

Vânia Calisto and Catarina I.A. Ferreira thank the Portuguese Science Foundation (FCT) for their postdoctoral (SFRH/BPD/78645/2011) and PhD grants (SFRH/BD/88965/2012), respectively. Marta Otero acknowledges financial support from the Spanish Ministry of Economy and Competitiveness, State Secretariat for Research, Development and Innovation (RYC-2010-05634). European Funds through COMPETE and by National Funds through the FCT within project PEst-C/MAR/LA0017/2013 are acknowledged. Authors also thank the kind collaboration of Eng Pedro Sarmento from RAIZ – Instituto de Investigação da Floresta e do Papel.

References

APHA-AWWA-WPCF, 2001. Standard Methods for the Examination of Water and Wastewater, 20th ed. American Public Health Association, Washington DC, USA.

Bolong, N., Ismail, A.F., Salim, M.R., Matsuurad, T., 2009. A review of the effects of emerging contaminants in wastewater and options for their removal. Desalination 239, 229–246.

Calisto, V., Ferreira, C.I.A., Santos, S.M., Gil, M.V., Otero, M., Esteves, V.I., 2014. Production of adsorbents by pyrolysis of paper mill sludge and application on the removal of citalopram from water. Bioresource Technol. 166, 335–344.

Calisto, V., Ferreira, C.I.A., Oliveira, J.A.B.P., Otero, M., Esteves, V. I., 2015. Adsorptive removal of pharmaceuticals from water by commercial and waste-based carbons. J. Environ. Manage. 152, 83–90.

CEPI, 2013. Confederation of European Paper Industries (CEPI). CEPI'S Online Sustainability Report. <http://www.cepi-sustainability.eu/> (last accessed on the 15th of January 2015).

Combarros, R.G., Rosas, I., Lavín, A.G., Rendueles, M., Díaz, M., 2014. Influence of biofilm on activated carbon on the adsorption and biodegradation of salicylic acid in wastewater. Water Air Soil Poll. 225, 1858–1869.

Domínguez, J.R., González, T., Palo, P., Cuerda-Correa, E., 2011. Removal of common pharmaceuticals present in surface waters by Amberlite XAD-7 acrylic-ester-resin: influence of pH and presence of other drugs. Desalination 269, 231–238.

Elliott, A., Mahmood, T., 2005. Survey benchmarks generation, management of solid residues. Pulp Pap. 79, 49–55.

Farré, M., Pérez, S., Kantiani, L., Barceló, D., 2008. Fate and toxicity of emerging pollutants, their metabolites and transformation products in the aquatic environment. Trends Anal. Chem. 27, 991–1007.

Freundlich, H., 1906. Über die adsorption in Lösungen. Z. Phys. Chem. 57, 385–470.

Ho, I.S., McKay, G., 1999. Pseudo-second order model for sorption processes. Process Biochem. 34, 451–465.

Ince, B.K., Cetecioglu, Z., Ince, O., 2011. Pollution Prevention in the Pulp and Paper Industries, Environmental Management in Practice, Dr. Elzbieta Broniewicz (Ed.), ISBN: 978-953-307-358-3, InTech, DOI: 10.5772/23709. <http://www.intechopen.com/books/environmental-management-in-practice/pollution-prevention-in-the-pulp-and-paper-industries> (last accessed on the 19th of November 2015).

Kovalova, L., Knappe, D.R.U., Lehnberg, K., Kazner, C., Hollender, J., 2013. Removal of highly polar micropollutants from wastewater by powder activated carbon. Environ. Sci. Poll. Res. 20, 3607–3615.

Lagergren, S., 1898. Zur theorie der sogenannten adsorption gelöster stoffe. Kungliga Svenska Vetenskapsakademiens. Handlingar 24, 1–39.

Langmuir, I., 1918. The adsorption of gases on plane surfaces of glass, mica and platinum. J. Am. Chem. Soc. 40, 1361–1403.

Méndez, A., Fidalgo, J.M., Guerrero, F., Gascó, G., 2009. Characterization and pyrolysis behaviour of different paper mill waste materials. J. Anal. Appl. Pyrol. 86, 66–73.

Méndez-Díaz, J.D., Abdel daiem, M.M., Rivera-Utrilla, J., Sánchez-Polo, M.Bautista-Toledo, I., 2012. Adsorption/bioadsorption of phthalic acid, an organic micropollutant present in landfill leachates, on activated carbons. J. Colloid Interface Sci. 369, 358–365.

Monte, M.C., Fuente, E., Blanco, A., Negro, C., 2009. Waste management from pulp and paper production in the European Union. Waste Manage. 29, 293–308.

Pokhrel, D., Viraraghavan, T., 2004. Treatment of pulp and paper mill wastewater- a review. Sci. Total Environ. 333, 37–58.

Priac, A., Morin-Crini, N., Druart, C., Gavoille, S., Bradu, C., Lagarrigue, C., Torri, G., Winterton, P., Crini, G., 2014. Alkylphenol and alkylphenol polyethoxylates in water and wastewater: a review of options for their elimination. Arab. J. Chem. http://dx.doi.org/10.1016/j.arabjc.2014.05.011.

Ridout, A.J., Carrier, M., Görgens, J., 2015. Fast pyrolysis of low and high ash paper waste sludge: influence of reactor temperature and pellet size. J. Anal. Appl. Pyrol. 111, 64–75.

Santos, L.H.M.L.M., Araujo, A.N., Fachinia, A., Pena, A., Delerue-Matos, C., Montenegro, M.C.B.S.M., 2010. Review. Ecotoxicological aspects related to the presence of pharmaceuticals in the aquatic environment. J. Hazard Mater. 175, 45–95.

Saravia, F., Frimmel, F.H., 2008. Role of NOM in the performance of adsorption-membrane hybrid systems applied for the removal of pharmaceuticals. Desalination 224, 168–171.

Sips, R., 1948. Combined form of Langmuir and Freundlich equations. J. Chem. Phys. 16, 490–495.

Sotelo, J.L., Rodríguez, A.R., Mateos, M.M., Hernández, S.D., Torrellas, S.A., Rodríguez, J.G., 2012. Adsorption of pharmaceutical compounds and an endocrine disruptor from aqueous solutions by carbon materials. J. Environ. Sci. Health – Part B. Pestic. Food Contam. Agric. Wastes 47, 640–652.

Yang, Y., Brammer, J.G., Ouadi, M., Samanya, J., Hornung, A., Xu, H.M., Li, Y., 2013. Characterisation of waste derived intermediate pyrolysis oils for use as diesel engine fuels. Fuel 103, 247–257.

Anexo V

Coimbra, R.N., Escapa, C., Paniagua, S., Otero, M., *in press*. Adsorptive removal of diclofenac from ultrapure and wastewater: a comparative assessment on the performance of a polymeric resin and activated carbons. Desalination and Water Treatment.
http://dx.doi.org/10.1080/19443994.2016.1186398

Taylor & Francis
Taylor & Francis Group

Desalination and Water Treatment

ISSN: 1944-3994 (Print) 1944-3986 (Online) Journal homepage: http://www.tandfonline.com/loi/tdwt20

Adsorptive removal of diclofenac from ultrapure and wastewater: a comparative assessment on the performance of a polymeric resin and activated carbons

R.N. Coimbra, C. Escapa, S. Paniagua & M. Otero

To cite this article: R.N. Coimbra, C. Escapa, S. Paniagua & M. Otero (2016): Adsorptive removal of diclofenac from ultrapure and wastewater: a comparative assessment on the performance of a polymeric resin and activated carbons, Desalination and Water Treatment

To link to this article: http://dx.doi.org/10.1080/19443994.2016.1186398

Published online: 20 May 2016.

Submit your article to this journal

View related articles

View Crossmark data

Full Terms & Conditions of access and use can be found at
http://www.tandfonline.com/action/journalInformation?journalCode=tdwt20

Download by: [Marta Otero] **Date:** 21 May 2016, At: 01:38

Desalination and Water Treatment
www.deswater.com
doi: 10.1080/19443994.2016.1186398

(2016) 1–10

Taylor & Francis
Taylor & Francis Group

Adsorptive removal of diclofenac from ultrapure and wastewater: a comparative assessment on the performance of a polymeric resin and activated carbons

R.N. Coimbra, C. Escapa, S. Paniagua, M. Otero*

Faculty of Environmental and Biological Sciences, Department of Applied Chemistry and Physics, Institute of Environment, Natural Resources and Biodiversity (IMARENABIO), University of León, Campus de Vegazana, 24071 León, Spain,
emails: ricado.decoimbra@unileon.es (R.N. Coimbra), carla.escapa@unileon.es (C. Escapa), sergio.paniagua@unileon.es (S. Paniagua), Tel. +34 987293541; email: marta.otero@unileon.es (M. Otero)

Received 1 October 2015; Accepted 22 March 2016

Downloaded by [Marta Otero] at 01:38 21 May 2016

ABSTRACT

This work aimed to compare the adsorptive removal of diclofenac from ultrapure and wastewater by different adsorbents. Batch kinetic and equilibrium experiments were carried out using two different activated carbons (GPP20 and WP70, from Chemviron Carbon) and a non-ionic polymeric resin (SP207, from Resindion). The pseudo-second-order equation fitted the kinetic experimental results and the corresponding k_2 (g mg^{-1} min^{-1}) determined for the activated carbons was one order of magnitude higher than for the polymeric resin. The equilibrium results were fitted by the Langmuir–Freundlich isotherm. The determined maximum adsorption capacity (Q_m, mg g^{-1}) and the adsorbent–adsorbate affinity parameter (K_{LF}, mg g^{-1} (mg L^{-1})$^{-1/n}$) were one order of magnitude higher for the activated carbons than for the polymeric resin. With respect to the influence of the aqueous matrix, both the k_2 and the Q_m remained the same in ultrapure as in wastewater. Differently, the K_{LF} showed one order of magnitude higher values in waste than in ultrapure water. WP270 displayed the best adsorptive performance providing 0.00106 g mg^{-1} min^{-1} (k_2), 315 mg g^{-1} (Q_m), and 1.7 mg g^{-1} (mg L^{-1})$^{-1/n}$ (K_{LF}) for the adsorption of diclofenac from wastewater. These results support the practical application of activated carbon for the removal of diclofenac during the tertiary treatment of waste effluents.

Keywords: Emerging contaminants; Pharmaceutical industry; Wastewater; Adsorption; Water framework directive

1. Introduction

Emerging contaminants (ECs) are compounds that are not currently covered by existing water regulations, but are thought to be threat to environmental ecosystems and human health [1]. Among ECs, pharmaceuticals represent an especially worrying class since they were designed to cause a physiological response and their presence in the environment may

*Corresponding author.

Presented at the International Conference on Industrial Waste and Wastewater Treatment and Valorization (IWWTV 2015) May 21–23, 2015, Athens, Greece

1944-3994/1944-3986 © 2016 Balaban Desalination Publications. All rights reserved.

Downloaded by [Marta Otero] at 01:38 21 May 2016

affect non-target individuals and species [2]. Also, possible negative impacts on human health cannot be neglected [3].

In the last years, the identification and quantification of many previously undetected ECs in natural and wastewaters has remarkably progressed along with the development of analytical techniques [4]. Wide-ranging monitoring programs have been launched (e.g. [5]), which have confirmed the presence of ECs in natural waters and have raised concern about their effects. These programs have pointed to sewage treatment plants (STPs) as important sources of ECs in the aquatic environment [1,3]. These contaminants originated either from domestic sewage or from hospital or industrial discharges enter municipal STPs [6]. However, STPs are not efficient on the removal of ECs since they were not originally designed for this purpose due to the non-existence of limiting regulations on their discharge [7,8].

In the European context, the Water Framework Directive (2000/60/EC) (WFD) represented a breakthrough in EU policy by setting out strategies against water pollution. In this sense, a first list of priority substances was established (Decision 2455/2001/EC). This was replaced by Annex II of the Directive on Environmental Quality Standards (Directive 2008/105/EC) (EQSD). Later, it was foreseen by the Commission proposal of 31 January 2012 the inclusion of diclofenac, 17-beta-estradiol (E2), and 17-alpha-ethinylestradiol (EE2). However, under Directive 2013/39/EU, the Commission established the creation of a watch list of substances to be monitored in all member states to support future reviews of the priority substances list. It was then established that diclofenac, together with the hormones E2 and EE2, would be included in the first watch list.

Diclofenac (2-(2-(2,6-dichlorophenylamino)phenyl) acetic acid) is a non-steroidal anti-inflammatory drug (NSAID), which is prescribed as oral tablets or as a topical gel, has a yearly consumption that varies between 195 and 940 mg per inhabitant in different countries [9]. Its fate in the human body and during the municipal wastewater treatment, mechanisms of sorption, and biotransformation as well as formation of transformation products were recently reviewed and discussed by Vieno and Sillanpää [9]. These authors [9] concluded that diclofenac is only moderately or poorly biodegradable and therefore incomplete elimination during the conventional wastewater treatment can be expected. In fact, diclofenac is among the most frequently detected pharmaceuticals in the effluents of municipal wastewater treatment plants [10].

Given social and political concern at the EU about ECs, and, specifically about diclofenac, it is expectable that legislation on its discharge will come out in the near future. However, research on the removal of this pharmaceutical is even at a more incipient state than that on its occurrence and fate in the environment. Bolong et al. [8] have recently reviewed literature on treatment technologies applied for the removal of ECs from water, highlighting the necessity of research on this matter, and pointing out the potential of adsorption onto activated carbon. Main advantages of adsorption treatments for the removal of ECs are that they produce high-quality effluents, do not involve the generation of degradation products, which may have similar or even worse effects in aquatic systems, and are relatively cheap to perform [11].

Recently, a few works have been published on the removal of diclofenac from water by adsorption onto commercial activated carbon (e.g. [11,12]). Also, some alternative activated carbons have been produced and used for the adsorption of diclofenac (e.g. [13,14]). Non-ionic polymeric resins have been used with success for the adsorptive removal of different pharmaceuticals such as salicylic acid, vitamin B12, and cephalosporin C [14–16] but, to our best knowledge, there is not information on their utilization for the adsorption of diclofenac. Therefore, the aim of this work was to compare the diclofenac adsorption kinetics and capacity of a polymeric resin and two activated carbons. With this purpose, the performance of these materials from either ultrapure or wastewater has been evaluated. This is an important novelty, since most of the published works on the adsorptive removal of pharmaceuticals report results only from ultrapure or distilled aqueous solutions.

2. Materials and methods

2.1. Adsorbent materials

Two different activated carbons were used in this study, namely GPP20 and WP270, which were kindly provided by Chemviron Carbon (Feluy, Belgium). The utilization of both these carbons was recommended by Chemviron Carbon for their application in adsorption of pharmaceuticals from wastewater GPP20 is an activated carbon suitable for wastewater treatment applications, namely for the removal of aromatic compounds; and WP270 is an activated carbon originally designed for the treatment of drinking water, with promissory application for the removal of micropollutants from wastewater. The polymeric resin Sepabeads SP207 (Mitsubishi Chemical Corp., Tokyo, Japan) was gentle offered by Resindion (Rome, Italy). Table 1 shows the physical characteristics of these adsorbents, as supplied by the manufacturers.

Table 1
Physical properties of adsorbents used for diclofenac acid adsorption

Adsorbent	GPP20	Pulsorb WP270	Sepabeads SP207
Matrix	Coal-based steam-activated carbon	Coal-based steam-activated carbon	Styrene and DVD copolymer
Color	Black carbon	Black carbon	Yellowish opaque beads
Specific surface area ($m^2\ g^{-1}$)	725	1,050	630
Mean particle diameter (mm)	0.04	0.03	0.4

Downloaded by [Marta Otero] at 01:38 21 May 2016

2.2. Chemicals and analytic methods

Diclofenac sodium (≥99%) was purchased from Sigma-Aldrich (Steinheim, Germany). A waters HPLC 600 equipped with a 2487 Dual λ Absorbance Detector was used for determining the concentration of diclofenac in the aqueous phase. A Phenomenex C18 column (5 μm, 250 × 4.6 mm) was used for the separation. The mobile phase consisted of a mixture of acetonitrile:water:orthophosphoric acid (70:30:0.1, v/v/v) and the wavelength of detection was 276 nm. HPLC quality acetonitrile (CH_3CN) from LAB-SCAN, orthophosphoric acid (H_3PO_4) from Panreac, and ultrapure water obtained by a Millipore System were used for the preparation of the mobile phase. Before use, the homogenized mobile phase was passed through a Millipore 0.45-μm-pore size filter and degasified in an ultrasound bath during 30 min. For the chromatographic analysis, the mobile phase flow rate was 1 mL min^{-1} and the injection volume was 50 μL. For each aliquot, four replicated injections were carried out.

2.3. Wastewater

The secondary effluent collected from the STP of León (Spain) was used in this work. This secondary effluent is directly discharged at the Bernesga River, a tributary of the Esla River that is 77 km long and goes through the town of León. The STP consists of primary and secondary stage treatments. The primary stage comprises a sequence of treatments consisting of screening, sand removal, fat removal, and primary clarification. Then, the secondary stage involves a plug-flow activated sludge with nitrification/denitrification followed by secondary clarification. The plant was designed to treat the wastewater of 330,000 equivalent inhabitants and has an inflow of 123,000 $m^3\ d^{-1}$ with a hydraulic retention time (HRT) of about 6 h.

Wastewater quality parameters, namely pH, conductivity, total suspended solids (TSS), biological oxygen demand at five days (BOD_5), chemical oxygen demand (DQO), NTK, N-NH_4, N-NO_3, N-NO_2, total P-PO_4, were determined using Standard Methods (APHA-AWWA-WPCF, 2001). Table 2 depicts the obtained results from these analyses.

2.4. Adsorption experiments

Adsorption experiments were performed using a batch experimental approach. Adsorption kinetic experiments were first carried out in order to determine the time necessary to attain equilibria (t_{eq}). Then, equilibrium experiments were performed to determine the adsorption isotherm. All experiments were carried out in triplicate by agitating (250 rpm) a known mass of adsorbent together with 100 mL of ultrapure or wastewater in 250-mL Erlenmeyer flasks. Initial concentration of diclofenac sodium was 100 ± 1 mg L^{-1}. Diclofenac sodium solutions were not buffered and pH was monitored throughout adsorption experiments. This allowed verifying that the pH of diclofenac sodium solutions in contact with each adsorbent material was equal to the point of zero charge (PZC) of the latter. Therefore, adsorbents maintained a net charge of zero throughout experiments. On the other hand, for the three adsorbents here used, the PZC was higher

Table 2
Main properties of wastewater used in this work

pH	Conductivity (μS cm^{-1})	TSS (mg L^{-1})	BOD_5 (mg L^{-1})	COD (mg L^{-1})	NTK (mg L^{-1})	N-NH_4 (mg L^{-1})	N-NO_3 (mg L^{-1})	N-NO_2 (mg L^{-1})	Total P-PO_4 (mg L^{-1})
7.8 ± 0.2	612 ± 3	22 ± 1	21 ± 2	47 ± 3	17 ± 2	13.10 ± 0.42	1.73 ± 0.18	0.48 ± 0.09	1.75 ± 0.13

Downloaded by [Marta Otero] at 01:38 21 May 2016

than the pK_a of diclofenac sodium ($pK_a = 4$), so ensuring that the adsorbate remained in its neutral form. Experiments were done at a constant temperature of 25 ± 2°C controlled by means of a thermostatically regulated incubator. Triplicate control experiments, with no adsorbent, were run in parallel with adsorption experiments in order to verify if the concentration of the target pharmaceutical was stable throughout the duration of the experiments.

In the kinetic experiments, Erlenmeyer flasks were progressively withdrawn from the shaker after pre-set time intervals. Then, from each flask, three aliquots were taken, filtered, and chromatographically analyzed to determine the concentration of diclofenac. The amount of diclofenac adsorbed onto each adsorbent at each time, q_t (mg g^{-1}), was calculated by a mass balance relationship as follows:

$$q_t = (C_0 - C_t)\frac{V}{W} \tag{1}$$

where C_0 (mg L^{-1}) and C_t (mg L^{-1}) are the initial and the liquid-phase concentrations of diclofenac at a time t, respectively, V is the volume of the solution (L) and W is the mass (g) of adsorbent.

For equilibrium experiments, Erlenmeyer flasks containing different masses of the corresponding adsorbent material were agitated throughout 1,000 min in the case of the activated carbons and 6,000 min in the case of the polymeric resin, in order to ensure that equilibrium was attained. Then, from each flask, three aliquots were taken, filtered, and chromatographically analyzed to determine the equilibrium concentration (C_e, mg L^{-1}) of diclofenac. The amount of pharmaceutical adsorbed onto PS800-150 at the equilibrium, q_e (mg g^{-1}), was calculated by the following mass balance relationship:

$$q_e = (C_0 - C_e)\frac{V}{W} \tag{2}$$

where C_0 (mg L^{-1}) and C_e (mg L^{-1}) are the initial and the liquid-phase concentrations of pharmaceutical at the equilibrium, respectively, V is the volume of the solution (L) and W is the mass (g) of adsorbent.

2.5. Modeling of adsorption results

Fittings of the experimental kinetic results to the pseudo-first-order [17] and the pseudo-second-order [18] equations were obtained by GraphPad Prism6 (trial version, last accessed on the 10 March 2015). Both the pseudo-first-order (Eq. (3)) and the pseudo-second-order (Eq. (4)) are empirical rate equations based on the overall sorption rate:

$$q_t = q_e(1 - e^{-k_1 t}) \tag{3}$$

$$q_t = \frac{q_e^2 k_2 t}{1 + q_e k_2 t} \tag{4}$$

where k_1 (min^{-1}) and k_2 (mg g^{-1} min) are the pseudo-first- and the pseudo-second-order rate constants, respectively.

In order to describe the adsorption equilibrium results, fittings to the main two parameter isotherms, namely the Freundlich isotherm [19] and the Langmuir isotherm [20], which are described by Eqs. (5) and (6), were determined. Then, the Sips isotherm [21], also known as the Langmuir–Freundlich equation, which is a three parameter model, as described by Eq. (7), was also used to fit the experimental results.

$$q_e = K_F C_e^{1/n} \tag{5}$$

$$q_e = \frac{Q_m K_L C_e}{1 + K_L C_e} \tag{6}$$

$$q_e = \frac{Q_m K_{LF} C_e^{1/n}}{1 + K_{LF} C_e^{1/n}} \tag{7}$$

$$q_e = q_\infty \frac{K_1 C_e\left(1/r + K_2 C_e^{r-1}\right)}{1 + K_1 C_e\left(1 + K_2 C_e^{r-1}\right)} \tag{8}$$

where K_F is the Freundlich adsorption constant (mg g^{-1} (mg $L^{-1})^{-1/n}$); n is the degree of non-linearity; Q_m is the maximum adsorption capacity (mg g^{-1}); K_L (L mg^{-1}) and K_{LF} (mg g^{-1} (mg $L^{-1})^{-1/n}$) are the Langmuir and Langmuir–Freundlich affinity coefficients, respectively.

3. Results and discussion

The parameters analyzed on the secondary effluent used in this work (Table 2) showed typical values of a municipal STP effluent and accomplished with European regulations on the discharge of this sort of effluents (35 mg L^{-1} TSS, 25 mg L^{-1} BOD_5, and 125 mg L^{-1} COD as established by the EU Council Directive 91/271/EEC).

Control experiments carried out allowed verifying that diclofenac concentration remained the same during the agitation times here considered, either in ultrapure or in wastewater.

Downloaded by [Marta Otero] at 01:38 21 May 2016

The kinetic experimental data on the adsorption of diclofenac from ultrapure and wastewater are shown in Figs. 1 and 2, respectively, together with fittings to the pseudo-first-order and the pseudo-second-order kinetic equations. Parameters determined from these fittings are depicted in Table 3.

As evidenced by Fig. 1, in ultrapure water, the adsorption of diclofenac onto the polymeric resin is slower than onto both the activated carbons, which displayed similar kinetics. Furthermore, as seen in Fig. 1 and for all the adsorbent materials, the pseudo-second-order equation fits experimental results slightly better than the pseudo-first-order model, which is also true for the adsorption kinetics of diclofenac from wastewater, as seen in Fig. 2. This observation is further supported by parameters in Table 3, which show that, in all cases, higher R^2 and lower S_{xy} have been determined for fittings to the pseudo-second-order kinetic equation, as compared to the pseudo-first-order one. Still, by comparing Figs. 1 and 2, it may be seen that, for each adsorbent, the adsorption kinetics of diclofenac from ultrapure and wastewater are very similar. This is confirmed by the kinetic constants in Table 3, since there are no significant differences between the k_2 determined for the adsorption of diclofenac from ultrapure or wastewater onto the adsorbents here considered. Therefore, it may be said that the velocity of the diclofenac adsorption was not reduced when the aqueous matrix was as complex as the wastewater used in this work.

The experimental adsorption isotherms determined for the adsorption of diclofenac from ultrapure and

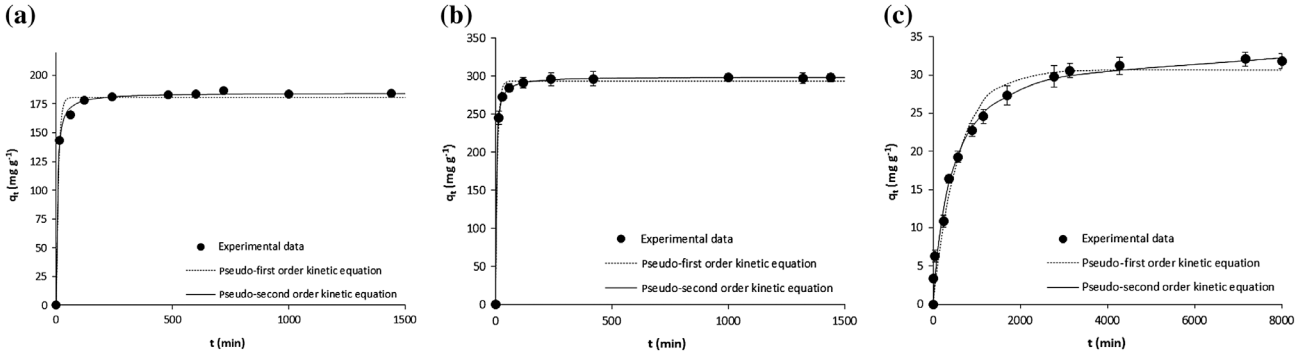

Fig. 1. Kinetic results on the adsorptive removal of diclofenac from ultrapure water by adsorption onto the adsorbents used in this work: (a) activated carbon GPP20, (b) activated carbon WP270, and (c) a polymeric resin Sepabeads SP207. Experimental results throughout time are shown together with the corresponding fittings to the pseudo-first- and to the pseudo-second-order kinetic equations. Error bars stand for standard deviation of three experimental replications.
Note: For a better visualization of fittings, the scale of axis Y in figures (a), (b), and (c) has been adjusted to results.

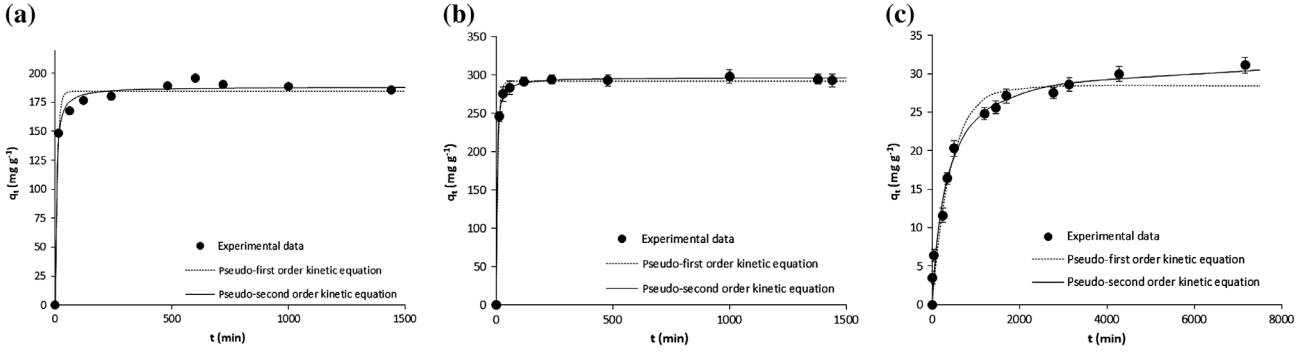

Fig. 2. Kinetic results on the adsorptive removal of diclofenac from wastewater by adsorption onto the adsorbents used in this work: (a) activated carbon GPP20, (b) activated carbon WP270, and (c) a polymeric resin Sepabeads SP207. Experimental results throughout time are shown together with the corresponding fittings to the pseudo-first- and to the pseudo-second-order kinetic equations. Error bars stand for standard deviation of three experimental replications.
Note: For a better visualization of fittings, the scale of axis Y in figures (a), (b), and (c) has been adjusted to results.

Downloaded by [Marta Otero] at 01:38 21 May 2016

Table 3
Kinetic parameters obtained from the fittings of experimental results on the adsorption of diclofenac from ultrapure water (UPW) and from wastewater (WW) to the pseudo-first- and to the pseudo-second-order equations

		GPP20		WP270		SP207	
		UPW	WW	UPW	WW	UPW	WW
Pseudo-first-order	k_1 (min^{-1})	0.104 ± 0.011	0.108 ± 0.015	0.115 ± 0.008	0.119 ± 0.007	0.0017 ± 0.0002	0.0023 ± 0.0003
	q_e (mg g^{-1})	180.90 ± 2.13	184.40 ± 2.96	293.50 ± 2.27	291.90 ± 1.89	30.64 ± 0.83	28.45 ± 0.84
	R^2	0.9903	0.9820	0.996	0.9972	0.9734	0.9692
	S_{xy}	5.99	8.33	6.16	5.14	1.92	1.98
Pseudo-second-order	k_2 (g mg^{-1} min^{-1})	0.00119 ± 0.00010	0.00118 ± 0.00020	0.00106 ± 0.00003	0.00117 ± 0.00008	0.00007 ± 0.00001	0.00010 ± 0.00002
	q_e (mg g^{-1})	188.70 ± 1.01	188.40 ± 2.09	299.1 ± 0.45	296.90 ± 1.09	33.94 ± 0.83	31.83 ± 0.92
	R^2	0.9983	0.993	0.9999	0.9993	0.9869	0.9835
	S_{xy}	2.50	5.22	1.06	2.58	1.35	1.45

wastewater are represented in Figs. 3 and 4, respectively. Fittings to the Freundlich, Langmuir, and Langmuir–Freundlich isotherm models are shown together with experimental results and the corresponding parameters are depicted in Table 4.

Equilibrium results in Fig. 3 make evident that the diclofenac adsorption capacity of the polymeric resin from ultrapure water is one order of magnitude smaller than that of the activated carbons, among which the WP270 displays the highest capacity. As seen in Fig. 3, the Langmuir–Freundlich isotherm model fits the adsorption of diclofenac onto the three adsorbent materials considered in this work. Coincidently, Fig. 4 shows that the Langmuir–Freundlich isotherm fits experimental adsorption results from wastewater better than the Langmuir and Freundlich isotherms. Also, the diclofenac adsorption capacity of each of the three adsorbent materials from wastewater (Fig. 4) is equivalent to its respective capacity from ultrapure water (Fig. 3). However, for the three adsorbents, the rise of the isotherm curves close to the origin is steeper for the adsorption from wastewater (Fig. 4) than from ultrapure water (Fig. 3). Parameters in Table 4 confirm the previous observations. For all the three adsorbents and from both ultrapure and wastewater, the Langmuir–Freundlich isotherm is the model that best fit the experimental results, as reflected by the highest R^2 and the lowest S_{xy} in Table 4. Then, the performance of the adsorbent materials here used may be compared on the basis of the Langmuir–Freundlich isotherm parameters. However, it must be highlighted that, for GPP20, the Freundlich isotherm also fits the diclofenac equilibrium adsorption from ultrapure water, as it may be observed in Fig. 3 and inferred by the corresponding R^2 and S_{xy}. Therefore, in this case and as a consequence of the absence of a clear plateau, the deviation associated to the Langmuir–Freundlich maximum adsorption capacity (Q_m (mg g^{-1})) is very large. On the contrary, for the polymeric resin SP207, as seen in Fig. 3, the Langmuir isotherm fits diclofenac equilibrium adsorption from ultrapure water, the corresponding R^2 and S_{xy} being equivalent to those regarding the Langmuir–Freundlich isotherm.

According to the fitted Langmuir–Freundlich Q_m, it may be confirmed that the diclofenac adsorption capacity of the activated carbons is one order of magnitude higher than that of the polymeric resin. In any case, as seen in Table 4, for all the adsorbents here considered, the Q_m remains the same in ultrapure as in wastewater. This is contrary to the findings on the adsorption of highly polar ECs, namely cytarabine (CytR) and 5-fluorouracil (5-Fu), on powdered activated carbon by Kovalova et al. [22]. These authors [22] found that the presence of organic matter in a

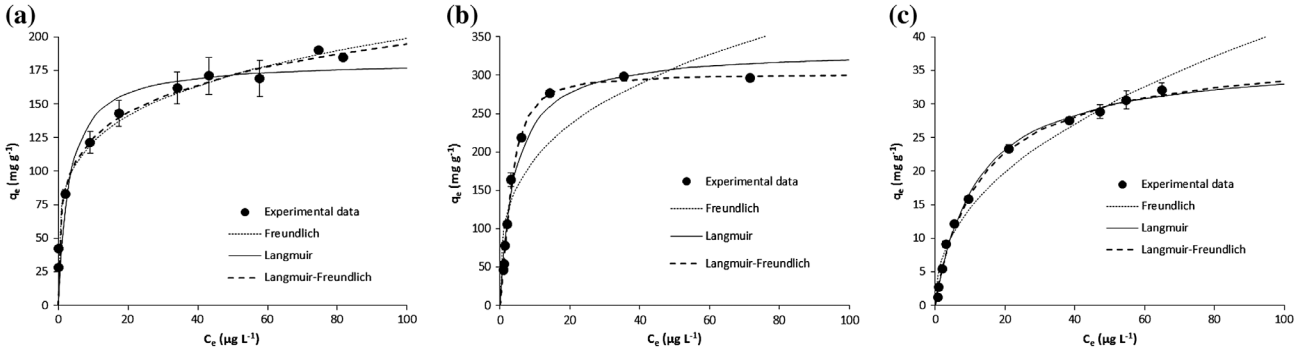

Fig. 3. Equilibrium results on the adsorptive removal of diclofenac from ultrapure water by adsorption onto the adsorbents used in this work: (a) activated carbon GPP20, (b) activated carbon WP270, and (c) a polymeric resin Sepabeads SP207. Experimental results are shown together with fittings to the Freundlich, to the Langmuir, and to the Langmuir–Freundlich isotherm models. Error bars stand for standard deviation of three experimental replications.
Note: For a better visualization of fittings, the scale of axis Y in figures (a), (b), and (c) has been adjusted to results.

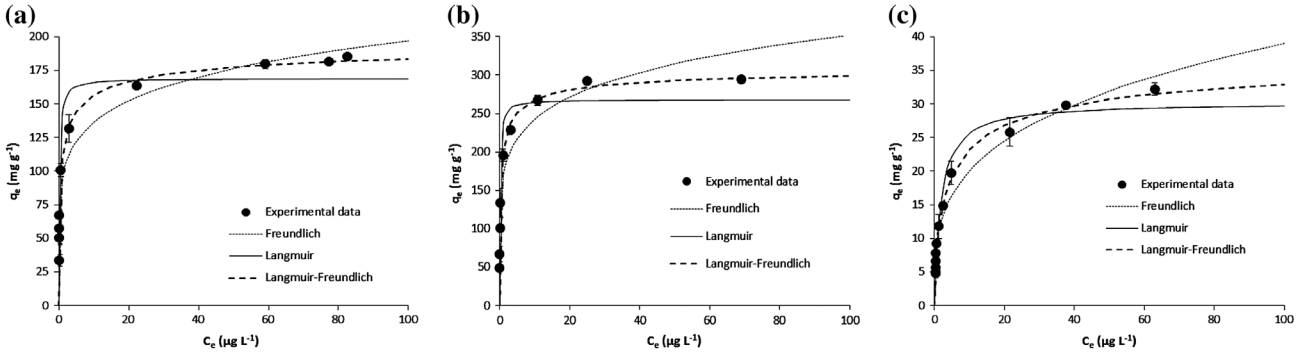

Fig. 4. Equilibrium results on the adsorptive removal of diclofenac from wastewater by adsorption onto the adsorbents used in this work: (a) activated carbon GPP20, (b) activated carbon WP270, and (c) a polymeric resin Sepabeads SP207. Experimental results are shown together with fittings to the Freundlich, to the Langmuir, and to the Langmuir–Freundlich isotherm models. Error bars stand for standard deviation of three experimental replications.
Note: For a better visualization of fittings, the scale of axis Y in figures (a), (b), and (c) has been adjusted to results.

Downloaded by [Marta Otero] at 01:38 21 May 2016

wastewater effluent lowered the adsorption uptake of CytR and 5-Fu. However, our results are coincident with those by Méndez-Díaz et al. [23], who found that the phthalic acid (PA) adsorption capacity of two different activated carbons was larger from wastewater than from ultrapure water. These authors [23] attributed differences to the action of micro-organisms in wastewater. Unfortunately, no comparative isotherms in ultrapure and wastewater have been found in the literature on the adsorption of diclofenac. Therefore, we cannot contrast our results with those obtained by other authors.

With respect to the K_{LF}, values corresponding to activated carbons are one order of magnitude higher than those of the polymeric resin. The activated carbon WP270 displayed the highest values of K_{LF}, which may be related to the affinity of the adsorbent for the adsorbate. Also, the K_L determined for the adsorbents here considered followed the same order than the Q_m, that is: WP270 > GPP20 > SP207. However, and differently from the Q_m, one order of magnitude higher K_{LF} were determined for each of the adsorbents in wastewater than in ultrapure water. This is in agreement with the steeper isotherms in wastewater (Fig. 4) as compared with those in ultrapure water (Fig. 3). In wastewater, a 3% increase of the activated carbon affinity for PAC was determined by Méndez-Díaz et al. [23], as compared with ultrapure water. These authors [23] attributed this increase to an increase of the hydrophobicity of the activated carbon surface due to the attachment of micro-organisms, which external walls are formed by phospholipids. On the other hand, the presence of salts is known to affect the adsorbent–adsorbate affinity [24], to increase water

Downloaded by [Marta Otero] at 01:38 21 May 2016

Table 4
Isotherm parameters obtained from the fittings of the equilibrium experimental results on the adsorption of diclofenac from ultrapure water (UPW) and from wastewater (WW) to the isotherm models of Freundlich, Langmuir, and Langmuir–Freundlich

		GPP20		WP270		SP207	
		UPW	WW	UPW	WW	UPW	WW
Freundlich	K_F (mg g^{-1} (mg L^{-1})$^{-1/n}$)	74.53 ± 2.73	94.30 ± 5.39	96.07 ± 19.17	167.20 ± 12.05	5.12 ± 0.70	10.28 ± 0.63
	n	4.689 ± 0.214	6.252 ± 0.598	3.343 ± 0.678	6.186 ± 0.8822	2.212 ± 0.182	3.454 ± 0.225
	R^2	0.9932	0.954	0.8116	0.90742	0.9728	0.9689
	S_{yx}	5.14	13.72	48.62	31.3	2.042	1.85
Langmuir	Q_m (mg g^{-1})	182.10 ± 11.06	169.00 ± 8.10	333.00 ± 15.82	268.10 ± 12.78	36.90 ± 0.86	30.23 ± 1.19
	K_L (L mg^{-1})	0.327 ± 0.138	5.334 ± 1.440	0.246 ± 0.038	7.157 ± 1.890	0.084 ± 0.006	0.551 ± 0.078
	R^2	0.9019	0.9252	0.9712	0.9371	0.9959	0.9695
	S_{yx}	19.57	17.49	19.02	25.79	0.89	1.836
Langmuir–Freundlich	Q_m (mg g^{-1})	445.50 ± 254.70	202.60 ± 12.59	300.80 ± 5.17	315.00 ± 18.64	38.63 ± 2.59	37.94 ± 2.31
	K_{LF} (mg g^{-1} (mg L^{-1})$^{-1/n}$)	0.158 ± 0.086	1.198 ± 0.259	0.182 ± 0.015	1.698 ± 0.422	0.087 ± 0.008	0.385 ± 0.038
	n	3.670 ± 0.495	2.208 ± 0.302	0.646 ± 0.038	1.912 ± 0.261	1.070 ± 0.092	1.628 ± 0.126
	R^2	0.9952	0.9896	0.9969	0.9868	0.9962	0.9953
	S_{yx}	4.62	6.98	6.72	12.78	0.81	0.76

Downloaded by [Marta Otero] at 01:38 21 May 2016

surface tension and to decrease adsorption free energy of organic solutes [25]. For example, Chang et al. [26] verified that the presence of inorganic salts in relative high concentration significantly enhanced the removal of 2-ethyl-1-hexanol from aqueous solutions by adsorption on activated carbon.

On the whole, in this work, it may be said that none of the adsorbents considered displayed lower capacity in waste than in ultrapure water. Moreover, all of them showed a higher affinity for the adsorption of diclofenac from waste than from ultrapure water. From a practical point of view, these findings are quite relevant for the application of the adsorbents.

4. Conclusions

The adsorption kinetics of diclofenac both onto the activated carbons (GPP20 and WP270) and onto the polymeric resin (SP207) was described by the pseudo-second-order kinetic model. The fitted pseudo-second-kinetic constant (k_2) for the activated carbons and for the polymeric resin were around 0.001 and 0.0001 g mg^{-1} min^{-1}, respectively. For each of the considered adsorbents, no differences were observed between k_2 determined for the adsorption from ultrapure or wastewater. The three parameters Langmuir–Freundlich isotherm fitted equilibrium adsorption results onto the three adsorbent materials. The activated carbons displayed the same order maximum adsorption capacity (Q_m), which was one order of magnitude higher than that of the polymeric resin (around 38 mg g^{-1}). As for the k_2, for each of the adsorbents, the Q_m remained the same in ultrapure than in wastewater. Differently, steeper isotherms were obtained in waste than in ultrapure water and so, for each of the adsorbents, higher fitted K_{LF} were determined in waste than in ultrapure water. Therefore, an increased affinity for diclofenac occurred in wastewater for all the adsorbents tested. In any case, results obtained in this work support the utilization of the activated carbon for the adsorptive removal of diclofenac from wastewater, the WP270 being specially recommended.

Acknowledgments

P. Quintans, Process and Laboratory Manager at the STP of León (Spain), is acknowledged for her friendly assistance. C. Escapa and S. Paniagua thank the Spanish Ministry of Education, Culture and Sports for their PhD fellowships (FPU12/03073 and FPU14/05846, respectively). Also, Marta Otero acknowledges support from the Spanish Ministry of Economy and Competitiveness, State Secretariat for Research, Development and Innovation (RYC-2010-05634).

References

[1] M. Farré, S. Pérez, L. Kantiani, D. Barceló, Fate and toxicity of emerging pollutants, their metabolites and transformation products in the aquatic environment, TrAC, Trends Anal. Chem. 27 (2008) 991–1007.
[2] L.H.M.L.M. Santos, A.N. Araújo, A. Fachini, A. Pena, C. Delerue-Matos, M.C.B.S.M. Montenegro, Ecotoxicological aspects related to the presence of pharmaceuticals in the aquatic environment, J. Hazard. Mater. 175 (2010) 45–95.
[3] A. Pal, Y. He, M. Jekel, M. Reinhard, K.Y.-H. Gin, Emerging contaminants of public health significance as water quality indicator compounds in the urban water cycle, Environ. Int. 71 (2014) 46–62.
[4] S.D. Richardson, Water analysis: Emerging contaminants and current issues, Anal. Chem. 81 (2009) 4645–4677.
[5] R. López-Roldán, M. López de Alda, M. Gros, M. Petrovic, J. Martín-Alonso, D. Barceló, Advanced monitoring of pharmaceuticals and estrogens in the Llobregat River basin (Spain) by liquid chromatography–triple quadrupole-tandem mass spectrometry in combination with ultra performance liquid chromatography–time of flight-mass spectrometry, Chemosphere 80 (2010) 1337–1344.
[6] M.I. Badawy, R.A. Wahaab, A.S. El-Kalliny, Fenton-biological treatment processes for the removal of some pharmaceuticals from industrial wastewater, J. Hazard. Mater. 167 (2009) 567–574.
[7] D. Barceló, M. Petrovic, Reducing the environmental risk from emerging pollutants: Report on the 1st EMCO Workshop "Analysis and Removal of Contaminants from Wastewaters for the Implementation of the Water Framework Directive (WFD)", Dubrovnik, Croatia, 20–21 October 2005.
[8] N. Bolong, A.F. Ismail, M.R. Salim, T. Matsuura, A review of the effects of emerging contaminants in wastewater and options for their removal, Desalination 239 (2009) 229–246.
[9] N. Vieno, M. Sillanpää, Fate of diclofenac in municipal wastewater treatment plant—A review, Environ. Int. 69 (2014) 28–39.
[10] P. Verlicchi, M. Al Aukidy, E. Zambello, Occurrence of pharmaceutical compounds in urban wastewater: Removal, mass load and environmental risk after a secondary treatment—A review, Sci. Total Environ. 429 (2012) 123–155.
[11] J.L. Sotelo, G. Ovejero, A. Rodríguez, S. Álvarez, J. Galán, J. García, Competitive adsorption studies of caffeine and diclofenac aqueous solutions by activated carbon, Chem. Eng. J. 240 (2014) 443–453.
[12] J.L. Sotelo, A. Rodríguez, S. Álvarez, J. García, Removal of caffeine and diclofenac on activated carbon in fixed bed column, Chem. Eng. Res. Des. 90 (2012) 967–974.
[13] S. Jodeh, F. Abdelwahab, N. Jaradat, I. Warad, W. Jodeh, Adsorption of diclofenac from aqueous solution using *Cyclamen persicum* tubers based activated carbon (CTAC), J. Assoc. Arab Univ. Basic Appl. Sci. (in press), doi: 10.1016/j.jaubas.2014.11.002.
[14] C. Saucier, M.A. Adebayo, E.C. Lima, R. Cataluña, P.S. Thue, L.D.T. Prola, M.J. Puchana-Rosero, F.M. Machado, F.A. Pavan, G.L. Dotto, Microwave-assisted activated carbon from cocoa shell as adsorbent for

removal of sodium diclofenac and nimesulide from aqueous effluents, J. Hazard. Mater. 289 (2015) 18–27.
[15] A.M. Ramos, M. Otero, A.E. Rodrigues, Recovery of Vitamin B12 and cephalosporin-C from aqueous solutions by adsorption on non-ionic polymeric adsorbents, Sep. Purif. Technol. 38 (2004) 85–98.
[16] M. Otero, M. Zabkova, C. Grande, A.E. Rodrigues, Fixed-bed adsorption of salicylic acid onto polymeric adsorbents and activated charcoal, Ind. Eng. Chem. Res. 44(4) (2005) 927–936.
[17] S. Lagergren, Zur theorie der sogenannten adsorption gelöster stoffe (About the theory of so-called adsorption of soluble substances), Kungliga Svenska Vetenskapsakademiens, Handlingar 24 (1898) 1–39.
[18] Y.S. Ho, G. McKay, Pseudo-second order model for sorption processes, Process Biochem. 34 (1999) 451–465.
[19] H. Freundlich, Uber die adsorption in losungen, Z. Phys. Chem. 57 (1906) 385–470.
[20] I. Langmuir, The adsorption of gases on plane surfaces of glass, mica and platinum, J. Am. Chem. Soc. 40 (1918) 1361–1403.
[21] R. Sips, On the structure of a catalyst surface, J. Chem. Phys. 16 (1948) 490–495.
[22] L. Kovalova, D.R.U. Knappe, K. Lehnberg, C. Kazner, J. Hollender, Removal of highly polar micropollutants from wastewater by powdered activated carbon, Environ. Sci. Pollut. Res. 20 (2013) 3607–3615.
[23] J.D. Méndez-Díaz, M.M. Abdel Daiem, J. Rivera-Utrilla, M. Sánchez-Polo, I. Bautista-Toledo, Adsorption/bioadsorption of phthalic acid, an organic micropollutant present in landfill leachates, on activated carbons, J. Colloid Interface Sci. 369 (2012) 358–365.
[24] L.M. Pastrana-Martínez, M.V. López-Ramón, M.A. Fontecha-Cámara, C. Moreno-Castilla, Batch and column adsorption of herbicide fluroxypyr on different types of activated carbons from water with varied degrees of hardness and alkalinity, Water Res. 44 (2010) 879–885.
[25] K. Sahu, V.F. McNeill, K.B. Eisenthal, Effect of salt on the adsorption affinity of an aromatic carbonyl molecule to the air-aqueous interface: Insight for aqueous environmental interfaces, J. Phys. Chem. C 114 (2010) 18258–18262.
[26] G. Chang, Z. Bao, Z. Zhang, H. Xing, B. Su, Y. Yang, Q. Ren, Salt-enhanced removal of 2-ethyl-1-hexanol from aqueous solutions by adsorption on activated carbon, J. Colloid Interface Sci. 412 (2013) 7–12.

Downloaded by [Marta Otero] at 01:38 21 May 2016